



**HAL**  
open science

# Systèmes multiporteuses à postfixes pseudo aléatoires

Markus Muck

► **To cite this version:**

Markus Muck. Systèmes multiporteuses à postfixes pseudo aléatoires. domain\_other. Télécom Paris-Tech, 2006. English. NNT: . pastel-00002834

**HAL Id: pastel-00002834**

**<https://pastel.hal.science/pastel-00002834>**

Submitted on 28 Sep 2007

**HAL** is a multi-disciplinary open access archive for the deposit and dissemination of scientific research documents, whether they are published or not. The documents may come from teaching and research institutions in France or abroad, or from public or private research centers.

L'archive ouverte pluridisciplinaire **HAL**, est destinée au dépôt et à la diffusion de documents scientifiques de niveau recherche, publiés ou non, émanant des établissements d'enseignement et de recherche français ou étrangers, des laboratoires publics ou privés.



# Thèse

présentée pour obtenir le grade de docteur

## Markus Mück

### Systèmes multiporteuses à postfixes pseudo aléatoires

#### Pseudo Random Postfix Orthogonal Frequency Division Multiplexing

Soutenance le 09-mai-2006 devant le jury composé de

Hikmet Sari

Président

David Falconer  
Jean-François Hérald

Rapporteurs

Pierre Duhamel  
Jean-Claude Belfiore  
Marc De Courville

Examineurs



*Und sehe, daß wir nichts wissen KÖNNEN !  
Das will mir schier das Herz verbrennen.  
Faust, Goethe*



# Acknowledgements

I would like to start expressing my profound thanks to Marc De Courville who gave me the opportunity to pursue this thesis at Motorola Labs in Paris, France while I was working as a research engineer. I did not only learn a lot on a technical and human level from Marc, but we also had great fun in challenging internal projects, during our participation to standardization bodies (in particular IEEE 802.11n) where we started off as underdogs, fought many battles against challenging and sometimes vicious opponents and finally ended up as quite influential participants, etc. I would like to thank him sincerely for the time we have been working together and hope that we will still be able to commonly explore both new and crazy ideas.

I am also deeply thankful to Pierre Duhamel of LSS Supelec Gif-sur-Yvette, France who supervised my thesis from the university side. I had a great time working with Pierre and appreciated his human and technical qualities in any way. He led me onto many interesting and challenging paths and was very available for me despite of his numerous involvements in organizational tasks (ICASSP 2006, etc., etc.). Thank you very much, Pierre, for the nice time we had together !

Let me extend these thanks to all members of my PhD jury. First of all, there is Jean-Claude Belfiore who kindly accepted to take the responsibility of being the official supervisor of this thesis at the Ecole Nationale Supérieure des Télécommunications (ENST) de Paris. Thank you, Jean-Claude, for being always available, for the great technical discussions (in particular on Golden Codes) and your didactic courses at ENST. I would also like to express my deep thanks to David Falconer from Carleton University, Canada. I had many great discussions with Dave and his staff in the framework of the European Project IST-WINNER. I am very grateful, Dave, that you accepted to participate in the jury of my thesis. Moreover, many thanks to Jean-François Hélar from the Institut National des Sciences Appliquées (INSA) Rennes, France who kindly accepted to evaluate my thesis; thank you very much, Jean-François, for your positive and constructive report and all the great discussions we still had off-line. Last, but not least, I am deeply thankful to Hikmet Sari of Supelec Gif-sur-Yvette, France for accepting the role as president of my jury. Merci, Hikmet, for your availability and the great technical discussions we had during and after the defense.

I would also like to express my thanks to all my colleagues at Motorola Labs in Paris. It is difficult to name everyone, but in particular, I am thinking of Laurent Mazet who likes Cuban Cigars and gives great advice in Digital Signal Processing and about 100 programming languages. Thank you also very much, Stephanie Rouquette-Léveil, for the great time we've been working together on IEEE 802.11n and all the discussions, publications, disclosures, etc. Among the first people I met when joining Motorola were Véronique Buzenac and Sébastien Simoens - thanks again very much, Véro, for the common projects and the great time we had; thanks also, Seb, for all our discussions on Signal Processing, black chocolate and beyond. I express also my thanks to Patrick Labbé - we had a great time working together and had many nice discussions about Scuba Diving and other fun activities. There is obviously also Philippe Bernardin

with whom I was working for a long time and who I appreciate very much; thanks again, Philippe, for our time in Motorola and all the discussions about Jazz and music. Obviously, I was also working with colleagues in the Schaumburg Labs, USA; there, I wish to thank in particular Yufei Blankenship who is a great teacher and provided valuable comments on the LDPC chapter of this thesis. Finally, I wish to express all my thanks to Jean-Noël Patillon who took the crazy decision of hiring me at the Motorola Labs; he also supported me strongly in the endeavor of this thesis and I thank him very much for his support.

Moreover, I wish to thank the new colleagues I started recently to work with. There's Didier Bourse who's a great, hard working colleague who's introduced me in the weird world of European IPs (Integrated Projects). Thank you very much, Didier, for the great fun we had by now - I sincerely hope that we will have the opportunity to make lots of crazy things happen. Thank you also, Sophie Gault and David Grandblaise for our great and motivating cooperation and in particular to you, David, for giving valuable advice on the french part of this thesis.

In the following I wish to express my sincere thanks to several former PhD students of Motorola Labs: there are Merouane Debbah and Samson Lasaulce, now with Eurecom and Supelec, who were always enriching teachers and great friends giving clear guidance on the spiritual paths. Thank you very much, Merouane and Samson for the fun we had together. There are also Emilio Strinati and Mohamed Kamoun who I wish to thank for their friendship and all our enriching discussions.

In this context, I wish to express my deep appreciation to Prof. Paul J. Kühn of the Institut für Kommunikationsnetze und Rechnersysteme at the University of Stuttgart, Germany. He organized the double-diploma exchange programme between the University of Stuttgart and the ENST in Paris and it is clearly due to him that I was able to live this great experience here in France. Thank you very much for having organized all this and your valuable help in integrating a very different environment !

Finally I wish to express all my thanks and affection to my parents, Christa Mück and Gunter Mück as well as to my sister Anja Mück. They have always been a great support even in the most difficult moments while being abroad. Many, many thanks also to my francophile relatives in Stuttgart, Rose, Florian and Klaus Heuser. They helped me very much in absorbing the french language and in guiding my (hopeless ?) artistic tendencies.

Thanks again very much to all of you,

Markus

## Abstract

This thesis presents a novel *Orthogonal Frequency Division Multiplexing (OFDM)* modulation scheme replacing the cyclic extension known from classical *Cyclic Prefix OFDM (CP-OFDM)* by a deterministic *pseudo randomly weighted postfix* sequence: **Pseudo Random Postfix OFDM (PRP-OFDM)** [1–26].

The postfix sequence is known to both, the transmitter and the receiver and can thus be exploited for order-one (semi-)blind channel estimation without any repeated introduction of learning symbols and/or pilot tones within a frame. The corresponding overhead, usually present in CP-OFDM and Zero-Padded OFDM (ZP-OFDM) systems, is thus reduced or even avoided leading to an improved spectral efficiency. Suitable approaches, including postfix design considerations, are discussed for both, single-antenna and multiple-antennas systems in static and time-variant environments.

The studies are then further extended to time and frequency synchronization [2]. It is shown how to exploit the pseudo-randomly weighted postfixes for the refinement of an initial (rough) time/frequency synchronization. This part is followed by a study on Low-Density Parity Check (LDPC) coded OFDM systems [27, 28], proposing an adaptation of the LDPC code word mapping onto OFDM carriers to the constraints of OFDM systems in a frequency selective fading environment; this approach can be interpreted as the design of an adaptive interleaver for a specific context. For a given irregular LDPC code, a low-complexity algorithm is derived indicating which code word bits should be modulated onto which OFDM carriers in function of a known or estimated channel impulse response.

The PRP-OFDM modulation scheme is one of several modulations considered in the framework of the European Projects IST-BroadWay [14–20, 29] and more recently IST-WINNER [21–24, 30]: IST-WINNER is a 6<sup>th</sup> framework Integrated Project (IP) with the goal to study candidate air interfaces for future (4<sup>th</sup> generation) mobile communication systems preparing a corresponding standardization phase. The study results on LDPC codes in combination with OFDM modulators have been presented at the IEEE 802.11n standardization group; they are currently under consideration for implementation in the standard [31, 32].

Finally, conclusions are drawn on the future research topics in connection with this work. Note that all chapters start with a definition of symbols in order to facilitate the lecture of this thesis, in particular for readers who wish to read selected chapters only.

**Keywords:** Cyclic Prefix Orthogonal Frequency Division Multiplexing (CP-OFDM), FFT equalization, Frequency Synchronization, Low-Density Parity Check (LDPC) codes, Minimum Mean Square Error, Pseudo Random Postfix Orthogonal Frequency Division Multiplexing (PRP-OFDM), Time Synchronization, Zero Padded Orthogonal Frequency Division Multiplexing (ZP-OFDM).

## Résumé en français

Dans le contexte de cette thèse, un nouveau schéma de modulation est proposé en introduisant une séquence déterministe pondérée par un scalaire pseudo aléatoire: **Pseudo Random Postfix OFDM (PRP-OFDM)**. Il est proposé de remplacer l'extension cyclique du Cyclic Prefix OFDM (CP-OFDM) classique par un postfixe connu à l'émetteur et au récepteur [1–26].

Grâce à la nature déterministe de cette séquence, le récepteur peut exploiter sa connaissance afin d'estimer la réponse impulsionnelle du canal de propagation par une approche semi-aveugle d'ordre un. Ceci permet d'éviter l'introduction des séquences d'apprentissage ou des symboles pilotes. L'efficacité spectrale du système est donc améliorée par rapport à des architectures classiques comme le CP-OFDM, Zero-Padded OFDM (ZP-OFDM), etc. Par la suite, plusieurs algorithmes sont proposés. Ceux-ci permettent d'effectuer une estimation du canal dans un contexte statique et dans un contexte de mobilité. En delà, la dérivation d'une séquence de postfixe optimisée est présentée.

Ensuite, les études sont étendues à un raffinement de la synchronisation temporelle et fréquentielle d'une estimation initiale approximative. Après, une utilisation optimale des codes LDPC (Low Density Parity Check) est discutée dans le contexte de l'OFDM: il est montré comment il faut attribuer des mots de codes LDPC à des porteuses OFDM en prenant en compte une connaissance préalable du canal de propagation à l'émetteur.

Le schéma de modulation PRP-OFDM est une de plusieurs propositions dans le contexte du projet européen IST-BroadWay [14–20, 29] et plus récemment par IST-WINNER [21–24, 30]: IST-WINNER est un projet IP (Integrated Project) du 6ème framework qui cible l'étude des systèmes candidats pour la prochaine génération de la communication sans file (4ème génération). Concernant l'optimisation des codes LDPC pour une utilisation avec l'OFDM, les résultats de cette thèse ont été présentés à la standardisation de IEEE802.11n; ils sont actuellement en considération pour l'adoption dans la norme [31, 32].

Efin, le dernier chapitre présente les conclusions des travaux de recherche de cette thèse, ainsi que de futurs axes de recherche.

**Mots clés:** Cyclic Prefix Orthogonal Frequency Division Multiplexing (CP-OFDM), FFT equalization, Frequency Synchronization, Low-Density Parity Check (LDPC) codes, Minimum Mean Square Error, Pseudo Random Postfix Orthogonal Frequency Division Multiplexing (PRP-OFDM), Time Synchronization, Zero Padded Orthogonal Frequency Division Multiplexing (ZP-OFDM).

## Résumé étendu en français

La théorie des communications numériques connaît actuellement une nouvelle phase d'application: des progrès récents dans la technologie des semi-conducteurs permettent l'utilisation des algorithmes puissants, mais complexes dans le cadre des produits de large échelle. Par exemple, la future génération des réseaux locaux sans fils (WLAN) proposera un débit élevé de 500Mbps et en delà de la couche MAC (Medium Access Control); ce système est en phase de normalisation sous l'acronyme IEEE802.11n [31, 32]. Afin d'arriver à des performances élevées, IEEE802.11n s'appuie sur la modulation CP-OFDM (*Cyclic Prefix Orthogonal Frequency Division Multiplexing*) en combinaison avec des techniques d'antennes multiples à l'émetteur et au récepteur (*Multiple Transmit Multiple Receive (MTMR)* antennes): le multiplexage spatial (*Spatial Division Multiplexing (SDM)*) est normalisé au niveau de l'émetteur; un décodage efficace nécessite l'implémentation des schémas à moindres carrés (*Minimum Mean Square Error (MMSE)*) ou à maximisation de vraisemblance (*Maximum Likelihood (ML)*). La robustesse d'un lien point à point est améliorée en définissant des schémas d'adaptation au canal (*TX beamforming*) basés sur une décomposition en valeurs singulières (*Singular Value Decomposition (SVD)*) du canal de propagation. Le dernier est disponible grâce à un retour explicite par le récepteur. Concernant le codage de canal, l'évolution actuelle tend vers l'utilisation des codes LDPC (*Low Density Parity Check codes*). Ces codes améliorent les performances du système d'environ 2dB à 3dB par rapport à des codes convolutifs classiques. Les bases théoriques de ces schémas sont pour la plupart connues et publiées; en revanche, il a y de nombreux aspects pratiques qui restent à étudier. En particulier, une utilisation conjointe des schémas nommées ci-dessus nécessite toujours une évaluation détaillée.

Cette thèse présente les aspects pratiques suivants qui peuvent servir à améliorer des systèmes de communication numérique comme celui cité ci-dessus: une modification du CP-OFDM classique est proposée; ceci permet au récepteur d'effectuer une estimation ou mise à jour de l'estimation du canal de propagation semi aveugle d'ordre un: **Pseudo Random Postfix OFDM (PRP-OFDM)** [1–26]. En conséquence, l'OFDM devient utilisable dans un contexte de mobilité élevée (une vitesse de 72m/s à une fréquence porteuse de 5GHz est considéré dans le cadre de ce document) sans avoir besoin des séquences d'apprentissage ou des symboles pilotes. Cette propriété aide à améliorer l'efficacité spectrale du système. A cet effet, plusieurs algorithmes sont proposés, avec des différences en terme de qualité d'estimation et latence. Le dernier chapitre s'intéresse à une optimisation conjointe des codes LDPC en combinaison avec les propriétés d'un système OFDM dans le contexte d'un canal sélectif en fréquence.

Dans la suite, un compte rendu des chapitres du rapport de thèse est présenté:

### Orthogonal Frequency Division Multiplexing

Le chapitre 2 introduit une définition de l'OFDM en temps continu basée respectivement sur un schéma de bancs de filtres - CP-OFDM, Zero Padded OFDM (ZP-OFDM) et PRP-OFDM. Le modulateur du PRP-OFDM comprend une transformation de Fourier inverse comme le CP-OFDM classique; cette opération est suivie de l'ajout du postfixe pondéré par un scalaire complexe pseudo aléatoire de moyenne zéro, préférablement de module un. Le postfixe est composé d'une séquence prédéfinie, typiquement d'après les critères suivants: facteur de crête, radiation hors-bande et homogénéité du signal in-bande (voir chapitre 4). Fig. 1 illustre la définition du CP-OFDM, Fig. 2 la définition du ZP-OFDM et Fig. 3 la définition du PRP-OFDM.

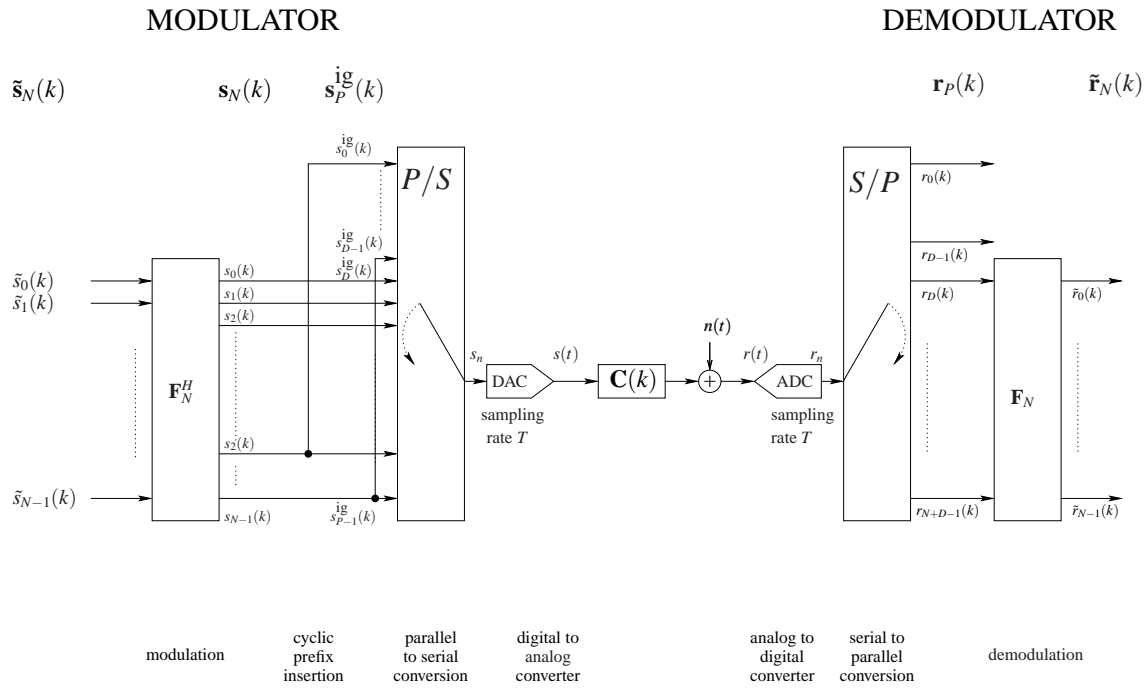


Figure 1: Modèle discret du modulateur CP-OFDM.

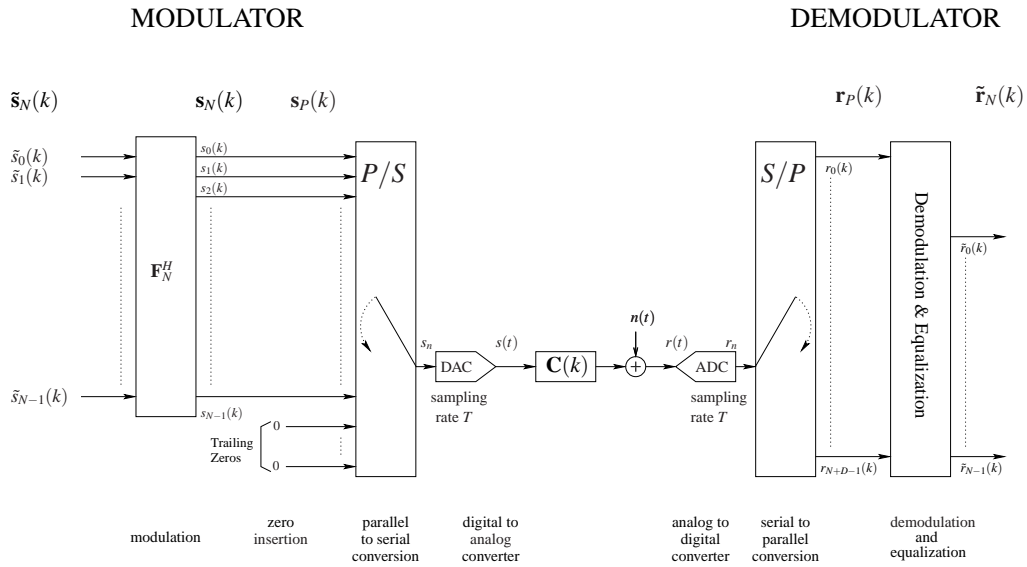


Figure 2: Modèle discret du modulateur ZP-OFDM.

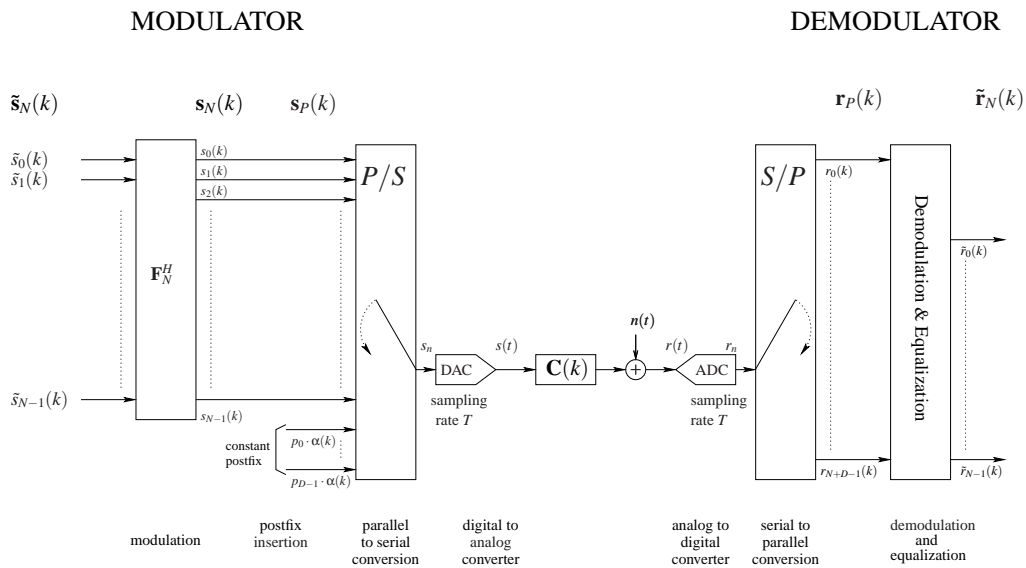


Figure 3: Modèle discret du modulateur PRP-OFDM.

Il est ensuite expliqué comment PRP-OFDM arrive à avoir des propriétés semblables au CP-OFDM dans un contexte de propagation à chemins multiples:

- la séquence du postfixe pseudo-aléatoire prend un rôle similaire à l'intervalle de garde de CP-OFDM en évitant toute interférence entre des blocs.
- l'extension cyclique qui est introduite dans le cadre du CP-OFDM sert à rendre circulante la convolution avec le canal de propagation; puisque la matrice de convolution correspondante est diagonalisée dans une base de Fourier, la convolution du canal se traduit par une pondération de chaque porteuse par un coefficient distinct. Ce chapitre démontre une propriété proche de cette diagonalisation dans une base de Fourier dans le contexte du PRP-OFDM: on démontre que la convolution du canal n'est pas circulante, mais pseudo-circulante, c'est-à-dire que la matrice de convolution est circulante avec une pondération de la partie triangulaire supérieure par une constante qui dépend de la pondération pseudo-aléatoire des séquences des postfixes. On démontre alors que la matrice de convolution de canal est diagonalisée sur une nouvelle base similaire à la base de Fourier observée dans le contexte du CP-OFDM.

Ensuite, le modulateur PRP-OFDM est comparé au modulateur ZP-OFDM. Ceci s'explique par le fait que le chapitre 3 démontre que le PRP-OFDM possède aussi les avantages du ZP-OFDM. En particulier, il est possible de récupérer les symboles des données même en présence d'un gain nul de porteuses du canal de propagation.

Il est ensuite démontré qu'un décalage de synchronisation temporel limité est bien absorbé par la séquence du postfixe, comme c'est le cas pour l'intervalle de garde du CP-OFDM. Les effets d'une erreur de synchronisation fréquentielle sont également discutées et il est montré comment le PRP-OFDM fonctionne dans un contexte de offsets de synchronisation limités.

Pour donner un exemple d'un système OFDM avancé, nous choisissons de citer et de détailler la proposition *MITMOT* [33–36] à la standardisation IEEE802.11n: celle-ci présente un système CP-OFDM MTMR avec un nombre d'antennes inférieur ou égale à quatre au niveau de l'émetteur; le débit maximal monte jusqu'à 180Mbps (360Mbps) pour une largeur de bande de 20MHz (40MHz) et une constellation MAQ-64. Une application d'un modulateur PRP-OFDM peut-être envisagée pour un tel système dans

le contexte de mobilité pour un schéma mono-antenne et multi-antennes. En particulier, les propositions de MITMOT concernant des modes asymétriques sont compatibles avec le PRP-OFDM: un schéma de codage spatio-temporel est proposé. Celui-ci permet d'implémenter un nombre d'antennes différent au niveau de l'émetteur et récepteur. Ceci est particulièrement utile dans un contexte de téléphonie mobile où le mobile est supposé être équipé avec moins d'antennes par rapport au point d'accès.

### Pseudo Random Postfix OFDM: estimation de canal et égalisation

Le chapitre 3 continue l'étude d'un système PRP-OFDM basé sur le schéma de modulation proposé précédemment. En particulier, le chapitre explique comment les symboles de données de l'OFDM peuvent être vus comme du bruit Gaussien dans le domaine temporel qui s'ajoute au bruit thermique. En supposant un canal de propagation statique, ceci permet d'extraire la séquence du postfixe convolué par le canal de propagation en effectuant un moyennage sur une multitude de séquences, précédé par une multiplication par l'inverse des scalaires de pondération pseudo aléatoires qui sont connus au récepteur. La réponse impulsionnelle du canal est ensuite déterminée par une dé-convolution en forçage à zéro (*Zero Forcing (ZF)*) ou à moindres carrés (*Minimum Mean Square Error (MMSE)*). Puisqu'il est souvent utile d'introduire un postfixe qui possède des contributions spectrales près de zéro dans la partie hors-bande, un schéma d'estimation de canal gardant la partie d'interférence intra-symbole et la partie interférence entre-bloques séparée. En exprimant la convolution canal-postfix par une matrice circulante contenant des coefficients du postfix, cette opération permet d'améliorer le conditionnement de la matrice. En conséquence, l'amplification du bruit est limitée.

Afin de pouvoir effectuer l'estimation du canal de propagation dans un contexte de mobilité, il est d'abord constaté que le modèle d'évolution du canal et ses approximations inhérentes jouent un rôle important. La littérature propose souvent un schéma auto-régressif d'ordre un pour modéliser des corrélations du canal en fonction du temps. Nous montrons que cette approximation implique une forte limitation des performances du système à mobilité élevée; à la place, un filtrage de Wiener nécessitant aucune simplification est utilisé. La performance de l'estimation dépend finalement de la fréquence de Doppler et des contraintes sur la latence maximale de décodage. Des exemples démontrent l'application des algorithmes proposés dans un contexte des réseaux locaux sans fils à 5GHz jusqu'à une mobilité de 72m/s. En delà de ces considérations, le récepteur peut choisir entre un niveau de latence d'estimation du canal et l'erreur moyenne quadratique des estimations. Le schéma à latence minimale est illustrée dans la suite :

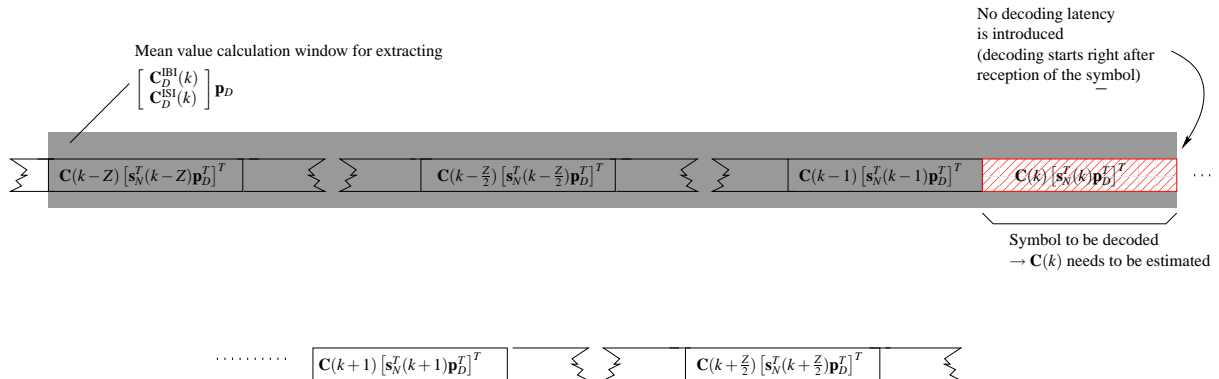


Figure 4: Estimation du canal à latence minimale.

Le schéma à l'erreur moyenne quadratique minimale est présenté dans la Fig. 5 :

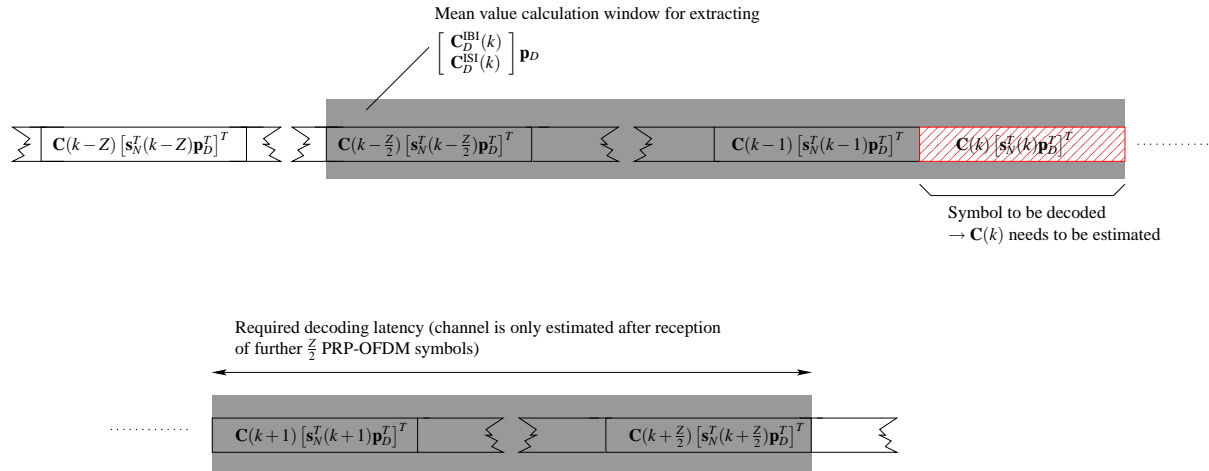


Figure 5: Estimation du canal à erreur moyenne quadratique minimale.

La performance de l'égalisation d'un signal PRP-OFDM au niveau du récepteur dépend de sa complexité en terme de puissance de calcul. Une architecture simple est proposée basée sur l'algorithme *Overlap-Add (OLA)*. Les performances du système en terme de *Bit Error Rate (BER)* et *Packet Error Rate (PER)* sont ensuite semblables à celles de CP-OFDM. Le coût de l'utilisation du PRP-OFDM est environ de l'ordre de grandeur de 16% en complexité arithmétique pour l'égalisation, ce qui permet d'effectuer le raffinement de l'estimation du canal comme présenté ci-dessus. Un gain d'environ 1dB à 1.5dB peut-être obtenu en s'appuyant sur des schémas d'égalisation à moindres carrés (*MMSE*). Les figures Fig.6 à Fig.10 illustrent des résultats de simulation en terme de BER (probabilité d'erreur de bits) et PER (probabilité d'erreur de trames) obtenus dans le contexte d'un canal BRAN-A [37] et pour des constellations QPSK et MAQ-16. Une trame se compose ici de 72 symboles OFDM.

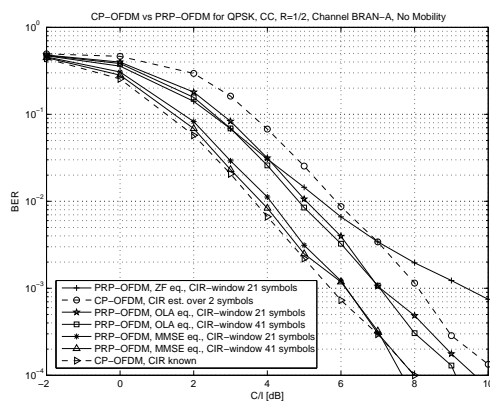


Figure 6: BER pour IEEE802.11a, BRAN canal

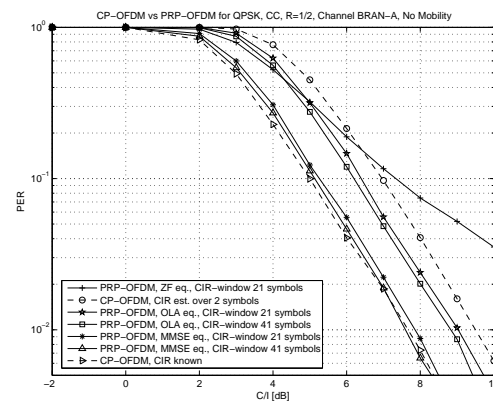


Figure 7: PER pour IEEE802.11a, BRAN canal A, QPSK.

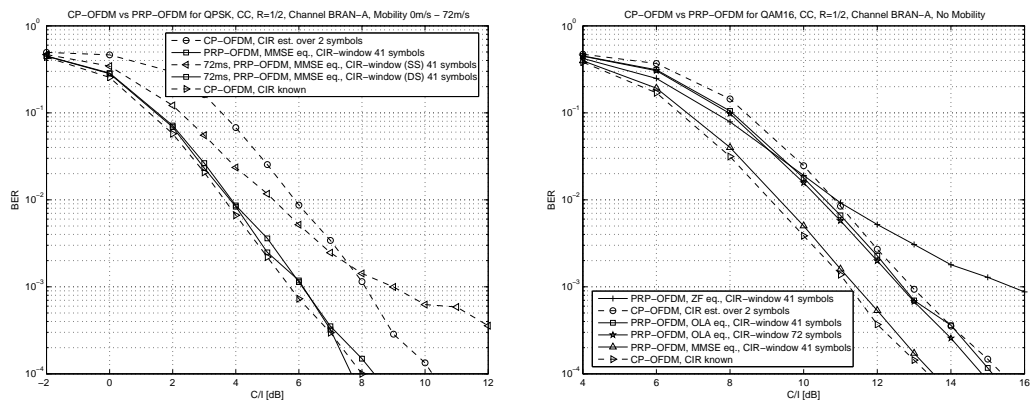


Figure 8: BER pour IEEE802.11a, BRAN canal Figure 9: BER pour IEEE802.11a, BRAN canal A, QPSK.

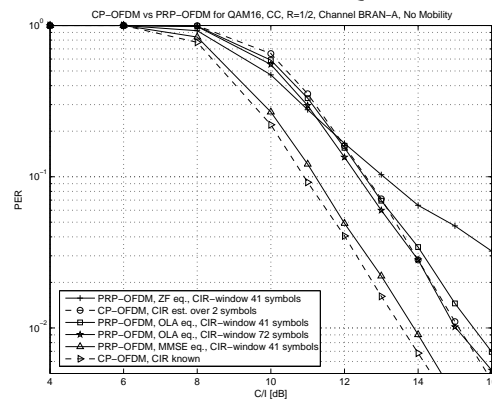


Figure 10: PER pour IEEE802.11a, BRAN canal A, MAQ-16.

## Pseudo Random Postfix OFDM: Conception du Postfix

Les chapitres présentés ci-dessus détaillent l'estimation du canal de propagation en exploitant la présence d'une séquence de postfixe à la suite de chaque symbole OFDM. Le chapitre 4 s'intéresse aux méthodes qui permettent de trouver une telle séquence en fonction de plusieurs critères. Dans le cadre de cette thèse, nous nous limitons à l'ensemble des critères suivants:

- minimisation du facteur de crête du signal temporel (*Peak-to-Average-Power-Ratio (PAPR)*).
- minimisation de la radiation hors-bande en concentrant l'énergie du signal sur des porteuses utiles.
- minimisation de l'ondulation du signal intra-bande, afin d'assurer une qualité d'estimation du canal de propagation qui est homogène sur tous les porteuses du système.
- toute cyclo-stationnarité est évitée en introduisant des scalaires de pondération pseudo-aléatoire de moyenne zéro.

Les séquences sont trouvées en exprimant chaque critère par une fonction de coût. Une fonction de coût globale est en suite définie par simple addition des fonctions par critère, pondérées par un scalaire :

- $\gamma^{\text{Flat}} J^{\text{Flat}}(\mathbf{p}_D)$  avec  $\gamma^{\text{Flat}} \in \mathbb{R}, J^{\text{Flat}}(\mathbf{p}_D) \in \mathbb{R}$  pour forcer le signal à être le plus plat possible dans la partie in-bande;
- $\gamma^{\text{Out}} J^{\text{Out}}(\mathbf{p}_D)$  avec  $\gamma^{\text{Out}} \in \mathbb{R}, J^{\text{Out}}(\mathbf{p}_D) \in \mathbb{R}$  pour minimiser la radiation hors-bande;
- $\gamma^{\text{Clip}} J^{\text{Clip}}(\mathbf{p}_D)$  avec  $\gamma^{\text{Clip}} \in \mathbb{R}, J^{\text{Clip}}(\mathbf{p}_D) \in \mathbb{R}$  pour minimiser le facteur crête.

La fonction de coût résultante est donc:

$$J^{\text{Tot}} := \gamma^{\text{Flat}} J^{\text{Flat}}(\mathbf{p}_D) + \gamma^{\text{Out}} J^{\text{Out}}(\mathbf{p}_D) + \gamma^{\text{Clip}} J^{\text{Clip}}(\mathbf{p}_D).$$

Nous proposons d'effectuer la recherche en utilisant un schéma itérative de gradient. Pour ce but, les dérivés de chaque fonction de coût sont proposées.

Finalement, des exemples sont donnés adaptés à un contexte des réseaux locaux sans fils comme l'IEEE802.11n: des séquences de longueur  $D = 16$ ,  $D = 32$  et  $D = 48$  échantillons sont présentées. Ces résultats sont comparés à des fenêtres de *Kaiser*, qui ont des meilleurs propriétés spectrales; en revanche, les séquences souffrent d'un facteur de crête temporel souvent très élevé. Dans le cas du postfixe de longueur  $D = 32$  échantillons, par exemple, la fenêtre de *Kaiser* est caractérisée par un facteur de crête temporel de  $14.443dB$  et la séquence optimisée par la technique proposée dans ce chapitre est de  $6.762dB$ .

Ci-dessous, des résultats d'optimisation de postfixes sont présentés.

Paramètres	fenêtre de Kaiser	PAPR opt. Postfix
PAPR $\frac{\ \mathbf{p}_D\ _{\infty}^2}{\frac{1}{D} \sum_{n=0}^{D-1}  p_n ^2}$	11.548dB	7.489dB
Radiation hors-bande $\frac{\sum_{n=0}^{N-1}  p_n^f ^2}{\sum_{n=0}^{N-1}  p_n^f ^2}, \mathbf{p}^f = \mathbf{F}_N \begin{bmatrix} \mathbf{p}_D \\ \mathbf{0}_{N-D,1} \end{bmatrix}$	-16.33dB	-12.581dB
Ripple in-bande calculé sur porteuses $C^2 = C \setminus \{21, \dots, 27, 39, \dots, 45\}$ (i.e. transition au stop-bande non prise en compte)	0.025dB	0.742dB

Table 1: Analyse des postfixes (16 échantillons postfix).

Paramètres	fenêtre de Kaiser	PAPR opt. Postfix
PAPR $\frac{\ \mathbf{p}_D\ _\infty^2}{\frac{1}{D} \sum_{n=0}^{D-1}  p_n ^2}$	14.443dB	6.7626dB
Radiation hors-bande $\frac{\sum_{n=0}^{N-1}  p_n^f ^2}{\sum_{n=0}^{N-1}  p_n^f ^2}, \mathbf{p}^f = \mathbf{F}_N \begin{bmatrix} \mathbf{p}_D \\ \mathbf{0}_{N-D,1} \end{bmatrix}$	-16.719dB	-31.501dB
Ripple in-bande calculé sur porteuses $C^2 = C \setminus \{21, \dots, 27, 39, \dots, 45\}$ (i.e. transition au stop-bande non prise en compte)	0.0252dB	1.986dB

Table 2: Analyse des postfixes (32 échantillons postfix).

Paramètres	fenêtre de Kaiser	PAPR opt. Postfix
PAPR $\frac{\ \mathbf{p}_D\ _\infty^2}{\frac{1}{D} \sum_{n=0}^{D-1}  p_n ^2}$	16.174dB	7.691dB
Radiation hors-bande $\frac{\sum_{n=0}^{N-1}  p_n^f ^2}{\sum_{n=0}^{N-1}  p_n^f ^2}, \mathbf{p}^f = \mathbf{F}_N \begin{bmatrix} \mathbf{p}_D \\ \mathbf{0}_{N-D,1} \end{bmatrix}$	-16.153dB	-39.715dB
Ripple in-bande calculé sur porteuses $C^2 = C \setminus \{21, \dots, 27, 39, \dots, 45\}$ (i.e. transition au stop-band non prise en compte)	0.017dB	0.000176dB

Table 3: Analyse des postfixes (48 échantillons postfix).

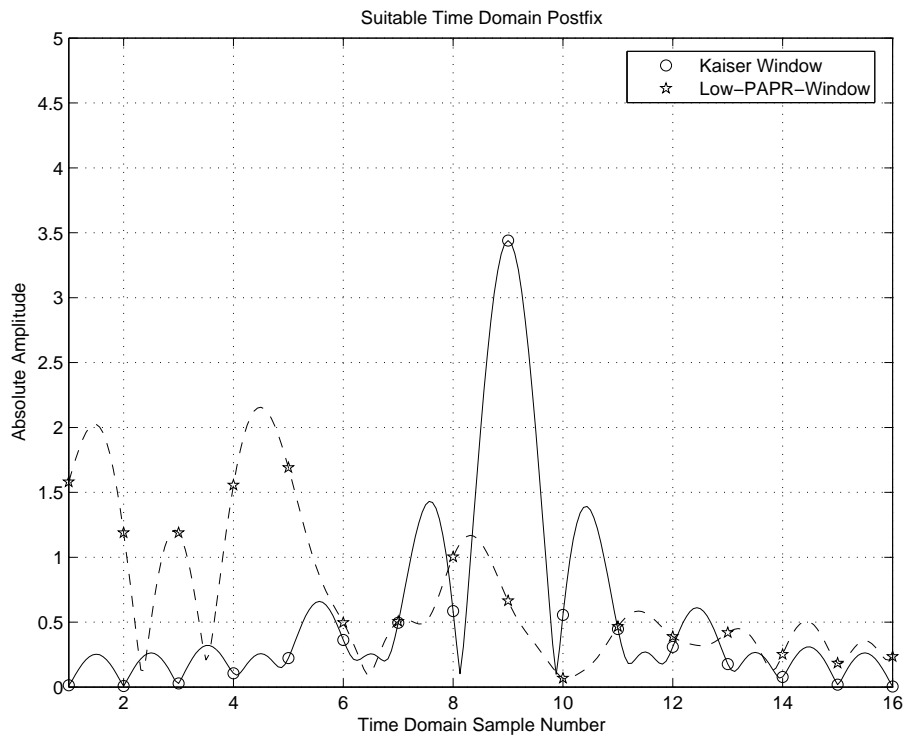


Figure 11: Différents postfixes en domaine temporel (16 échantillons).

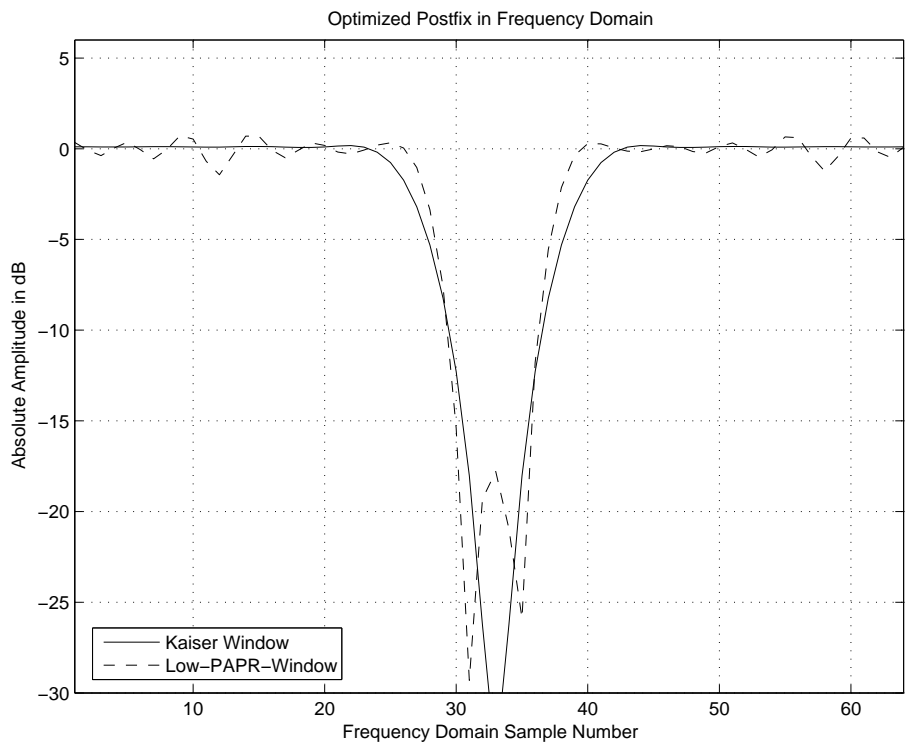


Figure 12: Différents postfixes en domaine fréquentiel (16 échantillons).

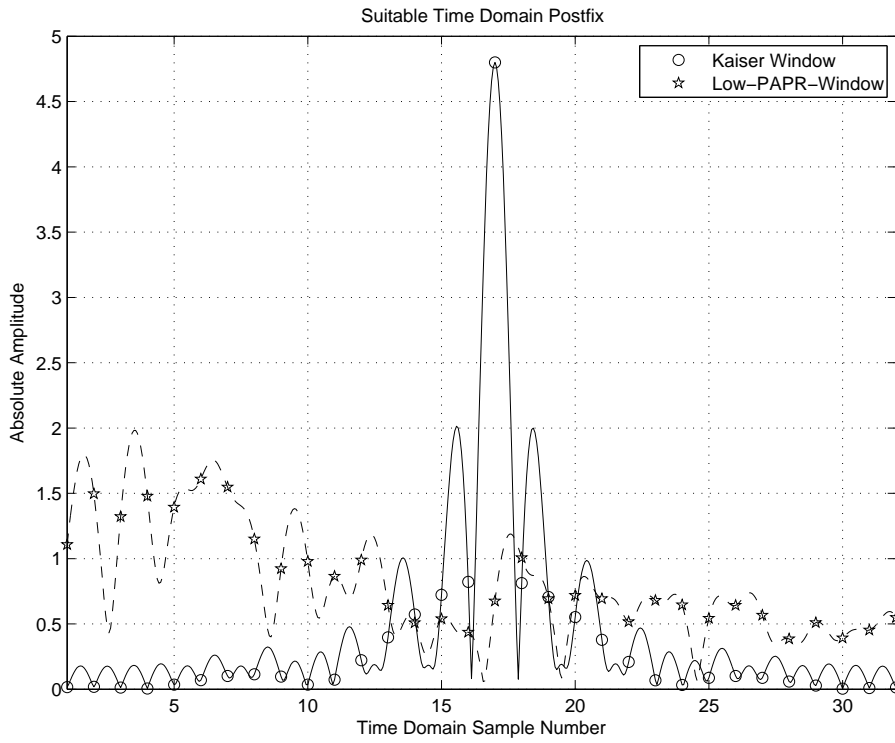


Figure 13: Différents postfixes en domaine temporel (32 échantillons).

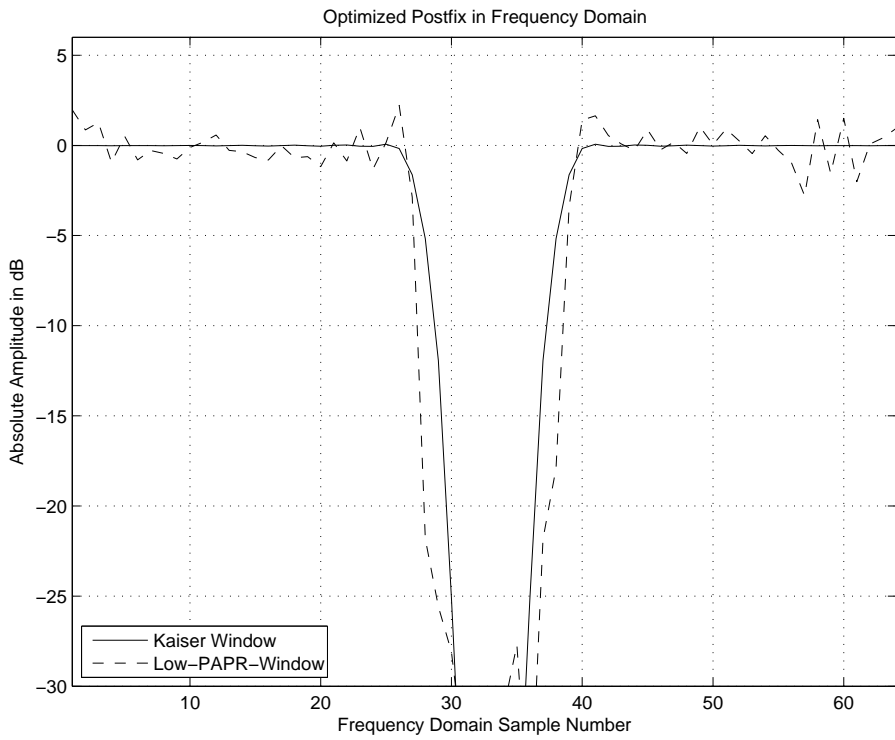


Figure 14: Différents postfixes en domaine fréquentiel (32 échantillons).

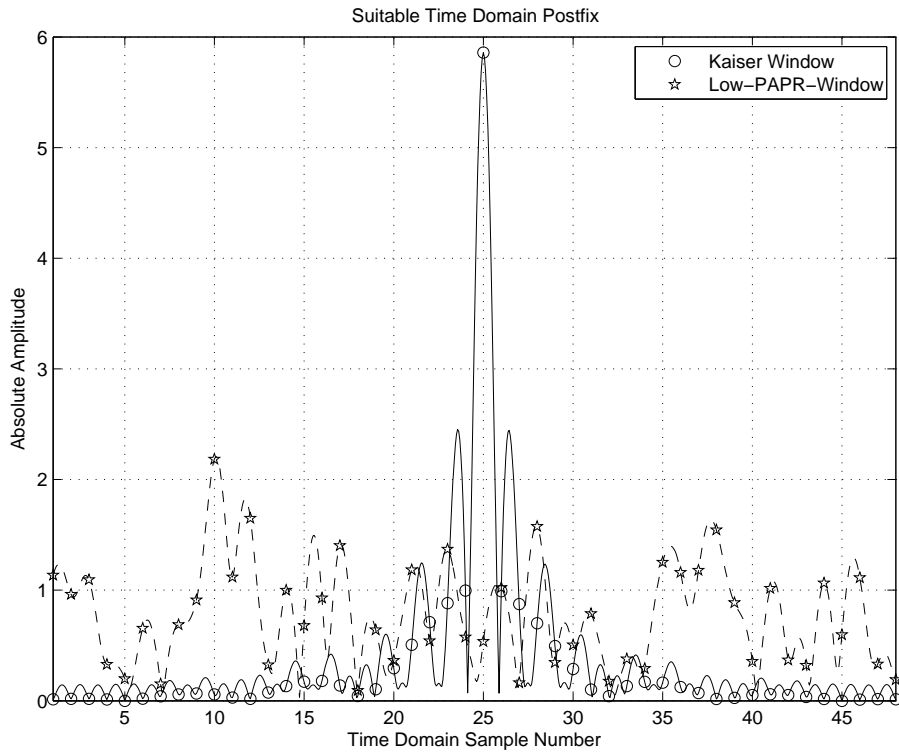


Figure 15: Différents postfixes en domaine temporel (48 échantillons).

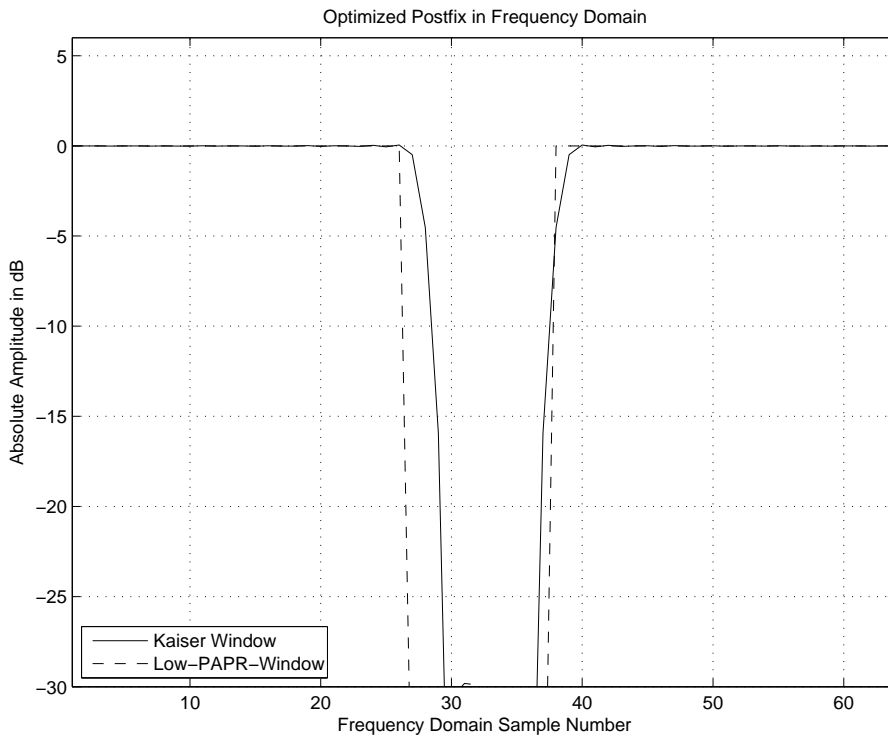


Figure 16: Différents postfixes en domaine fréquentiel (48 échantillons).

## Raffinement de la synchronisation pour le Pseudo Random Postfix OFDM

Le chapitre 5 s'intéresse à la question suivante: est-ce que le récepteur peut exploiter sa connaissance sur les séquences de postfixes pour améliorer une synchronisation temporelle et fréquentielle initiale. Cette estimation initiale n'est pas étudiée dans le cadre de ce chapitre et peut être effectuée, par exemple, sur une séquence d'apprentissage à l'entête de chaque trame. Ces techniques sont détaillées, entre autres, dans [38].

L'amélioration de la synchronisation temporelle permet de mieux utiliser le postfixe afin d'éviter une interférence entre bloques au niveau du récepteur: dans le cas optimale, la fenêtre d'observations à l'entrée de la transformation de Fourier ne contient que des échantillons d'un seul symbole OFDM. Avec une réponse impulsionnelle d'un canal assez longue, la marge d'erreur décroît. La synchronisation fréquentielle, en revanche, est importante afin d'éviter des interférences entre porteuses OFDM (interférence intra symbole).

Ce chapitre présente un algorithme de raffinement de la synchronisation temporelle basé sur une corrélation avec la séquence du postfixe, précédée par une pondération par l'inverse du scalaire pseudo-aléatoire de chaque postfixe. L'algorithme est optimal dans le sens de la maximisation de vraisemblance dans un contexte de bruit blanc Gaussien additive (*Additive White Gaussian Noise (AWGN)*). Les résultats de simulations montrent que ce schéma donne aussi des performances améliorées pour des canaux à trajets multiples sans connaissance préalable du canal au récepteur, mais la technique est sous-optimale. Dans l'exemple des réseaux locaux sans fils (IEEE802.11a) et d'un canal BRAN-A (*50ns rms delay spread*), des simulations montrent qu'un algorithme de référence de synchronisation temporelle donne une incertitude sur le début de la trame dans l'intervalle  $[-5; 5]$  échantillons (en ne prenant en compte que des échantillons des décalages de synchronisation temporelle qui apparaissent avec une probabilité supérieure à  $10^{-3}$ ). Le raffinement basé sur le PRP-OFDM permet d'améliorer ces résultats dans le contexte donné l'intervalle  $[-1;4]$  échantillons environ.

La synchronisation fréquentielle est raffinée en exploitant le fait qu'un décalage fréquentiel conduit à la présence d'une phase linéaire dans le signal temporel. Cette phase, et finalement le décalage fréquentiel, est estimée par une auto-corrélation. Des résultats de simulation montrent que dans le scénario donné l'ecart-type s'approche de zéro en moyennant sur environ 20 postfixes et à partir d'un rapport de signal à bruit d'environ 10dB. Pour un contexte d'une variance de bruit plus élevée, la fenêtre de moyennage doit évidemment être agrandie.

Pour le scénario d'une présence jointe d'un décalage temporel et fréquentiel, il est proposé d'effectuer d'abord le raffinement temporel. On montre que la présence d'une phase linéaire en temps ne dégrade que le rapport de signal à bruit des sorties du corrélateur. Ensuite, ce résultat est utilisé pour estimer le décalage fréquentiel.

## Pseudo Random Postfix Orthogonal Frequency Division Multiplexing pour des systèmes à antennes multiples

Le chapitre 6 étend l'étude PRP-OFDM au contexte d'antennes multiples au niveau de l'émetteur et du récepteur (*Multiple Transmit Multiple Receive (MTMR) antennas*). L'enjeu consiste maintenant à mettre en œuvre l'estimation des tous les canaux de propagation entre toutes les antennes d'émission et toutes les antennes de réception. Il est important de noter que ce problème est indépendant du schéma de codage spatial et temporel. Les résultats de ce chapitre seront donc applicables à tout choix d'un tel code.

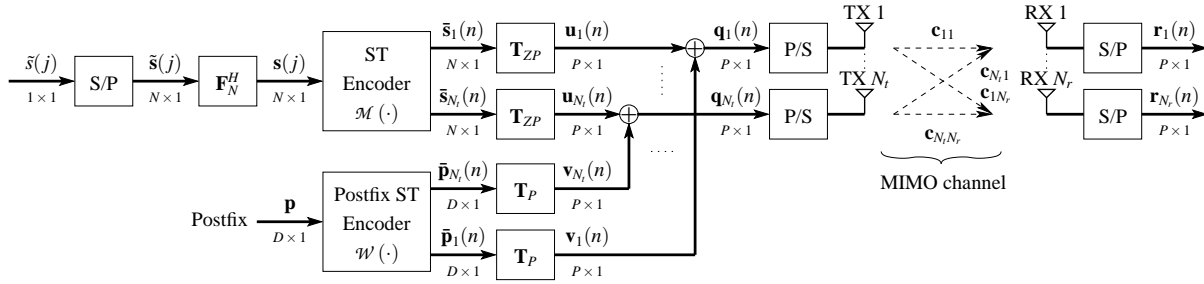


Figure 17: Modèle discret du modulateur MTMR PRP-OFDM.

L'idée consiste à introduire un seul scalaire de pondération pseudo-aléatoire pour un sous-ensemble de postfixes. Par la suite, chaque élément d'un sous-ensemble est pondéré par un nouveau facteur qui représente un élément d'une matrice unitaire et orthogonale, par exemple d'une matrice de Walsh-Hadamard ou d'une matrice de Fourier. Ceci permet d'extraire l'ensemble des différents canaux, appelé généralement canal à entrées et sorties multiples (*Multiple Input Multiple Output (MIMO) channel*). Les symboles des données ainsi que le bruit thermique sont traités comme du bruit Gaussien dont la variance est réduite en moyennant sur de nombreux blocs.

Deux exemples spécifiques sont donnés pour la mise en place d'un modulateur et démodulateur PRP-OFDM. La première proposition permet un décodage efficace en exploitant les propriétés des matrices pseudo-circulantes. Le deuxième cas nécessite une transformation du signal PRP-OFDM en ZP-OFDM au niveau du récepteur. Ensuite, des algorithmes d'égalisation ZP-OFDM peuvent être utilisés tels qu'ils sont disponibles dans la littérature [39, 40]. Dans l'exemple d'un contexte réseaux locaux sans fils, des résultats de simulation montrent qu'un récepteur MTMR PRP-OFDM avec deux antennes à l'émission et une antenne pour la réception permet d'obtenir une amélioration des performances d'environ 1.5dB par rapport au CP-OFDM classique pour des modulations BPSK, QPSK, MAQ-16 et MAQ-64. Dans un contexte de mobilité, des estimateurs dérivés en chapitre 3 sont adaptés au contexte MTMR. Pour l'exemple d'une mobilité de 32m/s et une fréquence porteuse de 5GHz, des résultats proche du cas statique sont obtenus pour le PRP-OFDM pour des constellations d'ordre inférieur (environ 0.3dB de perte pour BPSK, environ 0.5dB de perte pour QPSK et environ 1.5dB de perte pour MAQ-16). Pour les constellations MAQ-64, les dégradations de performances deviennent importantes (environ 4dB de dégradation pour un BER de  $10^{-3}$ ). Les figures Fig.18 à Fig.21 illustrent des résultats de simulation en terme de BER (probabilité d'erreur de bits) et PER (probabilité d'erreur de trame) obtenus dans le contexte d'un canal BRAN-A [37] et pour des constellations QPSK et MAQ-16 et une configuration avec deux antennes au niveau de l'émetteur et une antenne au niveau du récepteur. Une trame se compose ici de 72 symboles OFDM.

Pour l'instant, le PRP-OFDM n'est pas appliqué dans une norme MIMO de type IEEE 802.11n. En revanche, il est envisageable de proposer ces schémas pour un contexte de mobilité élevée (voir discussion ci-dessus) et dans un contexte d'un grand nombre d'antennes. Un grand nombre d'antennes nécessite des préambules de taille importante et introduit donc un over-head non-négligeable; le PRP-OFDM peut donc contribuer à une amélioration de l'efficacité spectrale en proposant que les canaux de propagation soient estimés à partir des postfixes.

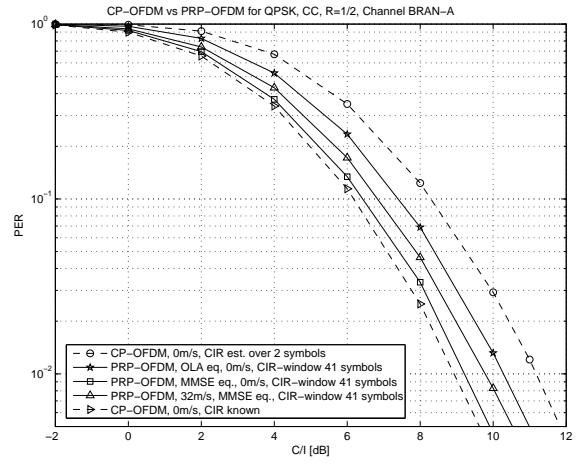
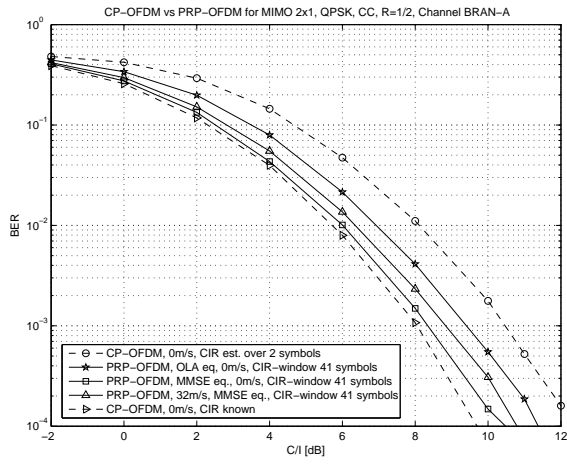


Figure 18: BER pour IEEE802.11a, MIMO 2x1, Figure 19: PER pour IEEE802.11a, MIMO 2x1, BRAN canal A, QPSK.

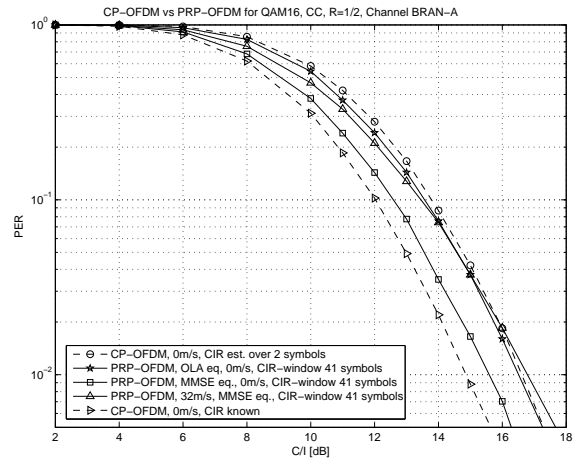
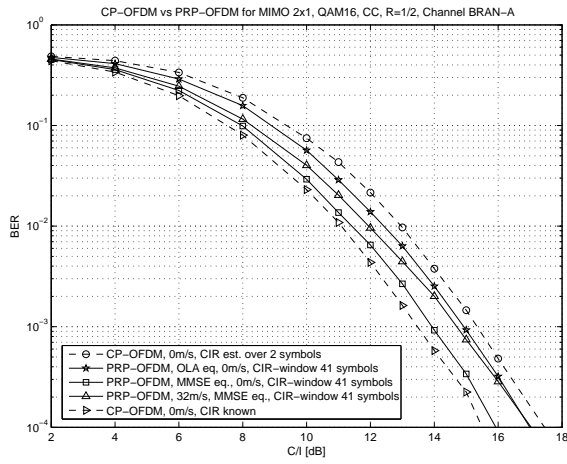


Figure 20: BER pour IEEE802.11a, MIMO 2x1, Figure 21: PER pour IEEE802.11a, MIMO 2x1, BRAN canal A, MAQ-16, Doppler.

## Suppression itérative d'interférence

Le chapitre 7 propose des moyens qui permettent d'améliorer les estimations du canal de propagation en supprimant une partie de l'interférence: l'idée consiste à décoder les données utiles en supposant qu'une première estimation (grossière) du canal est disponible. Ce décodage est supposé être effectué en utilisant un décodeur à sorties souples. Ensuite, ces données seront ré-encodées (en utilisant les sorties souples du décodeur), convoluées par l'estimation de la réponse impulsionnelle du canal et soustraites du signal reçu. Ensuite, le canal est estimé à nouveau en profitant du fait que l'interférence venant des symboles utiles est réduite ou (idéalement) supprimée.

Ce processus est illustré ci-dessous:

1. Estimation initiale de la reponse impulsionnelle du canal (CIR): à l'itération  $k = 0$ , effectuer une estimation initiale du canal de propagation  $\hat{\mathbf{c}}^0(i)$ , par exemple d'après l'algorithme proposé en section 7.3.1.
2. Incrémenter l'index d'itération:  $k \leftarrow k + 1$
3. Effectuer le décodage à sorties souples en utilisant la dernière estimation du canal  $\hat{\mathbf{c}}^{k-1}(i)$ : mémoriser les sorties du décodeur à sorties souples qui indiquent la probabilité d'erreur du  $l$ th bit décodé de la constellation sur porteuse  $n$  du symbole OFDM symbol  $i$ :  $p_l^k(x_n(i))$  avec  $n \in [0, \dots, N - 1]$  et  $l \in [0, \dots, \log_2(Q_M) - 1]$ ;  $Q_M$  est l'ordre de la constellation.
4. Estimation de l'interférence: comme détaillé en section 7.3.3, l'estimation de l'interférence  $\mathbf{u}_p^k(i)$  du symbole OFDM  $i$  est générée à partir des probabilités d'erreur  $p_l^k(x_n(i))$  et à partir des dernières estimations du canal  $\hat{\mathbf{c}}^{k-1}(i)$  comme indiqué par le théorème 7.3.1.
5. Suppression d'interférence: soustraire l'interférence estimée du vecteur reçu  $\mathbf{r}_p(i)$  et générer un nouveau vecteur d'observation:  $\bar{\mathbf{r}}_p^k(i) = \mathbf{r}_p(i) - \mathbf{u}_p^k(i)$ .
6. Estimation du canal: dériver une nouvelle estimation du canal  $\hat{\mathbf{c}}^k(i)$  à partir de  $\bar{\mathbf{r}}_p^k(i)$ , comme proposé par exemple dans la section 7.3.1. Le resultat  $\hat{\mathbf{c}}^k(i)$  montre typiquement une estimation plus exacte puisque l'interférence des symboles OFDM des données sur la séquence du postfixe a été réduite.
7. Itérer : autant que nécessaire.

Ce schéma peut être utilisée, entres autres, pour les applications pratiques suivantes:

- L'estimation du canal de propagation basée sur les postfixes PRP-OFDM devient utilisable dans le contexte des constellations d'ordre supérieure qui nécessitent un faible erreur sur les estimés. Il est possible d'effectuer une première estimation approximative du canal et ensuite un premier décodage qui conduit probablement à un niveau d'erreurs assez élevé. Après, l'interférence est calculée en prenant en compte les probabilités d'erreur des bits décodés et ce résultat permet d'améliorer l'estimation du canal dans l'étape suivante. Au bout de plusieurs itérations, des performances en PER du PRP-OFDM dépassent le CP-OFDM comme c'est montré par des simulations.
- Puisqu'il est possible de commencer un décodage itératif par des estimations grossières du canal de propagation à la première itération, cette technique permet de réduire la taille de la fenêtre d'observations qui est utilisée pour extraire la séquence du postfixe convoluée par le canal. Dans le cadre des constellations d'ordre inférieur (BPSK, QPSK), il est donc possible d'effectuer cette estimation dans un contexte de mobilité très élevée où une forte corrélation du canal ne peut être garantie que dans une telle petite fenêtre. Ceci permet donc d'améliorer la robustesse du système dans un contexte de mobilité.

Les résultats de simulations présentés ci-dessous qui illustrent l'évolution de l'erreur moyenne quadratique sur plusieurs itérations.

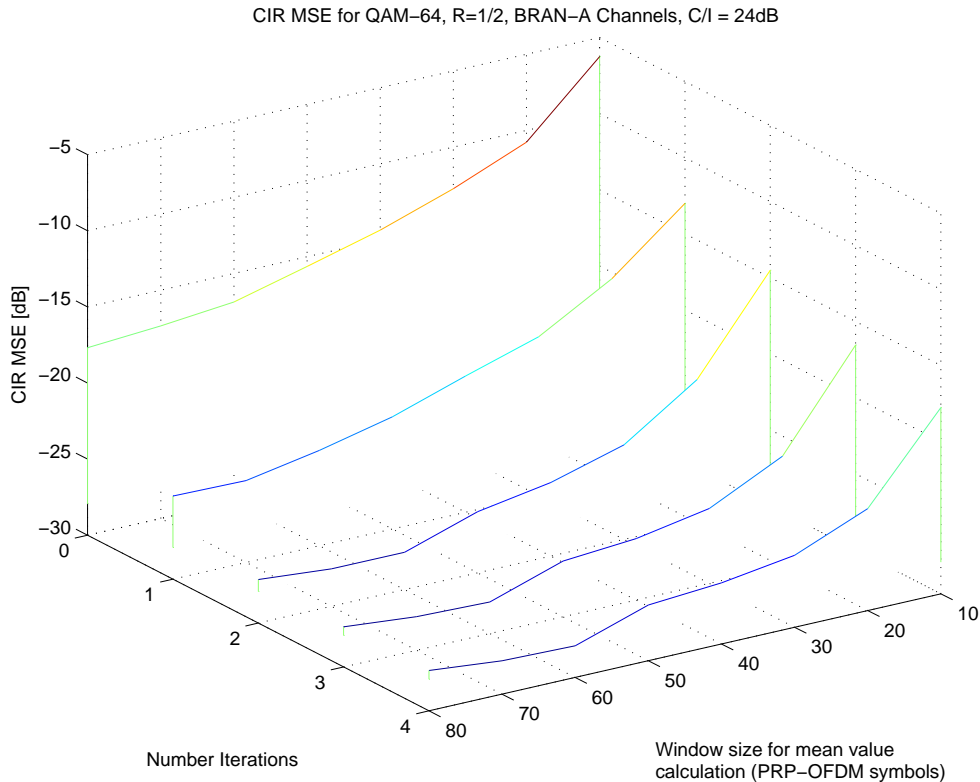


Figure 22: Erreur moyenne quadratique du CIR pour MAQ-64, BRAN-A, C/I=24dB.

### Codage Low Density Parity Check (LDPC) pour l'OFDM

Le chapitre 8 regarde les aspects de l'utilisation de l'OFDM dans un contexte pratique sous un angle différent. Puisque le problème de l'estimation du canal de propagation a été abordé dans des précédentes discussions, ce chapitre s'intéresse en particulier à une utilisation optimale des codes LDPC (*Low Density Parity Check*) en combinaison avec l'OFDM (PRP-OFDM, CP-OFDM, ZP-OFDM ou autre): dans des systèmes existants, l'attribution des mots de code LDPC aux porteuses OFDM est souvent linéaire (c'est-à-dire, il n'y a aucun algorithme d'adaptation). Il est démontré dans le contexte de cette thèse que les performances peuvent être améliorées d'environ 1.5dB en PER en appliquant un entrelacement optimisé en prenant en compte une connaissance du canal de propagation au niveau de l'émetteur. Cette connaissance peut être obtenue en pratique en exploitant la réciprocité du canal ou en utilisant des schémas de boucle fermée où le récepteur communique ses estimations de canal à l'émetteur. Cette étude se base sur des codes de taille infinie et sans cycles. Il est possible qu'une optimisation différente puisse donner de meilleurs résultats dans le contexte des codes utilisés en pratique, c'est-à-dire des codes de taille limitée et avec des cycles.

Une fois que la connaissance du canal est établie, un algorithme est proposé afin d'effectuer la recherche d'un entrelaceur. La complexité arithmétique de cet algorithme est très faible, puisqu'il consiste principalement en un triage du module des coefficients du canal en fréquence combiné avec un triage des degrés de nœud de variables du code LDPC.

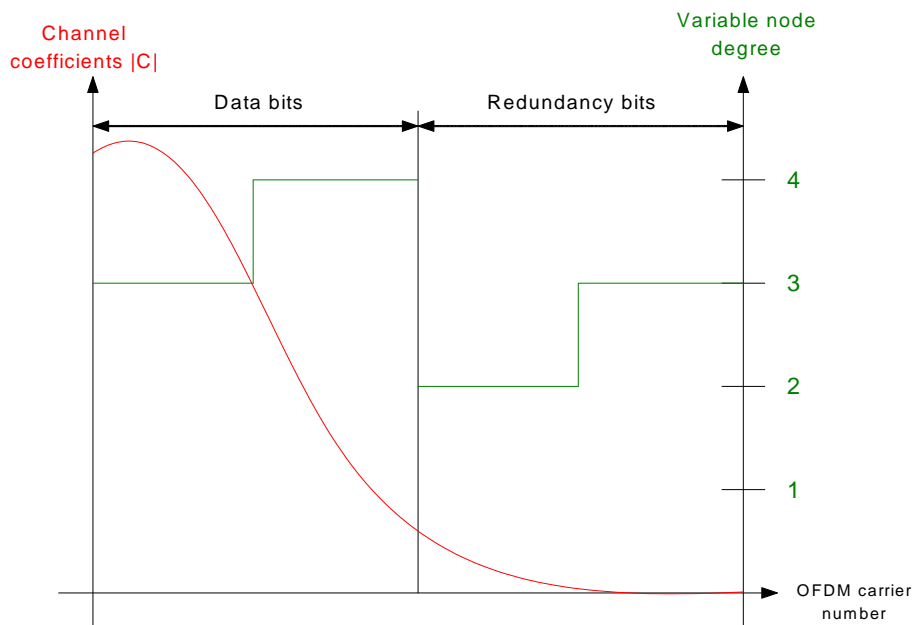


Figure 23: Exemple de l’optimisation du mapping des mots de code LDPC.

L’optimisation est effectuée en exploitant l’*approximation Gaussienne* connue de l’analyse théorique des codes LDPC. La littérature propose des outils qui permettent d’évaluer l’évolution des métriques pendant le codage itératif (en supposant un algorithme de *propagation de croyances*). Ces outils sont consultés afin de dériver des attributions optimales des bits des mots de code aux porteuses OFDM. Ensuite, une décomposition en série d’ordre deux est présentée afin de trouver un algorithme d’optimisation dans un contexte pratique où peu de degrés élevés de nœuds de variables existent.

Des résultats de simulations sont présentés pour le code LDPC proposé dans le contexte de la normalisation des réseaux locaux sans fils IEEE802.11n [41]. Nous choisissons une longueur de bloque de 576 bits et un canal de propagation à trajets multiples (BRAN-A [37]).

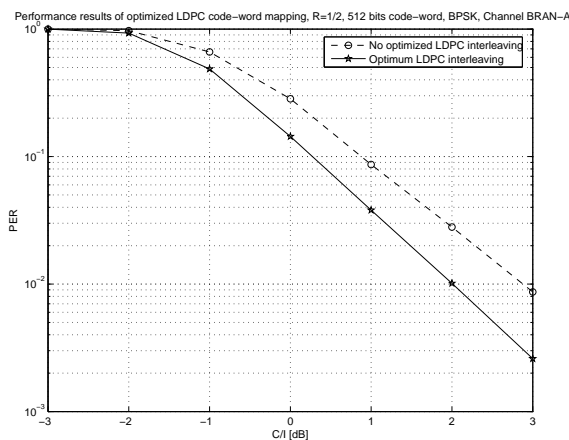
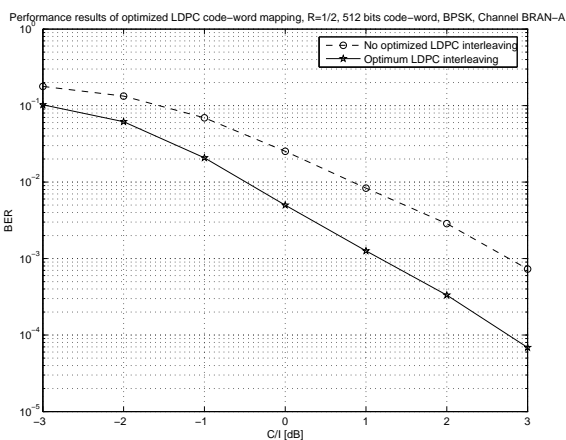


Figure 24: BER pour code LDPC après optimisation, Figure 25: PER pour code LDPC après optimisation, canal BRAN-A, 576 bits mot de code.

## Conclusion

Le chapitre 9 donne quelques conclusions et présente de futurs axes de recherche. Entre autres, les sujets suivants sont proposés:

- Etude d'architectures à faible complexité pour l'estimation du canal basée sur les postfixes PRP-OFDM.
- Etude d'architectures à faible complexité pour l'estimation du canal basée sur les postfixes PRP-OFDM en appliquant la suppression itérative d'interférence.
- Etude de l'influence du *power delay profile (PDP)* (et l'exactitude des estimations disponibles) sur l'estimation du canal.
- Etude LDPC: Prise en compte de connaissances sur des matrices LDPC à petite taille et en présence de cycles.

## Appendices

Les appendices présentent des outils et des démonstrations qui sont utilisés dans des chapitres principaux:

- L'appendice A présente une démonstration de diagonalisation des matrices pseudo-circulantes.

Proposition: La matrice  $\mathbf{C}_\alpha$  définie comme suit

$$\begin{aligned} \mathbf{C}_\alpha &:= \begin{bmatrix} c_0 & \alpha \cdot c_{N-1} & \alpha \cdot c_{N-2} & \rightarrow & \alpha \cdot c_1 \\ c_1 & c_0 & \alpha \cdot c_{N-1} & \rightarrow & \alpha \cdot c_2 \\ \downarrow & \searrow & \searrow & \searrow & \downarrow \\ c_{N-1} & \rightarrow & \rightarrow & \rightarrow & c_0 \end{bmatrix} \\ &= \mathbf{C}_{\text{ISI}} + \alpha \cdot \mathbf{C}_{\text{IBI}}, \end{aligned}$$

est diagonalisé comme indiquée ci-dessous:

$$\mathbf{C}_\alpha = \mathbf{V}_N^{-1} \text{diag} \left\{ C \left( \alpha^{-\frac{1}{N}} \right), \dots, C \left( \alpha^{-\frac{1}{N}} e^{j \frac{2\pi(N-1)}{N}} \right) \right\} \mathbf{V}_N$$

avec

$$\begin{aligned} \mathbf{V}_N &:= \left( \frac{1}{N} \sum_{n=0}^{N-1} |\alpha|^{-\frac{2n}{N}} \right)^{\frac{1}{2}} \mathbf{F}_N \text{diag} \left\{ 1, \dots, \alpha^{\frac{N-1}{N}} \right\}, \\ \mathbf{F}_N &:= \frac{1}{\sqrt{N}} \left( W_N^{ij} \right)_{0 \leq i < N, 0 \leq j < N}, W_N := e^{-j \frac{2\pi}{N}}, \\ C(z) &:= \sum_{n=0}^{N-1} c_n z^{-n} \text{ and } z, \alpha, c_0, \dots, c_{N-1} \in \mathbb{C}. \end{aligned}$$

- L'appendice B dérive des égaliseurs à moindre carrés (MMSE).

A partir d'un signal reçu PRP-OFDM comme présenté en chapitre 3,

$$\begin{aligned} \mathbf{r}_P(i) &= \mathbf{C}_{\beta_i} \left( \mathbf{F}_{\text{ZP}}^H \tilde{\mathbf{s}}_N(i) + \alpha(i) \mathbf{p}_P \right) + \mathbf{n}_P(i) \\ &= \mathbf{C}_{\beta_i} \begin{pmatrix} \mathbf{F}_N^H \tilde{\mathbf{s}}_N(i) \\ \alpha(i) \mathbf{p}_D \end{pmatrix} + \mathbf{n}_P(i), \end{aligned} \quad (1)$$

il est démontré comment dériver un égaliseur standard MMSE et un égaliseur sans biais d'après les travaux de [42–44]. L'égaliseur à moindre erreur moyenne quadratique déterminant les estimations de  $\tilde{s}_N(i)$  en (1) est donné par:

$$\begin{aligned} \mathbf{G}_{\text{MMSE}}^{\text{PRP}} &:= \mathbf{F}_N [\mathbf{I}_N \mathbf{0}_{N,D}] \mathbf{R}_{s_p} \mathbf{C}_{\beta_i}^H \mathbf{Q}^{-1} \\ &= \mathbf{F}_N [\mathbf{I}_N \mathbf{0}_{N,D}] \mathbf{R}_{s_p} \mathbf{V}_P^H(i) \mathbf{D}_i^H \hat{\mathbf{Q}}^{-1} \mathbf{V}_P(i), \end{aligned}$$

with  $\mathbf{Q} := \mathbf{R}_{n_p} + \mathbf{C}_{\beta_i} \mathbf{R}_{s_p} \mathbf{C}_{\beta_i}^H$ ,  $\hat{\mathbf{Q}} := \mathbf{R}_{n_p} + \mathbf{D}_i \hat{\mathbf{R}}_{s_p} \mathbf{D}_i^H$ ,  $\mathbf{R}_{n_p} := \text{E} [\mathbf{n}_P(i) \mathbf{n}_P^H(i)] = \sigma_n^2 \mathbf{I}_P$ ,  $\mathbf{R}_{s_p} := \text{E} [\mathbf{s}_P(i) \mathbf{s}_P^H(i)]$ ,  $\hat{\mathbf{R}}_{s_p} := \mathbf{V}_P(i) \mathbf{R}_{s_p} \mathbf{V}_P^H(i)$ .

□

L'égaliseur à moindre erreur moyenne quadratique et sans biais déterminant les estimations de  $\tilde{s}_N(i)$  en (1) est donné par

$$\begin{aligned} \mathbf{G}_{\text{MMSE,unb}}^{\text{PRP}} &:= (\mathbf{R}_{\tilde{s}_N} - \text{diag} \{\lambda_0, \dots, \lambda_{N-1}\}) \mathbf{F}_N \mathbf{C}_o^H \left[ \mathbf{C}_{\beta_i} \mathbf{R}_{s_p} \mathbf{C}_{\beta_i}^H + \mathbf{R}_n \right]^{-1} \\ &= \hat{\mathbf{G}} \mathbf{G}_{\text{MMSE}}^{\text{PRP}} \\ \hat{\mathbf{G}} &:= \mathbf{I} - \text{diag} \{\lambda_0, \dots, \lambda_{N-1}\} \mathbf{R}_{\tilde{s}_N}^{-1} \\ \lambda_n &:= [\mathbf{R}_{\tilde{s}_N} \mathbf{B}_i - \mathbf{I}_N]_{n,n} / [\mathbf{B}_i]_{n,n} \\ \mathbf{B}_i &:= \mathbf{F}_N \mathbf{C}_o^H \left[ \mathbf{C}_{\beta_i} \mathbf{R}_{s_p} \mathbf{C}_{\beta_i}^H + \mathbf{R}_n \right]^{-1} \mathbf{C}_o \mathbf{F}_N^H \end{aligned}$$

où  $\mathbf{R}_{\tilde{s}_N} = [\mathbf{I}_N \mathbf{0}_{N,D}] \mathbf{R}_{s_p} [\mathbf{I}_N \mathbf{0}_{N,D}]^H$  est supposée diagonale,  $\mathbf{R}_{s_p} = \text{E} [\mathbf{s}_P(i) \mathbf{s}_P^H(i)]$  et  $\mathbf{C}_o$  est la matrice de dimension  $P \times N$  contenant  $\mathbf{C}_{\text{ISI}}(P)$   $N$  premières colonnes.

□

- L'appendice C donne des résultats d'évaluation de complexité des architectures d'estimation de canal et d'égalisation pour le CP-OFDM et PRP-OFDM.
- L'appendice D présente et discute plusieurs schémas de modélisation de l'évolution du canal de propagation dans un contexte de mobilité.
- L'appendice E présente un théorème de permutation entre des matrices circulantes et des matrices de corrélation.

Proposition: A partir de la matrice suivante de corrélation  $J$ -circulante  $\mathbf{M}_J$  de taille  $P \times P$  par (5.6)

$$\mathbf{M}_J = \begin{bmatrix} p_0 & p_1 & \cdots & p_{D-1} & 0 & \rightarrow & \rightarrow & 0 \\ p_1 & & \nearrow & & & & & p_0 \\ \vdots & \nearrow & & & & & & \vdots \\ p_{D-1} & & & & & & & p_{D-2} \\ 0 & & & & & & & p_{D-1} \\ 0 & & & & & & \nearrow & 0 \\ 0 & & & & & \nearrow & \nearrow & 0 \\ \downarrow & & & & \nearrow & \nearrow & \nearrow & \downarrow \\ 0 & p_0 & \cdots & p_{D-2} & p_{D-1} & 0 & \rightarrow & 0 \end{bmatrix}$$

et de la matrice de convolution circulante  $\mathbf{C}_{\text{CIRC}}(P)$  de taille  $P \times P$ , la validité de l'expression suivante est démontrée:

$$\mathbf{M}_J \mathbf{C}_{\text{CIRC}}(P) = \mathbf{H}_{\text{CIRC}}^T(P) \mathbf{M}_J.$$

- L'appendice F rappelle quelques propriétés utiles des trace de matrice et de la dérivation de ces traces.

# Abbreviations, Definition of Operators and List of Symbols

## ABBREVIATIONS

ADC	Analog to digital conversion
ADSL	Asymmetric digital subscriber line
AP	Access Point
AR	Auto-Regressive
AWGN	Additive white Gaussian noise
BER	Bit error rate
CC	Convolutional coding
CDMA	Code Division Multiple Access
CIR	Channel Impulse Response
COFDM	Coded OFDM
CP	Cyclic prefix
CSI	Channel State Information
DAC	Digital to analog conversion
DFE	Decision feedback equalizer
DMT	Discrete Multi-tone Transmission
ETSI	European telecommunications standard institute
IBI	Inter-Block-Interference
i.i.d.	Independent and identically distributed
ICI	Inter-Carrier-Interference
ISI	Inter-Symbol-Interference
FIR	Finite impulse response
GI	Guard interval
(ID)FFT	(Inverse) Fast fourier transform
LLR	Log-Likelihood-Ratio
LOS	Line of Sight
MA	Moving-Average
MIMO	Multiple inputs multiple outputs
ML	Maximum likelihood
MMSE	Minimum mean square error
MT	Mobile terminal
MTMR	Multiple Transmit Multiple Receive antennas
OFDM	Orthogonal frequency division multiplexing
PA	Power Amplifier

PAPR	Peak to average power ratio
PDF	Probability density function
PDP	Power Delay Profile
PRP	Pseudo Random Postfix
QAM	Quaternary Amplitude Modulation
QPSK	Quadrature Phase shift keying
SDM	Spatial Division Multiplexing
SINR	Signal to Interference plus Noise Ratio
SISO	Single Input Single Output
SNR	Signal to Noise Ratio
STSR	Single Transmit Single Receive antenna
SVD	Singular Value Decomposition
TZ	$z$ transformation
WLAN	Wireless Local Area Network
ZF	Zero forcing
ZP	Zero Padded

## OPERATORS

$(\cdot) \star (\cdot)$	Convolution operator
$(\cdot) \otimes (\cdot)$	Kronecker multiplication
$(\cdot)^*$	Complex conjugation
$(\cdot)^F$	Operator which reads a vector in inverse order
$(\cdot)^T$	Transposition operator
$(\cdot)^H$	Hermitian transposition operator
$(\cdot)^\dagger$	Moore-Penrose pseudo-inverse
$\ \cdot\ ^2$	Corresponds to $E[ \cdot ^2]$
$\lfloor \cdot \rfloor$	Floor operator
$\text{col}_n(\cdot)$	$n$ th column of the matrix argument
$\det(\cdot)$	Determinant of the matrix argument
$\text{diag}(\cdot)$	Diagonal matrix whose diagonal elements are the components of vector $X$
$\text{rank}(\cdot)$	Matrix rank operator
$\text{row}_n(\cdot)$	$n$ th row of the matrix argument
$\text{rowmax}(\cdot)$	operator that is applied on a vector of real values returning the integer $row$ of the its largest element
$E[\cdot]$	Statistical expectation operator
$E_\alpha[\cdot]$	Statistical expectation operator including de-weighting by PRP-OFDM related pseudo-random weighting factors
$\mathcal{F}\{\cdot\}$	Fourier transformation
$\mathcal{F}^{-1}\{\cdot\}$	Inverse Fourier transformation
$z^{-1}$	Unit delay operator
$\nabla$	Nabla operator, derivation operator
$\tau(\cdot)$	Trace of a matrix
$\Re(\cdot)$	Real part operator
$\Im(\cdot)$	Imaginary part operator

## NOTATIONS

$\mathbf{0}_{D \times D}$	$D \times D$ matrix containing zero elements
$\mathbf{a}_N$	A $N \times 1$ vector containing arbitrary symbols
$\mathcal{C}_N$	Diagonal frequency channel matrix of size $N \times N$
$\mathbf{C}_{\text{ISI}}(P)$	$P \times P$ Intra-Symbol interference channel matrix
$\mathbf{C}_{\text{IBI}}(P)$	$P \times P$ Inter-Block interference channel matrix
$\mathbf{C}_{\text{ISI}}^{D \times N}(P)$	First $D$ rows of $P \times P$ Intra-Symbol interference channel matrix
$\mathbf{C}_{\text{IBI}}^{D \times N}(P)$	First $D$ rows of $P \times P$ Inter-Block interference channel matrix
$\mathbf{C}_{lm}^{\text{ISI}}$	Intra-Symbol interference MIMO channel matrix between $l$ th transmit and $m$ th receive antenna
$\mathbf{C}_{lm}^{\text{IBI}}$	Inter-Block interference MIMO channel matrix between $l$ th transmit and $m$ th receive antenna
$\mathbf{C}_{lm}^{\text{ISI},D}$	$D \times D$ Intra-Symbol interference MIMO channel matrix between $l$ th transmit and $m$ th receive antenna
$\mathbf{C}_{lm}^{\text{IBI},D}$	$D \times D$ Inter-Block interference MIMO channel matrix between $l$ th transmit and $m$ th receive antenna
$\mathbf{C}_{\text{CIRC}}(P)$	$P \times P$ circulant channel matrix
$\mathbf{C}_{\beta_k}$	Circulant channel convolution matrix with upper triangular part weighted by $\beta_k$
$\mathbf{C}_l^{\beta_k}$	MIMO channel convolution matrix for $l$ th transmit antenna with upper triangular part weighted by $\beta_k$
$\mathbf{C}_{\beta_i}^k(i)$	Estimated pseudo-circulant CIR matrix of $i$ th OFDM symbol at $k$ th iteration with upper triangular part weighted by $\beta_i$
$\mathbf{C}_o$	$P \times N$ channel convolution for ZP-OFDM context
$\mathbf{C}(z)$	Channel convolution matrix with upper triangular part weighted by $z^{-1}$
$\mathbf{C}_{lm}$	Channel convolution matrix between $l$ th transmit and $m$ th receive antenna
$\mathbf{c}_D$	$D \times 1$ vector containing the channel impulse response
$\mathbf{c}_{lm}$	Time domain vector containing the MIMO channel impulse response between $l$ th transmit and $m$ th receive antenna
$\hat{\mathbf{c}}^k(i)$	Estimated CIR at $k$ th iteration for $i$ th OFDM symbol
$\tilde{\mathbf{c}}_{lm}$	Frequency domain vector containing the MIMO channel impulse response between $l$ th transmit and $m$ th receive antenna
$\bar{\mathbf{c}}_n$	$D \times 1$ vector containing the channel impulse response plus noise
$\hat{\mathbf{c}}_D$	$D \times 1$ vector containing the channel impulse response estimates
$\hat{\mathbf{c}}_D^{\text{MMSE}}$	$D \times 1$ vector containing the channel impulse response estimates (based on a Minimum Mean Square Error (MMSE) estimation approach)
$\hat{\mathbf{c}}_D^{\text{ZF}}$	$D \times 1$ vector containing the channel impulse response estimates (based on a Zero Forcing (ZF) estimation approach)
$c(t)$	Continuous time domain channel impulse response
$\tilde{c}_k$	Channel frequency response on the $k$ th OFDM carrier
$c[T]$	Time domain channel impulse response sampled at instant $T$
$c(z)$	$z$ transformation of channel impulse response
$c_k(z)$	$z$ transformation of $k$ th sample of the channel impulse response over all OFDM symbols

$c_{\Delta T,k}(z)$	$z$ transformation of $k$ th sample of the channel impulse response over all OFDM symbols including a time synchronization offset
$c_k$	$k$ th time domain coefficient of the channel impulse response
$c_{lm}(k)$	$k$ th time domain coefficient of the MIMO channel impulse response between $l$ th transmit and $m$ th receive antenna
$\tilde{c}_k$	$k$ th frequency domain channel coefficient
$\check{\mathbf{c}}(n)$	Process noise
$c_L$	Clipping amplitude
$\mathbf{D}_k$	Diagonal matrix containing channel coefficients
$\mathbf{D}_J$	Diagonal matrix used for diagonalization of $\mathbf{M}_J$
$\tilde{\mathbf{D}}_l$	Diagonal matrix containing $l$ th frequency domain channel impulse response
$\tilde{\mathbf{D}}$	Matrix regrouping four $\tilde{\mathbf{D}}_l$
$D$	Size of the guard interval
$\text{DFT}_{\mathbb{C}}(N)$	Complexity of a Fast Fourier Transform
$\mathbf{d}_m^k(i)$	Sum of first and last $D$ elements of the received vector of $m$ th receive antenna and $k$ th OFDM symbol of the $i$ th received ST block de-weighted by the corresponding pseudo random weighting factor $\alpha(\cdot)$
$\mathbf{d}_m^k$	Expectation of $\mathbf{d}_m^k(i)$
$\mathbf{d}_{m,2D}^k$	Expectation of $\mathbf{d}_m^k(i)$ with IBI and ISI contributions kept separately
$\mathbf{d}_m$	Concatenation of all $\mathbf{d}_m^k$ for a given $m$
$d_c$	Variable node degree in LDPC code
$d_v$	Check node degree in LDPC code
$\mathbf{F}_N$	Matrix performing the Fourier Transform
$\mathbf{F}_{\text{CP}}^{\text{H}}$	Matrix performing the Inverse Fourier Transform combined with the insertion of the CP-OFDM cyclic prefix sequence
$\mathbf{F}_{\text{ZP}}^{\text{H}}$	Matrix performing the Inverse Fourier Transform combined with the insertion of the trailing zeros sequence
$\mathbf{F}(n, n-1)$	Transition matrix for Kalman filter process equation
$\mathbf{F}_C$	The sub-matrix of $\mathbf{F}_P$ stacking the rows associated to in-band carriers $C$
$\mathbf{F}_O$	The sub-matrix of $\mathbf{F}_P$ stacking the rows associated to out-of-band carriers $O$
$\mathbf{f}_n^c$	A $1 \times P$ vector containing the row of $\mathbf{F}_C$ corresponding to carrier $C_n$
$\mathbf{f}_n^o$	A $1 \times P$ vector containing the row of $\mathbf{F}_O$ corresponding to carrier $O_n$
$(\mathbf{f}_n^c)_m$	The $m$ th component of $\mathbf{f}_n^c$
$(\mathbf{f}_n^o)_m$	The $m$ th component of $\mathbf{f}_n^o$
$f_0$	Frequency offset
$\hat{f}_0$	Estimated frequency offset
$f_D$	Doppler frequency
$f_{\text{PA}}(z)$	Power Amplifier transfer function
$f_{u_0,l}$	Distribution of the $l$ th LLR message arriving at variable nodes in LDPC belief propagation decoder corresponding to a zero-bit
$\mathbf{G}$	Generic equalization matrix
$\mathbf{G}_c$	Channel estimator matrix
$\mathbf{G}_{\text{ZF}}$	Zero Forcing (ZF) based equalization matrix (ZP-OFDM based)
$\mathbf{G}_{\text{MMSE}}$	Minimum Mean Square Error (MMSE) based equalization matrix (ZP-OFDM based)

$\mathbf{G}_{ZF}^{\text{PRP}}(i)$	Zero Forcing (ZF) based equalization matrix (PRP-OFDM based) for $i$ th OFDM symbol
$\mathbf{G}_{\text{MMSE}}^{\text{PRP}}(i)$	Minimum Mean Square Error (MMSE) based equalization matrix (PRP-OFDM based) for $i$ th OFDM symbol
$\mathbf{G}(z)$	Ensemble of all $g_k^{(l)}(z)$ of all time domain samples $l$ and OFDM symbols
$\mathbf{G}_d$	Diagonal matrix containing carrier weighting factors after equalization
$\mathbf{G}_f$	Matrix detailing sample correlation after equalization
$g_k(t)$	shaping filter for $k$ th OFDM sub-carrier
$g'_k(t)$	cyclically extended shaping filter for $k$ th OFDM sub-carrier
$g_k^{(l)}(z)$	Sum over all OFDM symbols of the $l$ th time domain sample of shaping filter for $k$ th OFDM sub-carrier
$\mathbf{H}$	LDPC code matrix
$\mathbf{H}_b$	LDPC code base matrix
$\mathbf{I}_N$	$N \times N$ unitary matrix
$i_0$	OFDM symbol number used as a reference for channel estimation, synchronization refinement, etc.
$J_0(\cdot)$	0th order Bessel function of the first kind
$J_n$	Correlation coefficients
$J^{\text{Clip}}$	Sub-optimum cost function for criterion of clipping
$J^{\text{Clip,ideal}}$	Optimum cost function for criterion of clipping
$J^{\text{Flat}}$	Cost function for criterion of spectral flatness
$J^{\text{Out}}$	Cost function for criterion of out-of-band radiation
$J^{\text{Tot}}$	Total cost function of postfix optimization
$K$	Number of used sub-carriers per OFDM symbol
$L$	Channel order
$\mathbf{M}_J$	$J$ circulant correlation matrix for synchronization refinement
$M_{\text{LDPC}}$	Number of bits in an LDPC code-word
$M_b$	Number of columns in the LDPC base matrix
$\mathbf{m}_M$	LDPC code-word
$\mathbf{m}_{\text{ZLDPC}}^{\text{Data}}$	Data bits of an LDPC code-word
$\mathbf{m}_{\text{ZLDPC}}^{\text{Red}}$	Redundancy bits of an LDPC code-word
$m_u^{(l)}$	Mean value of messages $u$ in an LDPC belief propagation decoder at iteration $l$
$m_v^{(l)}$	Mean value of messages $v$ in an LDPC belief propagation decoder at iteration $l$
$\mathbf{N}(i)$	Matrix containing MTMR receiver noise vectors for $i$ th ST block
$\mathbf{n}_N(i)$	Time domain noise vector of size $N \times 1$ associated to the $i$ th OFDM symbol
$\bar{\mathbf{n}}_N$	Time domain estimation noise vector of size $N \times 1$
$\bar{\mathbf{n}}_N(i)$	Time domain estimation noise vector of size $N \times 1$ associated to the $i$ th OFDM symbol
$\mathbf{n}_{D,0}(i)$	First $D$ elements of the time domain noise vector of size $P \times 1$ associated to the $i$ th OFDM symbol
$\mathbf{n}_{D,1}(i)$	Last $D$ elements of the time domain noise vector of size $P \times 1$ associated to the $i$ th OFDM symbol
$\mathbf{n}_{m,0}(i)$	First $D$ elements of the MIMO time domain noise vector of size $P \times 1$ associated to the $i$ th OFDM symbol of the $m$ th receive antenna

$\mathbf{n}_{m,1}(i)$	Last $D$ elements of the MIMO time domain noise vector of size $P \times 1$ associated to the $i$ th OFDM symbol of the $m$ th receive antenna
$\tilde{\mathbf{n}}$	Frequency domain noise vector
$\tilde{\mathbf{n}}_N$	Frequency domain noise vector of size $N \times 1$
$\tilde{\mathbf{n}}_u$	Observation noise vector
$\mathbf{n}_W(i)$	Noise plus interference associated to the $i$ th OFDM symbol
$\mathbf{n}_{2ZD}(i)$	$Z$ regrouped vectors of $2D$ noise samples each
$\tilde{\mathbf{n}}_{2ZD}(i)$	$Z$ regrouped vectors of $2D$ noise samples each
$\mathbf{n}_m(i)$	Time domain noise vector on the $m$ th receive antenna
$\tilde{\mathbf{n}}_m^k$	Mean noise contribution (calculated over $Z$ observations) on $m$ th receive antenna and $k$ th symbol inside the current ST block
$\tilde{\mathbf{n}}_{m,2D}^k$	Mean noise contribution (calculated over $Z$ observations) on $m$ th receive antenna and $k$ th symbol inside the current ST block with IBI and ISI contributions kept separately
$\tilde{\mathbf{n}}_m$	Concatenation of all $\tilde{\mathbf{n}}_m^k$ for a given $m$
$\tilde{\mathbf{n}}_{m,2D}$	Concatenation of all $\tilde{\mathbf{n}}_m^k$ for a given $m$ with IBI and ISI contributions kept separately
$N$	Number of samples per OFDM symbol ( <i>not</i> including the prefix/postfix sequence)
$\tilde{N}$	Number of used (non-zero) carriers of an OFDM symbol
$N_r$	Number of receive antennas in the MTMR configuration
$N_t$	Number of transmit antennas in the MTMR configuration
$\mathbf{P}_Q$	Permutation matrix used for PRP-OFDM synchronization
$\mathbf{P}_D$	$D \times D$ circulant convolution matrix with postfix sequence coefficients
$\mathbf{P}_{\text{IBI},D}$	Upper triangular part of $D \times D$ circulant convolution matrix with postfix sequence coefficients
$\mathbf{P}_{\text{ISI},D}$	Lower triangular part of $D \times D$ circulant convolution matrix with postfix sequence coefficients
$\tilde{\mathbf{P}}_D$	$D \times D$ circulant convolution matrix with postfix sequence coefficients in frequency domain
$\mathbf{P}_N^0$	$N \times N$ permutation matrix
$\mathbf{P}_P^N$	$P \times P$ permutation matrix
$P$	Number of samples per OFDM symbol including the prefix/postfix sequence
$\mathbf{p}_D$	$D \times 1$ time domain postfix sequence vector
$\bar{p}_l(i)$	$i$ th $D \times 1$ time domain MIMO postfix sequence vector for $l$ th transmit antenna
$\mathbf{p}_P$	vector consisting of $N$ zero elements followed by the $D$ samples time domain postfix sequence vector
$\mathbf{p}_l^{\beta(i)}$	$l$ th interference vector used in MTMR decoder for $i$ th block
$\hat{\mathbf{p}}_P$	vector consisting of the $D$ samples time domain postfix sequence vector followed by $N$ zero elements
$p_s(t)$	Continuous time domain postfix sequence
$p^{(l)}(z)$	Sum over all OFDM postfix sequences of the $l$ th time domain sample of continuous postfix sequence
$p_l^k(x_n(i))$	Decoded bit-probabilities of the $l$ th encoded bit of the constellation on carrier $n$ of OFDM symbol $i$ on decoding iteration $k$

$\tilde{p}(z)$	$z$ transformation of time domain postfix sequence weighted by pseudo-random factors $\alpha(i)$
$p(z)$	$z$ transformation of OFDM postfix time domain samples ( <i>not</i> including OFDM data symbol)
$\mathbf{Q}(i)$	Matrix containing MTMR transmission vectors for $i$ th ST block
$Q$	Time synchronization offset
$Q_M$	Constellation order
$\hat{Q}$	Estimated time synchronization offset
$\bar{Q}$	Variable related to time synchronization offset
$\mathbf{q}_l(i)$	$l$ th output of ST encoder of $i$ th block including pseudo randomly weighted postfix sequences
$\mathbf{R}(i)$	Matrix containing MTMR receiver vectors for $i$ th ST block
$\hat{\mathbf{R}}(i)$	Matrix containing estimated MTMR receiver vectors for $i$ th ST block
$\mathbf{R}_{cD}$	Covariance matrix of $\mathbf{c}_D$
$\tilde{\mathbf{R}}_{cD}$	Covariance matrix of $\mathbf{c}_D$ in frequency domain
$\mathbf{R}_{\tilde{\mathbf{n}}_D}$	Covariance matrix of $\tilde{\mathbf{n}}_D$
$\tilde{\mathbf{R}}_{\tilde{\mathbf{n}}_D}$	Covariance matrix of $\tilde{\mathbf{n}}_D$ in frequency domain
$\mathbf{r}(i)$	Received vector of $i$ th OFDM symbol
$\tilde{\mathbf{r}}(i)$	Received vector of $i$ th OFDM symbol in frequency domain
$\mathbf{r}^{ZP}(i)$	Received vector of $i$ th OFDM symbol
$\mathbf{r}_m(i)$	Received vector of $i$ th OFDM symbol on the $m$ th receive antenna
$\mathbf{r}_N(i)$	Received vector of size $N \times 1$ of $i$ th OFDM symbol
$\mathbf{r}_{2ZD}(i)$	$Z$ regrouped vectors of $2D$ received samples each
$\mathbf{r}_N$	Received vector of size $N \times 1$
$\mathbf{r}_{D,0}$	First $D$ coefficients of the received vector of size $P \times 1$
$\mathbf{r}_{D,1}$	Last $D$ coefficients of the received vector of size $P \times 1$
$\mathbf{r}_{m,0}(i)$	First $D$ elements of the received vector of $i$ th OFDM symbol on the $m$ th receive antenna
$\mathbf{r}_{m,1}(i)$	Last $D$ elements of the received vector of $i$ th OFDM symbol on the $m$ th receive antenna
$\tilde{\mathbf{r}}_P^k(i)$	Received vector of size $P \times 1$ of $i$ th OFDM symbol including postfix sequence after interference suppression on $k$ th decoding iteration
$\hat{\mathbf{r}}_{c,0}$	Mean value of $\mathbf{r}_{D,0}$ de-normalized by pseudo random weighting coefficients
$\hat{\mathbf{r}}_{c,1}$	Mean value of $\mathbf{r}_{D,1}$ de-normalized by pseudo random weighting coefficients
$\hat{\mathbf{r}}_c$	Estimated postfix sequence circularly convolved by the channel of size $D \times 1$
$\hat{\mathbf{r}}_{c,2D}$	Estimated postfix sequence circularly convolved by the channel of size $2D \times 1$ keeping IBI and ISI parts separate
$\mathbf{r}(z)$	vector containing $z$ transformation of received samples
$r_k(n)$	$k$ th time domain component of the $N \times 1$ received vector $\mathbf{r}_N$ at OFDM symbol $n$
$r(t)$	Continuous time received signal
$[r(t)]_{\Delta T}$	Continuous time received signal including a time offset
$[r(t)]_{\Delta F}$	Continuous time received signal including a frequency offset
$r[T]$	Time domain received signal sampled at instant $T$
$r(z)$	$z$ transformation of the received time domain samples

$r_{\Delta T}(z)$	$z$ transformation of the received time domain samples including a time synchronization offset
$r_{\Delta F}(z)$	$z$ transformation of the received time domain samples including a frequency synchronization offset
$r_n(i)$	$n$ th sample of the received signal in the $i$ th OFDM symbol
$[r(t)]_{\Delta F}$	Continuous time received signal including a frequency offset
$r_l(z)$	$l$ th polyphase component of $z$ transformation of the received time domain samples
$r_k(z)$	$z$ transformation of $r_k(n)$
$R$	Code rate
$R_{s,s}^{(0)}(l,k)$	Sample correlation
$S_{s,s}^{(0)}(z)$	Cyclo-spectrum of order 0 of the transmitted time domain sequence
$\text{Rect}_T(t)$	Rectangular function
$\tilde{\mathbf{S}}(i)$	Grouped ST encoded outputs of $i$ th block
$\mathbf{s}_N$	$N$ -dimensional time domain transmit vector
$\mathbf{s}_{D,0}$	The first $D$ elements of the $N$ -dimensional time domain transmit vector
$\mathbf{s}_{D,1}$	The last $D$ elements of the $N$ -dimensional time domain transmit vector
$\mathbf{s}(i)$	$N$ -dimensional time domain transmit vector associated to $i$ th OFDM symbol
$\tilde{\mathbf{s}}(i)$	$N$ -dimensional frequency domain transmit vector associated to $i$ th OFDM symbol
$\tilde{\tilde{\mathbf{s}}}(i)$	Alternative $N$ -dimensional frequency domain transmit vector associated to $i$ th OFDM symbol
$\mathbf{s}^{\text{ig}}(i)$	$P \times 1$ vector containing $i$ th CP-OFDM symbol including cyclic prefix extension
$\tilde{\mathbf{s}}(z)$	$z$ transformation of $\tilde{\mathbf{s}}(n)$
$\tilde{\mathbf{s}}$	Estimated OFDM symbol in frequency domain
$\tilde{\mathbf{s}}_l(i)$	$l$ th ST encoder output of $i$ th block
$\tilde{\mathbf{s}}_{l,0}(i)$	First $D$ elements of $l$ th ST encoder output of $i$ th block
$\tilde{\mathbf{s}}_{l,1}(i)$	Last $D$ elements of $l$ th ST encoder output of $i$ th block
$s_k(n)$	$k$ th time domain component of the $N \times 1$ transmit vector $\mathbf{s}_N$ at OFDM symbol $n$
$\tilde{s}_k(n)$	$k$ th frequency domain component of the $N \times 1$ transmit vector $\mathbf{s}_N$ at OFDM symbol $n$
$\tilde{s}_k(z)$	$z$ transformation of $\tilde{s}_k(n)$
$s(z)$	$z$ transformation of OFDM data symbol time domain samples ( <i>not</i> including postfix sequence)
$s^{\text{CP}}(z)$	$z$ transformation of CP-OFDM data symbol time domain samples including cyclic prefix sequence
$\mathbf{T}_{ZP}$	ZP-OFDM precoding matrix
$T$	Sampling rate
$T_B$	OFDM symbol block duration (including prefix/postfix sequence)
$T_{CP}$	OFDM symbol prefix/postfix duration
$T_g$	OFDM symbol block duration ( <i>not</i> including prefix/postfix sequence)
$t$	Time variable
$t_c$	Variable node degree of regular LDPC codes
$t_{c,\max}$	Maximum variable node degree of an irregular LDPC code

$t_r$	Check node degree of regular LDPC codes
$t_{r,max}$	Maximum check node degree of an irregular LDPC code
$TZ[x_n]$	$z$ transformation of sequence $x_n$
$\mathbf{U}$	Observation matrix
$\tilde{\mathbf{u}}(z)$	$z$ transformation of $\tilde{\mathbf{u}}(n)$
$\mathbf{u}_l(i)$	$l$ th output of ST encoder of $i$ th block including trailing zeros
$\mathbf{u}_P^k(i)$	Estimated interference vector of size $P \times 1$ on $k$ th decoding iteration
$\mathbf{u}_{Z_{LDPC}}^{\text{Data}}$	Pointer to variable node degrees of data bits of an LDPC code-word
$\mathbf{u}_{Z_{LDPC}}^{\text{Red}}$	Pointer to variable node degrees of redundancy bits of an LDPC code-word
$u(t)$	Transmitted continuous OFDM time domain signal
$u[T]$	Transmitted continuous OFDM time domain signal sampled at instant $T$
$u_n(i)$	$n$ th sample of the $i$ th Transmitted continuous OFDM time domain symbol
$u_n(z)$	$z$ transformation of $u_n(i)$
$u_i$	LLR messages arriving at variable nodes in LDPC belief propagation decoder
$u^{(l)}$	LLR messages arriving at variable nodes in LDPC belief propagation decoder at iteration $l$
$u_{0,l}$	$l$ th LLR message arriving at variable nodes in LDPC belief propagation decoder corresponding to a zero-bit
$\mathbf{V}_P$	$P \times P$ matrix containing eigenvectors of pseudo-circulant channel convolution matrix
$\mathbf{v}_n$	Postfix sequence convolved by channel plus noise
$\mathbf{W}$	Orthogonal and unitary matrix
$\mathbf{W}_{N,K}$	Precoding matrix of size $N \times K$
$W_N$	Coefficient $e^{-j\frac{2\pi}{N}}$ used for definition of $\mathbf{F}_N$
$\mathbf{W}(i)$	Channel estimator matrix
$\mathbf{W}_H(i)$	Matrix regrouping several $\mathbf{C}_i^{\beta_k}$ weighted by coefficients of a Walsh Hadamard matrix
$\bar{\mathbf{W}}(k)$	Channel estimator matrix
$\tilde{\mathbf{w}}_N^k$	Residual noise plus interference expression on received vector after interference suppression on $k$ th iteration
$\mathbf{w}_{Z_{LDPC}}^{\text{Data}}$	Variable node degrees of data bits of an LDPC code-word
$\mathbf{w}_{Z_{LDPC}}^{\text{Red}}$	Variable node degrees of redundancy bits of an LDPC code-word
$w_l(i)$	$l$ th row and $i$ th column of the orthogonal and unitary matrix $\mathbf{W}$
$\mathbf{Y}_n$	Combination matrix for combining channel estimates with different noise contributions
$Z$	Length of OFDM symbol window size used for channel estimation
$Z_{LDPC}$	Number of LDPC parity check equations
$Z_b$	Number of rows in the LDPC base matrix
$\bar{Z}$	One-block observation window size
$\mathbb{C}$	Complex numbers
$\mathbb{N}$	Natural Numbers
$\mathbb{R}$	Real Numbers

$\mathbb{Z}$	Entire Numbers
$\mathcal{C}$	Set of in-band carriers
$\mathcal{M}(\cdot)$	A generic ST encoder for the OFDM data symbols
$\mathcal{X}(m, \sigma^2)$	Gaussian distribution with mean $m$ and variance $\sigma^2$
$\mathcal{O}$	Set of out-of-band carriers
$\mathcal{W}(\cdot)$	A generic ST encoder for the postfix sequence
$\alpha(i)$	Pseudo random weighting factor of postfix sequence on $i$ th OFDM symbol
$\alpha(z)$	$z$ transformation of $\alpha(i)$
$\alpha_{\mathbb{C}}$	Complexity of a complex addition
$\alpha_{\mathbb{R}}$	Complexity of a real addition
$\beta_k$	weighting of upper triangular part of channel convolution matrix for PRP-OFDM
$\gamma^{\text{Clip}}$	Cost function weight for criterion of clipping
$\gamma^{\text{Flat}}$	Cost function weight for criterion of spectral flatness
$\gamma^{\text{Out}}$	Cost function weight for criterion of out-of-band radiation
$\delta_{n,n'}$	Kronecker symbol
$\delta(t)$	Dirac's Delta function
$\Delta T$	Synchronization offset
$\varepsilon(i)$	Estimation error on $i$ th block
$\zeta(k)$	Node degree of LDPC code
$\eta$	A real, positive coefficient
$\phi(\cdot)$	Auxiliary function for LDPC message update calculation
$\lambda(x)$	Polynomial defining the variable node degrees of an irregular LDPC code
$\lambda_i$	Weight of degree $i$ variable nodes of an irregular LDPC code
$\tilde{\lambda}_i$	Alternative definition of weight of degree $i$ variable nodes of an irregular LDPC code
$\mu_{\mathbb{C}}$	Complexity of a complex multiplication
$\mu_{\mathbb{R}}$	Complexity of a real multiplication
$\mu_{\mathbb{R}\mathbb{C}}$	Complexity of a multiplication real $\times$ complex
$\mathbf{v}_i$	LLR messages leaving variable nodes in LDPC belief propagation decoder
$\mathbf{v}^{(l)}$	LLR messages leaving variable nodes in LDPC belief propagation decoder at iteration $l$
$\pi$	The constant $\pi \approx 3.141592653589793238462643383279502884197$
$\rho(x)$	Polynomial defining the check node degrees of an irregular LDPC code
$\rho_i$	Weight of degree $i$ check nodes of an irregular LDPC code
$\tilde{\rho}_i$	Alternative definition of weight of degree $i$ check nodes of an irregular LDPC code
$\sigma_n^2$	Noise variance
$\sigma_s^2$	Variance of time domain OFDM data samples
$\sigma_{tot}^2$	Variance of noise plus OFDM time domain samples
$\tau$	Time
$\Phi_{\alpha(i)}$	Phase of the pseudo random weighting factor of postfix sequence on $i$ th OFDM symbol

$\phi_{\text{const}}$	Constant phase offset
$\psi(k)$	Number of data bits in a given constellation
$\omega$	Frequency



# Contents

<b>1</b>	<b>General Introduction</b>	<b>1</b>
<b>2</b>	<b>Orthogonal Frequency Division Multiplexing</b>	<b>5</b>
2.1	History and recent evolutions of Orthogonal Frequency Division Multiplexing . . . . .	5
2.2	Filter-Bank based representation of Orthogonal Frequency Division Multiplexing and definition of Pseudo Random Postfix OFDM . . . . .	7
2.2.1	Definition of the CP-OFDM modulator . . . . .	7
2.2.2	Definition of the PRP-OFDM modulator . . . . .	8
2.3	Discrete representation of the sampled signal in the receiver . . . . .	9
2.3.1	Symbol reconstruction in absence of a channel . . . . .	9
2.3.2	Symbol reconstruction in presence of multi-path propagation . . . . .	11
2.3.3	Discrete Transceiver Architectures . . . . .	13
2.4	Impact of synchronization impairments . . . . .	17
2.4.1	Frequency offset . . . . .	17
2.4.2	Time Offset . . . . .	17
2.4.3	Sampling frequency offset . . . . .	18
2.5	Strengths and weaknesses of OFDM . . . . .	19
2.6	Example of an OFDM system . . . . .	20
2.7	Conclusion . . . . .	22
<b>3</b>	<b>Pseudo Random Postfix OFDM: channel estimation and equalization</b>	<b>23</b>
3.1	Introduction . . . . .	23
3.2	Notations and PRP-OFDM modulator . . . . .	24
3.3	Order one semi-blind channel estimation based on PRP-OFDM postfixes only . . . . .	26
3.3.1	Channel estimation in a time-invariant environment . . . . .	26
3.3.2	Channel estimation in a time-variant environment (presence of Doppler) . . . . .	31
3.4	Order one semi-blind channel estimation based on PRP-OFDM postfixes and preambles . . . . .	35
3.5	Symbol Recovery: Equalization . . . . .	37
3.5.1	Zero Forcing equalizers . . . . .	38
3.5.2	Minimum Mean Square Error equalizers . . . . .	38
3.6	Symbol Recovery: Metric derivation . . . . .	39
3.6.1	Metric derivation . . . . .	40
3.6.2	Low-complexity metric proposal . . . . .	40
3.7	Low complexity receiver architecture . . . . .	41
3.8	Simulation results . . . . .	42
3.8.1	Mean Square Error of Pseudo-Random-Postfix OFDM based channel estimates . . . . .	44
3.8.2	Simulation results for BRAN-A channel model . . . . .	45
3.8.3	Simulation results for BRAN-C channel model . . . . .	49

3.8.4	Simulation results for BRAN-E channel model . . . . .	52
3.8.5	Simulation results for BRAN-A channel model (uncoded) . . . . .	54
3.9	Conclusion . . . . .	56
<b>4</b>	<b>Pseudo Random Postfix OFDM: Postfix Design</b>	<b>57</b>
4.1	Introduction . . . . .	57
4.2	Notations and PRP-OFDM modulator . . . . .	58
4.3	PRP-OFDM Postfix Design Constraints . . . . .	59
4.3.1	Regulatory constraints . . . . .	59
4.3.2	System implementation constraints . . . . .	61
4.3.3	Base-band design constraints . . . . .	62
4.3.4	Conclusion: resulting postfix design constraints . . . . .	63
4.4	Iterative derivation of a suitable postfix . . . . .	63
4.4.1	Spectral flatness . . . . .	64
4.4.2	Out-of-band radiation . . . . .	64
4.4.3	Clipping . . . . .	65
4.5	Example of Postfix design . . . . .	65
4.6	Conclusion . . . . .	66
<b>5</b>	<b>Synchronization Refinement with Pseudo Random Postfix OFDM</b>	<b>75</b>
5.1	Introduction . . . . .	75
5.2	Notations and PRP-OFDM modulator . . . . .	76
5.3	Time synchronization aspects . . . . .	77
5.3.1	Refinement in the AWGN context . . . . .	78
5.3.2	Refinement in presence of ISI . . . . .	80
5.4	Frequency Offset Estimation . . . . .	82
5.5	Simultaneous presence of Time and Frequency Offsets . . . . .	84
5.6	Performance illustration for 5GHz WLAN . . . . .	86
5.7	Conclusion . . . . .	86
<b>6</b>	<b>Pseudo Random Postfix Orthogonal Frequency Division Multiplexing for multiple antennas systems</b>	<b>89</b>
6.1	Introduction . . . . .	89
6.2	MTMR PRP-OFDM modulation and demodulation . . . . .	90
6.3	Order-one MIMO channel estimation . . . . .	91
6.3.1	Static context : minimum dimension circular diagonalization . . . . .	92
6.3.2	Static context : carrier grid adaptation . . . . .	94
6.3.3	Doppler Context . . . . .	96
6.4	Examples of transceiver designs . . . . .	96
6.4.1	ZP-OFDM based decoding approach . . . . .	97
6.4.2	Decoding based on diagonalization of pseudo-circulant channel matrices . . . . .	98
6.5	Simulation results . . . . .	99
6.6	Conclusion . . . . .	101
<b>7</b>	<b>Iterative Interference Suppression</b>	<b>105</b>
7.1	Introduction . . . . .	105
7.2	Notations and PRP-OFDM modulator . . . . .	106
7.3	Channel estimation . . . . .	107
7.3.1	Standard channel estimation . . . . .	107

7.3.2	The new iterative channel estimation . . . . .	108
7.3.3	Practical considerations related to Iterative Interference Suppression . . . . .	110
7.4	Simulation Results . . . . .	111
7.5	Conclusion . . . . .	112
<b>8</b>	<b>Low Density Parity Check (LDPC) Coding for OFDM</b>	<b>117</b>
8.1	Introduction . . . . .	117
8.2	Notations and definitions . . . . .	118
8.3	LDPC Code optimization with known and time-invariant channel . . . . .	122
8.3.1	Properties of the Gaussian Approximation applied to the analysis of message passing decoding . . . . .	123
8.3.2	Direct interpretation of the message passing update equation . . . . .	125
8.3.3	Second order approximation of the message passing update equation . . . . .	126
8.3.4	An algorithm for LDPC code word mapping onto OFDM carriers . . . . .	128
8.4	Simulation results . . . . .	130
8.5	Conclusion . . . . .	131
<b>9</b>	<b>Conclusion</b>	<b>133</b>
<b>A</b>	<b>Proof of Diagonalization Properties of Pseudo circulant matrices</b>	<b>135</b>
<b>B</b>	<b>Biased and unbiased MMSE equalizers</b>	<b>137</b>
B.1	Biased MMSE equalizer . . . . .	137
B.2	Unbiased MMSE equalizer . . . . .	138
<b>C</b>	<b>Complexity Considerations</b>	<b>141</b>
C.1	The complexity of basic operations . . . . .	141
C.2	The complexity of Fast Fourier Transformation (FFT) algorithms . . . . .	141
C.3	PRP-OFDM Complexity Evaluation . . . . .	142
C.3.1	Generic Complexity Evaluation . . . . .	143
C.3.2	Numerical Examples . . . . .	143
C.4	Conclusion . . . . .	143
<b>D</b>	<b>Modeling of the channel evolution in a Doppler context</b>	<b>145</b>
D.1	Modeling time-variant channels . . . . .	145
D.2	Auto-Regressive model of first order . . . . .	146
D.3	Moving Average model . . . . .	147
<b>E</b>	<b>Permutation product theorem for correlation and channel matrices</b>	<b>149</b>
<b>F</b>	<b>Complex derivation</b>	<b>151</b>
	<b>List of tables</b>	<b>153</b>
	<b>List of figures</b>	<b>154</b>
	<b>Bibliography</b>	<b>163</b>



# Chapter 1

## General Introduction

Advanced digital communications theory is currently facing a considerable amount of attention: recent advances in semiconductor technology make the application of high performing, but complex algorithms attractive for mass-market products. To give an example, the future generation of high throughput *Wireless Local Area Networks* is about to be standardized in the IEEE802.11n Working Group [31, 32]. It will provide data throughput of 500Mbps and beyond above the *Physical Layer* (PHY), applying *Multiple Transmit Multiple Receive* (MTMR) *Orthogonal Frequency Division Multiplexing* (OFDM) architectures: *Spatial Division Multiplexing* (SDM) is standardized on the transmission side, while *Minimum Mean Square Error* (MMSE) and *Maximum Likelihood* (ML) receiver architecture are already a reality. In order to increase the link reliability in a point-to-point scenario, the draft standard proposes *Singular Value Decomposition* (SVD) based beam-forming approaches combined with explicit *Channel State Information* (CSI) feedback. On the channel coding side, the current evolution tends towards the use of *Low Density Parity Check* (LDPC) codes providing approx. 2dB to 3dB of coding gain compared to standard convolutional codes in a typical scenario. While the basic theory of these approaches is well known and extensively published, numerous practical aspects are still unresolved. In particular, the joint use of these advanced technologies still requires scientific studies.

This thesis addresses the following practical aspects targeting an improvement of communication systems as the one discussed above: a modification of standard *Cyclic Prefix OFDM* (CP-OFDM) is proposed which enables the receiver to perform a first-order semi-blind channel estimation and tracking approach: *Pseudo Random Postfix OFDM* (PRP-OFDM) [1, 3–26]. As a consequence, OFDM is applicable in a high-velocity scenario (up to 72m/s of mobility at a 5GHz carrier frequency is considered) avoiding the introduction of learning sequences and/or pilot tones. As a consequence, the spectral efficiency of the system is improved. Several efficient algorithms are proposed for this purpose, providing different trade-offs in terms of receiver performance and decoding latency. In the final chapter, an optimum use of LDPC codes in combination with the OFDM modulation scheme is addressed in a frequency selective propagation channel environment.

The chapters of this document are organized as follows:

- Chapter 2 gives a general overview on the OFDM modulation scheme and presents the novel Pseudo-Random-Postfix OFDM (PRP-OFDM) modulator. Standard receiver architectures are discussed and the impact of time and frequency synchronization errors is illustrated.
- The novel Pseudo-Random-Postfix OFDM (PRP-OFDM) modulation scheme is further studied in chapter 3. The focus is on the receiver architectures where the following two basic equalization approaches are proposed: i) it is shown how to transform the PRP-OFDM signal in the receiver to the known Zero-Padded OFDM (ZP-OFDM) which allows the use of available equalization schemes [39]; ii) alternatively, a symbol-based equalization approach is derived exploiting the diagonalization properties of pseudo-circulant matrices. Then, it is shown how to exploit the pseudo-randomly weighted postfix sequence of PRP-OFDM for channel estimation in both, a time-invariant and time-variant case. In the time-invariant scenario, a low-complexity receiver architecture is proposed. Simulation results show that PRP-OFDM allows to guarantee improved performances with respect to CP-OFDM for lower-order constellations (BPSK, QPSK, QAM-16); in a high-mobility context (considering velocities up to 72m/s at a carrier frequency of 5.2GHz), PRP-OFDM suffers only a slight performance degradation: in the example of QPSK constellations, rate  $R = 1/2$  convolutional channel coding and  $4.0\mu\text{s}$  OFDM symbols of 64 carriers plus 16 postfix samples each, approx. 0.4dB of performance penalty in packet error rate (PER) is observed compared to the time-invariant results with one packet containing 72 OFDM symbols.
- The specific design of the deterministic postfix sequences is addressed in chapter 4. For this purpose, several design criteria are taken into account: i) spectral flatness of the in-band signal, ii) minimum signal power on out-of-band carriers and ii) minimum *Peak-to-Average-Power-Ratio* (PAPR) in time domain. Exemplary postfix sequences are presented meeting these requirements.
- The exploitation of PRP-OFDM's pseudo-randomly weighted postfix sequences for time and frequency synchronization refinement is discussed in chapter 5, assuming that an initial synchronization is available based on standard techniques (e.g., [38]). The time synchronization is shown to be improved by performing a cross-correlation of the received PRP-OFDM signal by the deterministic postfix sequence. The frequency offsets are then refined by autocorrelation. Simulation results illustrate the performance of the proposed scheme in context of a frequency selective fading channel.
- Chapter 6 generalizes the PRP-OFDM modulation scheme to the MTMR antennas context: a block based approach is presented introducing orthogonal weighting factors on the different postfix sequences. The approach enables the receiver to estimate the channel impulse responses between any transmit and receive antenna of the system based on postfix sequences only. Two transmit/receiver architectures are derived: one is targeting a transformation of the received signal to ZP-OFDM (applying then known equalization and decoding approaches [39]); the second approach benefits from the diagonalization properties of pseudo-circulant matrices. Simulation results illustrate the system performance for different constellation types (BPSK, QPSK, QAM-16 and QAM-64) and velocities (0m/s to 32m/s at a 5GHz carrier frequency).
- An *Iterative Interference Suppression* (IIS) approach is presented in chapter 7. The idea consists in exploiting decoded OFDM data symbols in order to reduce the interference on PRP-OFDM postfix sequences; this approach helps to improve the channel estimation properties and makes PRP-OFDM applicable to higher-order constellations (QAM-64 and above). Moreover, it is explained

how IIS can be used in order to reduce the observation window length for estimation of the postfix sequences convolved by the propagation channel. This technique helps to further increase the robustness to mobility.

- Chapter 8 complements the PRP-OFDM related study results by considering an optimum use of OFDM in combination with LDPC coding. An adaptive interleaver is derived (assuming CSI to be known) guaranteeing an optimum mapping of LDPC code word bits onto OFDM carriers. The corresponding mapping algorithm mainly requires the sorting of the absolute value of channel coefficients and the degrees of LDPC variable nodes; it is therefore of limited complexity and expected to be applicable in practice: the proposed approach has been presented at the standardization Working Group IEEE802.11n. Simulation results show that the optimized scheme leads to approx. 0.95dB gain in PER performance over a random mapping.
- A final conclusion and further study ideas are presented in chapter 9.

The appendices are organized as follows:

- Appendix A presents a generic proof of the diagonalization properties of pseudo-circulant matrices. This theorem is applied throughout this thesis in order to derive low-complexity PRP-OFDM equalization architectures.
- Appendix B derives biased and unbiased MMSE equalizers for PRP-OFDM.
- Appendix C gives complexity estimates of the proposed PRP-OFDM equalization and channel estimation architectures.
- Appendix D presents several approaches for modeling the time evolution of time-variant propagation channels.
- Appendix E derives a permutation theorem that is useful for time synchronization refinement.
- Appendix F recalls several rules of how to differentiate the trace of complex matrices.



---

## Chapter 2

# Orthogonal Frequency Division Multiplexing

This chapter presents a novel *Orthogonal Frequency Division Multiplexing* (OFDM) based modulation scheme: **Pseudo Random Postfix OFDM** (PRP-OFDM) [1–26]. A time-continuous and time discrete model is presented and compared to the corresponding expressions for the classical *Cyclic-Prefix OFDM* (CP-OFDM) and the recently presented *Zero-Padded OFDM* (ZP-OFDM).

### 2.1 History and recent evolutions of Orthogonal Frequency Division Multiplexing

OFDM is a multi-carrier modulation technique which uses distinct and orthogonal carriers for signal transmission. [45] initially proposed the OFDM principles in 1966 and was granted a corresponding patent in 1970. The original system proposal, however, turned out to be challenging in terms of modulation, synchronization and coherent demodulation as soon as a large number of carriers is used [46]. Based on this observation, [47] proposed a modified modulation approach based on the Discrete Fourier Transform (DFT) in 1971. In order to fight Inter-Block-Interference (IBI), [48] originally proposed the use of a redundant cyclic prefix extension of each OFDM symbol in 1980. Also in 1980, [49] introduced an equalization algorithm for the suppression of Intra-Symbol-Interference (ISI) and IBI which may result from a frequency selective propagation channel, synchronization error or phase error. The same author applied Quadrature-Amplitude-Modulation (QAM) to OFDM sub-carriers, pilot tones and trellis based coding techniques leading to a high-speed OFDM system operating in the voice-band. In 1985, [50] introduced a pilot-based scheme which helps to reduce the interference from multi-path propagation. [51] proposed in 1987 a practical OFDM modulation concept based on the generation of a discrete time domain digital signal followed by a Digital-to-Analog (D/A) conversion. [52] proposed 1989 to allocate more data on the carriers near the DC component in order to increase the throughput. During the 1990s, OFDM was widely applied in standardization: Asynchronous Digital Subscriber Line (ADSL) [53] and ETSI's Digital-Audio-Broadcasting (DAB) [54] were among the first OFDM based standards published in 1993 and 1995 respectively, followed by terrestrial Digital-Video-Broadcasting (DVB-T) [55] in 1996, the WLAN standards IEEE802.11a [56] and ETSI BRAN HIPERLAN/2 [57] in 1999 and others. Later,

this trend continues as illustrated for example by the OFDM based standardization effort on a Multiple-Transmit-Multiple-Receive (MTMR) antennas WLAN system under the pseudonym IEEE802.11n [58] and the European Projects IST-BROADWAY IST-2001-32686 [14–20, 29] and IST-WINNER IST-2003-507581 [21–24, 30]: IST-BROADWAY proposes a hybrid WLAN standard operation at 5GHz and 60GHz; IST-WINNER studies candidate air interfaces for future (4<sup>th</sup> generation) mobile communication systems preparing a corresponding standardization phase.

All these standards are based on the classical CP-OFDM modulation scheme which was subject to further studies during recent years: to give a few examples, [59] introduced an efficient *Weighted Sub-Band Adaptive Filtering* (WSAF) algorithm, [60, 61] studied the use of *Linear Precoding* (LP) techniques in the framework of *Spread Spectrum OFDM* (SS-OFDM) [62] in order to increase the frequency diversity. Multi-User access schemes were proposed in the framework of *Multi-Carrier CDMA* (MC-CDMA) [63–65] and *Orthogonal Frequency Division Multiple Access* (OFDMA) [66, 67]. [68, 69] consider the so-called *Isotropic Orthogonal Transform Algorithm OFDM* (IOTA-OFDM) where any prefix/postfix sequence can be omitted due to a particular shape of the sub-band signals in both time and frequency domain. A comparison in a common framework of different OFDM schemes has recently been presented in [9].

More recently, it was proposed to replace the cyclic extension of CP-OFDM by a zero padding sequence of same duration leading to *Zero-Padded OFDM* (ZP-OFDM) [39, 40, 70–76]. It turns out that this modifications still permits to recover carriers even if they coincide with channel nulls. Moreover, the receiver may choose among a variety of decoding and equalization approaches with different performance/complexity trade-offs [39].

In the framework of this thesis, it is proposed to replace the Zero Padded sequence of ZP-OFDM by a pseudo-randomly weighted, deterministic sequence known to both the transmitter (TX) and receiver (RX). This allows to keep the advantages of ZP-OFDM and moreover, the deterministic part can be exploited for channel estimation and synchronization refinement without the typical overhead in terms of learning symbols and pilot tones. The novel modulation scheme is entitled *Pseudo Random Postfix OFDM* (PRP-OFDM) and is of advantage over known schemes if the system requires i) a minimum pilot overhead, ii) low-complexity channel tracking (e.g. a IEEE802.11a like system in a high mobility context) and iii) adjustable receiver complexity/performance trade-offs. The PRP-OFDM concept has been validated on an FPGA based prototyping platform operating at 5GHz and 60GHz [11].

Note that a constant prefix/postfix has been proposed in both, the single carrier [77] and multi-carrier [78] context, but neither exploitation of this known sequence nor more advanced than classical equalization schemes are proposed. Moreover spectrum wise, it is important to avoid i) highly variable carrier amplitudes and ii) the insertion of the same training sequence at each block since the repetition generates peaks in the transmitted signal spectrum. The pseudo-randomly weighted sequence proposed in this thesis avoids this issue [6].

The following sections will illustrate the CP-OFDM, ZP-OFDM and PRP-OFDM transceiver architectures, first in a continuous representation based on filter banks; then, a discrete digital representation is derived.

## 2.2 Filter-Bank based representation of Orthogonal Frequency Division Multiplexing and definition of Pseudo Random Postfix OFDM

The continuous representation of the CP-OFDM synthesis filter bank representation is discussed in detail in [79]. In the following, these definitions are briefly recalled and extended to the framework of PRP-OFDM (and ZP-OFDM).

### 2.2.1 Definition of the CP-OFDM modulator

Define the constellation symbols to be transmitted as  $\tilde{s}_k(n)$ ,  $k = 0, \dots, K-1$ ,  $n \in \mathbb{Z}$ . They are modulated onto  $K$  parallel and distinct sub-channels by shaping filters  $g_k(t)$ ,  $k = 0, \dots, K-1$  which form an orthogonal basis [80];  $g'_k(t)$  are cyclically extended versions of the shaping filters  $g_k(t)$  and will be discussed below. As illustrated by Fig. 2.1, the transmitted time domain signal  $u(t)$  of the CP-OFDM modulator is the sum of the filtered data symbols:

$$u(t) := \sum_{k \in \mathbb{Z}} \sum_{n=0}^{N-1} \tilde{s}_n(k) g'_n(t - kT_B) \quad (2.1)$$

$T_B$  is the duration of one OFDM symbol block.

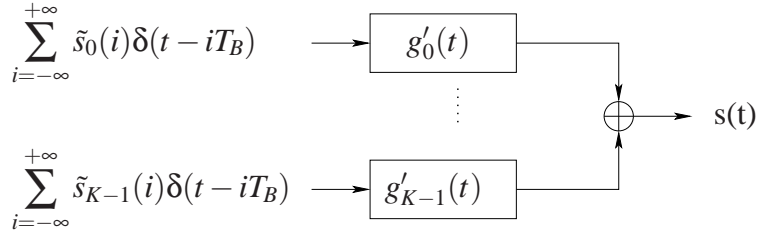


Figure 2.1: Continuous CP-OFDM modulator.

We define  $T_{cp}$  to be the duration of the Guard Interval and  $T_g = T_B - T_{cp}$ . In traditional OFDM systems, the filters  $g_n(t)$  and their extended versions  $g'_n(t)$  are chosen to be

$$g_n(t) := \frac{1}{\sqrt{T_g}} \text{Rect}_{T_g}(t) e^{2j\pi \frac{nt}{T_g}} \quad (2.2)$$

$$g'_n(t) := \frac{1}{\sqrt{T_g}} \text{Rect}_{T_B}(t) e^{2j\pi \frac{n(t-T_{cp})}{T_g}} \quad (2.3)$$

where  $\text{Rect}_T(t)$  is the window function of duration  $T$ :

$$\text{Rect}_T(t) := \begin{cases} 1 & 0 \leq t < T \\ 0 & \text{otherwise.} \end{cases} \quad (2.4)$$

It is straightforward from (2.2) and (2.3) to prove that the  $g'_n(t)$  and  $g_n(t)$  function basis meet the orthogonality constraints for  $0 \leq \Delta T \leq T_{cp}$ :

$$\int_{-\infty}^{+\infty} g'_n(t - kT_B) g_{n'}^*(t - k'T_B - \Delta T) dt = \delta_{n,n'} \delta_{k,k'} e^{2j\pi \frac{n'(\Delta T - T_{cp})}{T_g}},$$

where  $\delta_{k,k'}$  is the Kronecker symbol defined as

$$\delta_{i,j} := \begin{cases} 1 & \text{for } i = j; \\ 0 & \text{otherwise.} \end{cases}$$

## 2.2.2 Definition of the PRP-OFDM modulator

It will be shown in section 2.3.3 that the cyclic extension (or guard interval (GI)) of the CP-OFDM scheme leads to simple equalization approaches in the presence of a frequency selective fading channel. However, the GI contains redundant data and thus reduces the spectral efficiency of the system. This observation motivates the proposal of a new OFDM modulator which will be defined and studied in the framework of this thesis: the Pseudo-Random-Postfix OFDM (PRP-OFDM). The idea consists in replacing the (redundant) cyclic extension of CP-OFDM by a deterministic sequence of same power and duration (i.e. the spectral efficiency does not change); it will be shown that this sequence leads to several equalization trade-offs in terms of complexity/performance and it furthermore enables the receiver to estimate and track the channel impulse response in a static and mobility context at a low arithmetical complexity. The new scheme thus keeps the basic advantages of the classical CP-OFDM and adds means of simple channel estimation avoiding the typically required overhead in terms of pilot tones and learning symbols [1, 7].

The upper definitions are straightforwardly extended to the case of PRP-OFDM as illustrated by Figure 2.2; the transmitted time domain signal  $u(t)$  of the PRP-OFDM modulator is the sum of the filtered data symbols plus the deterministic and pseudo-randomly weighted postfix sequence  $p(t) = \sum_{i \in \mathbb{Z}} \alpha(i) p_s(t - iT_B)$ :

$$u(t) = \sum_{i \in \mathbb{Z}} \left[ \alpha(i) p_s(t - iT_B) + \sum_{k=0}^{K-1} \tilde{s}_k(i) g_k(t - iT_B) \right]$$

The block duration of a PRP-OFDM symbol including (excluding) its postfix is defined to be  $T_B$  ( $T_g$ ). PRP-OFDM symbol block  $i$  has one postfix  $p_s(t)$  attributed to it; it is weighted by a pseudo-random scalar  $\alpha(i) \in \mathbb{C}$  known to both the transmitter and the receiver [6]. In the framework of this document, all  $\alpha(i)$  are assumed to be a pure phase, i.e.  $\alpha(i) = e^{j\phi_{\alpha}(i)}$ .

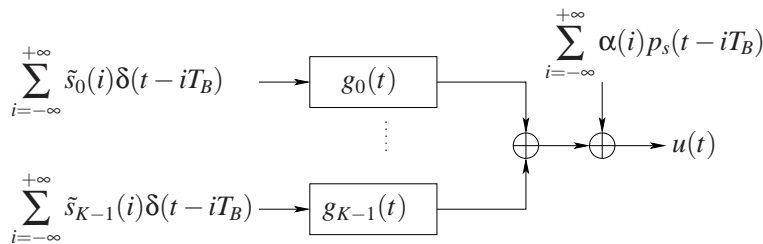


Figure 2.2: Continuous PRP-OFDM modulator.

Furthermore, the postfix sequence  $p_s(t)$  is usually chosen to be non-overlapping with the OFDM data symbols:  $p_s(t < T_g) = 0$  and  $p_s(t > T_B) = 0$ . See chapter 4 for details on the choice and design of postfix sequences. The expressions for ZP-OFDM are obtained by setting  $p_s(t) = 0 \forall t$ .

The corresponding frequency domain signal is obtained by a continuous Fourier transformation, denoted in the following as  $\mathcal{F}\{\cdot\}$ . Defining  $*$  as the convolution operator and with  $\text{sinc}(t) = \frac{\sin(\pi t)}{\pi}$ ,  $\mathcal{F}\{u(t)\}$  is given by

$$\tilde{u}(f) = \mathcal{F}\{u(t)\} = \sum_{i \in \mathbb{Z}} \left[ \alpha(i) \mathcal{F}\{p_s(t)\} e^{-2j\pi i T_B f} + \sum_{k=0}^{K-1} \tilde{s}_k(i) \delta(f - k/T_g) * [\sqrt{T_g} e^{-2j\pi i T_B f} \text{sinc}(T_g f)] \right] \quad (2.5)$$

The CP-OFDM signal is obtained from (2.5) by omitting the postfix related part and by replacing  $T_B$  by  $T_s$  in the remaining equation. The sub-carrier distance is  $T_g^{-1}$ . The synthesis of the PRP-OFDM signal is thus defined and the following sections derives the discrete time expressions of the sampled signal in the receiver.

## 2.3 Discrete representation of the sampled signal in the receiver

The reconstruction of the data symbols is first studied in the context of a channel impulse response (CIR) corresponding to a Dirac function  $c(t) = \delta(t)$  and assuming that no additive noise is present. In the subsequent sections these results are extended to the context of a multi-path channel.

### 2.3.1 Symbol reconstruction in absence of a channel

The sampling period in the receiver is assumed to be  $T$  with  $NT = T_g, N \in \mathbb{N}, T \leq \frac{T_g}{K}$ .  $P := \frac{T_g}{T}$  is the total number of samples in one PRP-OFDM symbol block  $k$ :

$$u_n(k) := u(kT_B + nT) = u[(kP + n)T], \quad 0 \leq n < P. \quad (2.6)$$

With these observations, the samples in the receiver are:

$$u_n(k) := \sum_{i \in \mathbb{Z}} \sum_{m=0}^{K-1} \tilde{s}_m(i) g_m[(k-i)PT + nT] + \sum_{i \in \mathbb{Z}} \alpha(i) p_s[(k-i)PT + nT]. \quad (2.7)$$

For a more useful representation, let us define

$$\begin{aligned} g_m^{(l)}(z) &:= \sum_{n \in \mathbb{Z}} g_m[(nP + l)T] z^{-n}, \quad 0 \leq l < P \\ \mathbf{G}(z) &:= \left[ g_m^{(l)}(z) \right]_{0 \leq l < P, 0 \leq m < K} \\ p^{(l)}(z) &:= \sum_{n \in \mathbb{Z}} p_s[(nP + l)T] z^{-n}, \quad 0 \leq l < P \end{aligned} \quad (2.8)$$

and define  $\text{TZ}[x_n] := \sum_{n \in \mathbb{Z}} x_n z^{-n}$  as the  $z$  transformation of any sequence  $(x_n)_{n \in \mathbb{Z}}$ . This allows to define  $s_n(z)$  as follows:

$$\begin{aligned} u_n(z) &:= \text{TZ}[u_n(k)] = \sum_{k \in \mathbb{Z}} u_n(k) z^{-k}, \\ \tilde{s}_n(z) &:= \text{TZ}[\tilde{s}_n(k)] = \sum_{k \in \mathbb{Z}} \tilde{s}_n(k) z^{-k} \text{ and} \\ \alpha(z) &:= \text{TZ}[\alpha(n)] = \sum_{n \in \mathbb{Z}} \alpha(n) z^{-n} \end{aligned}$$

$$\begin{aligned} u_n(z^P) &= \sum_{k \in \mathbb{Z}} u_n(k) z^{-kP} \\ &= \sum_{m=0}^{K-1} \sum_{i \in \mathbb{Z}} \tilde{s}_m(i) \sum_{k \in \mathbb{Z}} g_m[(k-i)PT + nT] z^{-kP} + \\ &\quad \sum_{i \in \mathbb{Z}} \alpha(i) \sum_{k \in \mathbb{Z}} p_s[(k-i)PT + nT] z^{-kP} \\ &= \sum_{i \in \mathbb{Z}} \sum_{m=0}^{K-1} \tilde{s}_m(i) z^{-iP} g_m^{(n)}(z^P) + \\ &\quad \sum_{i \in \mathbb{Z}} \alpha(i) z^{-iP} p^{(n)}(z^P) \\ &= \sum_{m=0}^{K-1} g_m^{(n)}(z^P) \tilde{s}_m(z^P) + \alpha(z^P) p^{(n)}(z^P) \\ &= \left[ g_0^{(n)}(z^P), \dots, g_{K-1}^{(n)}(z^P) \right] \tilde{\mathbf{s}}(z^P) + \alpha(z^P) p^{(n)}(z^P) \end{aligned}$$

where  $\tilde{\mathbf{s}}(z) := [\tilde{s}_0(z), \dots, \tilde{s}_{N-1}(z)]^T = \text{TZ}[\tilde{\mathbf{s}}(n)]$ . With  $\mathbf{u}(z) := [u_0(z), \dots, u_{N-1}(z)]^T = \text{TZ}[\mathbf{u}(n)]$  and  $\mathbf{p}(z) := \alpha(z) [p^{(0)}(z), \dots, p^{(P-1)}(z)]^T$  this proves that

$$\mathbf{u}(z) := [u_0(z), \dots, u_{P-1}(z)]^T = \mathbf{G}(z) \tilde{\mathbf{s}}(z) + \mathbf{p}(z). \quad (2.9)$$

The actually transmitted sequence is thus as illustrated in Fig.2.3:

$$u(z) := (1, z^{-1}, \dots, z^{-P+1}) \mathbf{u}(z^P). \quad (2.10)$$

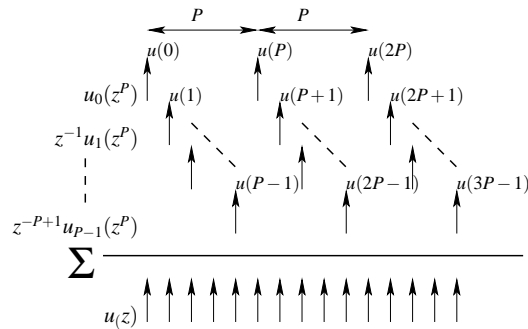


Figure 2.3: Illustration of the synthesis of  $u(z)$  based on its polyphase components

The contributions of the OFDM data symbols  $s(z)$  and of the postfix  $p(z)$  are extracted as follows with  $D = P - N$ :

$$s(z) := (1, z^{-1}, \dots, z^{-N+1}, 0, \dots, 0) \mathbf{u}(z^N), \quad (2.11)$$

$$p(z) := (0, \dots, 0, 1, z^{-1}, \dots, z^{-D+1}, \dots) \mathbf{u}(z^D), \quad (2.12)$$

The corresponding expressions for the digital filters of the synthesis filter bank are

$$g_m(z) := \sum_{l=0}^{N-1} g_m^{(l)}(z^P) z^{-l}, \quad 0 \leq m < K. \quad (2.13)$$

One way to model the digital synthesis of the signal  $s(z)$  is to use a polyphase matrix expression by filtering  $\tilde{\mathbf{s}}(z)$  by  $\mathbf{G}(z)$ ; in other words, the filter bank associated with  $\mathbf{G}(z)$  is applied whose filters are defined as  $g_m(z) = \sum_{l=0}^{N-1} g_m^{(l)}(z^N) z^{-l}$ . In the literature [81], the following notations are used:

- $\mathbf{G}(z)$  is the polyphase matrix [81] associated with the synthesis filter bank that is used for the modulation;
- $g_m(z)$  is the  $m^{\text{th}}$  filter of the synthesis filter bank;
- $g_m^{(l)}(z)$  is the  $l^{\text{th}}$  polyphase component of type I of  $g_m(z)$ .

Assuming that the filter bank consists of frequency shifted rectangular window functions as defined in (2.2) and (2.3), the polyphase components  $g_m^{(l)}(z)$  coincide with the coefficients of a size  $N \times N$  inverse Fourier matrix: with (2.8),  $g_m^{(l)}(z)$  is thus

$$g_m^{(l)}(z) := \begin{cases} \frac{1}{\sqrt{N}} \sum_{n \in \mathbb{Z}} e^{j \frac{2\pi}{N} ml} z^{-n} & 0 \leq l < N, 0 \leq m < N \\ 0 & \text{otherwise} \end{cases} \quad (2.14)$$

In the context of this thesis, equation (2.14) is assumed to be verified for all CP-OFDM, ZP-OFDM and PRP-OFDM modulator designs.

The CP-OFDM case is straightforwardly obtained by i) omitting the zeros sequence in (2.11), ii) omitting the postfix contribution (2.12) and iii) by replacing  $P$  in (2.13) by  $N$ . The final expression is thus  $s^{\text{CP}}(z) := [g_0(z), \dots, g_{K-1}(z)] \tilde{\mathbf{s}}(z^N)$ .

The following section introduces the convolution by the system filters and propagation channel. After these definitions, the analysis of the PRP-OFDM system in the context of synchronization offsets will be straightforward.

### 2.3.2 Symbol reconstruction in presence of multi-path propagation

By now, the propagation channel was neglected in the analysis of the received signal; thus, this section extends the preceding results to the presence of a frequency selective channel given by the CIR  $c(t)$ . The

signal to be sampled in the receiver is then no longer  $u(t)$ , but  $r(t) := c(t) * u(t)$ . Since the need for a vector model of the propagation channel is obvious, consider the polyphase type I components of the output signal  $r_k(z) := \sum_{i \in \mathbb{Z}} r[(iP+k)T]z^{-i}$ ,  $k = 0, \dots, P-1$  of the linear convolution of  $u(z)$  by the CIR as illustrated in figure 2.4.

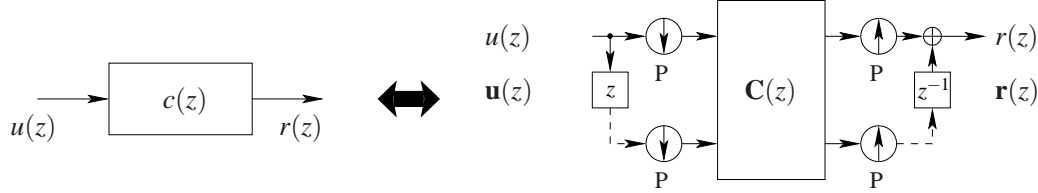


Figure 2.4: Equivalence between a linear scalar filter and the representation as polyphase sub-band filtering.

With  $c_k(z) := \sum_{i \in \mathbb{Z}} c[(iP+k)T]z^{-i}$ ,  $k = 0, \dots, P-1$ ,  $r(z)$  and  $c(z)$  are defined as follows:

$$r(z) := \sum_{k=0}^{P-1} r_k(z^P)z^{-k},$$

$$c(z) := \sum_{k=0}^{P-1} c_k(z^P)z^{-k}$$

The linear convolution results in

$$\begin{aligned} r(z) &= c(z)u(z) \\ &= \sum_{k,k' \in \mathbb{N}_p^2} u_k(z^P)c_{k'}(z^P)z^{-k-k'} \end{aligned} \quad (2.15)$$

and the polyphase components of  $r(z)$  are

$$r_l(z) := \sum_{k=0}^l u_k(z)c_{l-k}(z) + \sum_{k=l+1}^{P-1} u_k(z)c_{P+l-k}(z), \quad 0 \leq l < P$$

which corresponds to the following matrix representation:

$$\mathbf{r}(z) = \underbrace{\begin{bmatrix} c_0(z) & z^{-1}c_{P-1}(z) & \cdots & z^{-1}c_2(z) & z^{-1}c_1(z) \\ c_1(z) & c_0(z) & \searrow & & z^{-1}c_2(z) \\ \vdots & & \searrow & \searrow & \vdots \\ \vdots & & & \searrow & z^{-1}c_{P-1}(z) \\ c_{P-1}(z) & c_{P-2}(z) & \cdots & c_1(z) & c_0(z) \end{bmatrix}}_{\mathbf{C}(z)} \mathbf{u}(z) \quad (2.16)$$

The matrix  $\mathbf{C}(z)$  is of dimension  $P \times P$ ,  $\mathbf{r}(z) := [r_0(z), \dots, r_{P-1}(z)]^T$  and  $\mathbf{u}(z) := [u_0(z), \dots, u_{P-1}(z)]^T$ .

Assuming that the channel order  $L$  is smaller than the postfix length  $D$ , the matrix  $\mathbf{C}(z)$  leads to the following simplified expression:

$$\mathbf{C}(z) := \mathbf{C}_{\text{ISI}}(P) + z^{-1}\mathbf{C}_{\text{IBI}}(P) \quad (2.17)$$

where  $\mathbf{C}_{\text{ISI}}(P)$  and  $\mathbf{C}_{\text{IBI}}(P)$  are the following Toeplitz matrices of dimension  $P \times P$ :

$$\mathbf{C}_{\text{ISI}}(P) := \begin{bmatrix} c_0 & 0 & \rightarrow & \rightarrow & \rightarrow & 0 \\ \vdots & \searrow & \searrow & & & \downarrow \\ c_D & & \searrow & \searrow & & \downarrow \\ 0 & \searrow & & \searrow & \searrow & \downarrow \\ \downarrow & \searrow & \searrow & & \searrow & 0 \\ 0 & \rightarrow & 0 & c_D & \cdots & c_0 \end{bmatrix}, \quad (2.18)$$

$$\mathbf{C}_{\text{IBI}}(P) := \begin{bmatrix} 0 & \rightarrow & 0 & c_D & \cdots & c_1 \\ \downarrow & \searrow & & \searrow & \searrow & \vdots \\ \downarrow & & \searrow & & \searrow & c_D \\ \downarrow & & & \searrow & & 0 \\ \downarrow & & & & \searrow & \downarrow \\ 0 & \rightarrow & \rightarrow & \rightarrow & \rightarrow & 0 \end{bmatrix} \quad (2.19)$$

Figure 2.5 illustrates why it is important to impose the channel order to be inferior to the postfix duration:

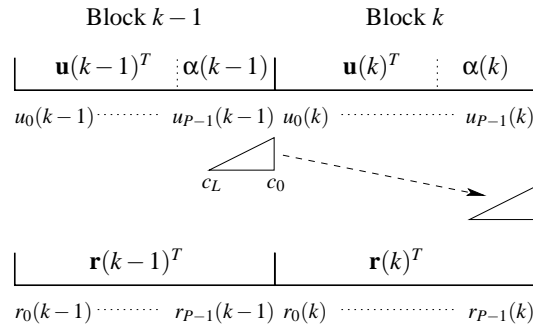


Figure 2.5: Illustration of Inter-Block-Interference.

The postfix plays a similar role as the guard interval of CP-OFDM systems and allows to represent the channel convolution as a multiplication of a pseudo-circulant channel matrix (see Appendix A) with  $\beta_i := \frac{\alpha(i-1)}{\alpha(i)}$ : instead of presenting the channel convolution as multiplication of  $(\mathbf{C}_{\text{ISI}}(P) + z^{-1}\mathbf{C}_{\text{IBI}}(P))$  by  $\mathbf{u}(z)$ , the channel matrix is substituted by  $(\mathbf{C}_{\text{ISI}}(P) + \beta_i\mathbf{C}_{\text{IBI}}(P))$  to be multiplied by a vector containing PRP-OFDM symbol  $i$  and the corresponding postfix. Like this, the inter-dependency between neighboring blocks is eliminated (i.e. there is no IBI present) and the equalization is greatly simplified (see chapter 3).

### 2.3.3 Discrete Transceiver Architectures

Following the upper definitions, the global transceiver architecture of a CP-OFDM system is illustrated by Fig. 2.6. The  $k^{\text{th}}$   $N \times 1$  input digital vector  $\tilde{\mathbf{s}}_N(k)$  is first modulated by the IFFT matrix  $\mathbf{F}_N^{\text{H}} := \frac{1}{\sqrt{N}}(W_N^{nm})^{\text{H}}$ ,  $0 \leq n < N$ ,  $0 \leq m < N$  and  $W_N := e^{-j\frac{2\pi}{N}}$ . Then, the guard interval is added by cyclicly

repeating the last  $D$  samples prior to the data symbol. With

$$\mathbf{F}_{\text{CP}}^{\text{H}} := \left[ \begin{array}{c|c} \mathbf{0}_{D,N-D} & \mathbf{I}_D \\ \hline & \mathbf{I}_N \end{array} \right]_{P \times N} \mathbf{F}_N^{\text{H}}.$$

the transmitted symbol is

$$\mathbf{s}^{\text{ig}}(k) := \mathbf{F}_{\text{CP}}^{\text{H}} \tilde{\mathbf{s}}_N(k) \quad (2.20)$$

The role of the cyclic prefix is to turn the linear convolution into a set of parallel attenuations in the discrete frequency domain.  $\mathbf{s}^{\text{ig}}(k)$  is then sent sequentially through the channel modeled here as an FIR filter of order  $L$ ,  $c(z) = \sum_{n=0}^L c_n z^{-n}$ . The OFDM system is designed such that the postfix duration exceeds the channel memory  $L < D$ . As already explained in [80], after guard interval suppression the received signal can be expressed as

$$\begin{aligned} \mathbf{r}_N(k) &:= \mathbf{C}_{\text{ISI}}(N) \mathbf{s}_N(k) + \mathbf{C}_{\text{IBI}}(N) \mathbf{s}_N(k-1) + \mathbf{n}_N(k) \\ &= \mathbf{C}_{\text{CIRC}}(N) \mathbf{s}_N(k) + \mathbf{n}_N(k) \\ &= \mathbf{F}_N^{\text{H}} \text{diag}\{\tilde{c}_0, \dots, \tilde{c}_{N-1}\} \tilde{\mathbf{s}}_N(k) + \tilde{\mathbf{n}}_N(k) \end{aligned} \quad (2.21)$$

Here,  $\mathbf{C}_{\text{CIRC}}(N) = \mathbf{C}_{\text{ISI}}(N) + \mathbf{C}_{\text{IBI}}(N)$  is a circulant matrix that is diagonalized on a Fourier basis and  $\mathbf{C}_{\text{ISI}}(N)$  and  $\mathbf{C}_{\text{IBI}}(N)$  represent respectively the intra and inter block interference.  $\mathbf{n}_N(k)$  is the  $k$ th AWGN vector of element variance  $\sigma_n^2$ ,  $[\tilde{c}_0, \dots, \tilde{c}_{N-1}]^T := \mathbf{F}_N \mathbf{c}_N$  and  $\tilde{\mathbf{n}}_N = \mathbf{F}_N \mathbf{n}_N = [\tilde{n}_0, \dots, \tilde{n}_{N-1}]^T$ . The main feature of OFDM becomes visible in equation (2.21): the channel convolution translates to distinct multiplicative coefficients in the discrete frequency domain; no inter-symbol-interference is present. Thus, the OFDM transceiver architecture can alternatively be represented by the parallel model illustrated in Fig.2.7.

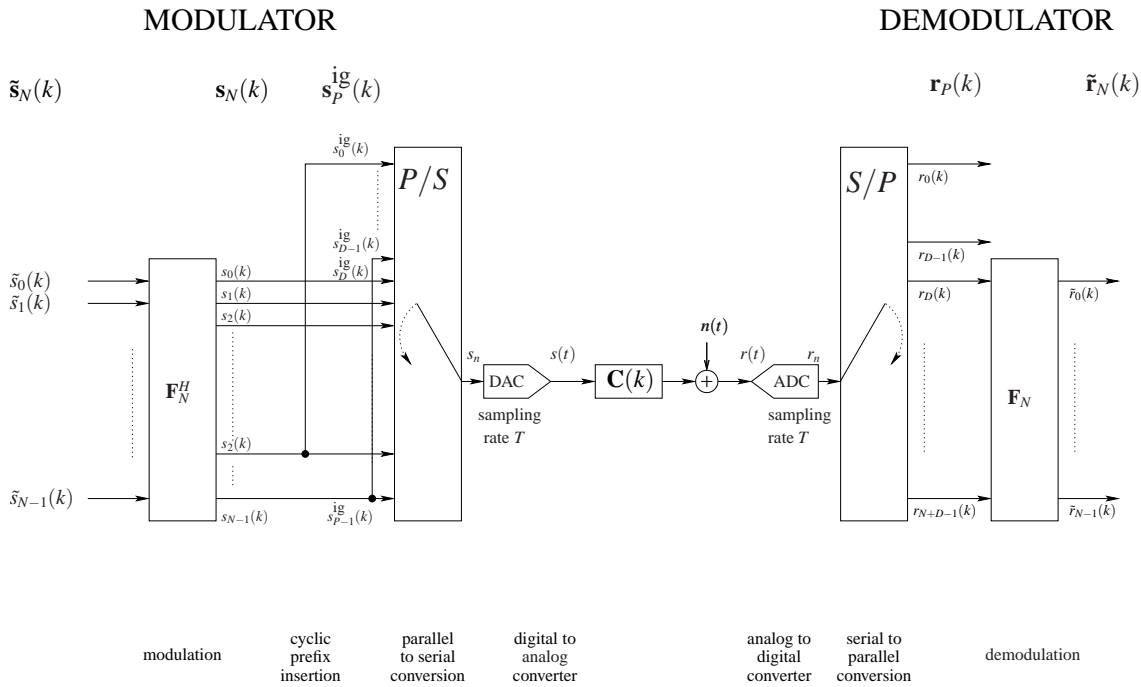


Figure 2.6: Discrete model of the CP-OFDM transceiver.

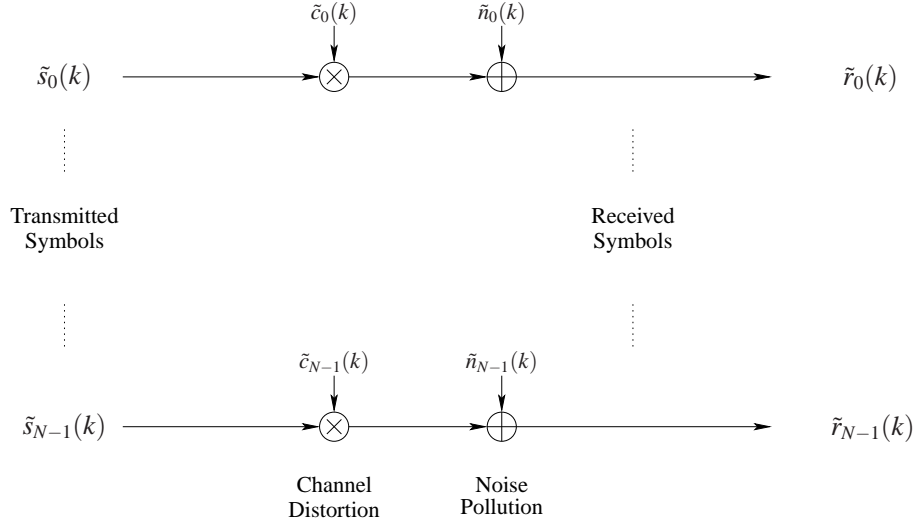


Figure 2.7: Parallel frequency domain representation of CP-OFDM.

A PRP-OFDM transceiver is illustrated in Fig.2.8. Instead of adding a cyclic prefix extension as shown above, a pseudo randomly weighted, deterministic postfix sequence follows each OFDM data symbol:

$$\mathbf{s}_P(k) := \mathbf{F}_{ZP}^H \tilde{\mathbf{s}}_N(k) + \alpha(k) \mathbf{p}_P$$

with  $P := N + D$ ,  $\mathbf{p}_P := (\mathbf{0}_{1,N} \mathbf{p}_D^T)^T$  and  $\mathbf{p}_D$  contains the postfix sequence samples. The expression of the received block is thus:

$$\begin{aligned} \mathbf{r}_P(k) &:= \mathbf{C}_{\beta_k} (\mathbf{F}_{ZP}^H \tilde{\mathbf{s}}_N(k) + \alpha(k) \mathbf{p}_P) + \mathbf{n}_P(k) \\ &= \mathbf{C}_{\beta_k} \begin{pmatrix} \mathbf{F}_N^H \tilde{\mathbf{s}}_N(k) \\ \alpha(k) \mathbf{p}_D \end{pmatrix} + \mathbf{n}_P(k) \end{aligned}$$

Hereby,  $\mathbf{C}_{\beta_k} := \mathbf{C}_{ISI}(P) + \beta_k \mathbf{C}_{IBI}(P)$ ,  $\alpha(k)$  is the pseudo-random weighting factor,  $\mathbf{n}_P$  contains the Gaussian noise contributions and  $\beta_k = \frac{\alpha(k-1)}{\alpha(k)}$ . Note that  $\mathbf{C}_{\beta_k}$  is diagonalized on a new basis which is different, but still similar to the Fourier basis as derived in annex A. The actual choice of the postfix sequence is discussed in chapter 4.

Since the postfix sequence and the CP-OFDM guard interval are of same power and duration as the guard interval of CP-OFDM, a higher spectral efficiency can be obtained; in particular, the typical overhead in terms of learning symbols and pilot tones for CP-OFDM is avoided.

The ZP-OFDM transceiver architecture follows from the PRP-OFDM representation by setting the postfix sequence to an all-zero vector as illustrated by Fig.2.9.

The corresponding discrete modulator is thus expressed as follows:

$$\begin{aligned} \mathbf{F}_{ZP}^H &:= \begin{bmatrix} \mathbf{I}_N \\ \mathbf{0}_{D,N} \end{bmatrix}_{P \times N} \mathbf{F}_N^H \\ \mathbf{s}_P(k) &:= \mathbf{F}_{ZP}^H \tilde{\mathbf{s}}_N(k) \end{aligned} \quad (2.22)$$

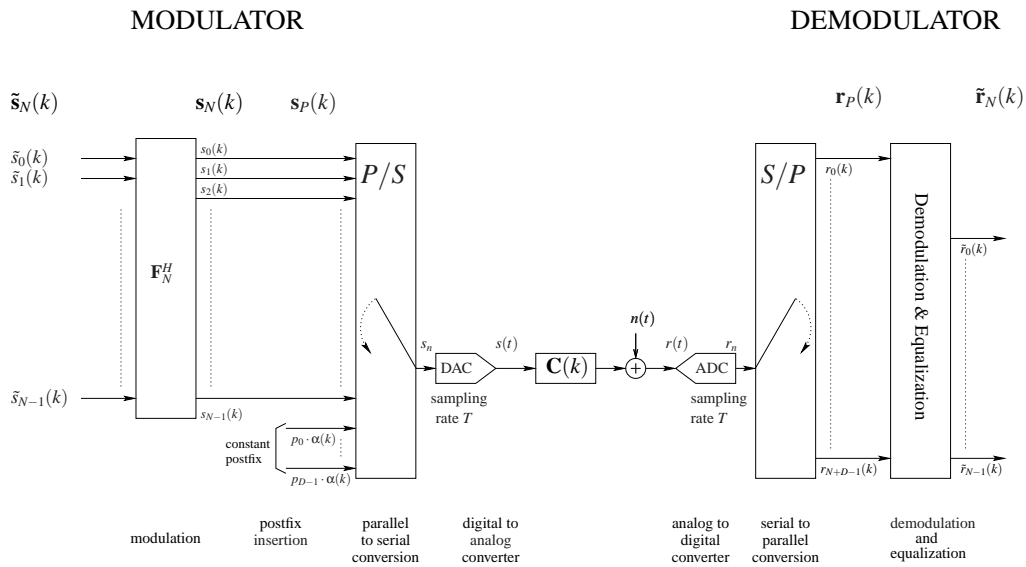


Figure 2.8: Discrete model of the PRP-OFDM transceiver.

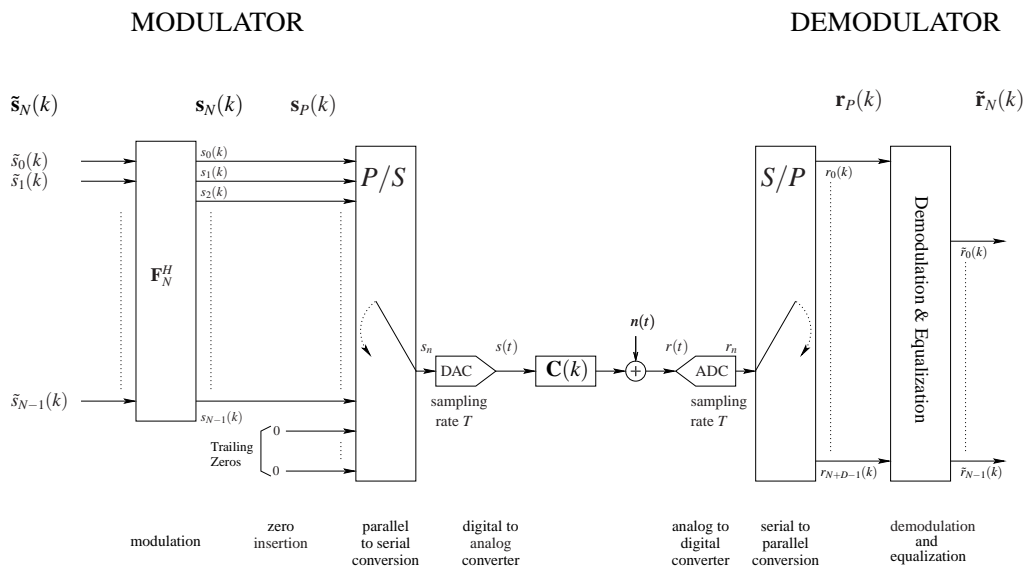


Figure 2.9: Discrete model of the ZP-OFDM transceiver.

With these definitions, it is straightforward to model the impact of synchronization offsets as it will be shown in the following sections.

## 2.4 Impact of synchronization impairments

This section derives the expressions of the received signal in the presence of synchronization offsets and indicates how the impairment correction can be performed in a typical receiver implementation. The considered offsets are: i) frequency offset, i.e. the received frequency domain signal is  $\tilde{u}(f - f_0)$  instead of  $\tilde{u}(f)$  as given by equation (2.5), ii) time offset, i.e. the received time domain signal is  $u(t - t_0)$  instead of  $u(t)$  and iii) sampling frequency offsets.

### 2.4.1 Frequency offset

In the presence of a frequency offset  $f_0$ , usually introduced by an offset of the reference clock in the RF front-ends, the received frequency domain signal is  $\tilde{r}(f - f_0)$  and the corresponding time domain signal is thus  $[r(t)]_{\Delta F} := \mathcal{F}^{-1}\{\tilde{r}(f - f_0)\} = \mathcal{F}^{-1}\{\tilde{r}(f)\}e^{j2\pi f_0 t}$ . The sampled expressions available in the receiver are now different from (2.6):

$$\begin{aligned} [r_n(k)]_{\Delta F} &:= r(kT_B + nT)e^{j2\pi f_0(kT_B + nT)}, \quad 0 \leq n < P \\ &= r[(kP + n)T]e^{j2\pi f_0(kP + n)T}. \end{aligned} \quad (2.23)$$

It is obvious that expression (2.23) is transformed to  $u_n(k)$  as given by (2.6) by

$$r_n(k) = [r_n(k)]_{\Delta F} e^{-j2\pi f_0(kP + n)T}$$

Thus, any frequency offset is straightforwardly corrected after the estimation of  $f_0$  which is usually performed based on preambles or training symbols.

Please note that the frequency offset is defined as the difference of the receiver clock frequency compared to the transmitter clock frequency. It does not make sense to introduce *two* frequency offsets, one for the offset in the transmitter and one for the offset in the receiver compared to the desired carrier frequency.

### 2.4.2 Time Offset

In the case that a time offset  $t_0$  remains in the receiver after an initial synchronization, the sampled signal in the receiver is

$$\begin{aligned} r_{\Delta T,k}(z) &:= \sum_{i \in \mathbb{Z}} r_{\Delta T}[(iP + k)T]z^{-i}, \\ r_{\Delta T}(t) &:= r(t - t_0) \\ &= \mathcal{F}^{-1}\{e^{-2j\pi f t_0} \mathcal{F}\{r(t)\}\} \end{aligned} \quad (2.24)$$

With  $r(t) = c(t) * u(t)$ ,  $r_{\Delta T}(t)$  is rewritten as

$$\begin{aligned} r_{\Delta T}(t) &:= \mathcal{F}^{-1} \left\{ e^{-2j\pi f t_0} \mathcal{F} \{ c(t) * u(t) \} \right\} \\ &= \mathcal{F}^{-1} \left\{ e^{-2j\pi f t_0} \mathcal{F} \{ c(t) \} \mathcal{F} \{ u(t) \} \right\} \\ &= \underbrace{\mathcal{F}^{-1} \left\{ e^{-2j\pi f t_0} \mathcal{F} \{ c(t) \} \right\}}_{=c_{\Delta T}(t)} * u(t) \end{aligned}$$

Consequently, equation (2.15) must be adapted in order to obtain the received sampled signal:

$$\begin{aligned} r_{\Delta T}(z) &:= c(z)_{\Delta T} u(z) \\ &= \sum_{k, k' \in \mathbb{N}_p^2} u_k(z^P) c_{\Delta T, k'}(z^P) z^{-k-k'} \end{aligned}$$

with  $c_{\Delta T, k}(z) = \sum_{i \in \mathbb{Z}} c_{\Delta T}[(iP+k)T] z^{-i}$ ,  $k = 0, \dots, P-1$ . It is thus obvious that a time offset can be modeled by a time shift in the CIR:  $c(t)$  is replaced by  $c_{\Delta T}(t)$ . If this modified CIR is estimated by a PRP-OFDM postfix based estimation technique, e.g. as presented in [4], any suitable equalization procedure will inherently correct the time offset assuming that the CIR convolution is still represented as given by (2.18) and (2.19) with the time shifted channel coefficients. The latter remark imposes two important constraints on the time offset which are possible to be corrected:

1. The time offset must be strictly positive, i.e.  $t_0 \geq 0$ . Otherwise, IBI from the previous OFDM data symbol is introduced onto the latest signal to be decoded. Moreover, the last samples of the current sequence will be missing.
2. The length of the CIR plus the maximum time offset to be tolerated must be smaller than the postfix duration. Similar constraints are imposed for CP-OFDM systems with respect to the guard interval size.

While this section has shown that fixed time offsets are inherently covered by PRP-OFDM based CIR estimation, in the sequel *time varying* time offsets are considered which usually occur due to offsets in the sampling clock frequency.

### 2.4.3 Sampling frequency offset

Let us assume that the offset in the sampling frequency  $f_{s,0}$  is small enough to be negligible over the mean-value window used for PRP-OFDM based channel estimation as defined in [4]. In this case, the sampling frequency offset leads to a time dependent *time offset* over long frames as discussed in section 2.4.2 and is inherently covered by the channel estimates when performed for each OFDM symbol separately. Again, the corresponding time offset is corrected by any equalization performed on these channel estimates.

Please note here the difference to legacy CP-OFDM systems [38, 79]: in the presence of sampling clock offsets, it is usually required to estimate the resulting linear phase in frequency domain based on several pilot tones (at least two). The phase correction requires a (different) complex multiplication on each carrier. This difference should be taken into account when comparing the decoder complexity of PRP-OFDM and CP-OFDM systems.

## 2.5 Strengths and weaknesses of OFDM

OFDM based system architectures have proven to be of advantage compared to traditional digital modulation schemes, such as single-carrier (SC) based approaches, in various contexts and in particular in presence of multi-path channels of large delay spread. However, OFDM also has inherent disadvantages which make it not always the preferable choice: a recent example is the choice of OFDM for terrestrial DVB [55] in contrast to SC which was the final choice for satellite DVB [82] due to its inherent small channel delay spreads.

This section will list and comment some strengths of OFDM as well as corresponding weaknesses. In most cases, an indicative comparison to SC based systems is given. The main strengths of OFDM are resumed in the following:

1. In the context of CP-OFDM, a multi-path channel is transformed into a set of parallel attenuations in the discrete frequency domain. Corresponding equalization algorithms only require one complex multiplication per sub-channel in order to obtain an estimate of the transmitted symbol. Consequently, the equalization complexity does not rise with the delay spread of the channel as it is the case for SC schemes; here, typically Decision-Feedback Equalization (DFE) architectures are applied whose complexity rises quickly with the channel length.
2. The equalization of received symbols requires the knowledge of the channel coefficients. OFDM provides several approaches for practical system implementation, typically leading to very simple solutions: in a quasi-static scenario, channel coefficients estimation is usually performed using known training sequences periodically transmitted (e.g. at the start of each frame), implicitly assuming that the channel does not vary between two training sequences. Wireless systems operating in a mobility context usually apply a combination of such initial training and Pilot-Symbol-Assisted Modulation (PSAM) schemes [83–85]. The pilots are exploited for channel tracking and estimation at the cost of a throughput reduction due to increased overhead. An alternative is to track the channel variations by refining the channel coefficients blindly using the training sequences as initializations for the estimator [71, 72, 86–88].
3. The available diversity over frequency (in presence of channels with a large inherent delay spread), time (typically in a mobility context where the channel coherence time is short) and space (in multiple-antennas systems) is straightforwardly exploited by interleaving over all dimensions, channel coding (e.g. convolutional codes [89], Turbo Codes [90] and LDPC Codes [91, 92]) and space-time coding (e.g. Alamouti's well known code [93]). A further increase of frequency diversity is obtained by spreading sequences, leading to Multi-Carrier OFDM (MC-CDMA) [63–65] and Spread-Spectrum OFDM (SS-OFDM) [62].
4. The link capacity is straightforwardly maximized by applying the *water-filling* principle [89]. Sub-optimum solutions consists, for example, in abandoning carriers with a poor inherent Signal-to-Noise-plus-Interference (C/I) ratio.
5. There is a high spectral efficiency due to overlapping, but still orthogonal carrier shaping.

The main weaknesses of OFDM are resumed below:

1. The OFDM modulator and demodulator require the implementation of a Discrete Fourier Transform. The inherent complexity is justified in the presence of multi-path propagation - in the context

of very short channel impulse responses, however, SC modulation schemes are often the better solution due to a lower implementation complexity.

2. OFDM receivers are very sensitive to both, time and frequency synchronization offsets [94]. This issue triggered a large quantity of studies on suitable solutions, e.g. [95–98].
3. The OFDM time domain signal is characterized by important power fluctuations over time - its complex samples are approximately distributed following a Rayleigh distribution [99]. This implies requirements for the power-amplifier in a practical system implementation which typically lead to an increase in power consumption compared to SC. Otherwise, signal clipping occurs which leads to both, inter-symbol-interference and (more importantly) growth of the out-of-band signal and thus interference to neighboring systems.
4. Plain OFDM (i.e. no coding, interleaving, etc. is applied) typically leads to poor system performances and is often outperformed by standard SC architectures. Only in combination with coding and interleaving (see above), the OFDM approach is suitable for practical use [100].
5. OFDM requires that the channel impulse response is shorter than the guard interval (CP-OFDM), postfix sequence (PRP-OFDM) and the zero-padding sequence (ZP-OFDM) respectively. Otherwise, IBI is present and typically an important error floor occurs.

Today, the weaknesses of OFDM are well understood. They are typically overcome by some increase in system complexity due to suitable synchronization algorithms, a proper design of the system parameters (GI length), etc. [101].

## 2.6 Example of an OFDM system

A typical example for an efficient CP-OFDM system is the IEEE802.11n MITMOT (Mac and mIMO Techniques for MOre Throughput) system proposal [33–36]. It is a multiple transmit multiple receive (MTMR) antennas system for high-throughput Wireless-LAN applications providing 100Mbps per links and beyond. The basic transmitter architecture is illustrated in Fig.2.10 and the basic system parameters are resumed in Tab.2.1 and Tab.2.2.

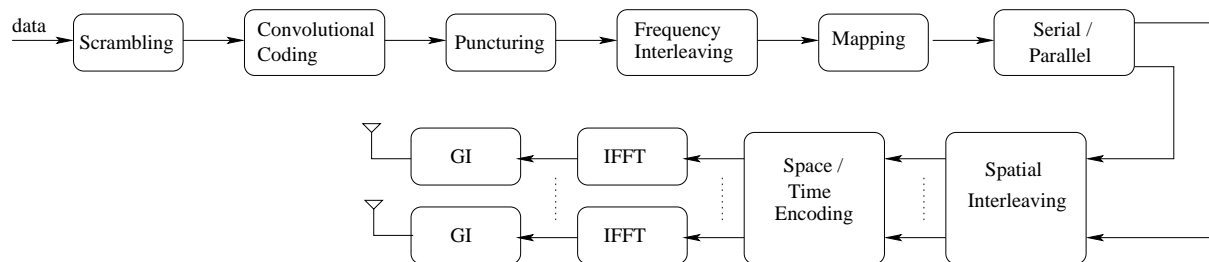


Figure 2.10: IEEE802.11n MITMOT transmitter architecture.

The incoming data bits first pass through the *scrambler* with the goal to provide i.i.d. entries to the rate  $R = 1/2$  *convolutional encoder* afterwards. Different coding rates are obtained by *puncturing*.

Transmit configuration	Data rate (Mbps)	Number of spatial streams	Modulation	Coding Rate
2Tx	6Mbps	1	BPSK	1/2
2Tx	12Mbps	1	QPSK	1/2
2Tx	18Mbps	1	QPSK	3/4
2Tx	24Mbps	1	16QAM	1/2
2Tx	36Mbps	1	16QAM	3/4
2Tx	48Mbps	1	64QAM	2/3
2Tx	60Mbps	1	64QAM	5/6
2Tx	72Mbps	2	16QAM	3/4
2Tx	96Mbps	2	64QAM	2/3
2Tx	108Mbps	2	64QAM	3/4
2Tx	120Mbps	2	64QAM	5/6

Table 2.1: Parameters of the 2Tx modes in 20MHz bandwidth (48 data subcarriers)

Transmit configuration	Data rate (Mbps)	Number of spatial streams	Modulation	Coding Rate
3Tx/4Tx	12Mbps	2	BPSK	1/2
3Tx/4Tx	24Mbps	2	QPSK	1/2
3Tx/4Tx	36Mbps	2	QPSK	3/4
3Tx/4Tx	48Mbps	2	16QAM	1/2
3Tx/4Tx	72Mbps	2	16QAM	3/4
3Tx/4Tx	96Mbps	2	64QAM	2/3
3Tx/4Tx	120Mbps	2	64QAM	5/6
3Tx/4Tx	144Mbps	3	64QAM	2/3
3Tx/4Tx	162Mbps	3	64QAM	3/4
3Tx/4Tx	180Mbps	3	64QAM	5/6

Table 2.2: Parameters of the 3Tx and 4Tx modes in 20MHz bandwidth (48 data subcarriers)

The corresponding outputs are *interleaved over frequency mapped* onto carrier amplitudes and *serial to parallel* converted. A *spatial interleaver* and the *space-time encoding* blocks follow. Finally, the different streams are converted to time domain by an *inverse discrete Fourier transform*, the cyclic prefix extension is added and the signals are transmitted from the corresponding antennas.

## 2.7 Conclusion

Standard CP-OFDM is well-established in digital communication standards and has proven to be an efficient modulation scheme providing decoding architectures of reasonable complexity [102]; it has moreover been proven to be robust against multi-path propagation as well as time and frequency synchronization errors. More advanced OFDM schemes, including ZP-OFDM, IOTA-OFDM and the novel PRP-OFDM are currently under investigation in the framework of research projects; to give a few examples, one can name the European Projects IST-BROADWAY IST-2001-32686 [14–20, 29] and IST-WINNER IST-2003-507581 [9, 21–24, 30]: IST-BROADWAY proposes a hybrid WLAN standard operation at 5GHz and 60GHz; IST-WINNER studies architectures for a 4<sup>th</sup> generation (4G) mobile communication system. PRP-OFDM has been accepted as an option in the IST-WINNER system concept [103].

## Chapter 3

# Pseudo Random Postfix OFDM: channel estimation and equalization

This chapter shows how to exploit the properties of the Pseudo-Random-Postfix OFDM (PRP-OFDM) modulation scheme that was defined in chapter 2. Low-complexity single-antenna receiver architectures and channel tracking algorithms are derived avoiding the typically required overhead in terms of learning symbols and pilot tones.

### 3.1 Introduction

This chapter builds on the novel Pseudo-Random-Postfix based OFDM (PRP-OFDM) transceiver architecture which is defined in chapter 2: instead of the classical cyclic prefix extension known from CP-OFDM [48] or the Zero-Padding introduced in the framework of ZP-OFDM [39], it is proposed to insert a known vector weighted by a pseudo random scalar sequence between classical OFDM symbols: the Pseudo Random Postfix OFDM (PRP-OFDM).

It is shown that PRP-OFDM capitalizes on the advantages of CP-OFDM [48] and ZP-OFDM [39, 40, 70–76]; furthermore, unlike former OFDM modulators, the receiver can exploit an additional information: the prior knowledge of a part of the transmitted block. It is explained how to build on this knowledge in order to perform an extremely low complexity order one semi-blind channel estimation and tracking. Moreover, several PRP-OFDM equalization architectures derived from the zero padded transmission scheme are proposed, allowing implementations ranging from low-complexity/medium performance to increased-complexity/high performance. PRP-OFDM is shown to be of advantage over existing modulation schemes if the target system requires i) a minimum pilot overhead, ii) low-complexity channel tracking (e.g. a IEEE802.11a like system in a high mobility context) and iii) adjustable receiver complexity/performance trade-offs. The PRP-OFDM concept has been validated on an FPGA based prototyping platform operating at 5GHz and 60GHz [11].

In the sequel, section 3.2 introduces the notations and presents the new PRP-OFDM modulator. Section 3.3 reveals how to exploit the postfix for performing blind channel estimation in the context

of both, low (Doppler is negligible) and high (Doppler is significant) mobility; it is further explained in section 3.4 how to combine estimates of different origins, e.g. preamble- and blind postfix-based results. Then suitable reception strategies are presented in section 3.5 including several equalization schemes (Zero Forcing, ZF and Minimum Mean Square Error, MMSE). Section 3.6 explains how to adapt the maximum likelihood (ML) decoding metrics in presence of bit interleaved convolutional coded modulation. Finally, section 3.7 presents a low complexity implementation architecture and simulations in section 3.8 illustrate the performances in both, a static and a mobility scenario reminiscent of the IEEE802.11a system.

## 3.2 Notations and PRP-OFDM modulator

Fig. 3.1 depicts the baseband discrete-time block equivalent model of an  $N$  carrier PRP-OFDM system. The  $i$ th  $N \times 1$  input digital vector  $\tilde{\mathbf{s}}_N(i)$  is first modulated by the IFFT matrix  $\mathbf{F}_N^H := \frac{1}{\sqrt{N}} (W_N^{kl})^H$ ,  $0 \leq k < N$ ,  $0 \leq l < N$  and  $W_N := e^{-j\frac{2\pi}{N}}$ .

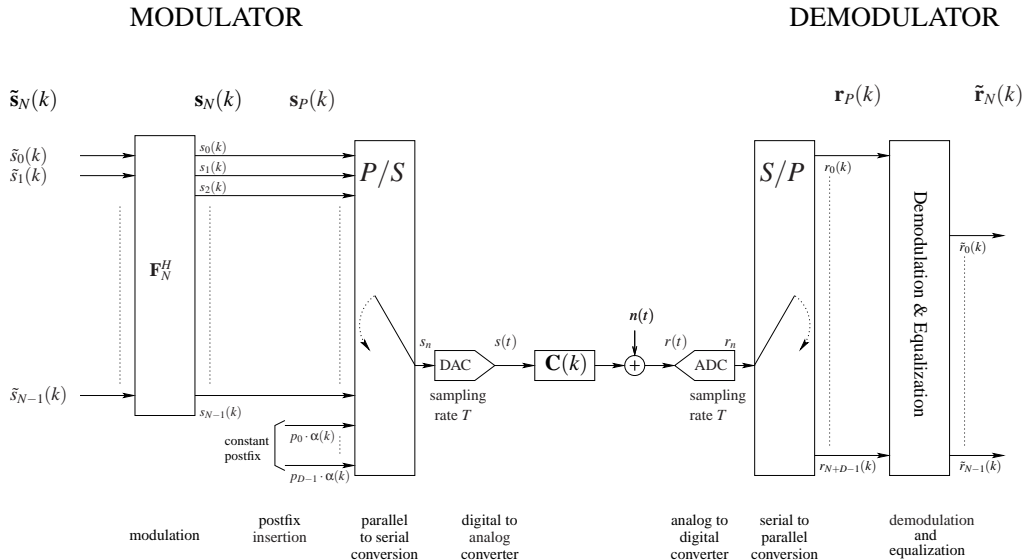


Figure 3.1: Discrete model of the PRP-OFDM transceiver.

Then, a deterministic postfix vector  $\mathbf{p}_D := (p_0, \dots, p_{D-1})^T$  weighted by a pseudo random value  $\alpha(i) \in \mathbb{C}$  is appended to the IFFT output  $\mathbf{s}_N(i)$ . With  $P := N + D$ , the corresponding  $P \times 1$  transmitted vector is

$$\mathbf{s}_P(i) := \mathbf{F}_{ZP}^H \tilde{\mathbf{s}}_N(i) + \alpha(i) \mathbf{p}_P, \quad (3.1)$$

where

$$\mathbf{F}_{ZP}^H := \begin{bmatrix} \mathbf{I}_N \\ \mathbf{0}_{D,N} \end{bmatrix}_{P \times N} \mathbf{F}_N^H \quad \text{and} \quad \mathbf{p}_P := (\mathbf{0}_{1,N} \mathbf{p}_D^T)^T$$

Without loss of generality, the elements of  $\mathbf{s}_N(i) = \mathbf{F}_N^H \tilde{\mathbf{s}}_N(i)$  are assumed to be i.i.d. and zero mean random variables of variance  $\sigma_s^2 = 1$  which are independent of  $\alpha(i) \mathbf{p}_D$ . The samples of  $\mathbf{s}_P(i)$  are then

sent sequentially through the channel modeled here as an FIR filter of order  $L$ ,  $C(z) := \sum_{n=0}^L c_n z^{-n}$ . The OFDM system is designed such that the postfix duration exceeds the channel memory  $L < D$ .

Let  $\mathbf{C}_{\text{ISI}}(P)$  and  $\mathbf{C}_{\text{IBI}}(P)$  be respectively the size  $P \times P$  Toeplitz inferior and superior triangular matrices of first column  $[c_0, c_1, \dots, c_L, 0, \dots, 0]^T$  and first row  $[0, \dots, 0, c_L, \dots, c_1]$ . As already explained in [80], the channel convolution can be modeled by  $\mathbf{r}_P(i) := \mathbf{C}_{\text{ISI}}(P)\mathbf{s}_P(i) + \mathbf{C}_{\text{IBI}}(P)\mathbf{s}_P(i-1) + \mathbf{n}_P(i)$ .  $\mathbf{C}_{\text{ISI}}(P)$  and  $\mathbf{C}_{\text{IBI}}(P)$  represent respectively the intra and inter block interference.  $\mathbf{n}_P(i)$  is the  $i$ th AWGN vector of element variance  $\sigma_n^2$ . Given the expression of equation (3.1), we have as illustrated by Fig. 3.2:

$$\mathbf{r}_P(i) = (\mathbf{C}_{\text{ISI}}(P) + \beta_i \mathbf{C}_{\text{IBI}}(P))\mathbf{s}_P(i) + \mathbf{n}_P(i) \quad (3.2)$$

where  $\beta_i := \frac{\alpha(i-1)}{\alpha(i)}$ .

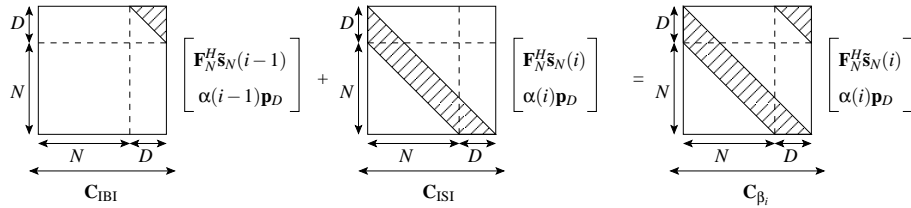


Figure 3.2: Circularization for PRP-OFDM.

Note that  $\mathbf{C}_{\beta_i} := (\mathbf{C}_{\text{ISI}}(P) + \beta_i \mathbf{C}_{\text{IBI}}(P))$  is pseudo circulant: i.e. a circulant matrix whose  $(D-1) \times (D-1)$  upper triangular part is weighted by  $\beta_i$ .

The expression of the received block is thus:

$$\mathbf{r}_P(i) := \mathbf{C}_{\beta_i} (\mathbf{F}_{\text{ZP}}^H \tilde{\mathbf{s}}_N(i) + \alpha(i) \mathbf{p}_P) + \mathbf{n}_P(i) \quad (3.3)$$

$$= \mathbf{C}_{\beta_i} \begin{pmatrix} \mathbf{F}_N^H \tilde{\mathbf{s}}_N(i) \\ \alpha(i) \mathbf{p}_D \end{pmatrix} + \mathbf{n}_P(i) \quad (3.4)$$

Please note that equation (3.3) is closely related to the CP and ZP modulation schemes. With  $\mathbf{C}_{\beta_i} = \mathbf{C}_{\text{ISI}}(P) + \mathbf{C}_{\text{IBI}}(P)$ ,  $\forall i$ , indeed ZP-OFDM corresponds to  $\alpha(i) = 0, \forall i$  and CP-OFDM is achieved for  $\alpha(i) = 0 \forall i$  when  $\mathbf{F}_{\text{ZP}}^H$  is replaced by  $\mathbf{F}_{\text{CP}}^H$ :

$$\mathbf{F}_{\text{CP}}^H := \left[ \begin{array}{c|c} \mathbf{0}_{D,N-D} & \mathbf{I}_D \\ \hline & \mathbf{I}_N \end{array} \right]_{P \times N} \mathbf{F}_N^H.$$

A different modulator also introducing a known postfix sequence is proposed in the literature [78]: a  $P \times 1$  frequency domain vector  $\tilde{\mathbf{s}}_P(i)$  is defined containing  $N$  frequency domain data carrier amplitudes  $\tilde{\mathbf{s}}_N(i)$  and  $D$  pilot tones. The pilot tones are chosen for each symbol in function of  $\tilde{\mathbf{s}}_N(i)$  such that the last (or first)  $D$  time domain samples of  $\mathbf{F}_P^H \tilde{\mathbf{s}}_P(i)$  correspond to the predefined postfix sequence; note that there is in general no equivalence between both schemes: in general  $\mathbf{F}_P^H \tilde{\mathbf{s}}_P(i) \neq \mathbf{F}_{\text{ZP}}^H \tilde{\mathbf{s}}_N(i) + \alpha(i) \mathbf{p}_P$  for an identical  $\tilde{\mathbf{s}}_N(i)$ . This approach has the advantage of simple inherent equalization schemes similar to the ones of CP-OFDM in combination with a larger FFT. However, the corresponding pilot amplitudes can vary significantly in amplitude which is in contradiction to a flat spectrum requirement: the impact of

channel fades on the system performance then depends on the affected frequency band. This undesired effect is avoided with the previously presented modulator.

Considering (3.4), it is shown in the sequel that  $\mathbf{C}_{\beta_i \mathbf{p}_P}$  can be retrieved by a simple averaging i.e. mean value calculation of the received samples if the OFDM data symbols  $\mathbf{F}_N^H \tilde{\mathbf{s}}_N(i)$  are assumed to be zero-mean. The channel can afterwards be extracted by de-convolution. Afterwards, it is shown that we can preserve the simple equalization/decoding properties of OFDM even with the introduction of the pseudo-random postfix.

### 3.3 Order one semi-blind channel estimation based on PRP-OFDM postfixes only

In a quasi-static scenario, channel coefficients estimation is usually performed using known training sequences periodically transmitted (e.g. at the start of each frame), implicitly assuming that the channel does not vary between two training sequences. Wireless systems operating in a mobility context usually apply a combination of such initial training and Pilot-Symbol-Assisted Modulation (PSAM) schemes [83–85]. The pilots are exploited for channel tracking and estimation at the cost of a throughput reduction due to increased overhead. An alternative is to track the channel variations by refining the channel coefficients blindly using the training sequences as initializations for the estimator. Such semi-blind equalization algorithms based on second order statistics have already been proposed for the CP-OFDM and ZP-OFDM modulators [71, 72, 86–88].

This section presents two different ways of estimating the CIR based on order one statistics. The first one exploits the  $D \times D$  circulant matrix containing the CIR convolved by the postfix yielding a low complexity estimation scheme. Then, a more general and powerful estimator is proposed playing with the two frequency domain grid resolutions:  $D$  and  $P$ . The second method leads to better results in cases where some frequency domain amplitudes of the postfix  $\mathbf{p}_D$  are close to zero. A discussion on channel estimation in a mobility context finalizes this section.

#### 3.3.1 Channel estimation in a time-invariant environment

##### Channel estimation using minimum dimension circular diagonalization

In this section, the Channel Impulse Response (CIR) is assumed static. Define  $\mathbf{C}_{\text{CIR}}(D) := \mathbf{C}_{\text{ISI}}(D) + \mathbf{C}_{\text{IBI}}(D)$  as the  $D \times D$  circulant channel matrix of first row  $\text{row}_0(\mathbf{C}_{\text{CIR}}(D)) = [c_0, 0, \dots, 0, c_L, \dots, c_1]$ . Note that  $\mathbf{C}_{\text{ISI}}(D)$  and  $\mathbf{C}_{\text{IBI}}(D)$  contain respectively the lower and upper triangular parts of  $\mathbf{C}_{\text{CIR}}(D)$ .

Denoting by  $\mathbf{s}_N(i) := [s_0(i), \dots, s_{N-1}(i)]^T$ , extracting two sub-vectors:  $\mathbf{s}_{D,0}(i) := [s_0(i), \dots, s_{D-1}(i)]^T$ ,  $\mathbf{s}_{D,1}(i) := [s_{N-D}(i), \dots, s_{N-1}(i)]^T$ , and performing the same operations for the noise vector:  $\mathbf{n}_P(i) := [n_0(i), \dots, n_{P-1}(i)]^T$ ,  $\mathbf{n}_{D,0}(i) := [n_0(i), \dots, n_{D-1}(i)]^T$ ,  $\mathbf{n}_{D,1}(i) := [n_{P-D}(i), \dots, n_{P-1}(i)]^T$ , the re-

ceived vector  $\mathbf{r}_P(i)$  can be expressed as:

$$\mathbf{r}_P(i) = \begin{pmatrix} \mathbf{C}_{\text{ISI}}(D)\mathbf{s}_{D,0}(i) + \alpha(i-1)\mathbf{C}_{\text{IBI}}(D)\mathbf{p}_D + \mathbf{n}_{D,0} \\ \vdots \\ \mathbf{C}_{\text{IBI}}(D)\mathbf{s}_{D,1}(i) + \alpha(i)\mathbf{C}_{\text{ISI}}(D)\mathbf{p}_D + \mathbf{n}_{D,1} \end{pmatrix}. \quad (3.5)$$

As defined earlier the transmitted time domain signal  $\mathbf{s}_N(i)$  is zero-mean. Thus the first  $D$  samples  $\mathbf{r}_{D,0}(i)$  of  $\mathbf{r}_P(i)$  and its last  $D$  samples  $\mathbf{r}_{D,1}(i)$  can be exploited very easily to retrieve the channel matrices relying on the deterministic nature of the postfix as follows:

$$\hat{\mathbf{r}}_{c,0} := \mathbb{E} \left[ \frac{\mathbf{r}_{D,0}(i)}{\alpha(i-1)} \right] = \mathbf{C}_{\text{IBI}}(D)\mathbf{p}_D, \quad (3.6)$$

$$\hat{\mathbf{r}}_{c,1} := \mathbb{E} \left[ \frac{\mathbf{r}_{D,1}(i)}{\alpha(i)} \right] = \mathbf{C}_{\text{ISI}}(D)\mathbf{p}_D. \quad (3.7)$$

Since  $\mathbf{C}_{\text{ISI}}(D) + \mathbf{C}_{\text{IBI}}(D) = \mathbf{C}_{\text{CIRC}}(D)$  is circulant and diagonalizable in the frequency domain  $\mathbf{F}_D$  combining equations (3.6) and (3.7) and using the commutativity of the convolution yields:

$$\hat{\mathbf{r}}_c := \hat{\mathbf{r}}_{c,0} + \hat{\mathbf{r}}_{c,1} = \mathbf{C}_{\text{CIRC}}(D)\mathbf{p}_D = \mathbf{P}_D\mathbf{c}_D = \mathbf{F}_D^H \tilde{\mathbf{P}}_D \mathbf{F}_D \mathbf{c}_D, \quad (3.8)$$

where  $\mathbf{P}_D$  is a  $D \times D$  circulant matrix with first row  $\text{row}_0(\mathbf{P}_D) := [p_0, p_{D-1}, p_{D-2}, \dots, p_1]$  and  $\tilde{\mathbf{P}}_D := \text{diag}\{\mathbf{F}_D \mathbf{p}_D\}$ .  $\text{diag}\{\cdot\}$  denotes a diagonal matrix whose components are given by the vector argument.

Since in practice the expectation  $\mathbb{E}[\cdot]$  in (3.6) is approximated by a mean value calculation over a limited number  $Z$  of symbols, we can model the estimation error as noise  $\tilde{\mathbf{n}}_D$  of covariance  $\mathbf{R}_{\tilde{\mathbf{n}}_D}$  (with  $\|\cdot\|^2 = E[|\cdot|^2]$ ):

$$\begin{aligned} \mathbf{R}_{\tilde{\mathbf{n}}_D} &= \mathbb{E} [\tilde{\mathbf{n}}_D \tilde{\mathbf{n}}_D^H] \\ &= 2 \frac{\sigma_n^2}{Z} \mathbf{I}_D + \frac{1}{Z} \mathbb{E} [\mathbf{C}_{\text{ISI}}(D)\mathbf{s}_{D,0}\mathbf{s}_{D,0}^H \mathbf{C}_{\text{ISI}}^H(D) + \mathbf{C}_{\text{IBI}}(D)\mathbf{s}_{D,1}\mathbf{s}_{D,1}^H \mathbf{C}_{\text{IBI}}^H(D)] \\ &= \mathbf{I}_D \left[ 2 \frac{\sigma_n^2}{Z} + \frac{\sigma_s^2}{Z} \sum_{p=0}^{D-1} \|c_p(k)\|^2 \right] \end{aligned}$$

Thus, an estimate of the CIR  $\hat{\mathbf{c}}_D$  can be retrieved by either a ZF or MMSE approach [104]:

$$\begin{aligned} \hat{\mathbf{c}}_D^{\text{ZF}} &:= \mathbf{P}_D^{-1} \hat{\mathbf{r}}_c \\ &= \mathbf{F}_D^H \tilde{\mathbf{P}}_D^{-1} \mathbf{F}_D \hat{\mathbf{r}}_c \\ \hat{\mathbf{c}}_D^{\text{MMSE}} &:= \mathbf{R}_{c_D} \mathbf{P}_D^H (\mathbf{R}_{\tilde{\mathbf{n}}_D}/D + \mathbf{P}_D \mathbf{R}_{c_D} \mathbf{P}_D^H)^{-1} \hat{\mathbf{r}}_c \\ &= \mathbf{F}_D^H \tilde{\mathbf{R}}_{c_D} \tilde{\mathbf{P}}_D^H (\tilde{\mathbf{R}}_{\tilde{\mathbf{n}}_D}/D + \tilde{\mathbf{P}}_D \tilde{\mathbf{R}}_{c_D} \tilde{\mathbf{P}}_D^H)^{-1} \mathbf{F}_D \hat{\mathbf{r}}_c \end{aligned} \quad (3.10)$$

where  $\mathbf{R}_{c_D} := \mathbb{E} [\mathbf{c}_D \mathbf{c}_D^H]$ ,  $\tilde{\mathbf{R}}_{c_D} := \mathbf{F}_D \mathbf{R}_{c_D} \mathbf{F}_D^H$ ,  $\mathbf{R}_{\tilde{\mathbf{n}}_D} := \mathbb{E} [\tilde{\mathbf{n}}_D \tilde{\mathbf{n}}_D^H]$  and  $\tilde{\mathbf{R}}_{\tilde{\mathbf{n}}_D} := \mathbf{F}_D \mathbf{R}_{\tilde{\mathbf{n}}_D} \mathbf{F}_D^H$ . Note that this ZF CIR estimation technique requires  $\mathbf{p}_D$  to be designed in such a way that  $\tilde{\mathbf{P}}_D$  is full rank. Since the channel power profile  $\mathbb{E} [\mathbf{c}_D \mathbf{c}_D^H]$  is not known, it is convenient to approximate it by the unitary matrix. If the order of the channel is over-estimated or the CIR contains zero contributions,  $\tilde{\mathbf{R}}_{c_D}$  is not invertible and (3.10) is only defined if the invertability is guaranteed by the properties of  $\tilde{\mathbf{R}}_{\tilde{\mathbf{n}}_D}$ .

### Channel estimation using frequency domain carrier grid adaptation

When designing practical multi-carrier systems,  $\tilde{\mathbf{P}}_D$  is often chosen rank deficient to ease compliance with the spectrum mask. Indeed for IEEE802.11a [56], implicit oversampling imposes null side carriers: actually only 52 out of the specified  $N = 64$  carriers are bearing information. Two typical postfix sequences suitable to this application are presented in Fig.3.3 in frequency domain (both sequences have different trade-offs in terms of Peak-to-Average-Power-Rate (PAPR), spectral flatness and out-of-band radiation; see chapter 4 for details on their derivation):

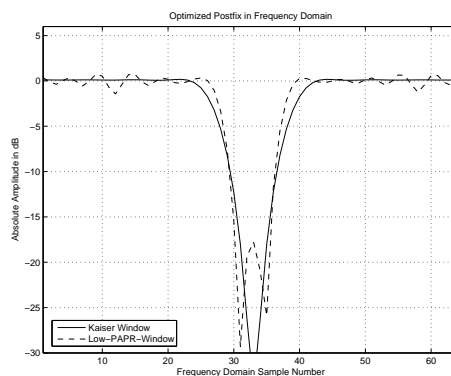


Figure 3.3: Postfixes with different trade-offs in frequency domain.

As a consequence even if the channel estimation is performed using a frequency grid of resolution  $D$ , some side coefficient of  $\tilde{\mathbf{P}}_D$  are not reliable. Fig.3.4 illustrates this effect (for sake of simplicity, a channel impulse response is assumed whose frequency domain coefficients are of constant modulus):

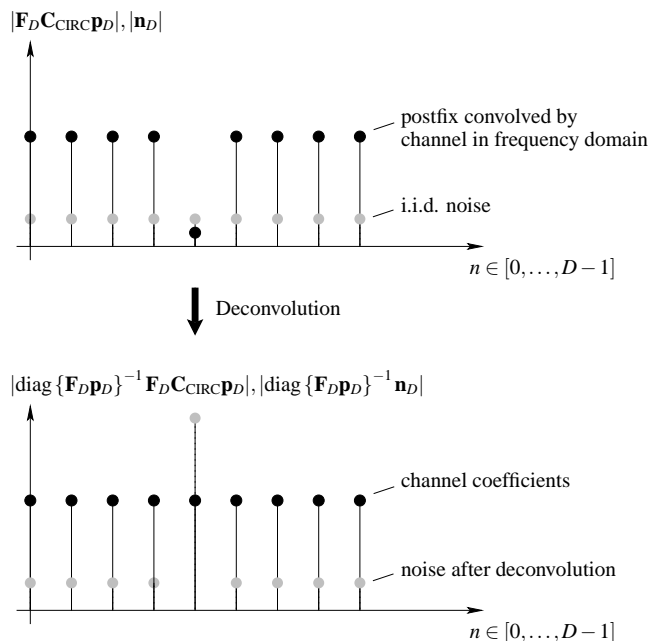


Figure 3.4: Illustration of channel extraction (representation in frequency domain).

Thus the derivation of the frequency domain CIR on a frequency grid of resolution  $N$  or  $P$  (required for equalization)  $\tilde{\mathbf{P}}_M$  where  $M \in \{N, P\}$  from  $\tilde{\mathbf{P}}_D$  using an oversampling matrix spreads the estimation error and noise yielding to a poor channel estimator as illustrated in Fig.3.5:

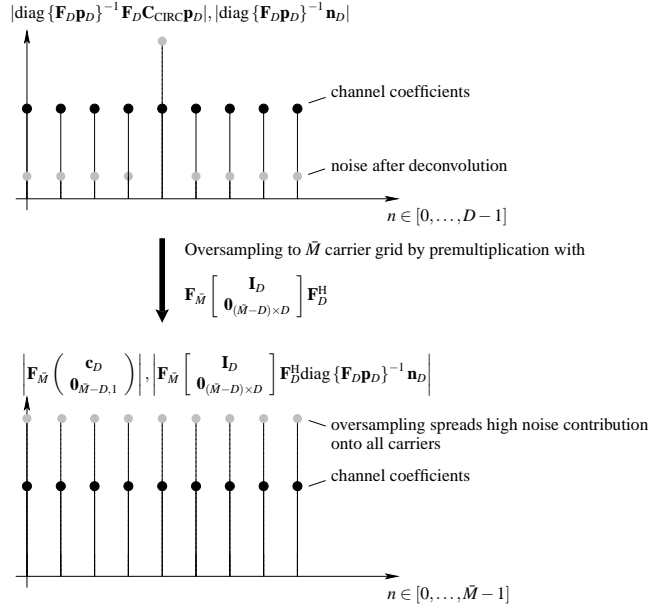


Figure 3.5: Illustration of noise amplification by de-convolution (representation in frequency domain).

This subsection provides two different way to overcome this issue: i) a MMSE based approach requiring a matrix multiplication and ii) a low-complexity ZF based approach in combination with a simple grid adaptation in time domain.

### Channel estimation using frequency domain carrier grid adaptation: MMSE approach

The goal is to estimate the frequency domain channel on the useful carriers (channel coefficients on zero carriers shall not be considered). For this purpose we define the matrix  $\mathbf{F}_u$  which is a sub-set of  $\mathbf{F}_{\bar{M}}$  containing only its first  $D$  columns and the rows corresponding to useful carriers (note that an equalization in the  $\bar{M} = P$  grid domain may require  $\mathbf{F}_u = \mathbf{F}_{\bar{M}}$ ). Grouping observations (3.6) and (3.7) in combination with a noise vector  $\mathbf{n}_{2D}$  and by constructing  $\mathbf{P}_{\text{IBI}}(D)$  and  $\mathbf{P}_{\text{ISI}}(D)$  as the corresponding IBI and ISI channel convolution matrices replacing the channel coefficients by postfix samples, the following expression is obtained:

$$\begin{aligned} \hat{\mathbf{r}}_{c,2D} &:= \begin{pmatrix} \mathbf{C}_{\text{IBI}}(D) \\ \mathbf{C}_{\text{ISI}}(D) \end{pmatrix} \mathbf{p}_D + \bar{\mathbf{n}}_{2D} \\ &= \begin{pmatrix} \mathbf{P}_{\text{IBI}}(D) \\ \mathbf{P}_{\text{ISI}}(D) \end{pmatrix} \mathbf{c}_D + \bar{\mathbf{n}}_{2D} \end{aligned}$$

The channel coefficients are extracted with the help of the following Wiener filtering matrix:

$$\begin{aligned}
\widehat{\mathbf{F}}_u \mathbf{c}_D &= \mathbf{G}_c \hat{\mathbf{f}}_{c,2D}, \\
\mathbf{G}_c &:= \underset{\mathbf{G}_c}{\operatorname{argmin}} \|\mathbf{G} \hat{\mathbf{f}}_{c,2D} - \mathbf{F}_u \mathbf{c}_D\|^2 \\
&= \mathbf{F}_u \mathbf{R}_{c_D} \begin{pmatrix} \mathbf{P}_{\text{IBI}}(D) \\ \mathbf{P}_{\text{ISI}}(D) \end{pmatrix}^H \left[ \begin{pmatrix} \mathbf{P}_{\text{IBI}}(D) \\ \mathbf{P}_{\text{ISI}}(D) \end{pmatrix} \mathbf{R}_{c_D} \begin{pmatrix} \mathbf{P}_{\text{IBI}}(D) \\ \mathbf{P}_{\text{ISI}}(D) \end{pmatrix}^H + \mathbf{R}_{\bar{\mathbf{n}}_{2D}} \right]^{-1} \quad (3.11)
\end{aligned}$$

with  $\mathbf{R}_{\bar{\mathbf{n}}_{2D}} := \mathbb{E} [\bar{\mathbf{n}}_{2D} \bar{\mathbf{n}}_{2D}^H]$  and  $\mathbf{R}_{c_D} := \mathbb{E} [\mathbf{c}_D \mathbf{c}_D^H]$  typically is a diagonal matrix where the channel power delay profile is contained in the main diagonal. Obviously, this estimator requires a full matrix multiplication for the extraction of the channel coefficients. Due to its inherent complexity, the following section will present a sub-optimum approach leading to a reasonable performance/complexity trade-off.

### Channel estimation using frequency domain carrier grid adaptation: ZF approach with simple grid adaptation

Exploiting relations (3.5), (3.6) and (3.7), we observe that

$$\begin{bmatrix} \hat{\mathbf{f}}_{c,0} \\ \mathbf{0}_{P-2D,1} \\ \hat{\mathbf{f}}_{c,1} \end{bmatrix} = \left( (\mathbf{C}_{\text{IBI}}(D) \mathbf{p}_D)^T \mathbf{0}_{P-2D}^T (\mathbf{C}_{\text{ISI}}(D) \mathbf{p}_D)^T \right)^T \quad (3.12)$$

It is possible to add or truncate any number of these zeros in order to adapt the grid resolution of the estimates. Contrarily to (3.8), this operation is not irreversible. Thus, a vector  $\hat{\mathbf{f}}_M(i)$  is created with  $M \geq 2D$  (e.g.  $M \in \{N, P\}$ ):  $\hat{\mathbf{f}}_M(i) := [(\mathbf{C}_{\text{IBI}}(D) \mathbf{p}_D)^T, \mathbf{0}_{M-2D}^T, (\mathbf{C}_{\text{ISI}}(D) \mathbf{p}_D)^T]^T$ . As in the previous section,  $\hat{\mathbf{f}}_M(i)$  can be expressed by a convolution of the postfix with the CIR:

$$\hat{\mathbf{f}}_M = \mathbf{C}_{\text{CIRC}}(M) (\mathbf{0}_{M-D}^T \mathbf{p}_D^T)^T = \mathbf{F}_M^H \tilde{\mathbf{P}}_M \mathbf{F}_M \mathbf{c}_M, \quad (3.13)$$

where  $\mathbf{P}_M$  is an  $M \times M$  circulant matrix with first row  $\text{row}_0(\mathbf{P}_M) := [0, p_{D-1}, p_{D-2}, \dots, p_0, 0, \dots, 0]$   $\tilde{\mathbf{P}}_M = \text{diag} \left\{ \mathbf{F}_M (\mathbf{0}_{M-D}^T \mathbf{p}_D^T)^T \right\}$ . The CIR estimates are derived similarly to (3.9) and (3.10). Using this procedure, the frequency domain channel coefficients are estimated for any desired carrier grid without requiring any up- or down-sampling after the postfix de-convolution. Particularly in combination with a ZF de-convolution approach, this is very convenient when some frequency domain amplitudes of the postfix  $\tilde{\mathbf{P}}_M$  are close to zero, since up-sampling matrices of the type  $\mathbf{F}_{\bar{M}} \begin{bmatrix} \mathbf{I}_M \\ \mathbf{0}_{(\bar{M}-M) \times M} \end{bmatrix} \mathbf{F}_{\bar{M}}^H, \bar{M} > M$  are full matrices which in general spread more evenly the estimation errors onto the carriers in the up-sampled domain. This effect can be avoided by directly estimating the CIR with the desired carrier grid.

We have detailed in these two sections very simple methods for blind estimation of the CIR only relying on first order statistics: an expectation of the received signal vector. Though the results presented above are based on the assumption that the channel does not vary, this method can be used to mitigate the effects of Doppler. Indeed this approach can be combined with the initial channel estimates derived from the preambles usually present at the start of the frame for either refining the channel estimates or tracking the channel variations. For WLANs this enables to operate at a mobility exceeding the specification of the standard (3m/s). In that case, MMSE channel estimates are usually more efficient than ZF ones.

### 3.3.2 Channel estimation in a time-variant environment (presence of Doppler)

This section details a suitable channel estimator in the presence of a time varying channel. For all derivations, the channel is assumed to vary insignificantly over one OFDM symbol; however, the variation can be considerable over the data frame.

In the context of a Doppler scenario, the choice of the Doppler model plays an essential role. Jakes' commonly accepted Doppler model [105] is used throughout this thesis stating that  $\alpha_D = E [c_l(n)c_l^*(n-1)] = J_0(2\pi f_D \Delta T) E [|c_l(n)|^2]$  with  $c_l(n)$  being the  $l^{th}$  component of the CIR  $\mathbf{c}(n)$  at instant  $T_n = n\Delta T$ ,  $J_0(\cdot)$  is the  $0^{th}$  order Bessel function of the first kind and  $f_D$  the Doppler frequency. A more detailed discussion of Jake's Doppler model and suitable approximations are discussed in annex D.

In the following, two different CIR estimation concepts are presented: i) a Kalman filtering based approach relying on a order-one auto-regressive channel evolution model and ii) a generic Wiener-filtering approach (including a study on different trade-offs in terms of decoding latency and robustness to high mobility).

#### Symbol based CIR update based on Kalman filtering

A Kalman filter allows to efficiently track a time-variant process, such as the channel impulse response  $\mathbf{c}(n)$ , based on a noisy observation  $\mathbf{u}(n) = \mathbf{U}\mathbf{c}(n) + \mathbf{n}_u$ ;  $\mathbf{U}$  is an observation matrix and the elements of the noise vector  $\mathbf{n}_u$  are i.i.d. and Gaussian. The Kalman filter outputs are optimum in the MMSE sense if the time-variant process is modeled as follows [104]:

$$\mathbf{c}(n) = \mathbf{F}(n, n-1)\mathbf{c}(n-1) + \check{\mathbf{c}}(n). \quad (3.14)$$

$\mathbf{F}(n, n-1)$  is the transition matrix and  $\check{\mathbf{c}}(n)$  is the so-called process noise which is i.i.d. and Gaussian. Unfortunately, Jakes' Doppler model leads to CIR correlation properties which cannot be modeled by (3.14) over an infinity of observations (since the correlations of the CIR at different instants of time are given by a Bessel function which is *non-linear*).

One way to overcome this problem is presented in annex D.3: Jake's model is closely approximated by a moving-average (MA) approach which is compatible with (3.14). As illustrated in Appendix D, this approach shows near-optimum performances, but the resulting Kalman filter is prohibitively complex in common scenarios (a large MA model leads to a large transition matrix  $\mathbf{F}(n, n-1)$  and thus to a arithmetically complex Kalman filter implementation [104]).

Another way has been discussed extensively by recent publications: the idea is to approximate Jakes' model by an low-order (typically order-one) auto-regressive (AR) filter given by [106]

$$\mathbf{c}(n+1) = J_0(2\pi f_D T_1)\mathbf{c}(n) + \check{\mathbf{c}}(n+1) \quad (3.15)$$

$\check{\mathbf{c}}(n+1)$  is the so-called process-noise. This model has several advantages; in particular, an MMSE estimator of the CIR  $\mathbf{c}(0)$  based on noisy observations  $\mathbf{c}(n) + \mathbf{n}(n)$  is straightforwardly derived by Kalman

filtering [107]. Due to the simplicity of the order-one model, the filtering equations are of reasonable complexity. An inherent issue, however, becomes apparent by rewriting equation (3.15) as follows:

$$\begin{cases} \mathbf{c}(0) = \check{\mathbf{c}}(0) \\ \mathbf{c}(1) = J_0(2\pi f_D T_1) \check{\mathbf{c}}(0) + \check{\mathbf{c}}(1) \\ \dots \\ \mathbf{c}(n) = \sum_{k=0}^n J_0^k(2\pi f_D T_1) \check{\mathbf{c}}(n-k) \end{cases}$$

clearly shows that the AR model inherently approximates  $J_0(2\pi f_D k \Delta T)$  by  $J_0^k(2\pi f_D \Delta T)$ . The latter expression is justified by the Bessel function addition theorem stating  $J_0(x+y) = \sum_{k=-\infty}^{\infty} (-1)^k J_k(x) J_k(y) \approx J_0(x) J_0(y)$  for small  $x$  and  $y$ . However, these approximations are not quite valid in the context of high Doppler frequencies which occur, for example, in the context of high mobility WLANs or at high carrier frequencies (60GHz).

This motivates the block based Wiener filtering approach presented in the following which does not require any approximation of Jake's correlation equation and it is still optimum in the MMSE sense: first, a minimum latency estimator is presented followed by a refined approach that improves the CIR estimation MSE with the drawback of an increased decoding delay.

### Block based CIR update based on Wiener filtering (minimum latency)

Contrarily to the previous approaches designed for the static context, the CIR is not estimated based on the result of a mean-value calculation process; instead, the observations of the postfix sequences convolved by the channel are concatenated over  $Z \in \mathbb{N}$  observations:

$$\mathbf{r}_{2ZD}(k) := \begin{bmatrix} \begin{bmatrix} \mathbf{P}_{\text{IBI},D} \mathbf{c}_D(k) \\ \mathbf{P}_{\text{ISI},D} \mathbf{c}_D(k) \\ \dots \\ \mathbf{P}_{\text{IBI},D} \mathbf{c}_D(k-Z+1) \\ \mathbf{P}_{\text{ISI},D} \mathbf{c}_D(k-Z+1) \end{bmatrix} \\ \end{bmatrix} + \mathbf{n}_{W,2ZD} \quad (3.16)$$

$$= [\mathbf{r}_{2D}^T(k), \mathbf{r}_{2D}^T(k-1), \dots, \mathbf{r}_{2D}^T(k-Z+1)]^T,$$

$$\mathbf{r}_{2D}(k) := \begin{bmatrix} \mathbf{C}_{\text{IBI}}^D(k) \\ \mathbf{C}_{\text{ISI}}^D(k) \end{bmatrix} \mathbf{p}_D + \alpha^{-1}(k) \mathbf{n}_W(k), \quad (3.17)$$

$$\mathbf{n}_W(k) := \begin{bmatrix} \mathbf{C}_{\text{ISI}}^D(k+1) \mathbf{s}_{D,0}(k+1) + \mathbf{n}_{D,0}(k+1) \\ \mathbf{C}_{\text{IBI}}^D(k) \mathbf{s}_{D,1}(k) + \mathbf{n}_{D,1}(k) \end{bmatrix}, \quad (3.18)$$

$$\mathbf{n}_{W,2ZD} := \begin{bmatrix} \mathbf{n}_W(k) \\ \dots \\ \mathbf{n}_W(k-Z+1) \end{bmatrix} \quad (3.19)$$

Fig. 3.6 illustrates the corresponding received samples taken into account for the channel estimation:

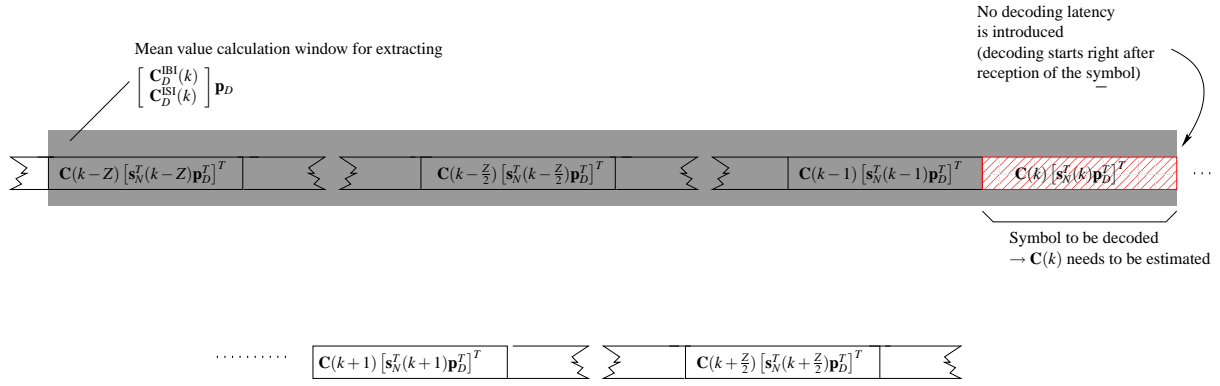


Figure 3.6: Received symbols exploited for channel estimation (minimum latency).

Using a standard Wiener filtering approach [108], the optimum estimator of  $\mathbf{c}_D(k)$  in the MMSE sense is given by the following theorem:

**Theorem 3.3.1** *The MMSE estimator of  $\mathbf{c}_D(0)$  form (3.16) is given by*

$$\begin{aligned} \mathbf{W}(k) &:= \underset{\mathbf{W}}{\operatorname{argmin}} \|\mathbf{W} \mathbf{r}_{2DZ}(k) - \mathbf{c}_D(k)\|^2 \\ &= \left( [1J_1 \cdots J_{Z-1}] \otimes (\mathbf{R}_{\mathbf{c}_D(k)} [\mathbf{C}_{IBI}^H \mathbf{C}_{ISI}^H]) \right) [\mathbf{T}(k) + \mathbf{R}_{\hat{\mathbf{n}}}(k) + \sigma_s^2 \mathbf{I}_Z \otimes \Delta_{2D}(k)]^{-1}, \end{aligned} \quad (3.20)$$

with

$$\begin{aligned} \mathbf{T}(k) &:= \begin{bmatrix} 1 & J_1 & J_2 & \cdots & J_{Z-1} \\ J_1 & 1 & J_1 & \cdots & J_{Z-2} \\ \vdots & \ddots & \ddots & \ddots & \vdots \\ J_{Z-1} & J_{Z-2} & J_{Z-3} & \cdots & 1 \end{bmatrix} \otimes \left( \begin{bmatrix} \mathbf{C}_{IBI}(D) \\ \mathbf{C}_{ISI}(D) \end{bmatrix} \mathbf{R}_{\mathbf{c}_D(k)} \begin{bmatrix} \mathbf{C}_{IBI}(D) \\ \mathbf{C}_{ISI}(D) \end{bmatrix}^H \right), \\ \mathbf{R}_{\hat{\mathbf{n}}}(k) &:= \mathbb{E} \left[ \left( \mathbf{n}_{D,0}^T(k+1), \mathbf{n}_{D,1}^T(k), \dots, \mathbf{n}_{D,1}^T(k-Z+1) \right)^T \left( \mathbf{n}_{D,0}^H(k+1), \mathbf{n}_{D,1}^H(k), \dots, \mathbf{n}_{D,1}^H(k-Z+1) \right) \right] \\ &= \sigma_n^2 \mathbf{I}_{2DZ}, \\ \Delta_{2D}(k) &:= \operatorname{diag} \left[ \|c_0(k)\|^2, \sum_{p=0}^1 \|c_p(k)\|^2, \dots, \sum_{p=0}^{D-1} \|c_p(k)\|^2, \sum_{p=1}^{D-1} \|c_p(k)\|^2, \sum_{p=2}^{D-1} \|c_p(k)\|^2, \dots, \|c_{D-1}(k)\|^2, 0 \right] \end{aligned} \quad (3.21)$$

$\otimes$  is the Kronecker product,  $\mathbf{R}_{\mathbf{c}_D(k)} := \mathbb{E} [\mathbf{c}_D(k) \mathbf{c}_D^H(k)]$ ,  $J_n = J_0(2\pi f_D n \Delta T)$  and  $\|\cdot\|^2 := \mathbb{E} (|\cdot|^2)$ .  $\square$

Contrary to the approach presented in section 3.3.2 based on an AR-1 approximation, the block based Wiener filtering approach does not require any approximation.

The following section will explain how to further improve the performance of the Wiener filtering approach at the expense of an increase in system latency.

### Block based CIR update based on Wiener filtering (increased latency)

In order to increase the performance of the upper approach, it is proposed to replace the observation window as defined in (3.16) by the following (with  $Z$  odd):

$$\bar{\mathbf{r}}_{2ZD}(k) = \begin{bmatrix} \left[ \begin{array}{c} \mathbf{P}_{IBI,D} \mathbf{c}_D(k - \frac{Z-1}{2}) \\ \mathbf{P}_{ISI,D} \mathbf{c}_D(k - \frac{Z-1}{2}) \\ \dots \\ \mathbf{P}_{IBI,D} \mathbf{c}_D(k + \frac{Z-1}{2}) \\ \mathbf{P}_{ISI,D} \mathbf{c}_D(k + \frac{Z-1}{2}) \end{array} \right] \end{bmatrix} + \bar{\mathbf{n}}_{W,2ZD} \quad (3.22)$$

$$\bar{\mathbf{n}}_{W,2ZD} = \begin{bmatrix} \mathbf{n}_W(k - \frac{Z-1}{2}) \\ \dots \\ \mathbf{n}_W(k + \frac{Z-1}{2}) \end{bmatrix} \quad (3.23)$$

with  $\mathbf{r}_{2D}(k)$  and  $\mathbf{n}_W(k)$  as defined in (3.17) and (3.18) respectively.

Fig. 3.6 illustrates the corresponding received samples taken into account for the channel estimation:

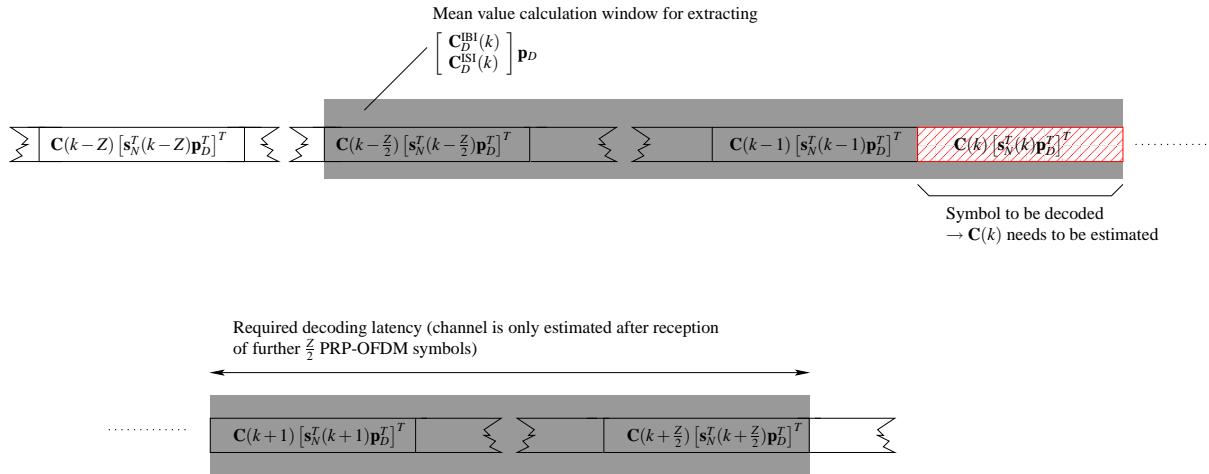


Figure 3.7: Received symbols exploited for channel estimation (increased latency).

It is obvious that only symbol observations with indices  $k - \frac{Z-1}{2}, \dots, k + \frac{Z-1}{2}$  are used in order to estimate the channel coefficients for equalization of received symbol  $\mathbf{r}_{2D}(k)$ ; the corresponding channel

correlations  $\mathbb{E}[\mathbf{c}_D^H(k - \frac{Z-1}{2})\mathbf{c}_D(k)], \dots, \mathbb{E}[\mathbf{c}_D^H(k + \frac{Z-1}{2})\mathbf{c}_D(k)]$  are thus globally higher compared to the previous case:  $\mathbb{E}[\mathbf{c}_D^H(k - Z + 1)\mathbf{c}_D(k)], \dots, \mathbb{E}[\mathbf{c}_D^H(k)\mathbf{c}_D(k)]$ . This explains an improved estimation MSE of the CIR with the drawback that symbol  $\mathbf{r}_{2D}(k)$  can only be decoded after reception of further  $\frac{Z-1}{2}$  PRP-OFDM symbols. The required increase in system latency corresponds thus to the duration of  $\frac{Z-1}{2}$  symbols including the postfix sequences.

Using again a standard Wiener filtering approach [108], the optimum estimator of  $\mathbf{c}_D(k)$  in the MMSE sense is given by the following theorem:

**Theorem 3.3.2** *The MMSE estimator of  $\mathbf{c}_D(0)$  form (3.22) is given by*

$$\begin{aligned} \bar{\mathbf{W}}(k) &:= \underset{\bar{\mathbf{W}}}{\operatorname{argmin}} \|\bar{\mathbf{W}}\bar{\mathbf{r}}_{2DZ}(k) - \mathbf{c}_D(k)\|^2 \\ &= \left( \left[ J_{-\frac{Z-1}{2}} \cdots 1 \cdots J_{\frac{Z-1}{2}} \right] \otimes (\mathbf{R}_{\mathbf{c}_D(k)} [\mathbf{C}_{|BI}^H \mathbf{C}_{|SI}^H]) \right) [\mathbf{T}(k) + \mathbf{R}_{\hat{\mathbf{n}}}(k) + \sigma_s^2 \mathbf{I}_Z \otimes \Delta_{2D}(k)]^{-1}, \end{aligned} \quad (3.24)$$

with  $\mathbf{T}(k)$  as defined in (3.21). Furthermore,  $\otimes$  is the Kronecker product,  $\mathbf{R}_{\mathbf{c}_D(k)} := \mathbb{E}[\mathbf{c}_D(k)\mathbf{c}_D^H(k)]$ ,  $J_n := J_0(2\pi f_D n \Delta T)$  and  $\|\cdot\|^2 = \mathbb{E}(|\cdot|^2)$ .  $\square$

The corresponding performance increase of this new estimator is discussed in section 3.8. In the extreme case (with a high Doppler frequency such that

$$\mathbb{E}[\mathbf{c}_D^H(k - Z + 1)\mathbf{c}_D(k)] \approx 0, \dots, \mathbb{E}\left[\mathbf{c}_D^H(k - \frac{Z-1}{2} - 1)\mathbf{c}_D(k)\right] \approx 0),$$

3dB of increase in the CIR estimation MSE can theoretically be achieved.

Obviously, however, equation (3.20) and (3.24) are of a certain complexity and do not seem to be compatible with low-complexity hardware implementation constraints. However, they only depend on the Doppler frequency  $f_D$ , channel statistics  $\mathbf{R}_{\mathbf{c}_D(k)}$  and the noise covariance  $\mathbf{R}_{\hat{\mathbf{n}}}(k)$ . In practice, these quantities are difficult to estimate and usually only rough approximations are available. This is why it is recommended to precalculate  $\mathbf{W}(k)$  and  $\bar{\mathbf{W}}(k)$  for a limited number of such parameter sets. The corresponding estimation matrices are then stored in look-up tables in a hardware implementation and are available without requiring any computations. Then, each CIR estimation requires only  $D \times 2DZ$  complex multiplications and a corresponding number of additions.

The performance of these estimators are illustrated in section 3.8.

### 3.4 Order one semi-blind channel estimation based on PRP-OFDM postfixes and preambles

Considering a practical system, CIR estimation is usually not performed based on PRP-OFDM postfix statistics only, but rather by combining several estimates affected by additive noise vectors of different

covariance. These estimates can be derived for example from reference signals (preambles, pilot tones, etc). A special case is well illustrated by semi-blind methods which rely on an initial CIR estimate as an initialization.

Let us consider the case of two channel estimates, both affected by noise contributions of known covariance:

$$\bar{\mathbf{c}}_1 := \mathbf{c}_D + \mathbf{n}_1, \quad (3.25)$$

$$\bar{\mathbf{c}}_2 := \mathbf{c}_D + \mathbf{n}_2. \quad (3.26)$$

As derived in [108], the optimum estimator of  $\mathbf{c}_D$  in the MMSE sense is thus given by Theorem 3.4.1.

**Theorem 3.4.1** *The MMSE estimator of  $\mathbf{c}_D$  in (3.25) and (3.26) is given by*

$$\begin{aligned} \hat{\mathbf{c}}_D &:= \mathbf{Y}_1 \bar{\mathbf{c}}_1 + \mathbf{Y}_2 \bar{\mathbf{c}}_2, \\ \mathbf{Y}_1 &:= [\mathbf{I} + \mathbf{R}_{\mathbf{n}_1} \mathbf{R}_{\mathbf{n}_2}^{-1} + \mathbf{R}_{\mathbf{n}_1} \mathbf{R}_{\mathbf{c}_D}^{-1}]^{-1}, \\ \mathbf{Y}_2 &:= [\mathbf{I} + \mathbf{R}_{\mathbf{n}_2} \mathbf{R}_{\mathbf{n}_1}^{-1} + \mathbf{R}_{\mathbf{n}_2} \mathbf{R}_{\mathbf{c}_D}^{-1}]^{-1} \end{aligned} \quad (3.27)$$

with  $\mathbf{R}_{\mathbf{c}_D} := \mathbb{E}[\mathbf{c}_D \mathbf{c}_D^H]$ ,  $\mathbf{R}_{\mathbf{n}_1} := \mathbb{E}[\mathbf{n}_1 \mathbf{n}_1^H]$ ,  $\mathbf{R}_{\mathbf{n}_2} := \mathbb{E}[\mathbf{n}_2 \mathbf{n}_2^H]$  and  $\mathbb{E}[\mathbf{n}_1 \mathbf{n}_2^H] = \mathbf{0}$ .  $\square$

The results obtained in previous subsection are now applied to the PRP-OFDM case for which several estimates (direct or indirect ones) of the channel impulse response are available. The goal is to combine them in the MMSE sense.

For illustration purposes, the following case is considered below: the channel estimation is based on two observations:

1. the convolution of a learning symbol by the channel  $\mathbf{c}_D$ , expressed as:

$$\mathbf{v}_1 := \bar{\mathbf{P}} \mathbf{c}_D + \tilde{\mathbf{n}}_1 \quad (3.28)$$

$\bar{\mathbf{P}}$  is a circulant convolution matrix built from the learning symbol coefficients,  $\tilde{\mathbf{n}}_1$  is a white Gaussian noise.

2. the pseudo random postfix convolved by the channel. This data is extracted by mean-value calculation over  $K$  received PRP-OFDM symbols. The IBI and ISI contributions are added up as previously presented in order to obtain a circular convolution of  $\mathbf{C}_D$ . The noise contribution can be split into 2 terms: a white Gaussian noise  $\tilde{\mathbf{n}}_2$  and the mean value of the OFDM data symbol interference over the  $K$  symbols considered for the estimation:

$$\begin{aligned} \mathbf{v}_2 &:= \mathbf{P} \mathbf{c}_D + \frac{1}{K} \sum_{i=0}^{K-1} \left( \tilde{\mathbf{n}}_2(i) + \mathbf{C}_{\text{ISI}}^{D \times N} \mathbf{F}_N^H \tilde{\mathbf{s}}_N(i) + \mathbf{C}_{\text{IBI}}^{D \times N} \mathbf{F}_N^H \tilde{\mathbf{s}}_N(i) \right), \\ \mathbf{C}_{\text{ISI}}^{D \times N} &:= [\mathbf{C}_{\text{ISI}}(D) \mathbf{0}_{D \times (N-D)}], \\ \mathbf{C}_{\text{IBI}}^{D \times N} &:= [\mathbf{0}_{D \times (N-D)} \mathbf{C}_{\text{IBI}}(D)]. \end{aligned} \quad (3.29)$$

Some reformatting of equations (3.28) and (3.29) is required in order to match expressions of (3.25) and (3.26). For that purpose (3.28) is pre-multiplied by  $\bar{\mathbf{P}}^{-1}$  and (3.29) by  $\mathbf{P}^{-1}$  resulting in:

$$\begin{aligned}\bar{\mathbf{c}}_1 &:= \mathbf{c}_D + \bar{\mathbf{P}}^{-1} \tilde{\mathbf{n}}_1, \\ \bar{\mathbf{c}}_2 &:= \mathbf{c}_D + \mathbf{P}^{-1} \frac{1}{K} \sum_{i=0}^{K-1} \left( \tilde{\mathbf{n}}_2(i) + \mathbf{C}_{\text{ISI}}^{D \times N} \mathbf{F}_N^H \tilde{\mathbf{s}}_N(i) + \mathbf{C}_{\text{IBI}}^{D \times N} \mathbf{F}_N^H \tilde{\mathbf{s}}_N(i) \right),\end{aligned}$$

In the following, the noise covariance expressions are computed for direct utilization of (3.27).

$$\begin{aligned}\mathbf{R}_{\mathbf{n}_1} &:= \mathbb{E} \left[ \bar{\mathbf{P}}^{-1} \tilde{\mathbf{n}}_1 \tilde{\mathbf{n}}_1^H \bar{\mathbf{P}}^{-H} \right] = \sigma_{\tilde{\mathbf{n}}_1}^2 \bar{\mathbf{P}}^{-1} \bar{\mathbf{P}}^{-H}, \\ \mathbf{R}_{\mathbf{n}_2} &:= \frac{\sigma_{\tilde{\mathbf{n}}_2}^2}{K} \mathbf{P}^{-1} \mathbf{P}^{-H} + \\ &\quad \frac{1}{K} \mathbf{P}^{-1} \mathbb{E} \left[ \mathbf{C}_{\text{ISI}}^{D \times N} \mathbf{s}_N \mathbf{s}_N^H (\mathbf{C}_{\text{ISI}}^{D \times N})^H \right] \mathbf{P}^{-H} + \\ &\quad \frac{1}{K} \mathbf{P}^{-1} \mathbb{E} \left[ \mathbf{C}_{\text{IBI}}^{D \times N} \mathbf{s}_N \mathbf{s}_N^H (\mathbf{C}_{\text{IBI}}^{D \times N})^H \right] \mathbf{P}^{-H}\end{aligned}$$

with  $\mathbb{E} \left[ \mathbf{C}_{\text{IBI}}^{D \times N} \mathbf{s}_N \mathbf{s}_N^H (\mathbf{C}_{\text{IBI}}^{D \times N})^H \right] = \mathbf{0}_{D \times D}$  and  $\mathbf{R}_{\mathbf{s}_N} = \sigma_{s_n}^2 \mathbf{I}_N$ . With these expressions, the optimum combination for estimating  $\mathbf{c}_D$  in the MMSE sense is directly available from Theorem 3.4.1.

This finalizes the study of PRP-OFDM based channel equalization. In the sequel, the presentation of suitable equalization approaches follows.

### 3.5 Symbol Recovery: Equalization

When the channel is known, two steps are usually performed in order to retrieve the data : i) equalization of the received vector  $\mathbf{r}_P(i)$ , ii) soft decoding when forward error encoding is applied at the emitter. This section focuses on the equalization step and is followed by a section dealing with the soft decoding procedure.

Several equalization strategies can be proposed for the received vector  $\mathbf{r}_P(i)$ :

- one can first reduce (3.4) to the ZP-OFDM case by simple subtraction of the known postfix convolved by the pseudo-circulant channel matrix:  $\mathbf{r}_P^{\text{ZP}}(i) := \mathbf{r}_P(i) - \alpha(i) \hat{\mathbf{C}}_{\beta_i} \mathbf{p}_P$ , where  $\hat{\mathbf{C}}_{\beta_i}$  is derived from the current channel estimate. In that case all known methods related to the ZP-OFDM can be applied. Among others let us recall the corresponding ZF and MMSE equalizers provided in [40, 71, 72]:

$$\begin{aligned}\mathbf{G}_{\text{ZF}} &:= \mathbf{F}_N \mathbf{C}_o^\dagger, \\ \mathbf{G}_{\text{MMSE}} &:= \mathbf{F}_N \mathbf{C}_o^H (\sigma_n^2 \mathbf{I} + \mathbf{C}_o \mathbf{C}_o^H)^{-1},\end{aligned}\tag{3.30}$$

where  $(\cdot)^\dagger$  stands for the Moore-Penrose pseudo-inverse [104],  $\mathbf{C}_o$  is the  $P \times N$  matrix containing  $\mathbf{C}_{\text{ISI}}(P)$   $N$  first columns. The frequency domain symbols  $\tilde{\mathbf{s}}_N(i)$  are assumed uncorrelated and of unitary variance. Note that other alternatives exist [40] and that with an overlap-add (OLA) approach, ZP-OFDM-OLA can attain almost same performance and complexity as CP-OFDM.

- it is also possible to directly equalize (3.4) relying on the diagonalization properties of pseudo circulant matrices applied to  $\mathbf{C}_{\beta_i}$ . According appendix A, we have:

$$\begin{aligned} \mathbf{C}_{\beta_i} &:= \mathbf{V}_P^{-1}(i) \mathbf{D}_i \mathbf{V}_P(i), \\ \mathbf{D}_i &:= \text{diag} \left\{ C \left( \beta_i^{-\frac{1}{P}} \right), \dots, C \left( \beta_i^{-\frac{1}{P}} e^{j2\pi \frac{P-1}{P}} \right) \right\} \\ \mathbf{V}_P(i) &:= \left[ \frac{1}{P} \sum_{n=0}^{P-1} |\beta_i|^{-\frac{2n}{P}} \right]^{\frac{1}{2}} \mathbf{F}_P \text{diag} \left\{ 1, \beta_i^{\frac{1}{P}}, \dots, \beta_i^{\frac{P-1}{P}} \right\} \end{aligned} \quad (3.31)$$

In order to preserve the overall block variance and allow further simplifications, in the sequel,  $\beta_i$  is chosen as a pure phase  $M$ -PSK symbol:  $\beta_i := e^{j2\pi \frac{m_i}{M}}$ ,  $m_i \in \{0, 1, \dots, M-1\}$ . Under that condition (3.31) reduces to:

$$\mathbf{D}_i = \text{diag} \left\{ C \left( e^{-j2\pi \frac{m_i}{MP}} \right), \dots, C \left( e^{j2\pi \frac{(P-1)M - m_i}{PM}} \right) \right\}. \text{ Thus diagonal } \mathbf{D}_i \text{ is obtained for all } m_i \text{ by a FFT of size } PM \text{ of vector } (c_0, \dots, c_{L-1}, 0, \dots, 0)^T.$$

Since the ZP-OFDM case is entirely discussed by [40] et al., we discuss in the following the second case only, i.e. the equalization based on pseudo circulant matrices.

### 3.5.1 Zero Forcing equalizers

The equalization matrix for (3.4) verifying the ZF criterion for retrieving a minimum norm estimate of  $\hat{\mathbf{s}}_N(i)$  in (3.4) is  $\mathbf{G}_{\text{ZF}}^{\text{PRP}} := \mathbf{C}_o^\dagger$  applied to  $\hat{\mathbf{r}}_P(i) = \mathbf{r}_P(i) - \mathbf{C}_{\beta_i} \mathbf{p}_P$ . Following the idea presented in [40], when  $\mathbf{D}_i^{-1}$  is available, a practical low-complexity, but sub-optimum equalizer is:

$$\begin{aligned} \mathbf{G}_{\text{ZF,sub}}^{\text{PRP}} &= \mathbf{F}_N [\mathbf{I}_N \mathbf{0}_{N,D}] \mathbf{C}_{\beta_i}^{-1} \\ &= \mathbf{F}_N [\mathbf{I}_N \mathbf{0}_{N,D}] \mathbf{V}_P^H(i) \mathbf{D}_i^{-1} \mathbf{V}_P(i). \end{aligned}$$

Note that the simplified ZF equalization works well for Gaussian channel, but experiences severe drawbacks for frequency selective case. This can be shown by observing that  $\mathbf{D}_i^{-1}$  deals with the parallel equalization in the  $\mathbf{V}_P$  frequency domain (i.e. when dealing with Fourier transforms of length  $P > N$ ) which potentially enhances noise when a carrier undergoes deep attenuation. This becomes an issue when switching back to the original frequency domain ( $\mathbf{F}_N$ : grid of size  $N$ ) of the OFDM symbol through the non diagonal  $\mathbf{F}_N [\mathbf{I}_N \mathbf{0}_{N,D}] \mathbf{V}_P^H(i)$  multiplication. Indeed this has the effect of spreading the noise over all the carriers.

Thus  $\mathbf{G}_{\text{ZF,sub}}^{\text{PRP}}$  leads to poor performance and since  $\mathbf{G}_{\text{ZF}}^{\text{PRP}}$  is of considerable implementation complexity, this motivates the use of MMSE equalizers in order to mitigate this issue.

### 3.5.2 Minimum Mean Square Error equalizers

Using standard Wiener filtering approaches [42, 43, 108], the following theorem is obtained:

**Theorem 3.5.1** *The biased equalization matrix in the MMSE sense for retrieving an estimate of  $\tilde{\mathbf{s}}_N(i)$  in (3.4) is given by*

$$\begin{aligned} \mathbf{G}_{MMSE}^{\text{PRP}} &:= \mathbf{F}_N [\mathbf{I}_N \mathbf{0}_{N,D}] \mathbf{R}_{s_p} \mathbf{C}_{\beta_i}^H \mathbf{Q}^{-1} \\ &= \mathbf{F}_N [\mathbf{I}_N \mathbf{0}_{N,D}] \mathbf{R}_{s_p} \mathbf{V}_P^H(i) \mathbf{D}_i^H \hat{\mathbf{Q}}^{-1} \mathbf{V}_P(i), \end{aligned}$$

with  $\mathbf{Q} := \mathbf{R}_{n_p} + \mathbf{C}_{\beta_i} \mathbf{R}_{s_p} \mathbf{C}_{\beta_i}^H$ ,  $\hat{\mathbf{Q}} := \mathbf{R}_{n_p} + \mathbf{D}_i \hat{\mathbf{R}}_{s_p} \mathbf{D}_i^H$ ,  $\mathbf{R}_{n_p} := \mathbb{E} [\mathbf{n}_P(i) \mathbf{n}_P^H(i)] = \sigma_n^2 \mathbf{I}_P$ ,  $\mathbf{R}_{s_p} := \mathbb{E} [\mathbf{s}_P(i) \mathbf{s}_P^H(i)]$ ,  $\hat{\mathbf{R}}_{s_p} := \mathbf{V}_P(i) \mathbf{R}_{s_p} \mathbf{V}_P^H(i)$ .  $\square$

The wording *biased* indicates that the mean phase and amplitude offset of each carrier  $n$  after equalization is not necessarily zero. Please note that in combination with ML decoders, there is no disadvantage compared to *unbiased* equalizers as defined in [42, 43]: the resulting *unbiased* equalization matrix corresponds to the *biased* one combined with a pre-multiplication matrix. This leaves the ML decoding expression identical for both cases.

Contrary to the noise which has a diagonal autocorrelation in the  $\mathbf{V}_P$  domain:  $\mathbf{R}_{n_p} = \sigma_n^2 \mathbf{I}_P$ , this is no longer the case for the time domain vector  $\mathbf{r}_P(i)$  since it contains the deterministic postfix. Thus the expression of  $\mathbf{G}_{MMSE}^{\text{PRP}}$  doesn't allow an easy hardware implementation. In order to overcome this issue the following assumption can be made resulting in a suboptimal equalizer:

$$\mathbf{G}_{MMSE}^{\text{PRP}}(i) \approx \mathbf{F}_N [\mathbf{I}_N \mathbf{0}_{N,D}] \mathbf{V}_P^H(i) \mathbf{D}_i^H (\sigma_n^2 \mathbf{I} + \mathbf{D}_i \mathbf{D}_i^H)^{-1} \mathbf{V}_P(i).$$

This amounts to approximate  $\mathbb{E} [\mathbf{s}_P(i) \mathbf{s}_P^H(i)]$  by  $\sigma_s^2 \mathbf{I}_P$ . In the IEEE802.11a context one can check that with QPSK constellations this yields to almost identical results up to  $10^{-3}$  BER.

Globally, PRP-OFDM leads to a very simple modulation scheme on the transmitter side. In the receiver, a variety of demodulation and equalization approaches are possible, each characterized by different complexity/performance trade-offs. Note that the channel estimation and equalization schemes presented above can be adapted to a modulator that appends a postfix sequence not after each OFDM symbol, but after an ensemble of OFDM symbols. This allows to further reduce the overhead, but the possibility is lost to keep the standard CP-OFDM decoder in combination with the low-complexity OLA transformation.

Once the equalization is achieved, the next issue to solve is how to perform optimum decoding of the equalized data symbols which is covered in the next section.

## 3.6 Symbol Recovery: Metric derivation

In this subsection we assume that a bit interleaved convolutionally coded modulation is used at the emitter and explain how to derive the Viterbi metrics. For example for IEEE802.11a a rate  $R = \frac{1}{2}$ , constraint length  $K = 7$  Convolutional Code (CC) (o171/o133) is applied before bit interleaving over a single OFDM block followed by QAM mapping. First, the calculations are derived in general; then, a simplified low-complexity scheme is proposed for practical implementation purposes. Note that the approach detailed below is quite general and can be extended to other coding schemes.

### 3.6.1 Metric derivation

According to (3.4), after equalization by any of the  $N \times P$  matrices  $\mathbf{G}$  presented above, the vector to be decoded can generally be expressed by:  $\hat{\mathbf{s}} := \mathbf{G}\mathbf{r}_P(i) = \mathbf{G}_d\tilde{\mathbf{s}}_N(i) + \hat{\mathbf{n}}_N$  where  $\mathbf{G}_d$  is a diagonal weighting matrix and  $\hat{\mathbf{n}}_N$  the total noise plus interference contribution which for simplicity sake is approximated here as Gaussian and zero-mean.

For maximum-likelihood decoding, usually a log-likelihood approach is chosen based on a multivariate Gaussian law leading to the following expression [89, 108]:

$$\hat{\mathbf{d}} := \underset{\hat{\mathbf{d}}}{\operatorname{argmax}} \left\{ - \sum_{i=0}^{S-1} \left( \mathbf{G}_d m_N \left( \hat{\mathbf{d}}(i) \right) - \hat{\mathbf{s}}(i) \right)^H \mathbf{R}_{\hat{\mathbf{n}}_N}^{-1} \left( \mathbf{G}_d m_N \left( \hat{\mathbf{d}}(i) \right) - \hat{\mathbf{s}}(i) \right) \right\} \quad (3.32)$$

where vector  $\hat{\mathbf{d}}$  contains an estimation of the original uncoded information bits,  $\hat{\mathbf{d}}(i)$  gathers the corresponding bits after encoding, puncturing, etc. within the  $i$ th OFDM symbol.  $S$  is the number of OFDM symbols in the sequence to be decoded,  $m_N(\cdot)$  is an operator representing the mapping of encoded information bits onto the  $N$  constellations, one for each carrier of the OFDM symbol.

Thus all what is needed for performing the decoding is an estimation of the noise covariance matrix  $\mathbf{R}_{\hat{\mathbf{n}}_N}$  which requires the following derivations:

$$\hat{\mathbf{s}} = \mathbf{G}\mathbf{r}_P(i) = \mathbf{G}_d\tilde{\mathbf{s}}_N(i) + \mathbf{G}_f\tilde{\mathbf{s}}_N(i) + \alpha(i)\mathbf{G}_p\mathbf{p}_D + \mathbf{G}\mathbf{n}_P(i), \quad (3.33)$$

where  $\mathbf{G}_d$  is a  $N \times N$  diagonal matrix and  $\mathbf{G}_f$  a  $N \times N$  full matrix with the main diagonal being zero such that  $\mathbf{G}_d + \mathbf{G}_f := \mathbf{G}\mathbf{C}_{\beta_i} \left[ (\mathbf{F}_N^H)^T \mathbf{0}_{D,N}^T \right]^T = \mathbf{G}\mathbf{C}_{\beta_i} \left[ \mathbf{I}_N \mathbf{0}_{D,N}^T \right]^T \mathbf{F}_N^H$ .  $\mathbf{G}_p$  is a  $N \times D$  matrix containing the last  $D$  columns of the matrix  $\mathbf{G}\mathbf{C}_{\beta_i}$ . Thus,  $\mathbf{G}_f\tilde{\mathbf{s}}_N(i)$  represents the inter-symbol interference. The total noise plus interference vector is  $\hat{\mathbf{n}}_N = \mathbf{G}_f\tilde{\mathbf{s}}_N(i) + \mathbf{G}\mathbf{n}_P(i) + \alpha(i)\mathbf{G}_p\mathbf{p}_D$  and its covariance is

$$\mathbf{R}_{\hat{\mathbf{n}}_N} = \sigma_s^2 \mathbf{G}_f \mathbf{G}_f^H + \sigma_n^2 \mathbf{G} \mathbf{G}^H + \mathbf{G}_p \mathbf{p}_D \mathbf{p}_D^H \mathbf{G}_p^H \quad (3.34)$$

Please note that in order to deal with the non Gaussian nature of the term  $\mathbf{G}_p\mathbf{p}_D$  we could use a non linear equalization scheme that would suppress its contribution by substituting to (3.33) by  $\hat{\mathbf{s}}^{(2)} := \mathbf{G}\mathbf{r}_P(i) - \alpha(i)\mathbf{G}_p\mathbf{p}_D$ .

The trouble is that the overall noise covariance presented above is not diagonal which yields to a very high complexity decoding scheme if no approximation is applied. One way to achieve a reasonable decoding complexity is to approximate  $\mathbf{R}_{\hat{\mathbf{n}}_N}$  by a matrix containing only its main diagonal elements. Then, standard OFDM Viterbi decoding can be used. In that case equation (3.32) reduces to the classical weighted summation of the Euclidean distances by the inverse noise variances. In the following we call these weighted Euclidean distance the Viterbi metrics. Several further simplifications are discussed in the sequel.

### 3.6.2 Low-complexity metric proposal

Even when approximating (3.34) by a diagonal matrix, the metric calculation complexity is still considerably increased compared to CP-OFDM. For low complexity sake, we verify in the following that

applying the standard CP-OFDM metrics (i.e. without taking into account the inter-carrier-interference) only incurs a moderate loss in performance.

This approach is applied to optimum pseudo circulant MMSE equalization given by *Theorem 3.5.1*. However, in the metric derivation, the noise covariance matrix is approximated as presented in (3.35), where  $C_n, n = 0, \dots, N-1$  are the frequency domain channel coefficients:

$$\mathbf{R}_{\hat{\mathbf{n}}_N} = \sigma_n^2 \mathbf{G} \mathbf{G}^H \approx \sigma_n^2 \mathbf{F}_N^H \text{diag} \left( \frac{|C_0|^2}{(|C_0|^2 + \sigma_n^2)^2}, \dots, \frac{|C_{N-1}|^2}{(|C_{N-1}|^2 + \sigma_n^2)^2} \right) \mathbf{F}_N, \quad (3.35)$$

$$\mathbf{G}_d = \text{diag} \left( \mathbf{G} \mathbf{C}_{\beta_i} [ \mathbf{I}_N \mathbf{0}_{D,N}^T ]^T \mathbf{F}_N^H \right) \approx \text{diag} \left( \frac{|C_0|^2}{|C_0|^2 + \sigma_n^2}, \dots, \frac{|C_{N-1}|^2}{|C_{N-1}|^2 + \sigma_n^2} \right). \quad (3.36)$$

Basically this simplification amounts to use the standard CP-OFDM MMSE equalizer coefficients as the weights for the Viterbi algorithm metrics. Same simplification can be applied to matrix  $\mathbf{G}_d$  as indicated by (3.36).

In practice, one can verify that the above approximations degrade the bit-error-rate (BER) performance by approx. 0.2dB for a BPSK and 0.7dB for a QPSK constellation, which is acceptable in the WLAN context while granting for PRP-OFDM a low-cost equalization architectures.

### 3.7 Low complexity receiver architecture

Section 3.5 presents various equalization strategies leading to improved performances at the cost of an increased complexity. This section presents a low arithmetic complexity PRP-OFDM receiver architecture. This structure based on the 'overlap-add' [109] algorithm is shown to yield similar performances as the classical CP-OFDM with similar complexity.

Fig.3.8 illustrates the final receiver architecture.

Compared to a standard CP-OFDM system, the following steps are included here:

- Extract the postfix convolved by the channel, considering the IBI and the ISI part separately.
- Cancel the weighting by the pseudo-random values  $\alpha(i)$  and  $\alpha(i-1)$ . In practice, all  $\alpha(i)$  are chosen such that this operation is of minimum computational cost; with a typical  $\alpha(i) \in (1, -1, j, -j)$ , for example, only sign inversions and exchanges of real and imaginary parts are necessary. These operations are performed in combination with the following averaging steps.
- The *expectation* of the received values is calculated; in practice, this is done by simple averaging and takes  $2 \times D$  additions per OFDM symbol (in mobility context:  $4 \times D$  including subtraction of oldest contribution).
- The results of the *expectation* block are weighted again by the suitable pseudo-random weighting factors.

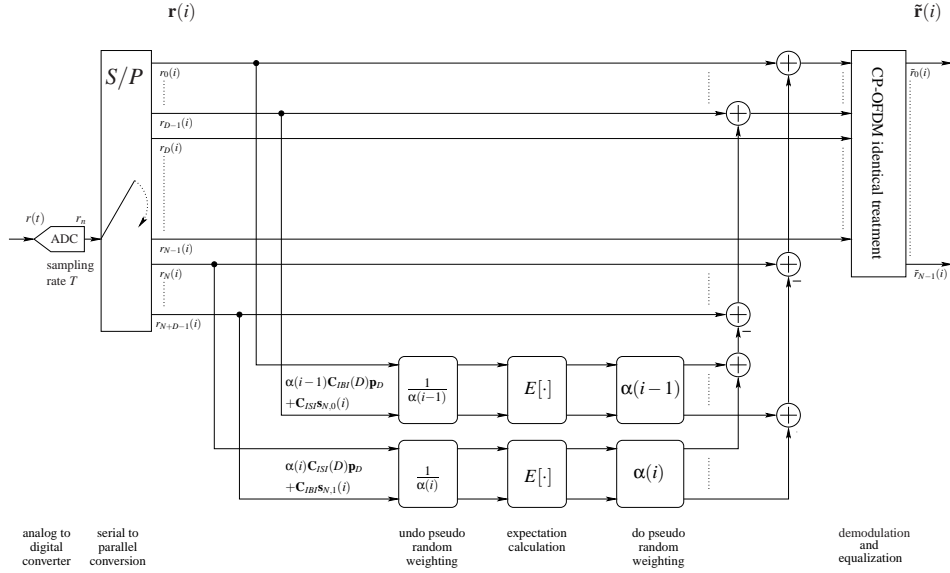


Figure 3.8: Discrete model of the PRP-OFDM OLA demodulator.

- The PRP-OFDM symbols are transformed to ZP-OFDM by subtraction of the postfix convolved by the channel. In the same time, the overlap-add operation is performed. This step takes  $2 \times D$  additions per OFDM symbol.
- The resulting OFDM symbol corresponds to the CP-OFDM case after truncation of the guard interval. All standard equalization approaches (ZF, MMSE) can be applied. Since the equalization can be performed on each carrier separately, no noise correlation issue arises.

Finally, the mean value calculation, the OLA operation and the postfix suppression takes up to  $6 \times D$  complex additions ( $4 \times D$  complex additions for the time-invariant case). Taking IEEE802.11a as an example, the OFDM-plus-postfix block is of size  $P = 5 \times D$  and thus an average of 1.2 complex additions are required per time domain sample. Each channel estimation takes an FFT operation (in order to transform the estimated postfix sequence convolved by the CIR into frequency domain) and one complex multiplication per useful carrier (assuming that the corresponding estimation coefficients have been pre-calculated). In a high mobility context, the calculation of the channel estimates requires a matrix multiplication: a number of received postfixes convolved by the channel are concatenated into a vector and multiplied by the (pre-calculated) estimator given in section 3.3.2. Numerical examples and further details on the calculation complexity are given in Appendix C.

### 3.8 Simulation results

In order to illustrate the performances of our approach, simulations have been performed in the IEEE802.11a [56] (equivalent to HIPERLAN/2 [110]) WLAN context: a  $N = 64$  carrier 20MHz bandwidth broadband wireless system operating in the 5.2GHz band using a 16 sample prefix or postfix. A rate  $R = \frac{1}{2}$ , constraint length  $K = 7$  Convolutional Code (CC) (o171/o133) is used before bit interleaving followed by constellation mapping (BPSK, QPSK, QAM16, QAM64). Each frame is preceded and followed by

dummy PRP-OFDM frames ensuring a seamless CIR estimation; in practice, these dummy symbols may correspond to frames that are not destined to the current user. The pseudo-random weighting factors are chosen to be a zero-mean pseudo-random  $\pm 1$  sequence. Both, Bit-Error-Rate (BER) and Packet-Error-Rate (PER) performance results are presented, setting the packet size to 72 OFDM symbols for all constellation types (the number of useful data bits are adapted appropriately). All data frames are assumed to be preceded and succeeded by a sufficient number of PRP-OFDM dummy symbols which are exploited for CIR estimation.

Monte carlo simulations are run and averaged over at least 2500 realizations of a normalized BRAN-A (office NLOS environment, 50ns rms delay spread), BRAN-C (large open space environment, 150ns rms delay spread) and BRAN-E (large open space environment, 250ns rms delay spread) [37] frequency selective channel with and without Doppler in order to obtain the performance curves.

In the following, section 3.8.1 presents an analysis of the Mean-Square-Error (MSE) of PRP-OFDM based channel estimates. Simulation results are presented for the coded case (convolutional encoder defined above) in sections 3.8.2, 3.8.3 and 3.8.4 for channels BRAN-A, BRAN-C and BRAN-E respectively [37]. Uncoded results follow in section 3.8.5 for channel BRAN-A. The curves compare the classical ZF CP-OFDM transceiver (standard IEEE802.11a) and PRP-OFDM with the MMSE equalizers combined with a transformation of the received symbols to ZP-OFDM, OLA and ZF equalization over the  $P = N + D$  carriers. In the case of CP-OFDM, each frame contains 2 known training symbols, followed by 72 OFDM data symbols.

For PRP-OFDM, the postfix is chosen as given by Tab.3.1:

Sample nb	Amplitude	Sample nb	Amplitude
1	1.5649-0.0356i	9	0.0832-0.6527i
2	-0.6961+ 0.9494i	10	0.0306+ 0.0594i
3	0.0874+ 1.1743i	11	0.4047+ 0.2204i
4	0.5737+ 1.4300i	12	-0.2723+ 0.2715i
5	-1.4368-0.8592i	13	0.3469-0.2291i
6	0.2212+ 0.4389i	14	0.0779-0.2369i
7	0.4137+ 0.2834i	15	0.1214+ 0.1355i
8	-0.0960+ 0.9893i	16	-0.2110-0.0972i

Table 3.1: Time domain samples of a suitable postfix.

It has been derived following the method in chapter 4 with respect to the following criteria:

- i) minimize the time domain peak-to-average-power ratio (PAPR);
- ii) minimize out-of-band radiations, i.e. concentrate signal power on useful carriers and
- iii) maximize spectral flatness over useful carriers since the channel is not known at the transmitter (do not privilege certain carriers).

The channel estimation is performed based on PRP-OFDM postfix sequences only using an averaging window over 21 and 41 OFDM symbols (BPSK and QPSK), 41 and 71 OFDM symbols (QAM-16) and

121 OFDM symbols (QAM-64) respectively. Preambles or pilot tones are not used for refining the estimates. When required by the equalization structure, only a-priori knowledge of the time domain channel confinement is used concerning its statistics:  $E[\mathbf{c}_D \mathbf{c}_D^H] \approx D^{-1} \mathbf{I}_D$ . In the mobility context, different CIR estimation approaches are compared as detailed in section 3.3.2:

- i) the 'Wiener (DS)' approach corresponds to a *double sided* (DS, increased latency) Wiener filter as illustrated in Fig. 3.7. It has the maximum performance of all estimators considered in this chapter.
- ii) the 'Wiener (SS)' approach corresponds to a *single sided* (SS, increased latency) Wiener filter as illustrated in Fig. 3.6.
- iii) the 'AR-1 Wiener (SS)' approach corresponds to the previous approach combined with an approximation of the CIR time-variant process as an Autoregressive model of order one as explained in section 3.3.2.
- vi) for sake for completeness, the upper approaches are compared to the static CIR estimator assuming that the CIR is time-invariant for the derivation of the Wiener filter.

### 3.8.1 Mean Square Error of Pseudo-Random-Postfix OFDM based channel estimates

The theoretically achieved MSE of the CIR estimation with (exact  $E[\mathbf{c}_D \mathbf{c}_D^H]$  known) and without ( $E[\mathbf{c}_D \mathbf{c}_D^H]$  is approximated by  $E[\mathbf{c}_D \mathbf{c}_D^H] \approx D^{-1} \mathbf{I}_D$  in the receiver) the knowledge of the channel statistics is illustrated in Fig. 3.9 to Fig. 3.10 for the static context (no mobility), in Fig. 3.11 and Fig. 3.12 at a mobility of 36m/s ( $\approx 130$ km/h) and in Fig. 3.14 and Fig. 3.14 at 72m/s ( $\approx 260$ km/h). In particular Fig. 3.11 to Fig. 3.14 illustrate the importance of a precise Doppler model - applying a standard first order Autoregressive (AR-1) model, for example, leads to an important degradation of the MSE at a high mobility and large observation window size (for 72m/s of velocity and a window size of 60 OFDM symbols, the AR-1 models leads to an CIR MSE of approx. -4dB while the optimum approach achieves approx. -18dB).

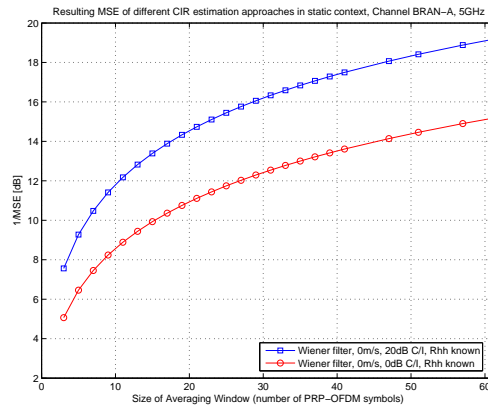
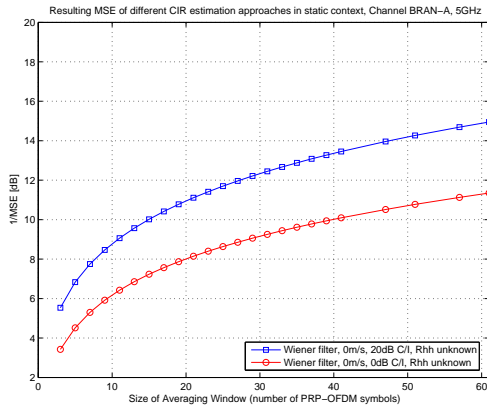


Figure 3.9: MSE of CIR estimates in Doppler scenario, no mobility (channel power profile is assumed to be rectangular). Figure 3.10: MSE of CIR estimates in Doppler scenario, no mobility (exact channel power profile is known).

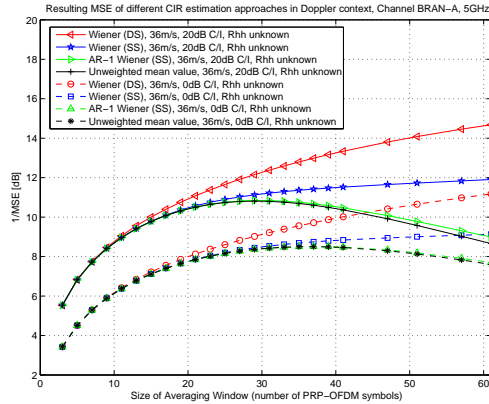


Figure 3.11: MSE of CIR estimates in Doppler scenario, mobility 36m/s (channel power profile is assumed to be rectangular).

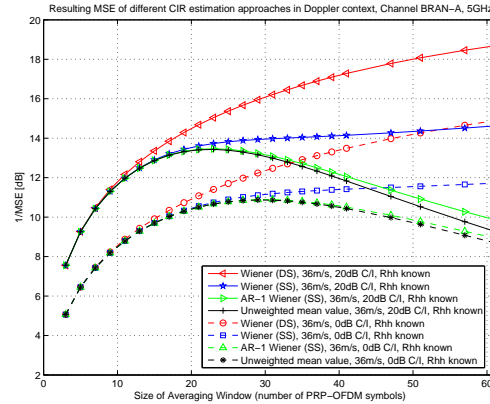


Figure 3.12: MSE of CIR estimates in Doppler scenario, mobility 36m/s (exact channel power profile is assumed to be rectangular).

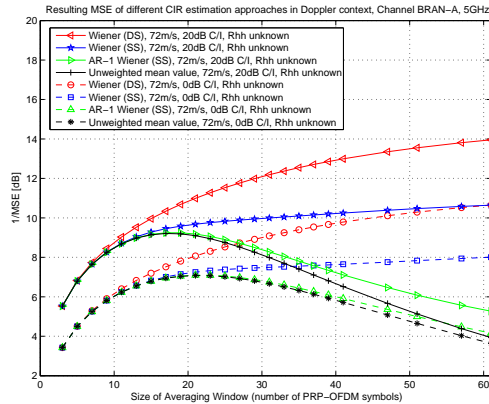


Figure 3.13: MSE of CIR estimates in Doppler scenario, mobility 72m/s (channel power profile is assumed to be rectangular).

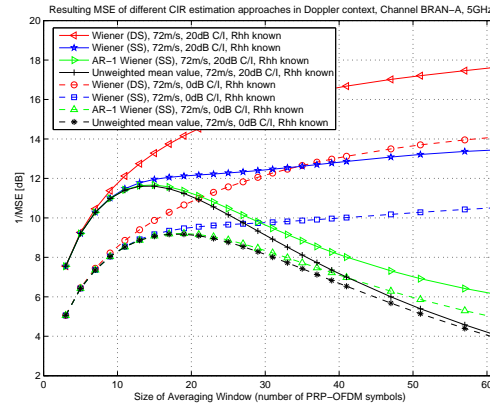


Figure 3.14: MSE of CIR estimates in Doppler scenario, mobility 72m/s (exact channel power profile is assumed to be rectangular).

### 3.8.2 Simulation results for BRAN-A channel model

BER and PER simulation results are presented in Fig. 3.15 to Fig. 3.26. As a comparison to the PRP-OFDM performances, the results are given for standard CP-OFDM with perfect CSI knowledge and for IEEE802.11a like channel estimation based on two learning symbols prior to the data symbol frame. No channel tracking/refinement is applied for CP-OFDM, neither in the static nor the mobility context. Concerning PRP-OFDM decoding techniques, the MMSE approach typically leads to the best performance results, followed by the OLA technique and finally the ZF approach. The ZF approach performs poorly due to the inherent noise correlation in PRP-OFDM equalization: a small channel coefficient leads to noise amplification during the equalization step including the spreading of this contribution over other carriers.

The BPSK simulation results in Fig. 3.15 and Fig. 3.17 illustrate the superior performance of PRP-OFDM based on MMSE equalization: a relatively small observation window size of 21 OFDM symbols

is sufficient in order to achieve BER/PER results that are close to CP-OFDM with perfect CSI. OLA based equalization is approx. 1dB below the MMSE results and the ZF equalization performs poorly as expected.

QPSK results are presented in Fig. 3.17, Fig. 3.18, Fig. 3.19 and Fig.3.20. The results are similar to the BPSK case: MMSE performs close to the CP-OFDM approach with perfect CSI, while OLA lies approx. 1dB behind. In the context of mobility (72m/s), the *SS* approach leads to an important error floor of approx.  $BER=3 \cdot 10^{-4}$ , but *DS* improves the inherent MSE of the CSI and the simulation performance is close to the time-invariant case.

Similarly, QAM-16 simulation results presented in Fig. 3.21, Fig. 3.22, Fig. 3.23 and Fig. 3.24 indicate MMSE based equalization results close to the CP-OFDM case with perfect CSI. However, the observation window size was increased to 41 symbols in order to achieve a sufficient CIR MSE. In the context of mobility, the *SS* approach leads to an error floor at approx.  $BER=1 \cdot 10^{-3}$  for 36m/s and  $BER=6 \cdot 10^{-3}$  for 72m/s. The improved window position of the *DS* approach, however, helps to avoid the error floor for the 72m/s case; at 36m/s, the resulting system performance is even close to the time-invariant case.

With QAM-64, the limitations of PRP-OFDM become visible. Even with a large observation window size of 121 OFDM symbols, the MMSE equalization is approx. identical to the CP-OFDM case with the CIR estimated over two learning symbols. It is obvious that PRP-OFDM is rather suited for lower-order constellations in order to mitigate high user mobility. Chapter 7, however, illustrates means that allow to bypass some of the limitations at the cost of a complexity increase.

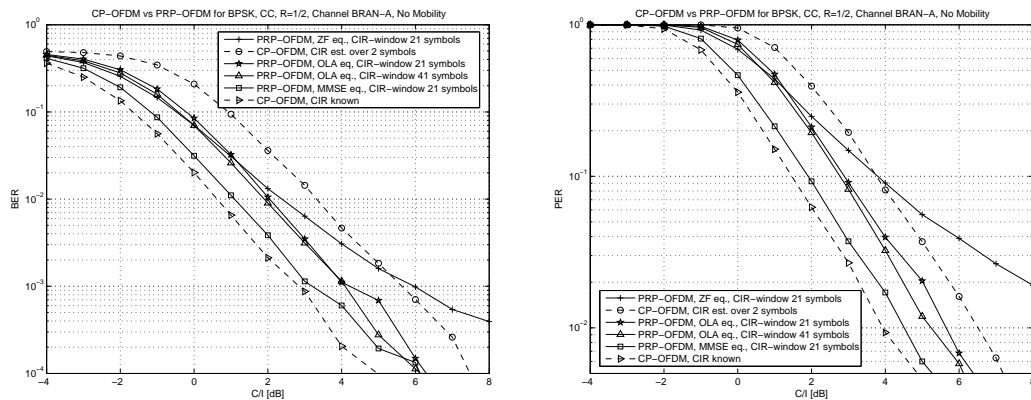


Figure 3.15: BER for IEEE802.11a, BRAN channel model A, BPSK, different decoding approaches. Figure 3.16: PER for IEEE802.11a, BRAN channel model A, BPSK, different decoding approaches.

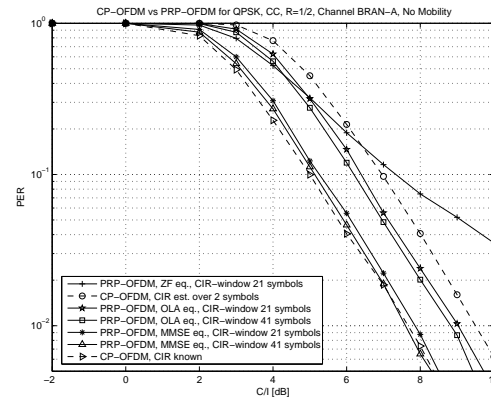
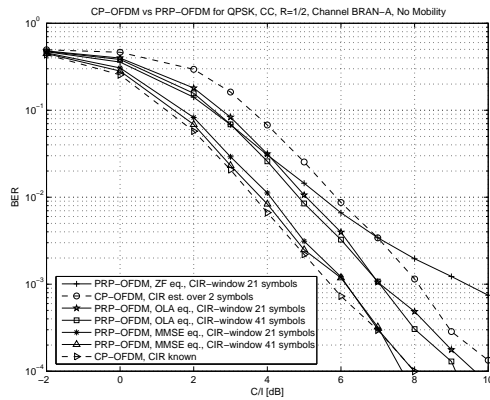


Figure 3.17: BER for IEEE802.11a, BRAN channel model A, QPSK, different decoding approaches. Figure 3.18: PER for IEEE802.11a, BRAN channel model A, QPSK, different decoding approaches.

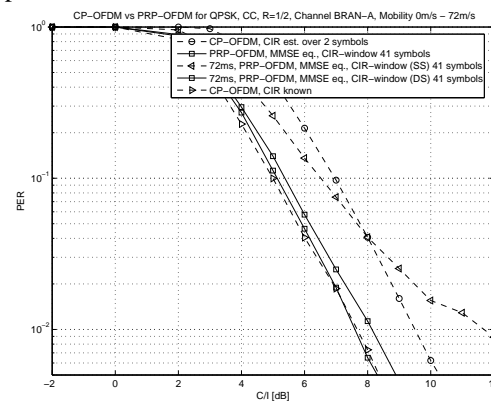
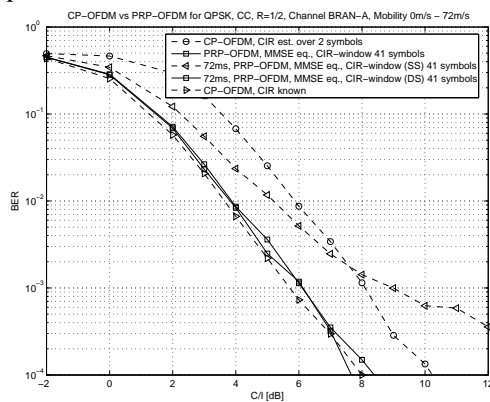


Figure 3.19: BER for IEEE802.11a, BRAN channel model A, QPSK, different decoding approaches, Doppler environment. Figure 3.20: PER for IEEE802.11a, BRAN channel model A, QPSK, different decoding approaches, Doppler environment.

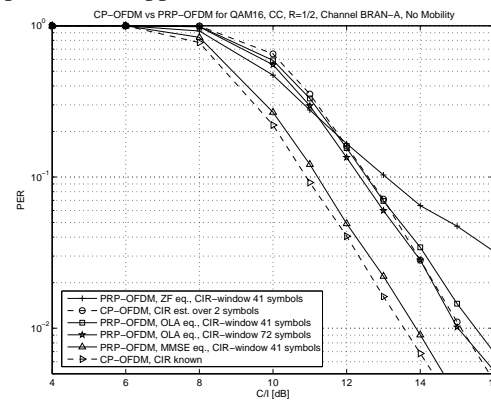
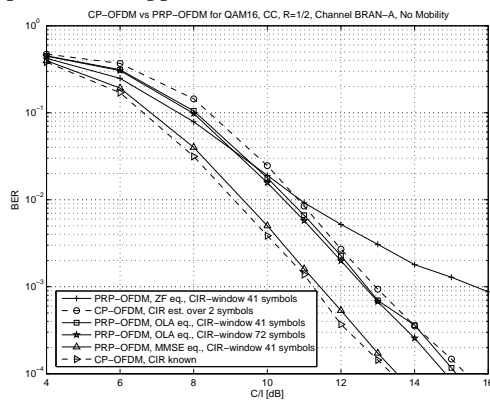


Figure 3.21: BER for IEEE802.11a, BRAN channel model A, QAM16, different decoding approaches. Figure 3.22: PER for IEEE802.11a, BRAN channel model A, QAM16, different decoding approaches.

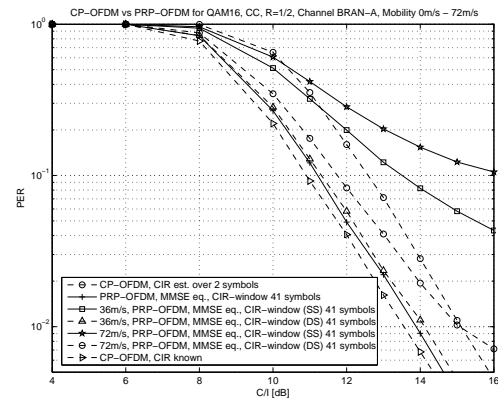
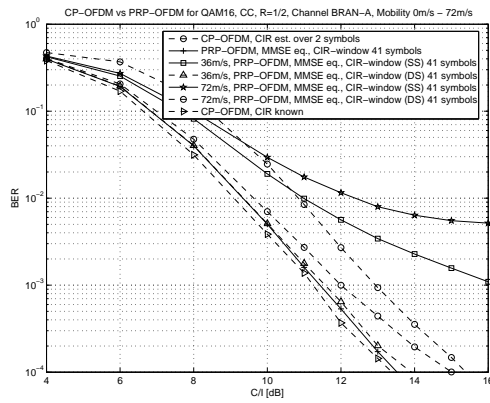


Figure 3.23: BER for IEEE802.11a, BRAN channel model A, QAM16, different decoding approaches, Doppler environment. Figure 3.24: PER for IEEE802.11a, BRAN channel model A, QAM16, different decoding approaches, Doppler environment.

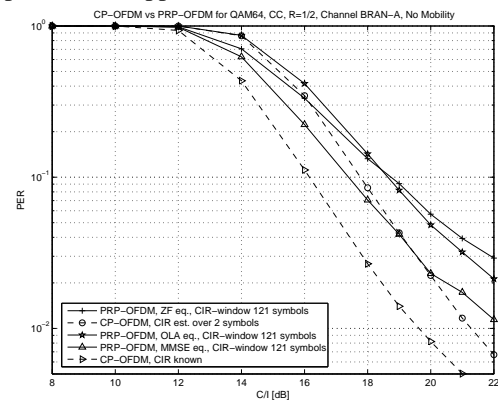
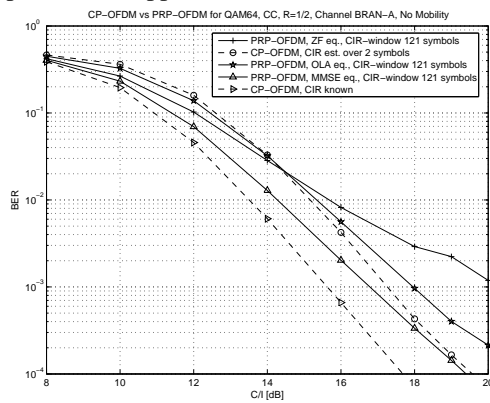


Figure 3.25: BER for IEEE802.11a, BRAN channel model A, QAM64, different decoding approaches. Figure 3.26: PER for IEEE802.11a, BRAN channel model A, QAM64, different decoding approaches.

### 3.8.3 Simulation results for BRAN-C channel model

Fig. 3.27 to Fig. 3.40 show the corresponding simulation results for the BRAN-C channel. The rms delay spread is increase to 150ns compared to 50ns for the BRAN-A case. Despite of the larger delay spread, the simulation results are very similar to the previous case: BPSK and QPSK constellations require a minimum observation window size of approx. 21 OFDM symbols, QAM-16 requires approx. 41 OFDM symbols or more and QAM-64 saturates even with an observation window size of 121 OFDM symbols. The MMSE equalization performs again close to the CP-OFDM case with perfect CSI knowledge and OLA loses approx. 1dB. ZF performs poorly for the reasons given above.

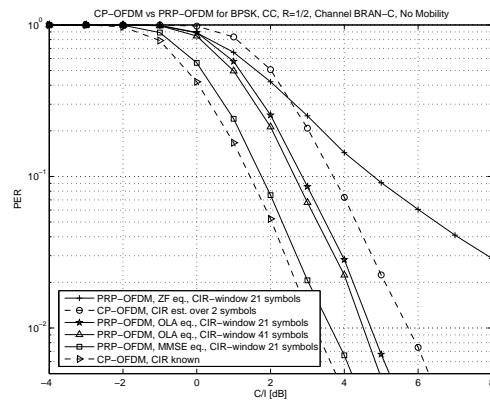
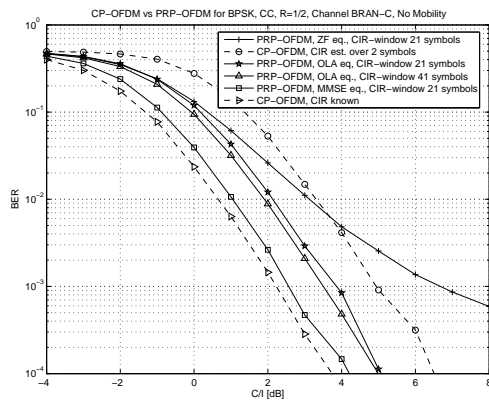


Figure 3.27: BER for IEEE802.11a, BRAN channel model C, BPSK, different decoding approaches. Figure 3.28: PER for IEEE802.11a, BRAN channel model C, BPSK, different decoding approaches.

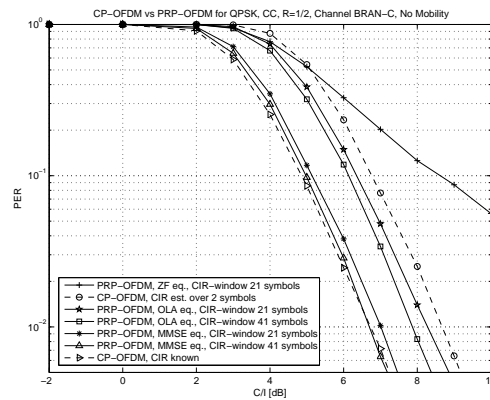
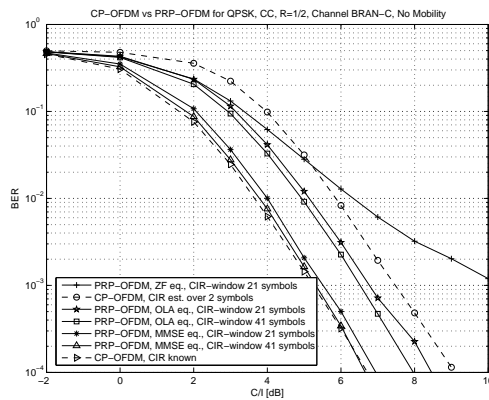


Figure 3.29: BER for IEEE802.11a, BRAN channel model C, QPSK, different decoding approaches. Figure 3.30: PER for IEEE802.11a, BRAN channel model C, QPSK, different decoding approaches.

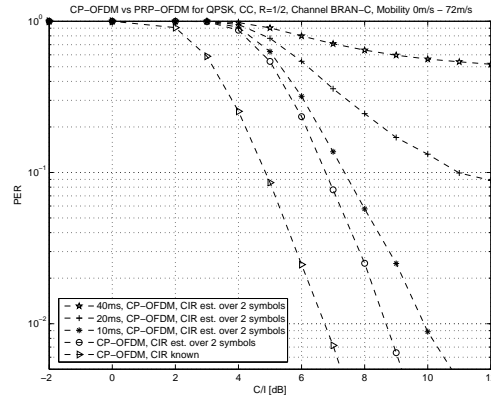
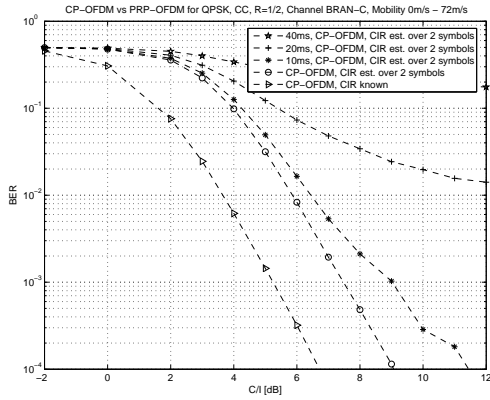


Figure 3.31: BER for IEEE802.11a, BRAN channel model C, QPSK, different decoding approaches, Doppler environment. Figure 3.32: PER for IEEE802.11a, BRAN channel model C, QPSK, different decoding approaches, Doppler environment.

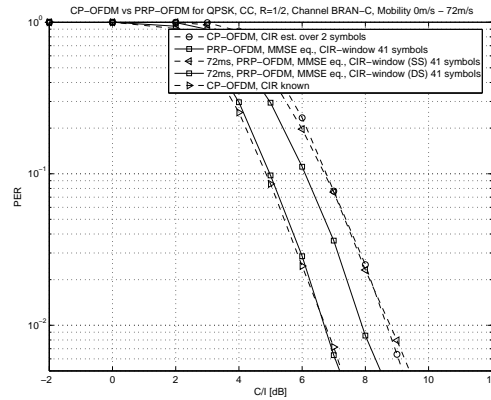
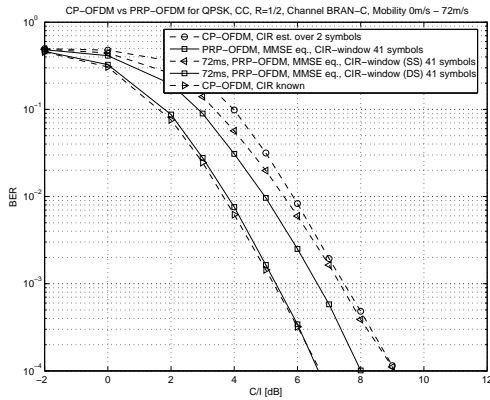


Figure 3.33: BER for IEEE802.11a, BRAN channel model C, QPSK, different decoding approaches, Doppler environment. Figure 3.34: PER for IEEE802.11a, BRAN channel model C, QPSK, different decoding approaches, Doppler environment.

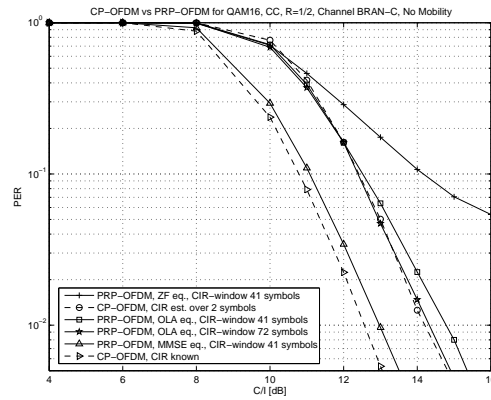
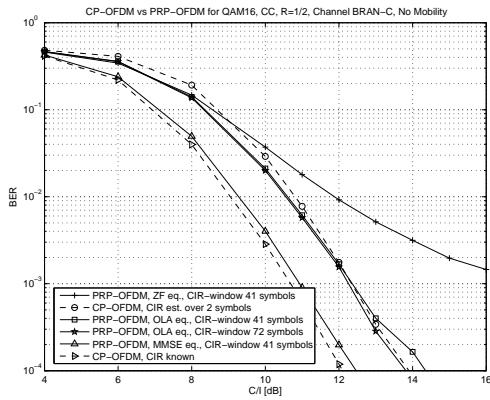


Figure 3.35: BER for IEEE802.11a, BRAN channel model C, QAM16, different decoding approaches. Figure 3.36: PER for IEEE802.11a, BRAN channel model C, QAM16, different decoding approaches.

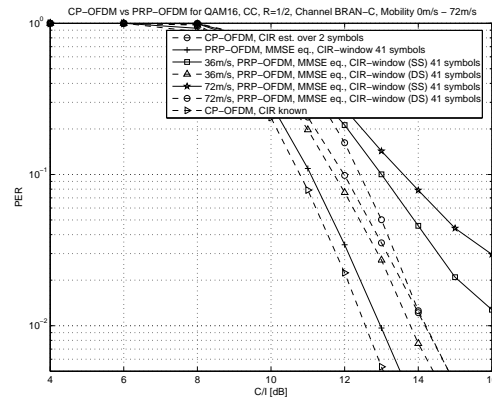
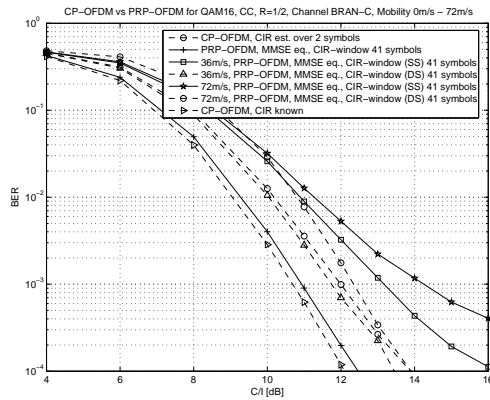


Figure 3.37: BER for IEEE802.11a, BRAN channel model C, QAM16, different decoding approaches, Doppler environment.

Figure 3.38: PER for IEEE802.11a, BRAN channel model C, QAM16, different decoding approaches, Doppler environment.

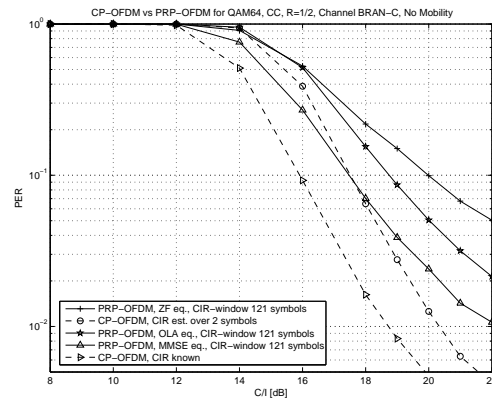
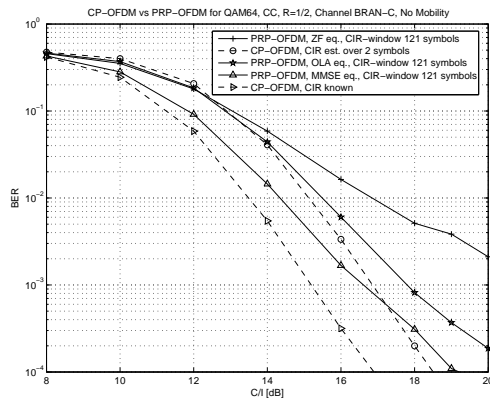


Figure 3.39: BER for IEEE802.11a, BRAN channel model C, QAM64, different decoding approaches.

Figure 3.40: PER for IEEE802.11a, BRAN channel model C, QAM64, different decoding approaches.

### 3.8.4 Simulation results for BRAN-E channel model

Fig. 3.41 to Fig. 3.52 show the corresponding simulation results for the BRAN-C channel. The rms delay spread is increase to 250ns compared to 50ns (150ns) for the BRAN-A (BRAN-C) case. Despite of the larger delay spread, the simulation results are very similar to the previous cases: BPSK and QPSK constellations require a minimum observation window size of approx. 21 OFDM symbols, QAM-16 requires approx. 41 OFDM symbols or more and QAM-64 saturates even with an observation window size of 121 OFDM symbols. The MMSE equalization performs again close to the CP-OFDM case with perfect CSI knowledge and OLA loses approx. 1dB. ZF performs poorly for the reasons given above.

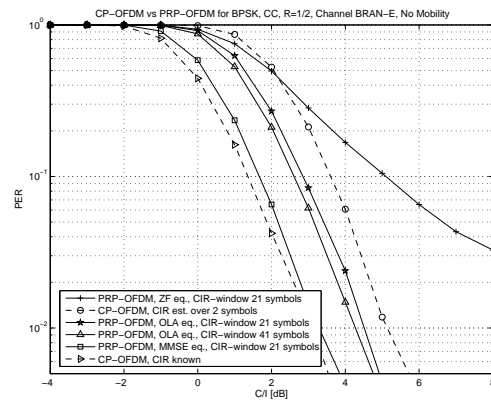
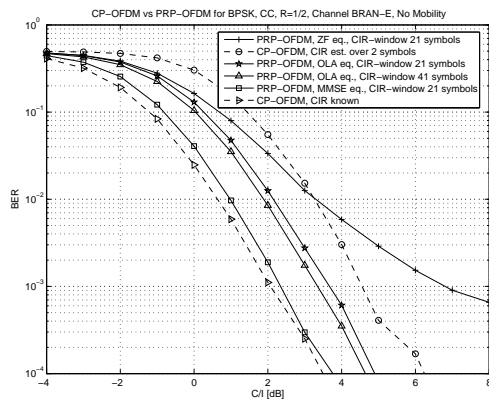


Figure 3.41: BER for IEEE802.11a, BRAN channel model E, BPSK, different decoding approaches. Figure 3.42: PER for IEEE802.11a, BRAN channel model E, BPSK, different decoding approaches.

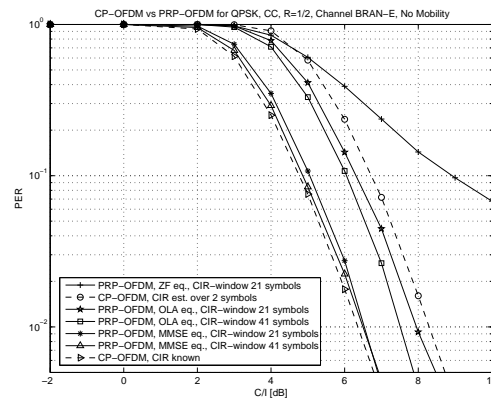
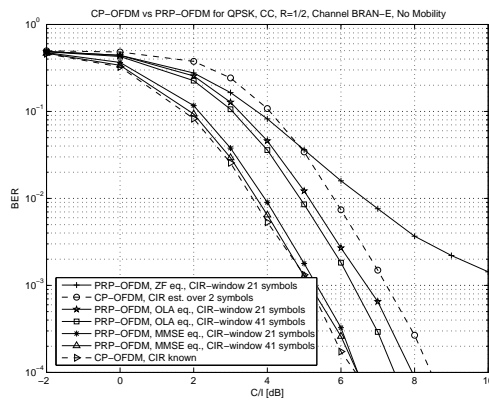


Figure 3.43: BER for IEEE802.11a, BRAN channel model E, QPSK, different decoding approaches. Figure 3.44: PER for IEEE802.11a, BRAN channel model E, QPSK, different decoding approaches.

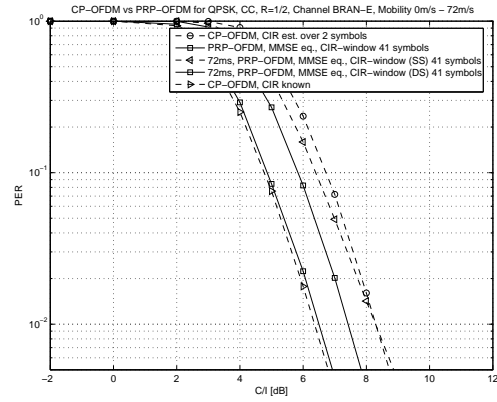
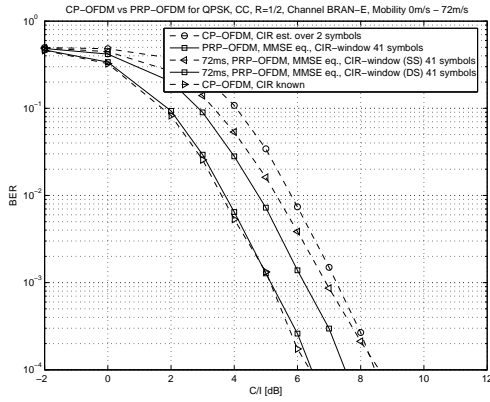


Figure 3.45: BER for IEEE802.11a, BRAN channel model E, QPSK, different decoding approaches, Doppler environment.

Figure 3.46: PER for IEEE802.11a, BRAN channel model E, QPSK, different decoding approaches, Doppler environment.

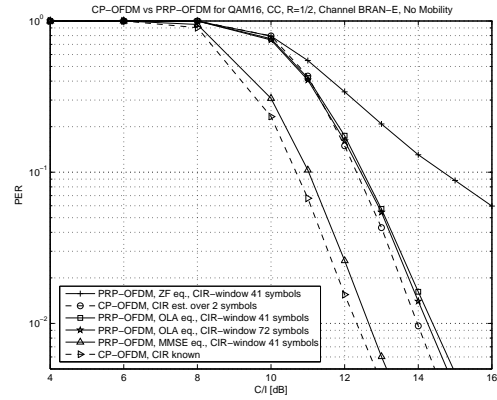
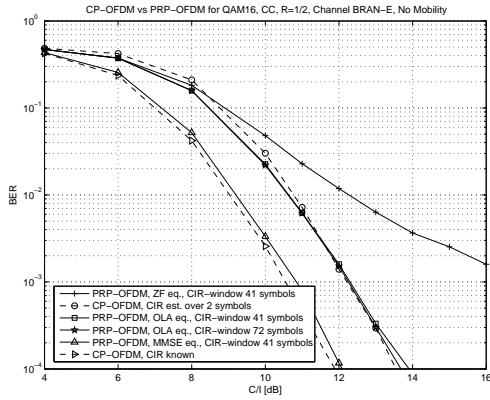


Figure 3.47: BER for IEEE802.11a, BRAN channel model E, QAM16, different decoding approaches.

Figure 3.48: PER for IEEE802.11a, BRAN channel model E, QAM16, different decoding approaches.

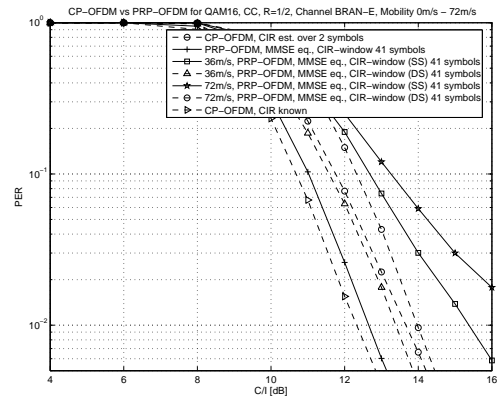
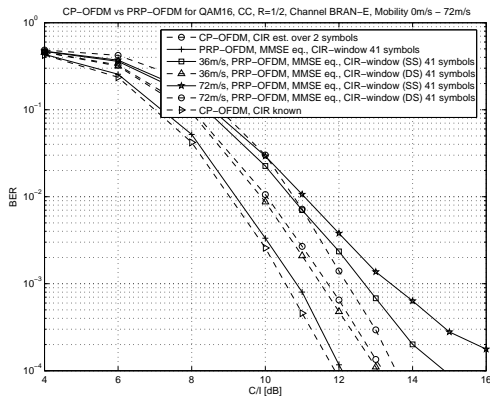


Figure 3.49: BER for IEEE802.11a, BRAN channel model E, QAM16, different decoding approaches, Doppler environment.

Figure 3.50: PER for IEEE802.11a, BRAN channel model E, QAM16, different decoding approaches, Doppler environment.

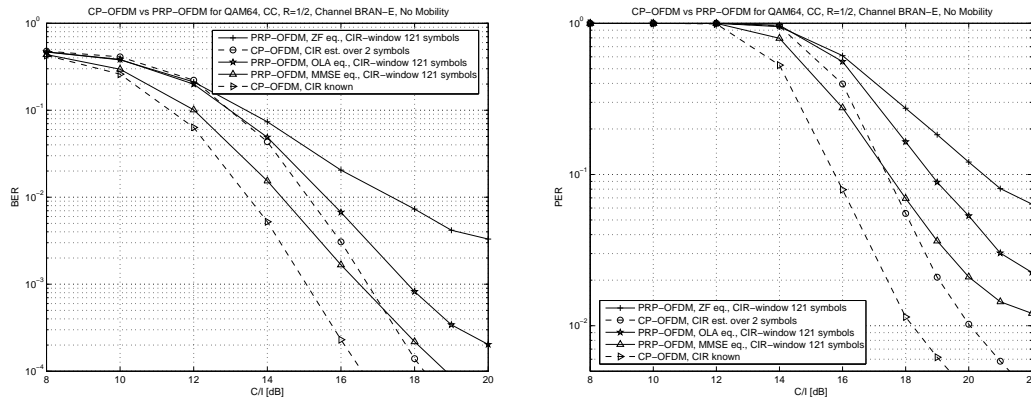


Figure 3.51: BER for IEEE802.11a, BRAN channel model E, QAM64, different decoding approaches. Figure 3.52: PER for IEEE802.11a, BRAN channel model E, QAM64, different decoding approaches.

### 3.8.5 Simulation results for BRAN-A channel model (uncoded)

This section presents simulation results for an uncoded transmission. The BPSK BER/PER results presented in Fig. 3.53 and Fig. 3.54 indicate that an MMSE equalization shows an error floor of approx.  $BER=7 \cdot 10^{-4}$  for an observation window size of 41 OFDM symbols for channel estimation. Increasing this window size to 121 symbols avoids this error floor and leads to results that are close to CP-OFDM with perfect CSI knowledge.

For QPSK, presented in Fig. 3.55 and Fig. 3.56, it is interesting to note that the observation window size of 41 OFDM symbols always leads to an error floor while the 121 OFDM symbols window used for channel estimation leads to system performances *superior* to the CP-OFDM case with perfect CSI knowledge. This is explained by the additional diversity gain of PRP-OFDM equalization compared to CP-OFDM: the PRP-OFDM MMSE equalizer works on an frequency domain oversampled signal as explained in [39] for ZP-OFDM; it is thus possible to recover a carrier amplitude even if the CP-OFDM frequency domain sampling point is weighted by a very low or even zero-valued channel coefficient. An error floor occurs still at approx.  $BER=2 \cdot 10^{-4}$ .

Uncoded QAM-16 constellations (and higher) require very large observation windows for CIR estimation. Here, PRP-OFDM is clearly not suited as illustrated in Fig. 3.57 and Fig. 3.58.

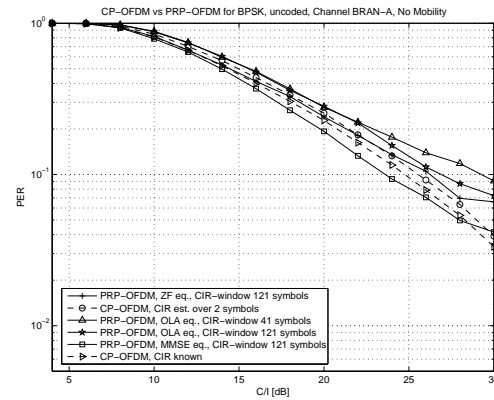
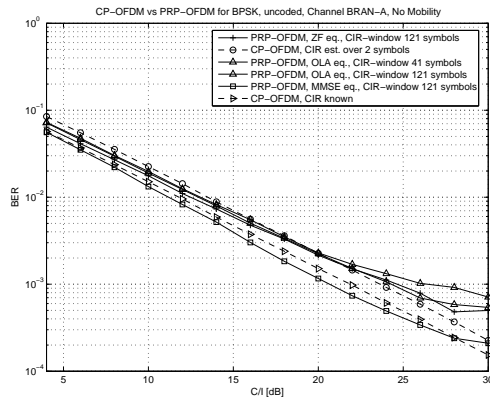


Figure 3.53: BER for IEEE802.11a, BRAN channel model A uncoded, BPSK, different decoding approaches.

Figure 3.54: PER for IEEE802.11a, BRAN channel model A uncoded, BPSK, different decoding approaches.

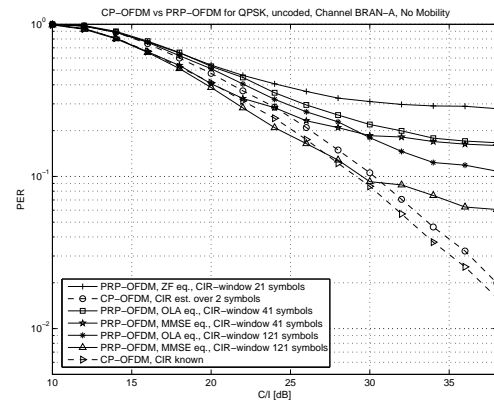
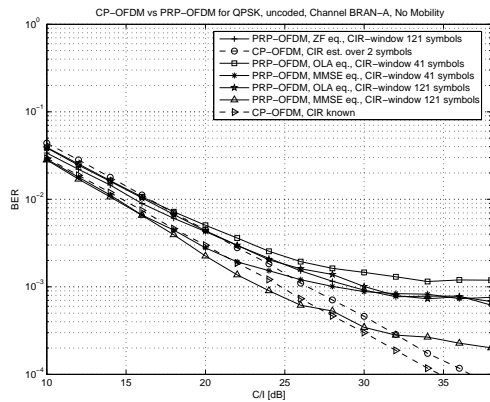


Figure 3.55: BER for IEEE802.11a, BRAN channel model A uncoded, QPSK, different decoding approaches.

Figure 3.56: PER for IEEE802.11a, BRAN channel model A uncoded, QPSK, different decoding approaches.

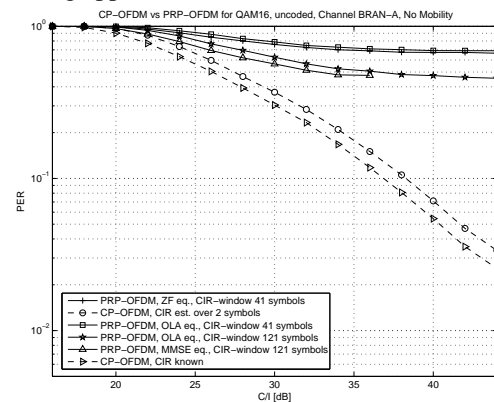
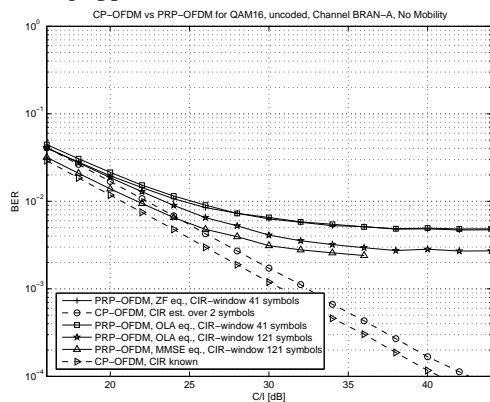


Figure 3.57: BER for IEEE802.11a, BRAN channel model A uncoded, QAM16, different decoding approaches.

Figure 3.58: PER for IEEE802.11a, BRAN channel model A uncoded, QAM16, different decoding approaches.

### 3.9 Conclusion

In this contribution a new OFDM modulation has been presented based on a pseudo random postfix: PRP-OFDM, using known samples instead of random data. This multi-carrier scheme has the advantage to inherently provide a very simple blind channel estimation exploiting this deterministic values. The same overhead as CP-OFDM is kept. Moreover several equalization approaches have been proposed with the same robustness granted by the ZP-OFDM receivers. Suboptimal arithmetic complexity yet efficient Viterbi decoding metrics have also been detailed. Simple channel estimates were shown to be feasible, leading to improved BER.

Due to the low additional complexity requirements for the simple decoding approaches derived in section 3.7, PRP-OFDM is of advantage compared to CP-OFDM and ZP-OFDM schemes if the target application requires: i) a minimum pilot overhead, ii) low-complexity channel tracking (e.g. a IEEE802.11a like system in a high mobility context) and iii) adjustable receiver complexity/performance trade-offs.

## Chapter 4

# Pseudo Random Postfix OFDM: Postfix Design

This part complements the definition of the Pseudo-Random-Postfix OFDM (PRP-OFDM) modulator presented in the chapters 2 and 3: the proper design of a postfix sequence is discussed which will replace the content of the guard interval known from classical Cyclic Prefix OFDM (CP-OFDM) systems.

### 4.1 Introduction

In previous chapters, the novel Pseudo-Random-Postfix OFDM (PRP-OFDM) modulation scheme was defined and studied: instead of the classical cyclic prefix extension known from CP-OFDM [48] or the Zero-Padding introduced in the framework of ZP-OFDM, it is proposed to insert a known vector weighted by a pseudo random scalar sequence between classical OFDM symbols: the Pseudo Random Postfix OFDM (PRP-OFDM). In chapter 3 it is shown that PRP-OFDM capitalizes on the advantages of CP-OFDM [48] and ZP-OFDM [39, 40, 70–76]; furthermore, unlike former OFDM modulators, the receiver can exploit an additional information: the prior knowledge of a part of the transmitted block. It is explained how to build on this knowledge in order to perform a low complexity order one semi-blind channel estimation and tracking. PRP-OFDM proves to be of advantage over existing modulation schemes if the target system requires i) a minimum pilot overhead, ii) low-complexity channel tracking (e.g. a IEEE802.11a like system in a high mobility context) and iii) adjustable receiver complexity/performance trade-offs. The PRP-OFDM concept has been validated on an FPGA based prototyping platform operating at 5GHz and 60GHz [11].

This chapter discusses the design of a proper postfix sequence. For this purpose, various constraints are taken into account: regulatory issues (such as spectrum mask requirements), system implementation (requirements on filter designs, Peak-to-Average-Power Ratio (PAPR)) and base-band design constraints (homogeneous mean-square-error (MSE) over all frequency domain channel coefficients, concentration of the signal power on in-band carriers). As a result, an iterative multi-dimensional optimization approach is proposed which helps to find suitable postfix sequences. Several examples are provided for the context of the 5GHz IEEE802.11a WLAN standard [56].

This chapter is organized as follows. Notations and a definition of the PRP-OFDM modulator are given section 4.2. Section 4.3.3 discusses the design constraints of the postfix sequence and demonstrates that a pseudo-random-weighting of the sequence leads to preferable spectral signal properties. An iterative optimization procedure for the derivation of postfix sequences with several trade-offs (e.g. low PAPR versus in-band flatness and low out-of-band radiation) is given in section 4.4 followed by a presentation of some examples of postfix sequences section 4.5. Finally, some conclusions are given section 4.6.

## 4.2 Notations and PRP-OFDM modulator

The baseband discrete-time block equivalent model of an  $N$  carrier PRP-OFDM system is considered as given by figure 4.1. The  $i$ th  $N \times 1$  input digital vector  $\tilde{\mathbf{s}}_N(i)$  is first modulated by the IFFT matrix  $\mathbf{F}_N^H := \frac{1}{\sqrt{N}} \left( W_N^{ij} \right)^H$ ,  $0 \leq i < N, 0 \leq j < N$  and  $W_N := e^{-j\frac{2\pi}{N}}$ .

Then, a deterministic postfix vector  $\mathbf{p}_D := (p_0, \dots, p_{D-1})^T$  weighted by a pseudo random value  $\alpha(i) \in \mathbb{C}$  is appended to the IFFT output  $\mathbf{s}_N(i)$ . With  $P := N + D$ , the corresponding  $P \times 1$  transmitted vector is  $\mathbf{s}_P(i) := \mathbf{F}_{ZP}^H \tilde{\mathbf{s}}_N(i) + \alpha(i) \mathbf{p}_P$ , where

$$\mathbf{F}_{ZP}^H := \begin{bmatrix} \mathbf{I}_N \\ \mathbf{0}_{D,N} \end{bmatrix}_{P \times N} \mathbf{F}_N^H \quad \text{and} \quad \mathbf{p}_P := (\mathbf{0}_{1,N} \mathbf{p}_D^T)^T$$

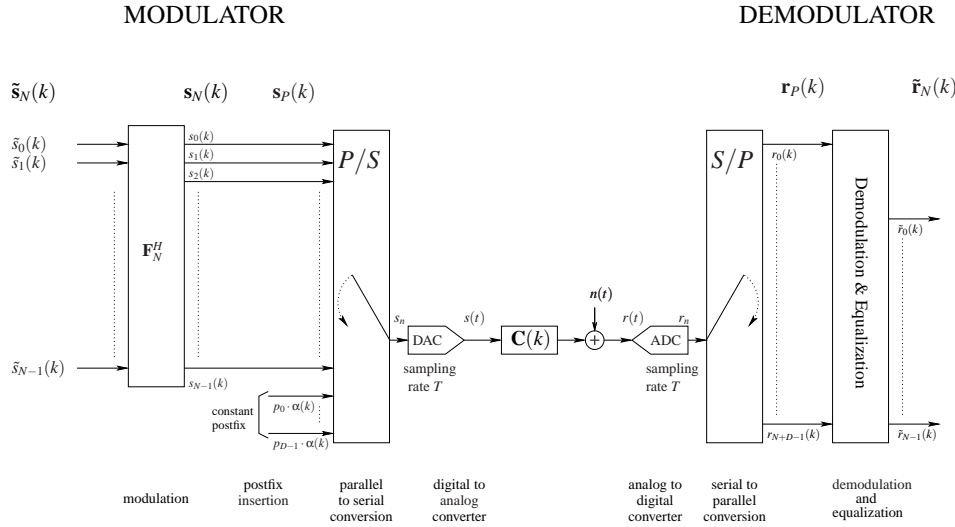


Figure 4.1: Discrete model of the PRP-OFDM modulator.

Without loss of generality, the elements of  $\mathbf{s}_N(i) = \mathbf{F}_N^H \tilde{\mathbf{s}}_N(i)$  are assumed to be i.i.d. and zero mean random variables of variance  $\sigma_s^2 = 1$  which are independent of  $\alpha(i) \mathbf{p}_D$ . The samples of  $\mathbf{s}_P(i)$  are then sent sequentially through the channel modeled here as an FIR filter of order  $L$ ,  $C(z) := \sum_{n=0}^L c_n z^{-n}$ . The OFDM system is designed such that the postfix duration exceeds the channel memory  $L < D$ .

Let  $\mathbf{C}_{ISI}(P)$  and  $\mathbf{C}_{IBI}(P)$  be respectively the size  $P$  Toeplitz inferior and superior triangular matrices of first column  $[c_0, c_1, \dots, c_L, 0, \dots, 0]^T$  and first row  $[0, \dots, 0, c_L, \dots, c_1]$ . As already explained in [80],

the channel convolution can be modeled by  $\mathbf{r}_P(i) := \mathbf{C}_{\text{ISI}}(P)\mathbf{s}_P(i) + \mathbf{C}_{\text{IBI}}(P)\mathbf{s}_P(i-1) + \mathbf{n}_P(i)$ .  $\mathbf{C}_{\text{ISI}}(P)$  and  $\mathbf{C}_{\text{IBI}}(P)$  represent respectively the intra and inter block interference.  $\mathbf{n}_P(i)$  is the  $i$ th AWGN vector of element variance  $\sigma_n^2$ . Since  $\mathbf{s}_P(i) = \mathbf{F}_{\text{ZP}}^H \tilde{\mathbf{s}}_N(i) + \alpha(i)\mathbf{p}_P$ , we have:

$$\mathbf{r}_P(i) := (\mathbf{C}_{\text{ISI}}(P) + \beta_i \mathbf{C}_{\text{IBI}}(P))\mathbf{s}_P(i) + \mathbf{n}_P(i) \quad (4.1)$$

where  $\beta_i := \frac{\alpha(i-1)}{\alpha(i)}$ . Note that  $\mathbf{C}_{\beta_i} := (\mathbf{C}_{\text{ISI}}(P) + \beta_i \mathbf{C}_{\text{IBI}}(P))$  is pseudo circulant: i.e. a circulant matrix whose  $(D-1) \times (D-1)$  upper triangular part is weighted by  $\beta_i$ .

In the sequel, the focus is on the proper design of postfix sequences as they are assumed to be available in the given references.

### 4.3 PRP-OFDM Postfix Design Constraints

Before considering the design of the postfix sequence itself, it is important to understand regulatory and system design constraint which have to be taken into account. The following points will be considered:

1. regulatory constraints on the power spectrum mask, such as limitations on the signal power distribution within the system bandwidth
2. system implementation constraints, such as non-linearities in the Power Amplifier (PA), limitations on filter impulse response lengths, etc.
3. base-band performance constraints, such as the requirement on a homogeneous MSE of the frequency channel coefficient estimates over all in-band carriers, etc.

All examples will be given in the context and with the system parameters of the IEEE802.11a 5GHz WLAN standard [56].

#### 4.3.1 Regulatory constraints

Any system implementation needs to meet the regulatory constraints. In the context of wireless systems, these are mainly limited to the center frequencies, the maximum mean level of output power and the definition of the spectrum mask. While the design of the PRP-OFDM postfix sequence is not affected by center frequency and system output power constraints, the definition of the spectrum mask is an important parameter. In the context of IEEE802.11a [56], it is defined as illustrated in Fig.4.2. Note that these limitations should be considered to be *moderate* and more restrictive spectrum mask constraints may be imposed in the future (e.g. in context of next generation wireless mobile phone standards as they are prepared in the context of the European Project IST-WINNER IST-2003-507581 [21–24, 30]):

By setting the sampling frequency of the complex time domain signal to 20MHz, the discrete time domain samples are efficiently generated by a 64-point Inverse Fast Fourier Transformation (IFFT). Among the 64 carriers, the DC carrier and 11 side-band carriers remain unused as illustrated in Fig.4.3 in order to facilitate the system conformance with the spectrum mask.

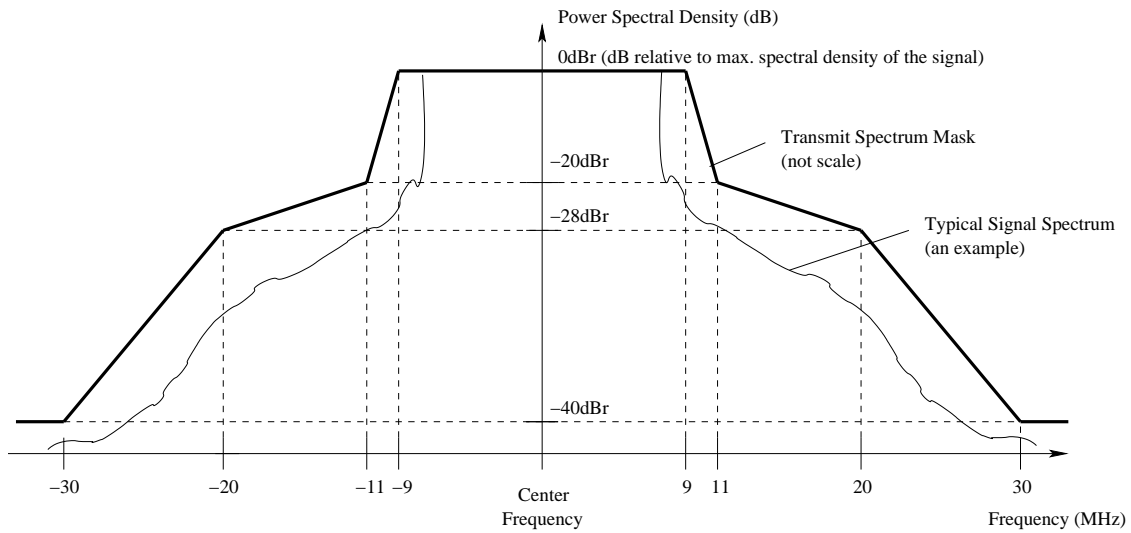


Figure 4.2: Transmission Spectrum Mask of IEEE802.11a.

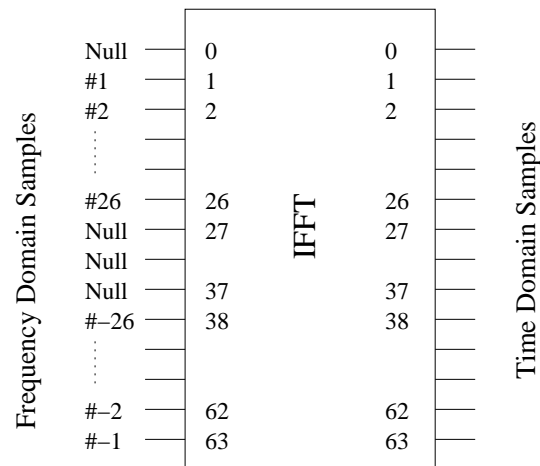


Figure 4.3: Time Domain Signal generation by means of an IFFT for IEEE802.11a.

Since the discrete time domain postfix sequence will typically be generated based on the same sampling frequency (and thus same bandwidth) as the OFDM data signal, the following design choices/constraints occur:

1. Design the postfix sequence such that it inherently meets the spectrum mask requirements. This approach considerably limits the possible design approach; in particular, any white PN-sequence is unsuitable.
2. Design the postfix sequence independently from any spectrum mask requirements. Suitable Low-Pass (LP) filters will adapt the signal to the spectrum mask requirements.
3. Avoid any (cyclo-)stationarity in the postfix sequences, since these would lead to peaks in the frequency domain which considerably lower the out-of-band radiation constraints given in the spectrum mask (see section 4.3.3).

While the trade-offs of the first approach are obvious, the second one will be considered in detail in the following section.

### 4.3.2 System implementation constraints

The study of the PRP-OFDM postfix design with respect to system implementation constraints will be performed based on the typical WLAN transmitter implementation architecture presented in Fig.4.4 [15]:

The analysis of this architecture leads to the identification of the following main implementation constraints:

1. The Peak-to-Average-Power-Ratio (PAPR) of the input signal fed to the Power Amplifier (PA) should be as low as possible in order to reduce backoff-constraints. This observation is important for the design of PRP-OFDM postfix sequences: Contrarily to CP-OFDM, where PAPR related problems are of a probabilistic nature, the effects become deterministic in the PRP-OFDM context; if postfix clipping occurs in the power amplifier of the transmitter, it occurs for all postfixes.
2. The system impulse response (i.e. the impulse response of the transmitter convolved by the impulse response of the over-the-air propagation channel convolved by the receiver impulse response) should be as short as possible in order to avoid Inter-Block-Interference (IBI). IBI occurs if the system impulse response length is longer than the postfix sequence (or the guard interval in traditional CP-OFDM systems). Since the main contributor to the transmitter/receiver impulse response length is the low-pass filter, its selectivity constraints be as moderate as possible (a high filter selectivity inherently requires a long filter impulse response).

These points indicate that the PAPR parameter of the postfix sequence should be inherently as low as possible; furthermore, the requirement on a moderate filter selectivity is in favor of a postfix design that inherently meets the spectrum mask requirements.

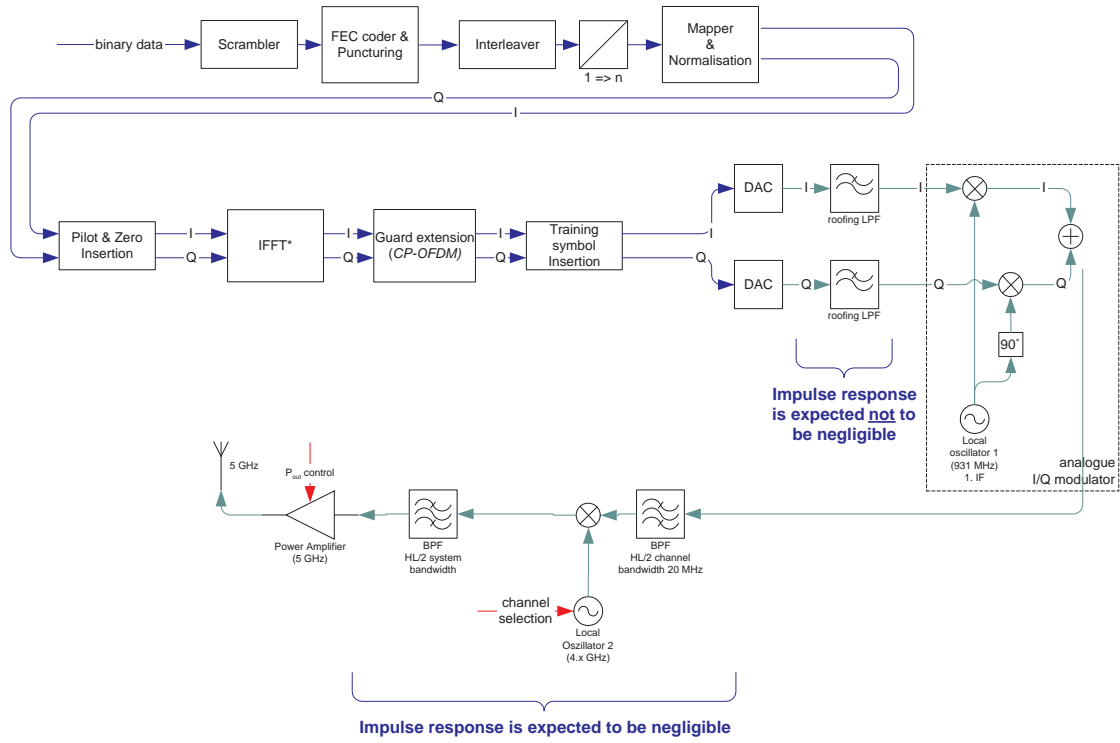


Figure 4.4: A typical transmitter implementation of IEEE802.11a.

### 4.3.3 Base-band design constraints

Following the arguments of section 4.3.1, it is desirable that the introduction of the pseudo random postfix results in a flat spectrum of the signal sent onto the channel. In order to analyze the spectral properties of the PRP-OFDM signal (since the signal is obviously not stationary but cyclo-stationary with periodicity  $P$  (duration of the OFDM block) [111]), the order 0 cyclo-spectrum of the transmitted time domain sequence  $s(k), k \in \mathbb{N}$  has to be calculated:

$$S_{s,s}^{(0)}(z) = \sum_{k \in \mathbb{Z}} z^{-k} \frac{1}{P} \sum_{l=0}^{P-1} R_{s,s}(l, k),$$

with  $R_{s,s}(l, k) = E [s_{l+k} s_l^*]$ . Hereby,  $R_{s,s}(l, k)$  is given for the symbol  $s(k = 0 \dots P-1)$  as

$$R_{s,s}(l, k) = \begin{cases} E [s_{l+k} s_l^*] & \text{for } k+l \geq 0 \text{ and } k+l < P \\ s_{l+k} s_l^* E_{\alpha} & \text{for } k+l \geq mP \text{ and} \\ & k+l < mP + D, m \in \mathbb{Z}/\{0\} \\ 0 & \text{otherwise.} \end{cases}$$

with  $E_{\alpha} = E [\alpha(\lfloor \frac{l+n}{P} \rfloor) \alpha^*(\lfloor \frac{l}{P} \rfloor)]$ . Now it is clear that it is desirable to choose  $\alpha(i), i \in \mathbb{Z}$  such that  $E_{\alpha} = 0$  in order to clear all influence of the deterministic postfix in the second order statistics of the transmitted signal. This is achievable by choosing  $\alpha(i)$  as a pseudo-random, zero-mean value.

### 4.3.4 Conclusion: resulting postfix design constraints

Following the argumentation presented in the previous section, the following criteria are recommended with respect to the design of the PRP-OFDM postfix sequence:

- i) minimize the time domain peak-to-average-power ratio (PAPR);
- ii) minimize out-of-band radiations, i.e. concentrate signal power on useful carriers;
- iii) maximize spectral flatness over useful carriers since the channel is not known at the transmitter (do not privilege certain carriers) and
- iv) avoid any signal (cyclo-)stationarity by applying a zero-mean pseudo-random weighting sequence to the postfix sequences.

The resulting postfix is obtained through a multi-dimensional optimization involving a complex cost function. A suitable procedure is studied in detail in the following sections. Note that if the PAPR criterion is not an issue, one can directly use the Kaiser-window [112].

## 4.4 Iterative derivation of a suitable postfix

Since the Kaiser-Window is optimum for all criteria defined before except the PAPR criterion, the idea is to take the Kaiser-Window as initial assumption and to trade-off low PAPR against out-of-band radiation and in-band flatness by iterative steepest-descent based optimization. For this reason, a weighted cost function is defined for each criterion. In another context, such an approach is commonly applied in the field of inverse problems, e.g. by [113].

The corresponding weighted cost functions introduced are:

- $\gamma^{\text{Flat}} J^{\text{Flat}}(\mathbf{p}_D)$  with  $\gamma^{\text{Flat}} \in \mathbb{R}, J^{\text{Flat}}(\mathbf{p}_D) \in \mathbb{R}$  cost function goal is to force spectral flatness over all in-band carriers;
- $\gamma^{\text{Out}} J^{\text{Out}}(\mathbf{p}_D)$  with  $\gamma^{\text{Out}} \in \mathbb{R}, J^{\text{Out}}(\mathbf{p}_D) \in \mathbb{R}$  cost function aims at setting the out-of-band carriers to approximately zero;
- $\gamma^{\text{Clip}} J^{\text{Clip}}(\mathbf{p}_D)$  with  $\gamma^{\text{Clip}} \in \mathbb{R}, J^{\text{Clip}}(\mathbf{p}_D) \in \mathbb{R}$  cost function role is to limit the time domain PAPR below a certain threshold.

Thus, the total cost function to be optimized is

$$J^{\text{Tot}} := \gamma^{\text{Flat}} J^{\text{Flat}}(\mathbf{p}_D) + \gamma^{\text{Out}} J^{\text{Out}}(\mathbf{p}_D) + \gamma^{\text{Clip}} J^{\text{Clip}}(\mathbf{p}_D).$$

Applying a simple steepest descent method, the minimum is found iteratively by setting  $\mathbf{p}_D(i+1) = \mathbf{p}_D(i) - \nabla J^{\text{Tot}}(i)$ , usually in combination with power normalization after each iteration. Hereby  $\nabla J^{\text{Tot}}(i) = 2 \frac{\partial}{\partial \mathbf{p}_D} J^{\text{Tot}}(\mathbf{p}_D)$  with  $\mathbf{p}_D = \mathbf{p}_D(i)$ , where  $\mathbf{p}_D$  is the vector containing the postfix of size  $D$ . The gradient of complex functions is used as defined by [104], Appendix B. In the following, both  $J^{\text{Tot}}(\mathbf{p}_D)$  and  $\nabla J^{\text{Tot}}(\mathbf{p}_D)$  are derived for each criterion. Since the channel is estimated over  $P$  carriers, all criteria are expressed in the  $P \times P$  Fourier domain.

#### 4.4.1 Spectral flatness

Denote by  $\mathcal{C}$  the set of integers gathering the row indices of the  $P \times P$  Fourier matrix  $\mathbf{F}_P$  corresponding to in-band carriers and  $\mathbf{F}_\mathcal{C}$  the sub-matrix of  $\mathbf{F}_P$  stacking these rows. With  $\hat{\mathbf{p}}_P = (\mathbf{p}_D^T \mathbf{0}_{1,N})^T$  a permuted version of vector  $\mathbf{p}_P$  is defined (which simplifies the presentation of the gradient calculation) and with  $\mathbf{f}_n^c$  a  $1 \times P$  vector containing the row of  $\mathbf{F}_\mathcal{C}$  corresponding to carrier  $c_n$ , i.e. the  $n$ th carrier of set  $\mathcal{C}$ , we have:

$$J^{\text{Flat}} := \sum_{n \in \mathcal{C}} \left[ |\mathbf{f}_n^c \hat{\mathbf{p}}_P| - \frac{1}{N_C} \sum_{k \in \mathcal{C}} |\mathbf{f}_k^c \hat{\mathbf{p}}_P| \right]^2$$

The gradient of  $J^{\text{Flat}}$  is given by  $\nabla J^{\text{Flat}} = 2 \left( \frac{\partial}{\partial p_0^*}, \dots, \frac{\partial}{\partial p_{D-1}^*} \right)^T J^{\text{Flat}}$  with

$$\frac{\partial J^{\text{Flat}}}{\partial p_m^*} = 2 \sum_{n \in \mathcal{C}} \left[ |\mathbf{f}_n^c \hat{\mathbf{p}}_P| - \overline{p}_F \right] \left( (\mathbf{f}_n^c)_m^* \frac{\mathbf{f}_n^c \hat{\mathbf{p}}_P}{2|\mathbf{f}_n^c \hat{\mathbf{p}}_P|} - \frac{\partial \overline{p}_F^{(m)}}{\partial p_m^*} \right)$$

Hereby,

$$\begin{aligned} \overline{p}_F &= \frac{1}{N_C} \sum_{n \in \mathcal{C}} |\mathbf{f}_n^c \hat{\mathbf{p}}_P|, \\ \frac{\partial \overline{p}_F^{(m)}}{\partial p_m^*} &= \frac{1}{N_C} \sum_{n \in \mathcal{C}} (\mathbf{f}_n^c)_m^* \frac{\mathbf{f}_n^c \hat{\mathbf{p}}_P}{2|\mathbf{f}_n^c \hat{\mathbf{p}}_P|} \end{aligned}$$

and  $(\mathbf{f}_n^c)_m^*$  is the  $m$ th component of  $(\mathbf{f}_n^c)^*$  and  $|\mathbf{f}_n^c \hat{\mathbf{p}}_P| = \sqrt{\mathbf{f}_n^c \hat{\mathbf{p}}_P \hat{\mathbf{p}}_P^H (\mathbf{f}_n^c)^H}$ .

#### 4.4.2 Out-of-band radiation

The out-of-band radiation is defined as the power over the unused carriers and is ideally zero. With  $\mathcal{O}$  being the set of  $N_O = |\mathcal{O}|$  out-of-band carriers, and  $\mathbf{F}_\mathcal{O}$  the subset of the  $\mathbf{F}_P$  Fourier matrix containing these rows  $\mathbf{f}_n^o$ . The expression of the cost function is:

$$J^{\text{Out}} := \sum_{n \in \mathcal{O}} \mathbf{f}_n^o \hat{\mathbf{p}}_P \hat{\mathbf{p}}_P^H (\mathbf{f}_n^o)^H$$

The expression of  $J^{\text{Out}}$  gradient is given by  $\nabla J^{\text{Out}} = 2 \left( \frac{\partial}{\partial p_0^*}, \dots, \frac{\partial}{\partial p_{D-1}^*} \right)^T J^{\text{Out}}$  with

$$\frac{\partial J^{\text{Out}}}{\partial p_m^*} = \sum_{n \in \mathcal{O}} (\mathbf{f}_n^o)_m^* \mathbf{f}_n^o \hat{\mathbf{p}}_P.$$

### 4.4.3 Clipping

The impact of the clipping is determined by the transfer function of the power amplifiers (PA) in the system. In the framework of this thesis, the following simple model is used:

$$f_{PA}(z) := \begin{cases} z & \text{for } |z| \leq c_L \\ c_L e^{j\phi(z)} & \text{for } |z| > c_L \end{cases}$$

where  $c_L \in \mathbb{R}^+$  is the clipping level and  $\phi(z)$  is the phase of  $z \in \mathbb{C}$ . The corresponding cost function is:

$$J^{\text{Clip,ideal}} := \sum_{n=0}^{D-1} \left[ \frac{1}{2} (|p_n| - c_L) \cdot [\text{sign}(|p_n|^2 - c_L^2) + 1] \right]^2.$$

In order to further improve the resulting postfix sequence, oversampling can be applied to the postfix sequence in the upper cost function. Note that  $\text{sign}(|p_n| - c_L) = \text{sign}(|p_n|^2 - c_L^2)$ . For the optimization, however, we substitute  $\text{sign}(x)$  by a  $C^1$  (differentiable) function; we choose  $\text{sign}(x) \approx \tanh(\eta x)$ ,  $\eta \in \mathbb{R}^+$ . Thus, the total cost function is

$$J^{\text{Clip}} := \sum_{n=0}^{D-1} \left[ \frac{1}{2} (|p_n| - c_L) \cdot [\tanh(\eta (|p_n|^2 - c_L^2)) + 1] \right]^2.$$

The gradient of  $J^{\text{Clip}}$  is given by  $\nabla J^{\text{Clip}} = 2 \left( \frac{\partial}{\partial p_0^*}, \dots, \frac{\partial}{\partial p_{D-1}^*} \right)^T J^{\text{Clip}}$  with

$$\frac{\partial J^{\text{Clip}}}{\partial p_m^*} = \frac{(|p_m| - c_L) p_m}{4|p_m|} [\tanh(\eta (|p_m|^2 - c_L^2)) + 1]^2 + \eta (|p_m| - c_L)^2 \frac{p_m [\tanh(\eta (|p_m|^2 - c_L^2)) + 1]}{2 \cosh^2(\eta (|p_m|^2 - c_L^2))}$$

with  $m = 0, \dots, D-1$ .

Now, the total cost function is defined and a corresponding postfix can be derived by the iteration  $\mathbf{p}_D(i+1) = \mathbf{p}_D(i) - \nabla J^{\text{Tot}}(i)$ .

## 4.5 Example of Postfix design

The upper steepest descent based postfix derivation is evaluated for the derivation of postfix sequences of 16, 32 and 48 samples. The optimized sequences are compared to a Kaiser window with respect to the following criteria: Peak-To-Average-Power-Ratio (PAPR), in-band ripple and out-of-band radiation. In all examples, the in-band carriers are defined corresponding to the definitions of IEEE802.11a as illustrated in Fig.4.3: the carriers  $\mathcal{O} = \{28, \dots, 38\}$  are out-of-band and  $\mathcal{C} = \{1, \dots, 27, 39, \dots, 64\}$  are useful carriers.

Fig.4.5 and Fig.4.6 present two postfixes with different trade-offs for the parameters  $D = 16$  (postfix size) and  $N = 64$  (OFDM symbol size) in time and frequency domain: A Kaiser Window as given by

Tab.4.1 and a postfix whose derivation is based on the upper optimization procedure, see Tab.4.2. As given by Tab.4.3, the Kaiser Window offers optimum spectral flatness and low out-of-band radiation with the drawback of a relatively high Peak-to-Average-Power-Ratio (PAPR): the PAPR is 11.548dB for the Kaiser window compared to 7.489dB for the optimized postfix sequence based on the upper steepest descent approach.

The spectral flatness vs PAPR trade-off becomes an issue if the size of the postfix sequence is further increased. Tab.4.4 and Tab.4.5 present the time domain samples of a corresponding Kaiser window and an optimized sequence, both of 32 samples. Fig.4.7 and Fig.4.8 illustrate the corresponding results in time and frequency domain. While the optimized sequence is superior compared to the Kaiser window in terms of PAPR (6.762dB vs 14.443dB), the ripple rises from 0.025dB to 0.742dB.

The ripple effect is reduced here for the 48 samples sequence as presented in Tab.4.7 and Tab.4.8 and illustrated in Fig.4.9 and Fig.4.10: the cost is a relatively high PAPR of 7.691dB. The same effect can be achieved for the upper postfixes, if desired. Note, however, that the ripple increases if the frequency resolution is higher; the postfix sequence was only improved for the  $N = 64$  considered carriers and may vary significantly on intermediate frequencies.

## 4.6 Conclusion

The design criteria for discrete postfix sequences have been discussed in the context of the Pseudo-Random-Postfix OFDM (PRP-OFDM) modulation scheme. A steepest descent based optimization algorithm has been proposed in order to trade-off different design-criteria, in particular the PAPR, the out-of-band radiation and spectral flatness. As an example, a resulting sequence is given for the IEEE802.11a WLAN context when the CP-OFDM modulator is replaced by the PRP-OFDM scheme. Further examples of 32 and 48 samples length are presented based on identical spectral requirements. While the postfix of 16 samples length is suitable for IEEE802.11a-like OFDM parameter sets, larger postfix sizes are applicable, for example, to a wider communication range context where typically longer OFDM symbols are used [24, 25]. PRP-OFDM thus allows to efficiently reduce the preamble and pilot overhead in a system design phase without any loss in system performances nor spectral efficiency.

Sample nb	Amplitude	Sample nb	Amplitude
1	0.0140	9	3.4066
2	-0.0079	10	0.5504
3	-0.0278	11	-0.4420
4	0.1045	12	0.3059
5	-0.2209	13	-0.1757
6	0.3597	14	0.0765
7	-0.4904	15	-0.0182
8	0.5792	16	-0.0042

Table 4.1: Time domain samples of a suitable postfix (Kaiser Window, 16 samples).

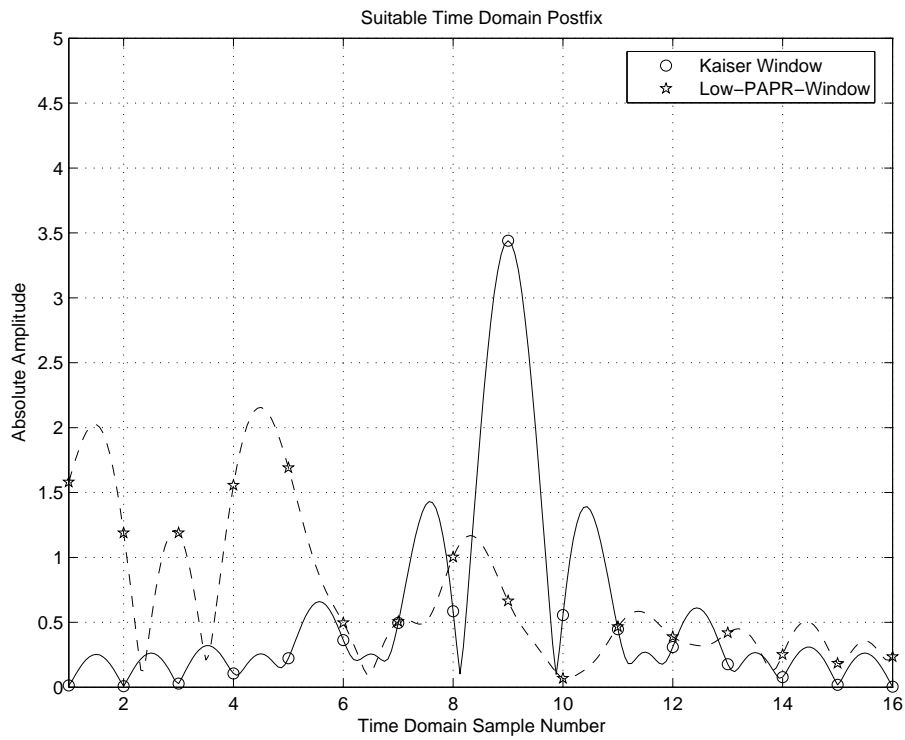


Figure 4.5: Postfixes with different trade-offs in time domain (16 samples).

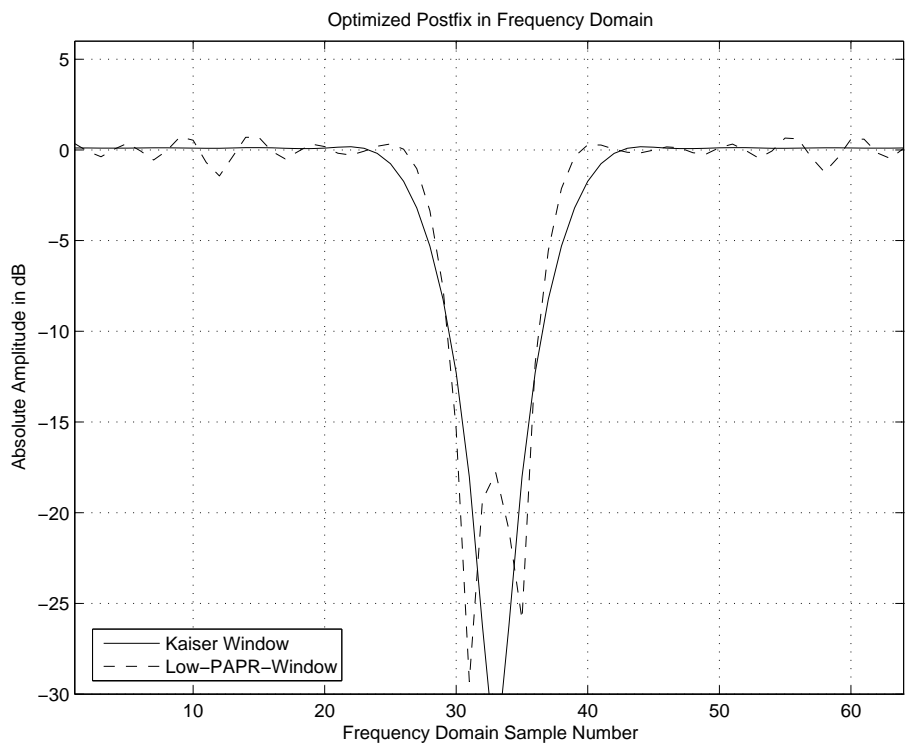


Figure 4.6: Postfixes with different trade-offs in frequency domain (16 samples).

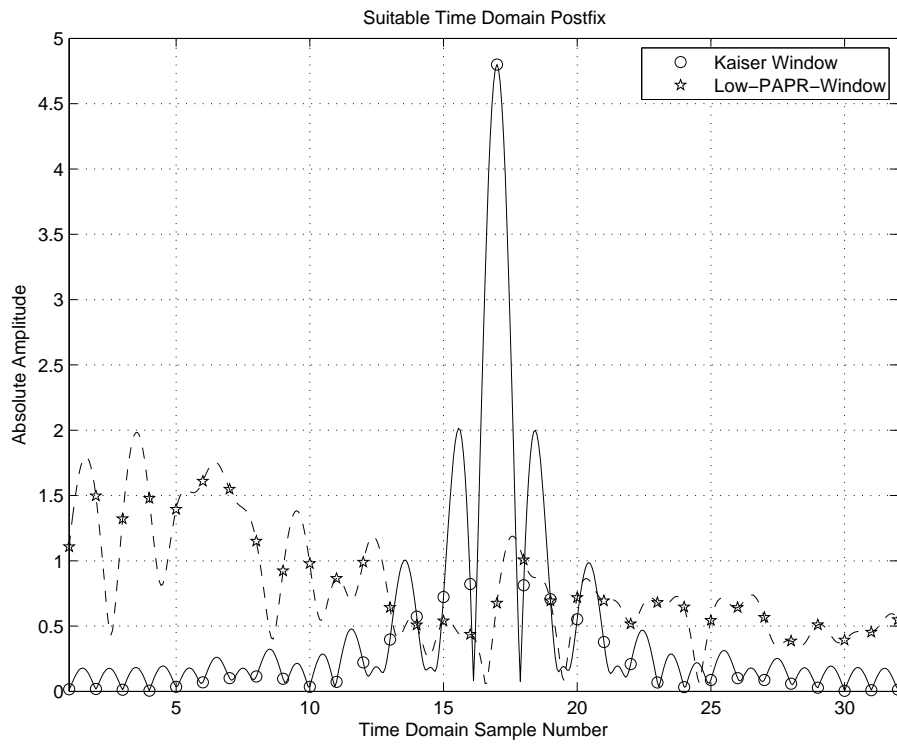


Figure 4.7: Postfixes with different trade-offs in time domain (32 samples).

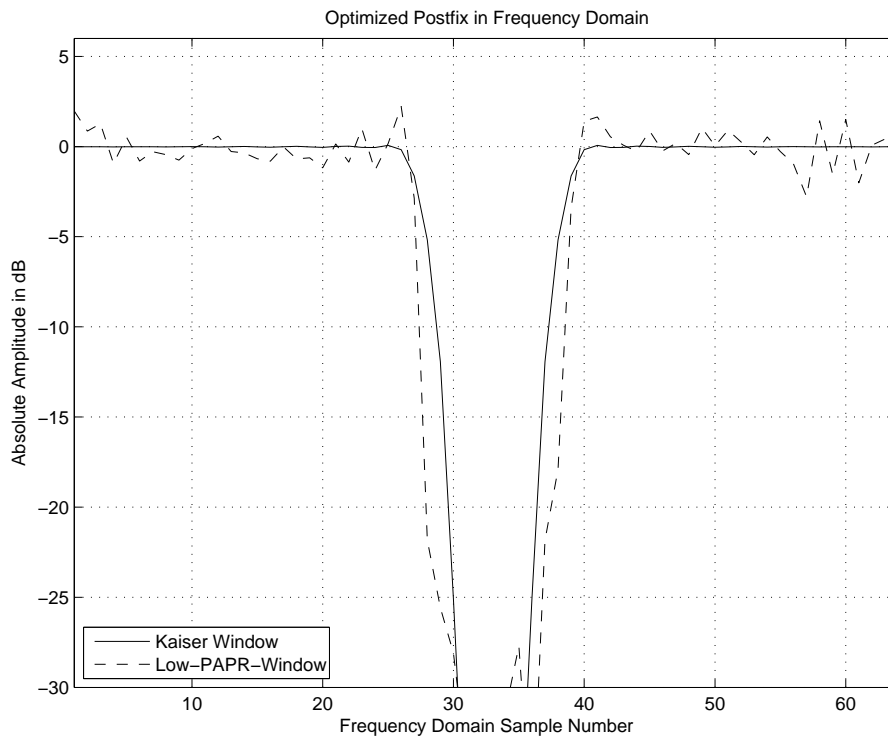


Figure 4.8: Postfixes with different trade-offs in frequency domain (32 samples).

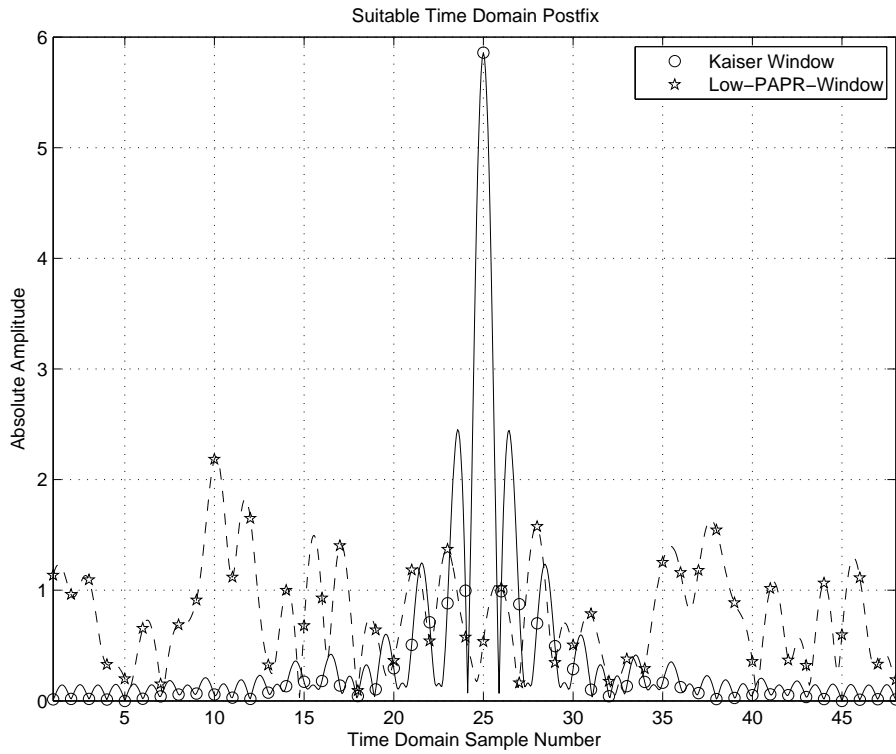


Figure 4.9: Postfixes with different trade-offs in time domain (48 samples).

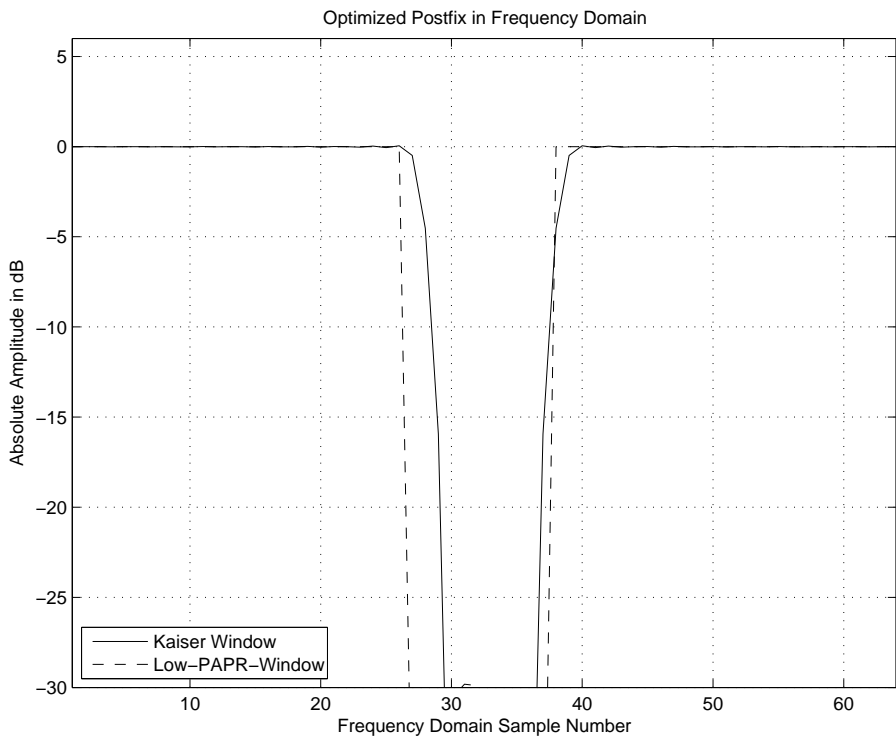


Figure 4.10: Postfixes with different trade-offs in frequency domain (48 samples).

Sample nb	Amplitude	Sample nb	Amplitude
1	1.5649-0.0356i	9	0.0832-0.6527i
2	-0.6961+ 0.9494i	10	0.0306+ 0.0594i
3	0.0874+ 1.1743i	11	0.4047+ 0.2204i
4	0.5737+ 1.4300i	12	-0.2723+ 0.2715i
5	-1.4368-0.8592i	13	0.3469-0.2291i
6	0.2212+ 0.4389i	14	0.0779-0.2369i
7	0.4137+ 0.2834i	15	0.1214+ 0.1355i
8	-0.0960+ 0.9893i	16	-0.2110-0.0972i

Table 4.2: Time domain samples of a suitable postfix (optimized 16 samples postfix).

Parameter	Kaiser Window	PAPR opt. Postfix
PAPR $\frac{\ \mathbf{p}_D\ _\infty^2}{\frac{1}{D} \sum_{n=0}^{D-1}  p_n ^2}$	11.548dB	7.489dB
Total out-of-band radiation $\frac{\sum_{n=0}^{N-1}  p_n^f ^2}{\sum_{n=0}^{N-1}  p_n^f ^2}, \mathbf{p}^f = \mathbf{F}_N \begin{bmatrix} \mathbf{p}_D \\ \mathbf{0}_{N-D,1} \end{bmatrix}$	-16.33dB	-12.581dB
Spectral in-band ripple Calculated over carriers $C^2 = C \setminus \{21, \dots, 27, 39, \dots, 45\}$ (i.e. transition to stop-band not considered)	0.025dB	0.742dB

Table 4.3: Comparison on postfix trade-offs (16 samples postfix).

Sample nb	Amplitude	Sample nb	Amplitude
1	-0.0159	17	4.7542
2	0.0181	18	0.8045
3	-0.0120	19	-0.6989
4	-0.0054	20	0.5471
5	0.0341	21	-0.3743
6	-0.0690	22	0.2069
7	0.1001	23	-0.0670
8	-0.1137	24	-0.0320
9	0.0956	25	0.0860
10	-0.0350	26	-0.1005
11	-0.0722	27	0.0867
12	0.2201	28	-0.0584
13	-0.3929	29	0.0281
14	0.5671	30	-0.0043
15	-0.7157	31	-0.0092
16	0.8141	32	0.0130

Table 4.4: Time domain samples of a suitable postfix (Kaiser Window, 32 Samples).

Sample nb	Amplitude	Sample nb	Amplitude
1	1.0678-0.2485i	17	-0.6305+ 0.2212i
2	-1.2244+ 0.8348i	18	-0.1557-0.9844i
3	-1.2278+ 0.4519i	19	0.4761-0.4938i
4	1.2361-0.7825i	20	-0.1803-0.6882i
5	-0.2617-1.3550i	21	0.5684-0.3849i
6	-1.0461+ 1.2017i	22	-0.1465+ 0.4904i
7	0.5739-1.4205i	23	0.0310-0.6722i
8	0.7884+ 0.8225i	24	0.6098-0.1938i
9	0.7616-0.5044i	25	-0.0338-0.5361i
10	-0.4033+ 0.8804i	26	0.6024-0.2020i
11	-0.6153+ 0.5960i	27	0.0316+ 0.5602i
12	-0.9602+ 0.1916i	28	0.2225-0.3104i
13	-0.1228-0.6236i	29	0.4748+ 0.1726i
14	0.2001-0.4621i	30	-0.2827-0.2660i
15	-0.5335-0.0187i	31	0.4158-0.1692i
16	-0.2175-0.3735i	32	0.1835+ 0.5114i

Table 4.5: Time domain samples of a suitable postfix (optimized 32 samples postfix).

Parameter	Kaiser Window	PAPR opt. Postfix
$\text{PAPR} = \frac{\ \mathbf{p}_D\ _\infty^2}{\frac{1}{D} \sum_{n=0}^{D-1}  p_n ^2}$	14.443dB	6.762dB
Total out-of-band radiation $\frac{\sum_{n \in O}  p_n^f ^2}{\sum_{n=0}^{N-1}  p_n^f ^2}, \mathbf{p}^f = \mathbf{F}_N \begin{bmatrix} \mathbf{p}_D \\ \mathbf{0}_{N-D,1} \end{bmatrix}$	-16.719dB	-31.501dB
Spectral in-band ripple Calculated over carriers $c^2 = C \setminus \{21, \dots, 27, 39, \dots, 45\}$ (i.e. transition to stop-band not considered)	0.0252dB	1.986dB

Table 4.6: Comparison on postfix trade-offs (32 samples postfix).

Sample nb	Amplitude	Sample nb	Amplitude
1	0.0127	25	5.8025
2	-0.0173	26	0.9814
3	0.0180	27	-0.8655
4	-0.0126	28	0.6936
5	0.0000	29	-0.4905
6	0.0187	30	0.2842
7	-0.0398	31	-0.1003
8	0.0577	32	-0.0419
9	-0.0654	33	0.1320
10	0.0569	34	-0.1693
11	-0.0290	35	0.1618
12	-0.0171	36	-0.1232
13	0.0745	37	0.0695
14	-0.1310	38	-0.0158
15	0.1710	39	-0.0267
16	-0.1778	40	0.0519
17	0.1378	41	-0.0590
18	-0.0435	42	0.0515
19	-0.1035	43	-0.0351
20	0.2918	44	0.0163
21	-0.5009	45	0.0000
22	0.7044	46	-0.0106
23	-0.8744	47	0.0148
24	0.9865	48	-0.0138

Table 4.7: Time domain samples of a suitable postfix (Kaiser Window, 48 Samples).

Sample nb	Amplitude	Sample nb	Amplitude
1	-0.3455+ 1.0703i	25	-0.4480-0.2845i
2	0.5167-0.8005i	26	0.7568+ 0.6750i
3	-1.0618+ 0.2140i	27	-0.0675+ 0.1458i
4	0.2655+ 0.1877i	28	-0.7098-1.3906i
5	-0.1938+ 0.0350i	29	-0.2838+ 0.1919i
6	-0.5792+ 0.2934i	30	0.3397+ 0.3671i
7	0.0908-0.1211i	31	0.4167-0.6586i
8	-0.2160-0.6457i	32	-0.1350+ 0.1112i
9	0.5287+ 0.7310i	33	-0.3572+ 0.1126i
10	-1.8827+ 1.0646i	34	0.2015+ 0.2065i
11	-0.9916-0.4922i	35	-1.1574-0.4457i
12	-0.1853-1.6238i	36	0.9955-0.5734i
13	0.0920-0.3074i	37	-1.1571-0.1639i
14	-0.1976-0.9700i	38	1.5059-0.2666i
15	-0.6025-0.3002i	39	-0.6689+ 0.5690i
16	0.9100+ 0.1404i	40	0.0296-0.3507i
17	0.7601-1.1629i	41	-0.6628-0.7569i
18	-0.0721-0.0574i	42	0.1214+ 0.3445i
19	0.1725+ 0.6107i	43	0.2804-0.1495i
20	0.3401-0.1199i	44	0.1323-1.0462i
21	-0.7860+ 0.8694i	45	0.2222-0.5485i
22	-0.3458-0.4107i	46	0.2851+ 1.0651i
23	0.7092-1.1569i	47	0.2972-0.1414i
24	-0.4684+ 0.3254i	48	-0.1216-0.1457i

Table 4.8: Time domain samples of a suitable postfix (optimized 48 samples postfix).

Parameter	Kaiser Window	PAPR opt. Postfix
PAPR $\frac{\ \mathbf{p}_D\ _\infty^2}{\frac{1}{D} \sum_{n=0}^{D-1}  p_n ^2}$	16.174dB	7.691dB
Total out-of-band radiation $\frac{\sum_{n=0}^{N-1}  p_n^f ^2}{\sum_{n=0}^{N-1}  p_n^f ^2}, \mathbf{p}^f = \mathbf{F}_N \begin{bmatrix} \mathbf{p}_D \\ \mathbf{0}_{N-D,1} \end{bmatrix}$	-16.153dB	-39.715dB
Spectral in-band ripple Calculated over carriers $C^2 = C \setminus \{21, \dots, 27, 39, \dots, 45\}$ (i.e. transition to stop-band not considered)	0.017dB	0.000176dB

Table 4.9: Comparison on postfix trade-offs (48 samples postfix).



## Chapter 5

# Synchronization Refinement with Pseudo Random Postfix OFDM

This chapters illustrates how to exploit the Pseudo Random Postfix OFDM frame structure in order to perform a time and frequency synchronization refinement [2]. After an initial (rough) synchronization, the proposed refinement algorithms rely on the deterministic postfix sequence only and do not require any signaling overhead.

### 5.1 Introduction

This chapter complements the PRP-OFDM related studies presented in the previous chapters of this document: it shows how to perform time and frequency synchronization (TS/FS) refinement (TSR/FSR) by exploiting the pseudo-randomly weighted deterministic postfix sequences [27, 28].

The proposed techniques allow thus to

1. refine an initial (rough) TS;
2. update the TS when a mobile terminal (MT) awakes from a sleep mode, which is a common scenario in the context of WLAN systems [58]: Automatic Power Save Delivery (APSD) [114] MAC (Medium Access Control) protocol is applied in order to inform the MT well in advance when it may receive and/or transmit data. In between, it switches to a (deep) sleep-mode in order to minimize power consumption. A common problem is to identify means for re-synchronization after the wake-up procedure: we propose to achieve this task by exploiting the Pseudo Random Postfix based TSR;
3. refine an initial (rough) FS.

The TSR helps to ensure that interference from adjacent OFDM symbols is entirely absorbed by the postfix interval (similar to the guard interval in the context of CP-OFDM) preventing any performance degradation introduced by Inter-Block-Interference (IBI). FSR helps to avoiding Inter-Carrier-Interference

(ICI) by adjusting the frequency domain sampling points. For an efficient hardware implementation, a Fast-Fourier-Transform (FFT) based TSR algorithm is proposed that is optimized in terms of calculation complexity: for the frequency-selective case, it is a sub-optimum approach where the inherent approximations, however, become rather accurate for low SNR where TSR/FSR is particularly useful.

Since the PRP-OFDM based synchronization refinement requires an initial TS/FS, in the framework of this thesis we assume that a first frame acquisition is achieved applying standard techniques: e.g., [38] presents suitable techniques applicable to IEEE802.11a 5GHz WLAN [56] preamble based TS/FS.

An alternative synchronization refinement has been studied for CP-OFDM in [98, 115] by correlating the guard interval with the tail of the corresponding OFDM symbol. This approach cannot be directly applied to the PRP-OFDM context, since the postfix-sequence is deterministic (and not quasi-Gaussian as it is the case for the CP-OFDM guard interval contents). [77] studies both, a FS and joint FS/TS in a single carrier (SC) context where every SC block is followed by a constant deterministic sequence. While its FS approach can be reused in the context of a frequency selective channel (see section 5.4 of this chapter), the joint FS/TS approach in [77] requires again Gaussian postfix sequences and is thus not applicable. A new TSR approach is thus derived which is efficiently applied after the FSR and frequency offset correction. A joint optimization is thus no longer required.

This chapter is organized as follows. Section 5.2 recalls basic definitions of the PRP-OFDM modulator followed by a presentation of suitable TS improvement techniques in section 5.3. In the context of an Additive White Gaussian Noise (AWGN) channel, a Maximum Likelihood (ML) estimate is derived. For frequency selective fading environments, the optimum ML decoder is typically replaced by a sub-optimum approach in practice, since the channel impulse response (not containing any time offset due to an imperfect initial synchronization) required for ML estimation cannot assumed to be known: corresponding sub-optimum approaches are derived. Section 5.4 extends the synchronization refinement to the frequency offset estimation, section 5.5 discusses the simultaneous time/frequency offset estimation (avoiding a joint detection approach) and section 5.6 presents simulation results. Final conclusion follow in section 5.7.

## 5.2 Notations and PRP-OFDM modulator

This section briefly presents the basic definitions introduced in chapters 2 and 3 for an  $N$  carrier PRP-OFDM system. The  $i$ th  $N \times 1$  input digital vector<sup>1</sup>  $\tilde{\mathbf{s}}_N(i)$  is first modulated by the IFFT matrix  $\mathbf{F}_N^H := \frac{1}{\sqrt{N}} \left( W_N^{ij} \right)^H, 0 \leq i < N, 0 \leq j < N$  where  $W_N := e^{-j\frac{2\pi}{N}}$ . Then, a deterministic postfix vector  $\mathbf{p}_D := (p_0, \dots, p_{D-1})^T$  weighted by a pseudo random value  $\alpha(i) \in \mathbb{C}$  is appended to the IFFT outputs  $\mathbf{s}_N(i)$ . With  $P := N + D$ , the corresponding  $P \times 1$  transmitted vector is  $\mathbf{s}_P(i) := \mathbf{F}_{ZP}^H \tilde{\mathbf{s}}_N(i) + \alpha(i) \mathbf{p}_P$ , where

$$\mathbf{F}_{ZP}^H := \begin{bmatrix} \mathbf{I}_N \\ \mathbf{0}_{D,N} \end{bmatrix}_{P \times N} \quad \mathbf{F}_N^H \quad \text{and} \quad \mathbf{p}_P := (\mathbf{0}_{1,N} \mathbf{p}_D^T)^T$$

<sup>1</sup>Lower (upper) boldface symbols will be used for column vectors (matrices) sometimes with subscripts  $N$  or  $P$  emphasizing their sizes (for square matrices only); tilde denotes frequency domain quantities; argument  $i$  will be used to index blocks of symbols;  $^H$  ( $^T$ ) denotes Hermitian (Transpose).

Without loss of generality, the elements of  $\mathbf{s}_N(i) = \mathbf{F}_N^H \tilde{\mathbf{s}}_N(i)$  are assumed to be i.i.d. and zero mean random variables of variance  $\sigma_s^2 = 1$  which are independent of  $\alpha(i)\mathbf{p}_D$ . The samples of  $\mathbf{s}_P(i)$  are then sent sequentially through the channel, modeled here as an  $L$ th-order FIR filter  $C(z) := \sum_{n=0}^L c_n z^{-n}$ . The OFDM system is designed such that the postfix duration exceeds the channel memory  $L < D$ .

Let  $\mathbf{C}_{\text{ISI}}(P)$  and  $\mathbf{C}_{\text{IBI}}(P)$  be respectively the Toeplitz lower and upper triangular matrices of first column  $[c_0, c_1, \dots, c_L, 0, \dots, 0]^T$  and first row  $[0, \dots, 0, c_L, \dots, c_1]$ . As already explained in [80], the channel convolution can be expressed as  $\mathbf{r}_P(i) := \mathbf{C}_{\text{ISI}}(P)\mathbf{s}_P(i) + \mathbf{C}_{\text{IBI}}(P)\mathbf{s}_P(i-1) + \mathbf{n}_P(i)$ .  $\mathbf{C}_{\text{ISI}}(P)$  and  $\mathbf{C}_{\text{IBI}}(P)$  represent respectively the intra-symbol and inter-block interference.  $\mathbf{n}_P(i)$  is the  $i$ th AWGN vector of i.i.d. elements with variance  $\sigma_n^2$ . Since  $\mathbf{s}_P(i) = \mathbf{F}_{\text{ZP}}^H \tilde{\mathbf{s}}_N(i) + \alpha(i)\mathbf{p}_P$ , we have:

$$\mathbf{r}_P(i) = (\mathbf{C}_{\text{ISI}} + \beta_i \mathbf{C}_{\text{IBI}})\mathbf{s}_P(i) + \mathbf{n}_P(i) \quad (5.1)$$

where  $\beta_i := \frac{\alpha(i-1)}{\alpha(i)}$ . Note that  $\mathbf{C}_{\beta_i} := (\mathbf{C}_{\text{ISI}} + \beta_i \mathbf{C}_{\text{IBI}})$  is pseudo circulant: i.e. a circulant matrix whose  $(D-1) \times (D-1)$  upper right triangular part is weighted by  $\beta_i$ . Such a matrix is no longer diagonal on a standard Fourier basis, but on a new one still allowing an efficient implementation based on FFTs (see Appendix A).

The expression of the received block thus becomes:

$$\begin{aligned} \mathbf{r}_P(i) &:= \mathbf{C}_{\beta_i} (\mathbf{F}_{\text{ZP}}^H \tilde{\mathbf{s}}_N(i) + \alpha(i)\mathbf{p}_P) + \mathbf{n}_P(i) \\ &= \mathbf{C}_{\beta_i} \begin{pmatrix} \mathbf{F}_N^H \tilde{\mathbf{s}}_N(i) \\ \alpha(i)\mathbf{p}_D \end{pmatrix} + \mathbf{n}_P(i) \end{aligned}$$

The following sections present TSR and FSR refinement techniques first independently; then, a discussion on a simultaneous presence of time/frequency offsets and considerations on the estimation/correction follows.

### 5.3 Time synchronization aspects

Due to the block transmission nature of OFDM systems, it is important to perform an accurate TS locating the start of the OFDM time domain symbols to be fed to the FFT demodulator in the receiver. In that respect, it is relevant to find TS algorithms that optimize the offset distribution of the estimated frame location: the real start of the frame and the estimated one provided by the time synchronization procedure need to coincide as closely as possible. If this property is not fulfilled, the system performance is impacted:

- a *late synchronization* leads to IBI with the subsequent OFDM symbol;
- an *early synchronization* leads to an extraction of OFDM symbols some samples earlier than required and subsequently reduces the duration margin of the OFDM guard time allocated for absorbing the IBI generated by a multi-path propagation channel (applicable to both, CP-OFDM or PRP-OFDM); this observation illustrates that in practice, the guard time role is to cope not only with the absorption of the IBI due to a CIR of significant memory, but also with the inherent delay offset remaining after TS.

In this chapter, it is assumed that an initial (rough) TS/FS has already been performed by standard means, e.g. see [38, 116]; so that TS false detection and detection failure [116] issues are not addressed. Usually, the TS is based on suitable preamble designs in combination with auto-correlation and peak-detection of the received signal. Correspondingly, FS is assumed to be performed on a suitable preamble. This section shows how to refine such a first estimation and hence aims at i) avoiding IBI and ii) increasing the spectral efficiency of the system by keeping the guard interval as short as possible. The case of an Additive White Gaussian Noise (AWGN) channel is first considered, and the general frequency selective case is derived subsequently.

### 5.3.1 Refinement in the AWGN context

For explanation sake, we first consider the received block vector  $\mathbf{r}_{P,Q}(i)$  in presence of an AWGN channel including an time synchronization offset  $Q$  and  $\mathbf{s}_N(i) = [s_0(i), \dots, s_{N-1}(i)]^T$  (similar to the noise vector  $\mathbf{n}_{P,Q}(i)$ ). For sake of simplicity we assume  $Q$  to belong to the interval of  $-D < Q < D$ :

$$\mathbf{r}_{P,Q}(i) := \mathbf{n}_{P,Q}(i) + \begin{cases} \begin{pmatrix} \mathbf{s}_N(i) \\ \alpha(i)\mathbf{p}_D \end{pmatrix} & \text{for } Q = 0 \\ \begin{pmatrix} s_Q(i) \\ \vdots \\ s_{N-1}(i) \\ \alpha(i)\mathbf{p}_D \\ s_0(i+1) \\ \vdots \\ s_{Q-1}(i+1) \end{pmatrix} & \text{for } Q > 0 \\ \begin{pmatrix} \alpha(i-1)p_{D+Q} \\ \vdots \\ \alpha(i-1)p_{D-1} \\ \mathbf{s}_N(i) \\ \alpha(i)p_0 \\ \vdots \\ \alpha(i)p_{D+Q-1} \end{pmatrix} & \text{for } Q < 0 \end{cases} \quad (5.2)$$

A corresponding vector  $\mathbf{n}_{P,Q}(i)$  needs to be defined for the Gaussian noise contributions. It is however sufficient to note that  $\mathbb{E}[\mathbf{n}_{P,Q}(i)\mathbf{n}_{P,Q}^H(i)] = \mathbb{E}[\mathbf{n}_P(i)\mathbf{n}_P^H(i)] = \sigma_n^2\mathbf{I}_N$ . The contribution of OFDM data samples in (5.2) shall be defined as  $\mathbf{s}_{P,Q}(i)$ ; it corresponds to  $\mathbf{r}_{P,Q}(i)$  setting all postfix and noise contributions to zero.

In order to prepare the synchronization refinement, we define  $\mathbb{E}_\alpha$  to be the expectation operator combined with de-weighting of postfixes by the corresponding inverse of the pseudo random weights  $\alpha(i)^{-1}$ ; with  $\alpha(i)$  being a pure phase ( $\alpha(i) = e^{j\phi_{\alpha(i)}}$ ), the variance of any weighted data/noise samples as well as their zero-mean properties remain unchanged; the offset  $Q$  introduced by the initial rough TS is

the parameter to be detected:

$$\mathbf{E}_\alpha[\mathbf{r}_{P,Q}(i)] = \begin{cases} \begin{pmatrix} \mathbf{0}_{P-D} \\ \mathbf{p}_D \end{pmatrix} & \text{for } Q = 0 \\ \begin{pmatrix} \mathbf{0}_{P-D-Q} \\ \mathbf{p}_D \\ \mathbf{0}_Q \end{pmatrix} & \text{for } Q > 0 \\ \begin{pmatrix} p_{D+Q} \\ \vdots \\ p_{D-1} \\ \mathbf{0}_{P-D} \\ p_0 \\ \vdots \\ p_{D+Q-1} \end{pmatrix} & \text{for } Q < 0 \end{cases} \quad (5.3)$$

In practice, this expectation  $\mathbf{E}_\alpha$  is approximated by a mean value calculation over a limited number of  $Z$  symbols (without loss of generality and for explanation sake,  $Z$  is assumed to be an odd integer:  $Z \in [3, 5, \dots]$ ). These are assumed to be grouped around the  $i_0$ th OFDM symbol ( $i_0 \geq \frac{Z-1}{2}$ ) in the frame:  $(\mathbf{s}_P(i_0 - \frac{Z-1}{2}), \dots, \mathbf{s}_P(i_0 + \frac{Z-1}{2}))$  and with

$$\hat{\mathbf{n}}_{P,Q}(i_0) = \frac{1}{Z} \sum_{i=0}^{Z-1} \left[ \mathbf{s}_{P,Q} \left( i_0 - \frac{Z-1}{2} + i \right) + \mathbf{n}_{P,Q} \left( i_0 - \frac{Z-1}{2} + i \right) \right] \quad (5.4)$$

the following expression is obtained:

$$\hat{\mathbf{r}}_{P,Q}(i_0) := \mathbf{E}_\alpha[\mathbf{r}_{P,Q}(i)] + \hat{\mathbf{n}}_{P,Q}(i_0). \quad (5.5)$$

We propose to determine the TS offset estimates  $\hat{Q}$  by a Maximum-Likelihood (ML) approach. In order to achieve this goal, let us first define the  $J$ -circulant correlation matrix  $\mathbf{M}_J$  of dimension  $P \times P$  as:

$$\mathbf{M}_J := \begin{bmatrix} p_0 & p_1 & \cdots & p_{D-1} & 0 & \rightarrow & \rightarrow & 0 \\ p_1 & & \nearrow & & & & & p_0 \\ \vdots & & \nearrow & & & & & \vdots \\ p_{D-1} & & & & & & & p_{D-2} \\ 0 & & & & & & & p_{D-1} \\ 0 & & & & & & \nearrow & 0 \\ 0 & & & & & \nearrow & \nearrow & 0 \\ \downarrow & & & & \nearrow & \nearrow & \nearrow & \downarrow \\ 0 & p_0 & \cdots & p_{D-2} & p_{D-1} & 0 & \rightarrow & 0 \end{bmatrix} \quad (5.6)$$

and  $\mathbf{m}_n$  as the  $n$ th column of  $\mathbf{M}_J$ ,  $n = 0, \dots, P-1$ . With  $p(\mathbf{E}_\alpha[\mathbf{r}_{P,Q}(i)] = \mathbf{m}_n | \hat{\mathbf{r}}_P(i_0))$  being the likelihood that  $\mathbf{E}_\alpha[\mathbf{r}_{P,Q}(i)] = \mathbf{m}_n$  knowing  $\hat{\mathbf{r}}_P(i_0)$  and with

$$\begin{aligned} \hat{Q} &:= \underset{n}{\operatorname{argmax}} \{ p(\mathbf{E}_\alpha[\mathbf{r}_{P,Q}(i)] = \mathbf{m}_n | \hat{\mathbf{r}}_P(i_0)) \} \\ &= \underset{n}{\operatorname{argmin}} \left\{ (\hat{\mathbf{r}}_{P,Q}(i_0) - \mathbf{m}_n)^H \mathbf{R}_n^{-1} (Q = n - D) (\hat{\mathbf{r}}_{P,Q}(i_0) - \mathbf{m}_n) \right\} \end{aligned} \quad (5.7)$$

the resulting Maximum Likelihood (ML) offset estimates are  $\hat{Q} = \bar{Q} - D$ . where  $\mathbf{R}_{\hat{n}}(Q)$  is defined with  $\mathbf{M}_{\alpha}(i) := \begin{bmatrix} \mathbf{I}_{\lfloor \frac{P}{2} \rfloor} \alpha^{-1}(i-1) & \mathbf{0} \\ \mathbf{0} & \mathbf{I}_{P-\lfloor \frac{P}{2} \rfloor} \alpha^{-1}(i) \end{bmatrix}$  as follows:

$$\begin{aligned} \mathbf{R}_{\hat{n}}(Q) &:= \mathbb{E}[\hat{\mathbf{n}}_{P,Q}(i_0) \hat{\mathbf{n}}_{P,Q}^H(i_0)] \\ &= \mathbf{I}_P \frac{\sigma_n^2}{Z} + \frac{1}{Z} \mathbb{E}[\mathbf{M}_{\alpha}(i) \mathbf{s}_{P,Q}(i) \mathbf{s}_{P,Q}^H(i) \mathbf{M}_{\alpha}^H(i)] \end{aligned}$$

$\mathbf{M}_{\alpha}(i)$  defines the de-weighting of the pseudo-random weighting factors  $\alpha(i)$  such that a maximum synchronization offset ( $\lfloor \frac{P}{2} \rfloor - L + 1$  samples) is covered. The final estimator is derived by defining "rowmax( $\cdot$ )" as an operator that is applied on a vector of real values returning the integer *row* of the its largest element and  $\Re(\cdot)$  is the classical real part operator. Reworking equation (5.7) by exploiting that  $\mathbf{R}_{\hat{n}}(Q)$  is diagonal and constant over the non-zero elements of  $\mathbf{m}_n$  leads to the following estimator:

$$\begin{aligned} \bar{Q} &= \text{rowmax} \left( \frac{Z}{\sigma_{\text{const}}^2} \Re\{\mathbf{M}_J^H \hat{\mathbf{r}}_{P,Q}(i_0)\} - \frac{1}{2} \underbrace{\begin{pmatrix} \mathbf{m}_0^H \mathbf{R}_{\hat{n}}^{-1}(Q = -D) \mathbf{m}_0 \\ \vdots \\ \mathbf{m}_{P-1}^H \mathbf{R}_{\hat{n}}^{-1}(Q = P-1-D) \mathbf{m}_{P-1} \end{pmatrix}}_{=\text{const}} \right) \\ &= \text{rowmax} (\Re\{\mathbf{M}_J^H \hat{\mathbf{r}}_{P,Q}(i_0)\}) \end{aligned} \quad (5.8)$$

$\mathbf{1}_P$  is a  $P \times 1$  vector containing '1' elements only. The computation of the cyclic correlation is performed in an efficient way based on the diagonalization of  $\mathbf{M}_J = \mathbf{F}_P \mathbf{D}_J \mathbf{F}_P$  with diagonal  $\mathbf{D}_J = \mathbf{F}_P^H \mathbf{M}_J \mathbf{F}_P$  and the efficient implementation of  $\mathbf{F}_P$  ( $\mathbf{F}_P^H$ ) by the (I)FFT:

$$\bar{Q} = \text{rowmax} (\Re\{\mathbf{F}_P^H \mathbf{D}_J^H \mathbf{F}_P^H \hat{\mathbf{r}}_{P,Q}(i_0)\}). \quad (5.9)$$

This finalizes the discussion on TSR in the AWGN context; for the case of a multi-path channel, either the knowledge of the CIR is required or some approximations need to be applied as it is proposed in the following section.

### 5.3.2 Refinement in presence of ISI

When the channel introduces ISI, the vector to be considered is with  $\mathbf{C}_{\text{CIRC}}(P) = \mathbf{C}_{\text{ISI}}(P) + \mathbf{C}_{\text{IBI}}(P)$ :

$$\begin{aligned} \hat{\mathbf{r}}_{P,Q}(i_0) &= \mathbb{E}_{\alpha} [\mathbf{r}_{P,Q}(i)] + \hat{\mathbf{n}}_{P,Q}(i_0) \\ &= \mathbf{P}_Q \mathbf{C}_{\text{CIRC}}(P) \mathbf{p}_P + \hat{\mathbf{n}}_{P,Q}(i_0) \end{aligned}$$

where  $\mathbf{P}_Q$  is a circulant permutation matrix representing the postfix offset in the received vector  $\hat{\mathbf{r}}_{P,Q}(i_0)$  due to the time synchronization offset  $Q$  and  $\mathbf{C}_{\text{CIRC}}(P)$  is a size  $P \times P$  circulant channel convolution matrix. Exploiting the relation  $\mathbf{M}_J \mathbf{C}_{\text{CIRC}}(P) = \mathbf{C}_{\text{CIRC}}^T(P) \mathbf{M}_J$ , derived in appendix E, the corresponding

ML estimator is thus:

$$\begin{aligned}
\bar{Q} &= \underset{n}{\operatorname{argmin}} \left\{ (\hat{\mathbf{r}}_P(i) - \mathbf{C}_{\text{CIRC}}(P)\mathbf{m}_n)^H \mathbf{R}_{\hat{\mathbf{n}}}^{-1}(Q = n - D) (\hat{\mathbf{r}}_P(i) - \mathbf{C}_{\text{CIRC}}(P)\mathbf{m}_n) \right\} \quad (5.10) \\
&= \operatorname{rowmax} \left\{ \left( \begin{array}{c} \Re\{\mathbf{m}_0^H \mathbf{C}_{\text{CIRC}}^H(P) \mathbf{R}_{\hat{\mathbf{n}}}^{-1}(Q = -D) \hat{\mathbf{r}}_{P,Q}(i_0)\} \\ \vdots \\ \Re\{\mathbf{m}_{P-1}^H \mathbf{C}_{\text{CIRC}}^H(P) \mathbf{R}_{\hat{\mathbf{n}}}^{-1}(Q = P - 1 - D) \hat{\mathbf{r}}_{P,Q}(i_0)\} \end{array} \right) - \right. \\
&\quad \left. \frac{1}{2} \left( \begin{array}{c} \mathbf{m}_0^H \mathbf{C}_{\text{CIRC}}^H(P) \mathbf{R}_{\hat{\mathbf{n}}}^{-1}(Q = -D) \mathbf{C}_{\text{CIRC}}(P) \mathbf{m}_0 \\ \vdots \\ \mathbf{m}_{P-1}^H \mathbf{C}_{\text{CIRC}}^H(P) \mathbf{R}_{\hat{\mathbf{n}}}^{-1}(Q = P - 1 - D) \mathbf{C}_{\text{CIRC}}(P) \mathbf{m}_{P-1} \end{array} \right) \right\} \\
&\approx \sigma_{\text{tot}}^2 \mathbf{1}_P \sum_{k=0}^{D-1} |[\mathbf{C}_{\text{CIRC}}(D)\mathbf{p}_D]_k|^2 = \text{const}, \\
&\quad \text{with the approximation } \mathbf{R}_{\hat{\mathbf{n}}}(Q) \approx \sigma_{\text{tot}}^2 \mathbf{I}, \text{ since} \\
&\quad \mathbf{m}_n^H \mathbf{C}_{\text{CIRC}}^H(P) \mathbf{C}_{\text{CIRC}}(P) \mathbf{m}_n = (\mathbf{C}_{\text{CIRC}}(P)\mathbf{m}_n)^H \mathbf{C}_{\text{CIRC}}(P)\mathbf{m}_n \\
&\quad = \sum_{k=0}^{D-1} |[\mathbf{C}_{\text{CIRC}}(D)\mathbf{p}_D]_k|^2 \\
&\approx \operatorname{rowmax} \left\{ \Re\{(\mathbf{C}_{\text{CIRC}}(P))^* \mathbf{M}_J^H \hat{\mathbf{r}}_{P,Q}(i_0)\} \right\} \quad (5.11)
\end{aligned}$$

with

$$\begin{aligned}
\mathbf{R}_{\hat{\mathbf{n}}}(Q) &= E[\hat{\mathbf{n}}_{P,Q}(i_0) \hat{\mathbf{n}}_{P,Q}^H(i_0)] \\
&= \mathbf{I}_P \frac{\sigma_n^2}{Z} + \frac{1}{Z} E[\mathbf{M}_\alpha(i) \mathbf{C}_{\beta_i} \mathbf{P}_Q \mathbf{s}_{P,Q=0}(i) \mathbf{s}_{P,Q=0}^H(i) \mathbf{P}_Q^H \mathbf{C}_{\beta_i}^H \mathbf{M}_\alpha^H(i)]
\end{aligned}$$

Equation (5.11) is based on the hypothesis that the noise covariance  $\mathbf{R}_{\hat{\mathbf{n}}}^{-1}(Q)$  contains i.i.d. contributions on the main diagonal and is zero elsewhere, which is a valid approximation for low SNR values. The resulting estimator becomes (applying approximation (5.11)):

$$\bar{Q} \approx \operatorname{rowmax} \Re[\mathbf{C}_{\text{CIRC}}^T(P) \mathbf{C}_{\text{CIRC}}^*(P) \mathbf{M}_J^H \mathbf{p}_P + (\mathbf{C}_{\text{CIRC}}(P) \mathbf{M}_J)^H \hat{\mathbf{n}}_P(i)] \quad (5.12)$$

As a matter of fact, the ML detector leads to an intuitive solution: the postfix sequence is pre-multiplied by a correlation matrix in order to find the synchronization offset similar to the AWGN case; for frequency selective channels, this expression is further weighted by the channel matrix and its hermitian.

Note that the ML estimator requires the knowledge of the CIR convolution matrix  $\mathbf{C}_{\text{CIRC}}(P)$ . This typically is not available; even if CIR coefficients can sometimes be estimated based on preamble symbols, this estimation contains an undesired offset due to the initial synchronization offset and is thus

unsuitable. The optimum ML estimator remains a theoretical limit which can be approximated in practice by sub-optimum approaches.

In the following, two simple approximations are discussed leading to sub-optimum estimators that do not require the knowledge of the CIR.

### Approximation I: Assume channel to be a Dirac function

The first idea consists in approximating the CIR by a Dirac function, i.e.  $\mathbf{C}_{\text{CIRC}}(P) \approx \mathbf{I}_P$ ; This approximation is justified by the fact that the value of  $\mathbf{m}_n^H \mathbf{E}_\alpha [\mathbf{r}_P(i)]$  in (5.12) typically decreases rapidly as a function of the synchronization offset in a Line Of Sight (LOS) scenario. Thus, the estimation of the TS offset is improved as for the AWGN case (5.9). As it will be explained in the following proposal of *Approximation II*, however, *Approximation I* should not be the preferred choice in the context of complex channel gains.

### Approximation II: Assume channel to be a Dirac function with a random phase

Typically, *Approximation I* has disadvantages if the channel coefficients are complex: replacing the real part operator  $\Re(\cdot)$  in (5.12) by an absolute value calculation avoids this problem with the expense of an increased noise variance. It typically leads to improved performances as it will be illustrated in the following section. *Approximation II* is thus a suitable approach in a practical context where CIR estimates (which must not contain offsets due to a synchronization offset) are typically not available.

## 5.4 Frequency Offset Estimation

The upper derivations show how to improve the TS in a practical system implementation. This section extends the technique to improving the frequency offset estimation which is equally important in order to minimize any loss in system performance due to Inter-Carrier-Interference (ICI).

The frequency offset leads to a linear phase shift of the received samples in time domain [38] expressed as  $[r_n(i)]_{\Delta F}$  which corresponds to the elements of (5.1) including a frequency offset of  $f_0$ . Defining  $T_B := (N + D)T$  as the duration of an OFDM symbol block including the postfix sequence and  $T$  as the sampling period, the resulting expression is

$$\begin{aligned} [r_n(i)]_{\Delta F} &:= r(iT_B + nT)e^{j2\pi f_0(iT_B + nT)}, \quad 0 \leq n < P \\ &= r[(iP + n)T]e^{j2\pi f_0(iP + n)T}. \end{aligned} \quad (5.13)$$

It is proposed to extract the frequency offset  $\Delta F = f_0$  by correlation of  $Z$  neighboring received postfix sequences corresponding to the definitions in section 5.3 and as illustrated in Fig.5.1 (with *MA* indicating *Moving Average*) and defined by equation (5.14) around the  $i_0$ th OFDM symbol ( $i_0 \geq \frac{Z-1}{2}$ ):

$$\hat{f}_0 := \frac{1}{2\pi(N+D)T} \text{angle} \left\{ \sum_{i=i_0-\frac{Z-1}{2}}^{i_0+\frac{Z-1}{2}} \alpha^{-1}(i)\alpha^{*-1}(i+1) \sum_{n=0}^{D-1} [r_{N+n}(i)]_{\Delta F} [r_{N+n}(i+1)]_{\Delta F}^* \right\} \quad (5.14)$$

Combining (5.13) and (5.14), the necessary condition to derive a unique frequency offset is

$$-\pi < 2\pi f_0 T_B < \pi$$

In other words, the shift from one OFDM symbol block to another may not exceed  $\pm\pi$ . This property needs to be met by an initial (rough) correction of the frequency offset.

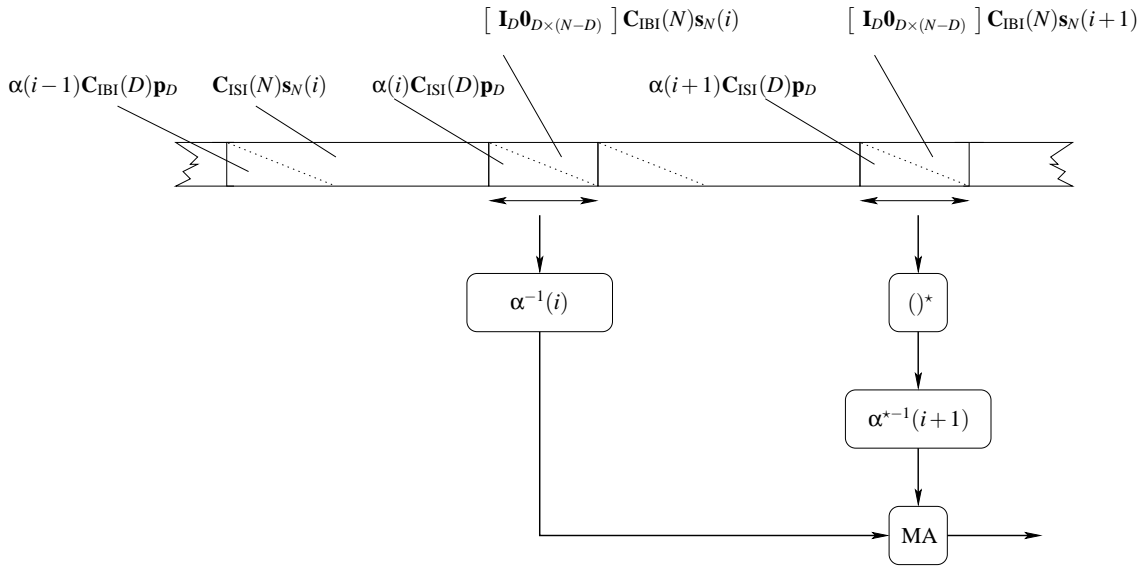


Figure 5.1: Illustration of FS refinement (1).

Contrary to the TSR, the resulting proposed FSR scheme applies to both, the AWGN and the multi-path propagation context without introducing any approximation. Assuming a channel impulse response of order  $L$  it is possible to exploit the IBI part of the postfix after convolution by the channel. As illustrated in Fig.5.2, it is proposed to add the following expression to equation (5.14), additionally exploiting the IBI contribution of the postfix after channel convolution, in order to refine the estimates (exploiting that the  $D$  samples postfix sequence convolved by a  $L+1$  samples CIR results in a sequence of  $D+L$  samples):

$$\frac{\text{angle} \left\{ \sum_{i=1+i_0-\frac{Z-1}{2}}^{1+i_0+\frac{Z-1}{2}} \alpha^{-1}(i-1)\alpha^{*-1}(i) \sum_{n=0}^{L-1} [r_n(i)]_{\Delta F} [r_n(i+1)]_{\Delta F}^* \right\}}{2\pi(N+D)T} \quad (5.15)$$

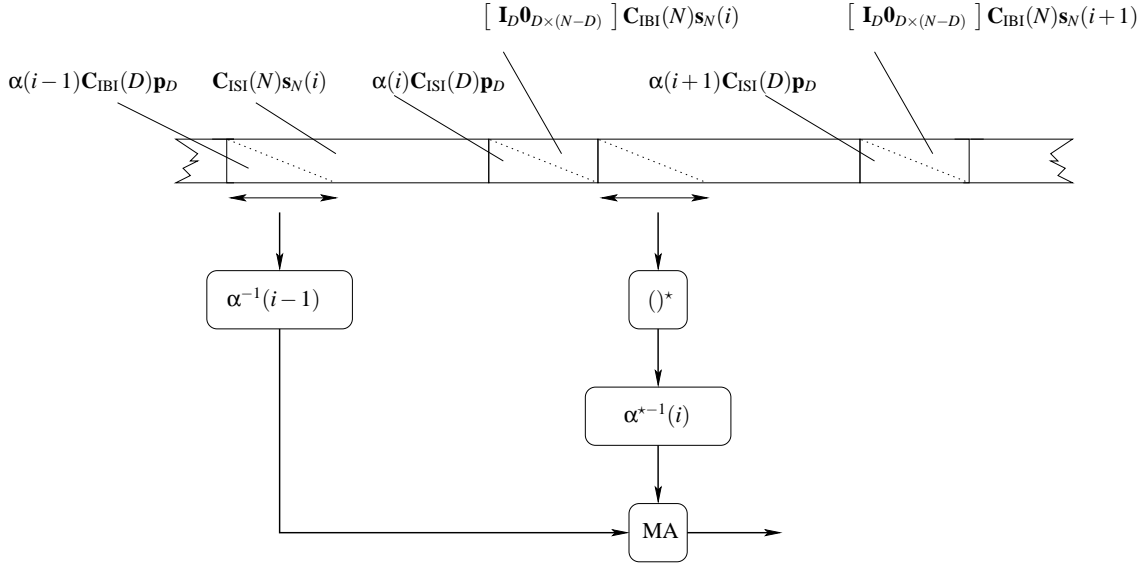


Figure 5.2: Illustration of FS refinement (2).

Since the channel order typically is not known in the receiver and expression (5.15) is expected to be corrupted by a high level of OFDM data symbol interference, in the framework of this chapter any optimization is performed with respect to (5.14).

As a final remark, note that in practice a sampling clock frequency offset needs to be taken into account additionally. In order to facilitate this detection, modern communication standards (such as IEEE802.11a [56]) require the mixer and sampling clock references to have the same source. Thus, the relative offset is identical; the sampling clock offset is obtained by scaling the center frequency offset estimates derived in this section correspondingly.

## 5.5 Simultaneous presence of Time and Frequency Offsets

Section 5.3 and 5.4 detailed the estimation of TS and FS offsets respectively, assuming the exclusive presence of either one. This section extends this analysis to the practical case where both, time and frequency offsets occur simultaneously. In order to perform the TSR/FSR after an initial acquisition, it is proposed to proceed as follows:

1. Estimate the FS offset as detailed in section 5.4 and perform a corresponding correction of the received PRP-OFDM frame.
2. Estimate the TS offset as detailed in section 5.3.

The FS offset estimation quality depends on the precision of the TS: a small TS offset is typically required in order to ensure a precise estimation of the FS offset. Otherwise, the refinement will be impacted by interference originating from preceding / following OFDM data samples: the corresponding sampling instants prior to / after the postfix can be assumed to carry zero-value postfix samples and i.i.d.

noise of element variance  $\sigma_s^2 + \sigma_n^2$  with  $\sigma_s^2 = E[s_n(i)s_n^*(i)]$ . Consequently, the frequency estimates are still valid but degraded by an increased noise contribution.

The TS offset estimates are impacted if the FSR estimates are not ideal and the corresponding linear phase in time domain is not completely corrected. Assuming that a small residual FS offset of  $\Delta F_R$  remains after correction and with the following definitions:

$$\begin{aligned} \mathbf{D}_{\Delta F_R}(i) &:= \text{Diag} \left\{ e^{j2\pi i P \Delta F_R T}, \dots, e^{j2\pi (iP+P-1) \Delta F_R T} \right\} \\ \phi_{\text{const}} &:= \pi(Z-1)P\Delta F_R T \end{aligned}$$

with  $P\Delta F_R T \frac{Z-1}{2} < 1$ , the frequency offset assumed to be negligible within one single received postfix sequence, the correlation outputs over  $Z$  postfixes are expressed as indicated by equation (5.16), exploiting (5.10), (5.12). As discussed in section 5.3 and with the approximation of  $\mathbf{R}_{\hat{\mathbf{n}}}(Q)$  having constant diagonal elements, the real part operator may be replaced by an absolute value calculation:

$$\bar{Q} = \underset{n}{\text{argmin}} \sum_{i=i_0-\frac{Z-1}{2}}^{i_0+\frac{Z-1}{2}} (\mathbf{M}_\alpha(i) \mathbf{D}_{\Delta F_R}(i) \mathbf{r}_{P,Q}(i) - \mathbf{C}_{\text{CIRC}}(P) \mathbf{m}_n)^H \mathbf{R}_{\hat{\mathbf{n}}}^{-1}(Q) (\mathbf{M}_\alpha(i) \mathbf{D}_{\Delta F_R}(i) \mathbf{r}_{P,Q}(i) - \mathbf{C}_{\text{CIRC}}(P) \mathbf{m}_n) \quad (5.16)$$

$$\begin{aligned} E_{\Delta F_R} &= \sigma_{\hat{\mathbf{n}}}^{-2} e^{j\phi_{\text{const}}} \left( 1 + \sum_{i=-\frac{Z-1}{2}}^{-1} [e^{-j2\pi i P \Delta F_R T} + e^{j2\pi i P \Delta F_R T}] \right) \Re \{ (\mathbf{C}_{\text{CIRC}}(P) \mathbf{M}_J)^H \hat{\mathbf{r}}_{P,Q}(i_0) \} \\ &= \sigma_{\hat{\mathbf{n}}}^{-2} e^{j\phi_{\text{const}}} \left( 2 \sum_{i=0}^{\frac{Z-1}{2}} \cos(2\pi i P \Delta F_R T) - 1 \right) \Re \{ (\mathbf{C}_{\text{CIRC}}(P) \mathbf{M}_J)^H \hat{\mathbf{r}}_{P,Q}(i_0) \} \\ &= \sigma_{\hat{\mathbf{n}}}^{-2} e^{j\phi_{\text{const}}} \underbrace{\left( 2 \frac{\cos\left(\pi \frac{(Z-1)P\Delta F_R T}{2}\right) \sin\left(\pi \frac{(Z+1)P\Delta F_R T}{2}\right)}{\sin(\pi P \Delta F_R T)} - 1 \right)}_{\text{Reduction of accumulated correlator outputs due to freq. offset } \Delta F_R} \Re \{ (\mathbf{C}_{\text{CIRC}}(P) \mathbf{M}_J)^H \hat{\mathbf{r}}_{P,Q}(i_0) \} \quad (5.17) \end{aligned}$$

With the hypothesis that  $\mathbf{R}_{\hat{\mathbf{n}}}(Q) \approx \sigma_{\hat{\mathbf{n}}}^2 \mathbf{I}$ , the expectation of the argmin argument in (5.16) and with  $\sum_{n=0}^Z \cos(nx) = \frac{\cos(\frac{1}{2}Zx) \sin(\frac{1}{2}(Z+1)x)}{\sin(\frac{1}{2}x)}$  becomes (5.17). The remaining common phase offset  $e^{j\phi_{\text{const}}}$  is considered to be contained in the CIR and does not intervene in the synchronization procedure.

Equation (5.17) presents the loss in signal power of the correlator outputs for TSR in presence of a residual FS offset, leading to the following SNR degradation:

$$SNR|_{\Delta F} = SNR|_{\Delta F=0} \frac{1}{Z} \left( 2 \frac{\cos\left(\pi \frac{(Z-1)P\Delta F_R T}{2}\right) \sin\left(\pi \frac{(Z+1)P\Delta F_R T}{2}\right)}{\sin(\pi P \Delta F_R T)} - 1 \right) \quad (5.18)$$

I.e. it is expected to obtain identical TS results compared to section 5.3 with a correspondingly reduced signal SNR.

## 5.6 Performance illustration for 5GHz WLAN

The performance of the TS/FS refinement techniques presented in this chapter are evaluated based on the following simulations: i) a standard IEEE802.11a preamble-based TS technique based on preamble-auto-correlation [38, 116] is applied, ii) improvement of the initial estimate based on the optimum ML estimator (perfect channel knowledge is assumed), iii) refinement of the initial estimate based on the *Approximation I* estimator and iv) improvement of the initial estimate based on the *Approximation II* estimator and v) refinement of FS by auto-correlation based estimation. The simulations are performed in an AWGN and a BRAN-A [37] multi-path channel environment at a SINR of 10dB. The frame structure defined by the IEEE802.11a standard [56] is used and BPSK symbols are chosen for the data carriers. For the PRP-OFDM approach, the mean value over 40 symbols (data plus postfix divided by corresponding pseudo-random weighting factors) is taken in order to refine the synchronization. The postfix sequence is chosen as presented in Tab.5.1.

Fig.5.3 presents the synchronization offset probabilities. The standard preamble-autocorrelation based technique leads to time offset probabilities above  $10^{-3}$  within an offset interval of  $[-5;5]$  for the BRAN-A channel model. Moreover, the offset probability density function is slowly decreasing for high offsets compared to the alternative proposals. In contrast to this approach, the ML estimator (assuming that the CIR is known) does not lead to any offset within  $10^6$  simulations for both, the AWGN and BRAN-A channel models.

With *Approximation II*, the performance lies in between these cases for BRAN-A channels: time offset probabilities above  $10^{-3}$  occur within an offset interval of  $[-1;4]$ . Beyond these values, the offset probability density function is quickly decreasing compared to the standard approach: the interval size is approx. divided by two. *Approximation I* performs poorly (i.e. there is some performance degradation with respect to the algorithm applied to CP-OFDM based TS at an offset beyond -5 samples) due to the reasons explained in section 5.3.2.

The frequency offset estimation analysis is performed for the example of a given frequency offset of  $\Delta F = 500\text{Hz}$  at a sampling frequency of 20MHz (leading to a carrier spacing of  $f_c = 0.3125\text{MHz}$  for  $N = 64$  sub-carriers). Fig.5.4 and Fig.5.5 show the mean estimated frequency offset and its standard deviation respectively. The results show that an averaging over 10 symbols is sufficient to achieve a mean frequency offset estimation error below 100Hz ( $= f_c/3125$  in the given context) for  $\text{SINR} \geq 0\text{dB}$ .

As a result, it can be stated that the use of a pseudo random postfix helps to increase the accuracy of the TS. This enables to reduce frame-mis-detection probabilities and thus makes corresponding receivers more robust. Note that in the PRP case, we can observe that the offset distribution is strictly lower bounded which indicates that we can safely limit the early synchronization to 2 samples in this practical context.

## 5.7 Conclusion

This chapter has shown that the PRP-OFDM inherent frame properties can be exploited for efficient refinement of the TS and FS: standard cross/auto-correlation based synchronization algorithms have been derived for this purpose. In a typical example, simulation results show that the corresponding TS offset

intervals are divided by two comparing to the standard WLAN auto-correlation approach performed on preambles with the PRP-OFDM based refinement. In the same context, FS refinement reduces the residual offset close to zero. Consequently, these techniques help to avoid IBI (due to improved TS) as well as ICI (due to improved FS) and thus improve the overall system performance.

Sample nb	Amplitude	Sample nb	Amplitude
1	1.5649-0.0356i	9	0.0832-0.6527i
2	-0.6961+ 0.9494i	10	0.0306+ 0.0594i
3	0.0874+ 1.1743i	11	0.4047+ 0.2204i
4	0.5737+ 1.4300i	12	-0.2723+ 0.2715i
5	-1.4368-0.8592i	13	0.3469-0.2291i
6	0.2212+ 0.4389i	14	0.0779-0.2369i
7	0.4137+ 0.2834i	15	0.1214+ 0.1355i
8	-0.0960+ 0.9893i	16	-0.2110-0.0972i

Table 5.1: Time domain samples of a suitable postfix (low PAPR).

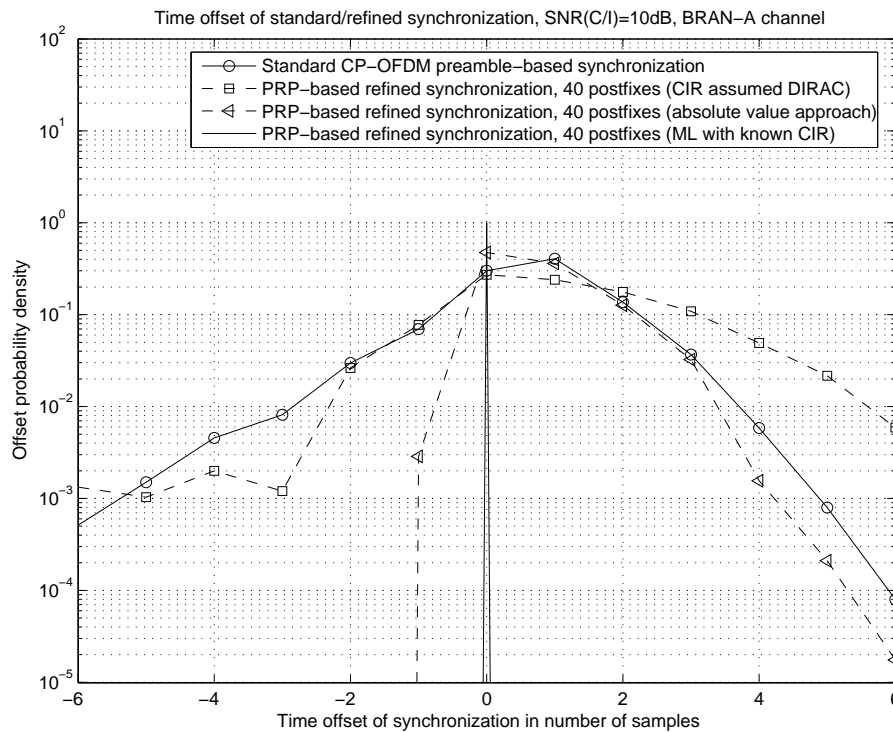


Figure 5.3: Synchronization offset probabilities.

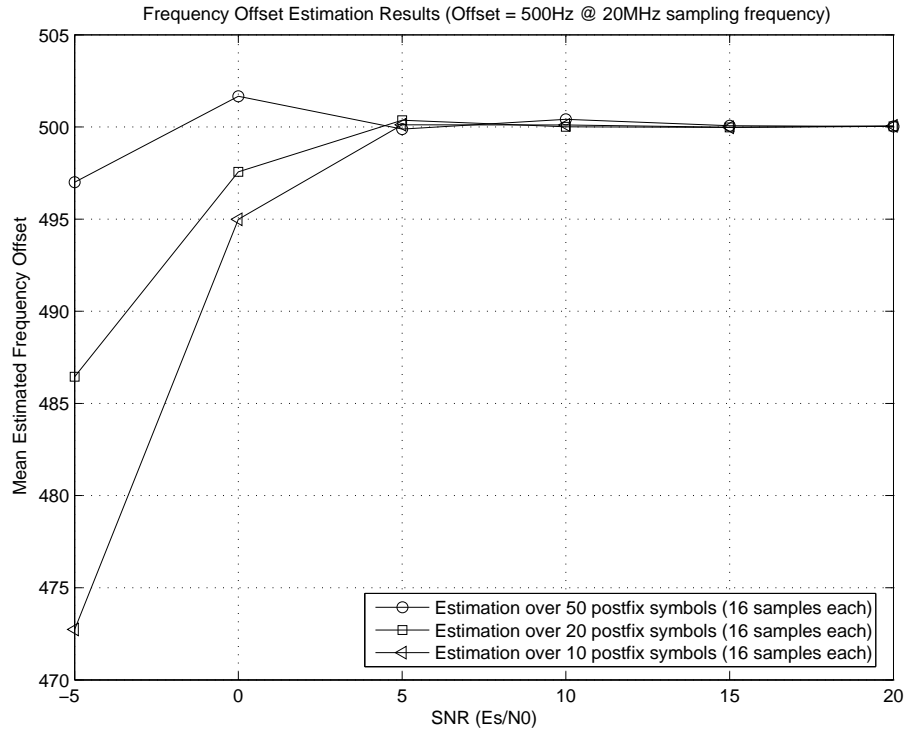


Figure 5.4: Example: mean estimated frequency offset.

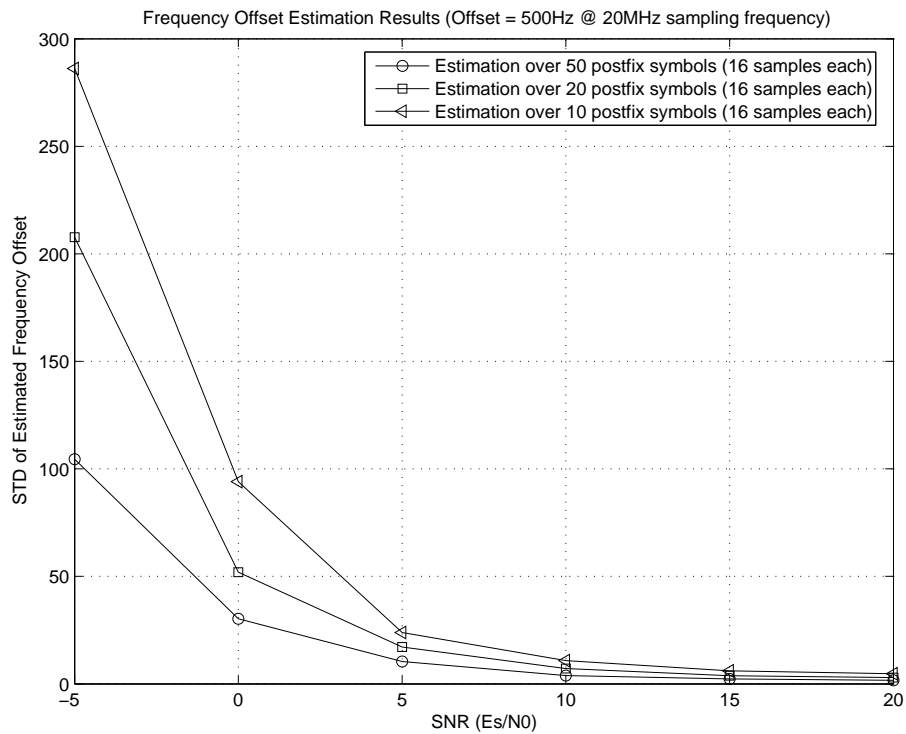


Figure 5.5: Example: standard deviation of the mean estimated frequency offset.

---

## Chapter 6

# Pseudo Random Postfix Orthogonal Frequency Division Multiplexing for multiple antennas systems

This chapter illustrates how to extend the Pseudo Random Postfix OFDM (PRP-OFDM) modulation concept to the Multiple-Transmit-Multiple-Receive (MTMR) antennas context.

### 6.1 Introduction

This chapter capitalizes on the single antenna Pseudo-Random-Postfix OFDM (PRP-OFDM) modulation scheme detailed in the previous chapters 2, 3, 4 and 5 and presents a novel extension of the PRP-OFDM transceiver to the Multiple-Transmit Multiple-Receive (MTMR) antennas case. It is shown how to estimate all propagation channel impulse responses between any TX and RX antenna based on space-time (ST) coded postfix sequences. The approach taken does neither limit the number of transmit and receive antennas nor impose a particular Space-Time Code (STC).

For coherent MTMR systems, the estimation and tracking of the Multiple Input Multiple Output (MIMO) channel is essential and becomes challenging in presence of high Doppler (either considering high mobility scenarios or high frequency bands). In the scheme considered, data and postfix vectors are independently encoded by two STCs; the new specific MTMR postfix design proposed in section 6.3 enables a semi-blind estimation of all the MIMO channel exploiting only the order-one statistics of the received signal. Moreover, after presenting the new channel estimator in the static case, a new one is derived for high mobility scenarios inspired by the derivations in chapter 3, section 3.3.2.

Section 6.4 proposes two transceiver architectures based on an Alamouti based STBC in order to illustrate the decoding and channel estimation steps. Two different decoding strategies are discussed. The first one is to convert the received blocks back to ZP-OFDM vectors through postfix contribution cancellation and then decode them using architectures proposed in [40, 117]. The second one proposes to equalize the full received vector exploiting the diagonalisation properties of pseudo-circulant matri-

ces (see chapter 3 and annex A). Section 6.5 finally presents simulation results and Section 6.6 draws conclusions.

## 6.2 MTMR PRP-OFDM modulation and demodulation

This section presents the digital PRP-OFDM MTMR modulator and recalls the discrete baseband channel model that is used in the framework of this thesis.

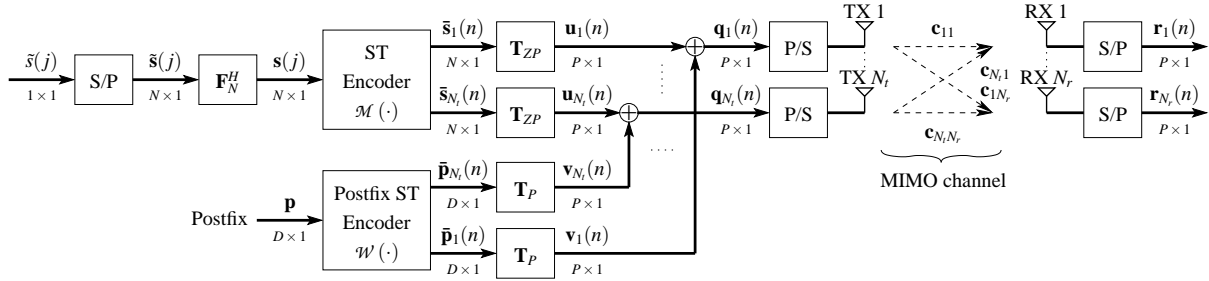


Figure 6.1: Discrete model of the MTMR PRP-OFDM modulator.

Figure 6.1 depicts the baseband discrete-time block equivalent model of a  $N$ -carrier PRP-OFDM MTMR transceiver with  $N_t$  transmit and  $N_r$  receive antennas. Please note that the proposed scheme is fully generic, but for concision sake we will limit the discussion here to Space-Time (ST) block codes. The initial serial stream of constellation symbols  $\tilde{s}(jN), \dots, \tilde{s}(jN + N - 1)$  is serial-to-parallel converted; the  $j$ th  $N \times 1$  input digital vector  $\tilde{\mathbf{s}}(j)$  is then modulated by the IFFT matrix  $\mathbf{F}_N^H$  with  $[\mathbf{F}_N]_{k,l} = (1/\sqrt{N})W_N^{kl}$ ,  $0 \leq k < N$ ,  $0 \leq l < N$  where  $W_N = e^{-j2\pi/N}$ . The resulting  $N \times 1$  time domain vector  $\mathbf{s}(j)$  is processed by any suitable ST encoder  $\mathcal{M}$  creating the outputs

$$\begin{aligned} \tilde{\mathbf{S}}(i) &:= \mathcal{M}(\mathbf{s}(iN_t), \dots, \mathbf{s}(iN_t + N_t - 1)) \\ &= \{\tilde{\mathbf{s}}_l(iM + k), 1 \leq l \leq N_t, 0 \leq k < M\} \end{aligned}$$

with  $i$  being the block number and  $n = iM + k$  indexing the outputs in Figure 6.1. Note that in the context of STBCs,  $M$  can differ from  $N_t$ . For example STBCs given in [118] lead to rectangular  $\tilde{\mathbf{S}}(i)$ , i.e.  $M > N_t$ . In the sequel, the  $\tilde{\mathbf{s}}_l(iM + k)$  are linearly precoded by a ZP-OFDM precoding matrix  $\mathbf{T}_{ZP}$

$$\mathbf{T}_{ZP} := \begin{bmatrix} \mathbf{I}_N \\ \mathbf{0}_{D,N} \end{bmatrix}_{P \times N}$$

with

$$\mathbf{u}_l(n) := \mathbf{T}_{ZP} \tilde{\mathbf{s}}_l(n) \text{ with } 1 \leq l \leq N_t. \quad (6.1)$$

A pseudo randomly weighted postfix, chosen with respect to the design criteria given in chapter 4, is appended afterwards. In the MTMR case, the deterministic  $D \times 1$  postfix vector  $\mathbf{p}$  is treated by a specific ST encoder  $\mathcal{W}$  which outputs the  $D \times 1$  vectors  $\tilde{\mathbf{p}}_l(n)$ ,  $1 \leq l \leq N_t$ . As it will be shown later,  $\mathcal{W}$  is there for ensuring identification of the complete MIMO channel. In order to avoid unpleasant spectrum

properties, the postfix vector is weighted by a scalar pseudo-random sequence (as discussed in chapter 4). The postfix vectors  $\bar{\mathbf{p}}_l(n)$  are then linearly precoded by the matrix  $\mathbf{T}_P$

$$\mathbf{T}_P := \left[ \frac{\mathbf{0}_{N,D}}{\mathbf{I}_D} \right]_{P \times D}$$

and the resulting  $\mathbf{v}_l(n)$  are finally added to the data symbols  $\mathbf{u}_l(n)$ :

$$\mathbf{q}_l(n) := \mathbf{u}_l(n) + \mathbf{v}_l(n) \text{ with } 1 \leq l \leq N_t \quad (6.2)$$

Let  $\mathbf{C}_{lm}$  be a  $P \times P$  circulant matrix whose first row is given by  $[c_{lm}(0), 0 \rightarrow 0, c_{lm}(L-1), \dots, c_{lm}(1)]$ , where  $\mathbf{c}_{lm} = [c_{lm}(0), \dots, c_{lm}(L-1), 0 \rightarrow 0]^T$  is the  $P \times 1$  channel impulse response between the  $l$ th transmit and the  $m$ th receive antenna;  $D$  is chosen such that  $L < D$ . Define  $\mathbf{C}_{lm}^{\text{ISI}}$  as the lower triangular part of  $\mathbf{C}_{lm}$  including the main diagonal which represents the Intra-Symbol-Interference (ISI);  $\mathbf{C}_{lm}^{\text{IBI}}$  shall contain the upper triangular part of  $\mathbf{C}_{lm}$  representing the Inter-Block-Interference (IBI), such that  $\mathbf{C}_{lm} = \mathbf{C}_{lm}^{\text{ISI}} + \mathbf{C}_{lm}^{\text{IBI}}$ . Therefore, the received vector on the  $m$ th antenna,  $1 \leq m \leq N_r$  is given by (compare with derivations in chapter 3)

$$\mathbf{r}_m(n) := \sum_{l=1}^{N_t} [\mathbf{C}_{lm}^{\text{ISI}} \mathbf{q}_l(n) + \mathbf{C}_{lm}^{\text{IBI}} \mathbf{q}_l(n-1)] + \mathbf{n}_m(n)$$

where  $\mathbf{n}_m(n)$  is an complex zero-mean additive white i.i.d. Gaussian noise term.

A choice of the pseudo random postfix ST encoder  $\mathcal{W}$  is discussed in the next section in order to allow a simple identification of all channels  $\mathbf{c}_{lm}$ ,  $1 \leq l \leq N_t$ ,  $1 \leq m \leq N_r$ .

### 6.3 Order-one MIMO channel estimation

The goal of this section is to extend the order-one channel estimation technique presented in chapter 3 to the MTMR case. First, a novel channel estimation algorithm is detailed, assuming the channel to be static. Then, a Doppler model is introduced for the mobility case and the corresponding optimum channel estimator in the Minimum Mean Square Error (MMSE) sense.

First let us express the received vector  $\mathbf{r}_m(n)$  in an exploitable form for the channel estimation. For that purpose let  $\mathbf{C}_{lm}^D$  be the  $D \times D$  circulant matrix of first row  $[c_{lm}(0), 0 \rightarrow 0, c_{lm}(L), \dots, c_{lm}(1)]$ . We define  $\mathbf{C}_{lm}^{\text{ISI},D}$  and  $\mathbf{C}_{lm}^{\text{IBI},D}$  as previously such that  $\mathbf{C}_{lm}^D := \mathbf{C}_{lm}^{\text{ISI},D} + \mathbf{C}_{lm}^{\text{IBI},D}$ . The signal  $\mathbf{r}_m(n)$ , received during the  $n$ th OFDM symbol on the  $m$ th antenna,  $1 \leq m \leq N_r$ , is equal to:

$$\mathbf{r}_m(n) = \sum_{l=1}^{N_t} \begin{bmatrix} \mathbf{C}_{lm}^{\text{ISI},D} \bar{\mathbf{s}}_{l,0}(n) + \mathbf{C}_{lm}^{\text{IBI},D} \bar{\mathbf{p}}_l(n-1) \\ \vdots \\ \mathbf{C}_{lm}^{\text{IBI},D} \bar{\mathbf{s}}_{l,1}(n) + \mathbf{C}_{lm}^{\text{ISI},D} \bar{\mathbf{p}}_l(n) \end{bmatrix} + \begin{bmatrix} \mathbf{n}_{m,0}(n) \\ \vdots \\ \mathbf{n}_{m,1}(n) \end{bmatrix} \quad (6.3)$$

where  $\bar{\mathbf{s}}_{l,0}(n)$ ,  $\bar{\mathbf{s}}_{l,1}(n)$ ,  $\mathbf{n}_{m,0}(n)$ ,  $\mathbf{n}_{m,1}(n)$  are respectively the first  $D$  and last  $D$  samples of  $\bar{\mathbf{s}}_l(n)$  and  $\mathbf{n}_m(n)$ .

Equation (6.3) tells that a super-imposition of the various postfixes convolved by the corresponding channels is interfering with the useful data. An easy independent retrieval of each of the channels based

on the sole observation of the postfixes contributions would be possible through isolation of each postfix convolved by its related channel. As detailed below, a way to achieve that condition is to use a weighting ST block coding scheme  $\mathcal{W}$  of the postfix  $\mathbf{p}$  using the following postfixes generation process :

$$\begin{bmatrix} \bar{\mathbf{p}}_1(iM) & \cdots & \bar{\mathbf{p}}_1(iM + M - 1) \\ \vdots & \ddots & \vdots \\ \bar{\mathbf{p}}_{N_t}(iM) & \cdots & \bar{\mathbf{p}}_{N_t}(iM + M - 1) \end{bmatrix} := \underbrace{\begin{bmatrix} w_1(0)\alpha(iM) & \cdots & w_1(M-1)\alpha(iM + M - 1) \\ \vdots & \ddots & \vdots \\ w_{N_t}(0)\alpha(iM) & \cdots & w_{N_t}(M-1)\alpha(iM + M - 1) \end{bmatrix}}_{\mathcal{W}} \otimes \mathbf{p} \quad (6.4)$$

where  $\otimes$  is the Kronecker product and  $\mathbf{p}$ ,  $\alpha(iM + k)$  are respectively the deterministic postfix and the pseudo-random weighting factors introduced in chapter 4. The pseudo-random weighting factors  $\alpha(iM + k)$  are used to convert the deterministic postfix  $\mathbf{p}$  into a pseudo-random one. Note that a new set of deterministic weighting factors is introduced, and gathered in the  $M \times N_t$  matrix  $\mathbf{W}$ , with  $[\mathbf{W}]_{k,l-1} = w_l(k)$ ,  $0 \leq k < M$ ,  $1 \leq l \leq N_t$ .  $\mathbf{W}$  is there to remove the interference between all transmitted postfixes and thus needs to be invertible:  $\mathbf{W}$  is of full column rank ( $\text{rank}(\mathbf{W}) = N_t$ ). In the following we choose  $\mathbf{W}$  orthogonal, such that  $\mathbf{W}^H \mathbf{W} = N_t \times \mathbf{I}_{N_t}$ .

### 6.3.1 Static context : minimum dimension circular diagonalization

We focus now on a static channel and detail an order-one channel estimator similar to the one presented in chapter 3.3.1, subsection *Channel estimation using minimum dimension circular diagonalization*. For the reasons given in 3.3.1, a carrier grid adaptation is useful in order to improve the estimation results if the postfix is rank deficient - this case is discussed in the following section.

For that purpose, denote respectively by  $\mathbf{r}_{m,0}(n)$  and  $\mathbf{r}_{m,1}(n)$  the first and last  $D$  samples of  $\mathbf{r}_m(n)$ . By setting  $n = iM + k$  and assuming the transmitted time domain signal  $\bar{\mathbf{s}}_l(n)$  to be zero mean for all  $l$ , we use (6.4) and (6.3) to compute for each  $k$ ,  $0 \leq k < M$ , the following  $D \times 1$  vector:

$$\mathbf{d}_m^k(i) := \frac{\mathbf{r}_{m,1}(iM + k) + \mathbf{r}_{m,0}(iM + k + 1)}{\alpha(iM + k)} \quad (6.5)$$

Define

$$\mathbf{d}_m^k := \mathbb{E}[\mathbf{d}_m^k(i)] \quad (6.6)$$

as the expectation of  $\mathbf{d}_m^k(i)$ . Thanks to the deterministic nature of the postfixes, it can be verified from (6.3) that:

$$\begin{aligned}
\mathbf{d}_m^k &= \sum_{l=1}^{N_t} [\mathbf{C}_{lm}^{\text{ISL},D} + \mathbf{C}_{lm}^{\text{IBL},D}] w_l(k) \mathbf{p} \\
&= \sum_{l=1}^{N_t} \mathbf{C}_{lm}^D w_l(k) \mathbf{p}
\end{aligned} \tag{6.7}$$

Note that in practice the expectation in (6.6) is estimated by averaging over  $Z$  observations (one observation is defined here as an STC block of  $M$  OFDM symbols per antenna) and thus approximate, and  $\mathbf{d}_m$  is corrupted by a residual additive noise  $\bar{\mathbf{n}}_m^k$ :

$$\bar{\mathbf{n}}_m^k := \frac{1}{Z} \sum_{i=0}^{Z-1} \left( \mathbf{n}_{m,0}(iM+k) + \mathbf{n}_{m,1}(iM+k) + \sum_{l=1}^{N_t} [\mathbf{C}_{lm}^{\text{ISL},D} \bar{\mathbf{s}}_{l,0}(iM+k) + \mathbf{C}_{lm}^{\text{IBL},D} \bar{\mathbf{s}}_{l,1}(iM+k)] \right)$$

thus the  $MD \times 1$  vectors

$$\mathbf{d}_m := [\mathbf{d}_m^{0T}, \dots, (\mathbf{d}_m^{M-1})^T]^T, \tag{6.8}$$

$$\bar{\mathbf{n}}_m := [\bar{\mathbf{n}}_m^{0T}, \dots, \bar{\mathbf{n}}_m^{(M-1)T}]^T \tag{6.9}$$

can be expressed for each receive antenna as:

$$\begin{aligned}
\mathbf{d}_m &= \sum_{l=1}^{N_t} \begin{bmatrix} \mathbf{C}_{lm}^D w_l(0) \mathbf{p} \\ \vdots \\ \mathbf{C}_{lm}^D w_l(M-1) \mathbf{p} \end{bmatrix} \\
&= (\mathbf{W} \otimes \mathbf{I}_D) \cdot \begin{bmatrix} \mathbf{C}_{lm}^D \mathbf{p} \\ \vdots \\ \mathbf{C}_{N,m}^D \mathbf{p} \end{bmatrix}, \tag{6.10} \\
\bar{\mathbf{n}}_m &= \frac{1}{Z} \begin{bmatrix} \sum_{i=0}^{Z-1} (\mathbf{n}_{m,0}(iM) + \mathbf{n}_{m,1}(iM)) \\ \vdots \\ \sum_{i=0}^{Z-1} (\mathbf{n}_{m,0}(iM+M-1) + \mathbf{n}_{m,1}(iM+M-1)) \end{bmatrix} + \\
&\quad \frac{1}{Z} \begin{bmatrix} \sum_{i=0}^{Z-1} \sum_{l=1}^{N_t} [\mathbf{C}_{lm}^{\text{ISL},D} \bar{\mathbf{s}}_{l,0}(iM) + \mathbf{C}_{lm}^{\text{IBL},D} \bar{\mathbf{s}}_{l,1}(iM)] \\ \vdots \\ \sum_{i=0}^{Z-1} \sum_{l=1}^{N_t} [\mathbf{C}_{lm}^{\text{ISL},D} \bar{\mathbf{s}}_{l,0}(iM+M-1) + \mathbf{C}_{lm}^{\text{IBL},D} \bar{\mathbf{s}}_{l,1}(iM+M-1)] \end{bmatrix}
\end{aligned}$$

Since  $\mathbf{W}$  is chosen orthogonal, multiplying each  $\mathbf{d}_m$ ,  $1 \leq m \leq N_r$  by  $(\mathbf{W} \otimes \mathbf{I}_D)^H$  removes completely the interference between channel contributions  $\mathbf{C}_{lm}^D$ ,  $1 \leq l \leq N_t$ :

$$\begin{aligned} N_t^{-1}(\mathbf{W} \otimes \mathbf{I}_D)^H \mathbf{d}_m &= N_t^{-1} \underbrace{(\mathbf{W} \otimes \mathbf{I}_D)^H (\mathbf{W} \otimes \mathbf{I}_D)}_{=N_t \mathbf{I}_{(D \times N_t)}} \cdot \begin{bmatrix} \mathbf{C}_{1m}^D \mathbf{p} \\ \vdots \\ \mathbf{C}_{N_t m}^D \mathbf{p} \end{bmatrix} \\ &= \begin{bmatrix} \mathbf{C}_{1m}^D \mathbf{p} \\ \vdots \\ \mathbf{C}_{N_t m}^D \mathbf{p} \end{bmatrix} \end{aligned} \quad (6.11)$$

In practice, an identical operation is performed on the noise:  $\bar{\mathbf{n}}_m \rightarrow N_t^{-1}(\mathbf{W} \otimes \mathbf{I}_D)^H \bar{\mathbf{n}}_m$ . In case  $\mathbf{W}$  containing unitary elements and assuming that the noise vector has i.i.d. Gaussian elements (including the data OFDM symbol part), this operation generates a new noise vector of identical noise variance.

Note that taking  $\mathbf{W}$  orthogonal also minimizes the mean square error of the least squares estimate of  $[(\mathbf{C}_{1m}^D \mathbf{p})^T, \dots, (\mathbf{C}_{N_t m}^D \mathbf{p})^T]^T$ . Note that  $\mathbf{W}$  can always be chosen to be a  $N_t \times N_t$  matrix, independently from  $M$  which is determined by the STC  $\mathcal{M}$ .

Once the interference between channel contributions is removed estimation algorithms of the single-antenna case apply as presented in chapter 3:

$$\begin{aligned} \mathbf{C}_{lm}^D \mathbf{p} &= \mathbf{p}_D \mathbf{c}_{lm}^D \\ &= \mathbf{F}_D^H \tilde{\mathbf{P}}_D \mathbf{F}_D \mathbf{c}_{lm}^D \end{aligned} \quad (6.12)$$

where  $\mathbf{p}_D$  is a  $D \times D$  circulant matrix with the first row  $[p(0), p(D-1), \dots, p(1)]$ ,  $\tilde{\mathbf{P}}_D = \text{diag}\{\mathbf{F}_D \mathbf{p}\}$ , and  $\mathbf{c}_{lm}^D$  represents the  $D$  first coefficients of  $\mathbf{c}_{lm}$ . Hence, the estimate  $\hat{\mathbf{c}}_{lm}^D$  of the time domain channel impulse response  $\mathbf{c}_{lm}^D$  is obtained by pre-multiplying  $\mathbf{C}_{lm}^D \mathbf{p}$  by  $\mathbf{F}_D^H \tilde{\mathbf{P}}_D^{-1} \mathbf{F}_D$ ,  $1 \leq l \leq N_t$ ,  $1 \leq m \leq N_r$  (Zero Forcing approach as given by equation (3.9) for the STSR case) or by performing an MMSE estimation taking the final noise-covariance  $N_t^{-1}(\mathbf{W} \otimes \mathbf{I}_D)^H \bar{\mathbf{n}}_m$  into account similar to equation (3.10).

Note that  $\tilde{\mathbf{P}}_D^{-1}$  is a diagonal matrix that is a-priori known to both the transmitter and receiver and can thus be pre-calculated. Subsequently,  $\hat{\mathbf{c}}_{lm}^D$  is usually transformed to the  $P \times 1$  frequency domain vector

$$\hat{\mathbf{c}}_{lm} = \mathbf{F}_P [\mathbf{I}_D^T, \mathbf{0}_{N,D}^T]^T \hat{\mathbf{c}}_{lm}^D. \quad (6.13)$$

### 6.3.2 Static context : carrier grid adaptation

As discussed in chapter 3.3.1, section *Channel estimation using frequency domain carrier grid adaptation*, in practice it is often of advantage to keep the IBI and ISI parts of the received postfixes separated.

In particular, this allows an efficient estimation of channel coefficients if the postfix is rank deficient (e.g. in order to keep the out-of-band radiation as low as possible). This section presents how to modify the upper equations in order to achieve this goal.

Contrary to equation (6.7), the ISI and IBI parts of the received signal are kept separately:

$$\begin{aligned} \mathbf{d}_{m,2D}^k &:= \sum_{l=1}^{N_t} \begin{bmatrix} \mathbf{C}_{lm}^{\text{ISI},D} \\ \mathbf{C}_{lm}^{\text{IBI},D} \end{bmatrix} w_l(k) \mathbf{p} \\ \bar{\mathbf{n}}_{m,2D}^k &:= \frac{1}{Z} \sum_{i=0}^{Z-1} \left( \begin{bmatrix} \mathbf{n}_{m,0}(iM+k) \\ \mathbf{n}_{m,1}(iM+k) \end{bmatrix} + \sum_{l=1}^{N_t} \begin{bmatrix} \mathbf{C}_{lm}^{\text{ISI},D} \bar{\mathbf{s}}_{l,0}(iM+k) \\ \mathbf{C}_{lm}^{\text{IBI},D} \bar{\mathbf{s}}_{l,1}(iM+k) \end{bmatrix} \right) \end{aligned} \quad (6.14)$$

Again, in practice it is useful to group all  $M$  observations of a STC block into a single vector, similar to equations (6.8) and (6.9):

$$\begin{aligned} \mathbf{d}_{m,2D} &:= [\mathbf{d}_{m,2D}^{0T}, \dots, (\mathbf{d}_{m,2D}^{(M-1)T})^T]^T, \\ \bar{\mathbf{n}}_{m,2D} &:= [\bar{\mathbf{n}}_{m,2D}^{0T}, \dots, \bar{\mathbf{n}}_{m,2D}^{(M-1)T}]^T \end{aligned}$$

The different contributions

$$\begin{bmatrix} \mathbf{C}_{lm}^{\text{ISI},D} \\ \mathbf{C}_{lm}^{\text{IBI},D} \end{bmatrix} \mathbf{p}$$

are extracted by pre-multiplication of  $\mathbf{d}_{m,2D}$  by  $(\mathbf{W} \otimes \mathbf{I}_{2D})^H$  instead of  $(\mathbf{W} \otimes \mathbf{I}_D)^H$  as used in equation (6.11):

$$N_t^{-1} (\mathbf{W} \otimes \mathbf{I}_{2D})^H \mathbf{d}_{m,2D} = N_t^{-1} \underbrace{(\mathbf{W} \otimes \mathbf{I}_{2D})^H (\mathbf{W} \otimes \mathbf{I}_{2D})}_{=N_t \mathbf{I}_{2D \cdot N_t}} \begin{bmatrix} \begin{bmatrix} \mathbf{C}_{lm}^{\text{ISI},D} \\ \mathbf{C}_{lm}^{\text{IBI},D} \end{bmatrix} \mathbf{p} \\ \vdots \\ \begin{bmatrix} \mathbf{C}_{N_t m}^{\text{ISI},D} \\ \mathbf{C}_{N_t m}^{\text{IBI},D} \end{bmatrix} \mathbf{p} \end{bmatrix}. \quad (6.15)$$

The resulting noise expression is given by  $N_t^{-1} (\mathbf{W} \otimes \mathbf{I}_{2D})^H \bar{\mathbf{n}}_{m,2D}$ .

The channel coefficients are finally extracted by a MMSE approach as given in chapter 3.3.1 by equation (3.11).

### 6.3.3 Doppler Context

Let extend the above channel estimator to mobile environments. For this purpose, it is assumed that the CIR remains static within one STC block of  $M$  OFDM symbols.

With these assumptions, let us investigate how to estimate the channel coefficients if the mean value window size is set to  $\bar{Z} = 1$ : then, the extraction of  $[\mathbf{C}_{lm}^{\text{ISL},D} + \mathbf{C}_{lm}^{\text{IBL},D}] \mathbf{p}$  or  $\begin{bmatrix} \mathbf{C}_{lm}^{\text{ISL},D} \\ \mathbf{C}_{lm}^{\text{IBL},D} \end{bmatrix} \mathbf{p}$  is not impacted as given by equation (6.11) and (6.15) respectively. Based on this observation, it is clear that the CIR estimation methodology derived in chapter 3.3.2 is straightforwardly applied to the MTMR case by performing the following steps:

1. extract the channel convolved by the postfix sequences assuming that a mean value window over  $\bar{Z} = 1$  STC block is used.
2. perform the first step  $Z$  times leading to  $Z$  independent observations of the postfix sequences convolved by the channel plus noise.
3. regroup all  $Z$  postfix sequences convolved by the channel for each  $\mathbf{C}_{lm}^{\text{ISL},D}$ ,  $\mathbf{C}_{lm}^{\text{IBL},D}$  separately and treat these observations as in the STSR case presented in chapter 3.3.2.

Similar to the STSR results presented in chapter 3.3.2, different trade-offs are possible in terms of system latency and MSE of the CIR estimates.

## 6.4 Examples of transceiver designs

This section presents two Alamouti [93] based modulators that are adapted to the use of pseudo-random postfixes at the transmitter and also to the equalizer structures detailed in this section. The two equalizers proposed are based on the ones already derived for the Single Transmit Single Receive (STSR) case in chapter 3: one is based on the transformation of the received PRP-OFDM vector to the ZP-OFDM case, the other one on the equalization of the full received block.

The system of interest is chosen to have  $N_t = 2$  transmit and  $N_r = 1$  receive antennas. The ST encoder operates over  $N_t \times M$  vectors with  $M = N_t = 2$ . Since  $N_r = 1$ , the subscript  $1 \leq m \leq N_r$  is not used in the sequel. A perfect knowledge of the channels  $\mathbf{c}_l$ ,  $1 \leq l \leq N_t$  is assumed.

Section 6.4.1 first defines a transmission scheme that targets in the receiver a transformation of the received symbols to a MTMR ZP-OFDM context (see for example [39] for more details on MTMR ZP-OFDM). The corresponding receiver is derived by extending the derivations presented in chapter 3 to the single antenna case. Then, section 6.4.2 illustrates how to define a transmission scheme that allows an equalization based on the properties of pseudo-circulant channel convolution matrices; as an advantage, the postfix suppression step is (partially) avoided.

### 6.4.1 ZP-OFDM based decoding approach

Let apply at the transmit the  $2 \times 1$  ST encoder  $\mathcal{M}$  proposed by [119] in the ZP single-carrier context, which takes two consecutive OFDM symbols  $\mathbf{s}(2i)$  and  $\mathbf{s}(2i+1)$  to form the following coded matrix:

$$\begin{bmatrix} \bar{\mathbf{s}}_1(2i) & \bar{\mathbf{s}}_1(2i+1) \\ \bar{\mathbf{s}}_2(2i) & \bar{\mathbf{s}}_2(2i+1) \end{bmatrix} := \begin{bmatrix} \mathbf{s}(2i) & -\mathbf{P}_N^0 \mathbf{s}^*(2i+1) \\ \mathbf{s}(2i+1) & \mathbf{P}_N^0 \mathbf{s}^*(2i) \end{bmatrix} \quad (6.16)$$

where the permutation matrices  $\mathbf{P}_N^p$  are such that, for a  $J \times 1$  vector  $\mathbf{a} = [a(0), \dots, a(J-1)]^T$ ,  $\{\mathbf{P}_N^p \mathbf{a}\}_p = a((J-1-p+n) \bmod J)$ , with  $0 \leq p \leq J-1$ . Note that (6.16) reduces to the Alamouti ST block code [93] if  $N = 1$ :

$$\begin{bmatrix} \bar{s}_1(2i) & \bar{s}_1(2i+1) \\ \bar{s}_2(2i) & \bar{s}_2(2i+1) \end{bmatrix} = \begin{bmatrix} s(2i) & -s^*(2i+1) \\ s(2i+1) & s^*(2i) \end{bmatrix} \quad (6.17)$$

Since the channel is known, as for the single antenna case in chapter 3, it is always possible to retrieve the MTMR ZP-OFDM signals from (6.3) by subtracting from the received signal the known PRP contribution where  $\hat{\mathbf{C}}_l^{\text{IBI}}$  and  $\hat{\mathbf{C}}_l^{\text{ISI}}$  are estimates of the channel matrices  $\mathbf{C}_l^{\text{IBI}}$  and  $\mathbf{C}_l^{\text{ISI}}$  respectively:

$$\mathbf{r}^{\text{ZP}}(n) := \mathbf{r}(n) - \sum_{l=1}^2 [\hat{\mathbf{C}}_l^{\text{IBI}} \mathbf{v}_l(n-1) + \hat{\mathbf{C}}_l^{\text{ISI}} \mathbf{v}_l(n)] \quad (6.18)$$

which leads to

$$\mathbf{r}^{\text{ZP}}(n) = \sum_{l=1}^2 \mathbf{C}_l \mathbf{T}_{\text{ZP}} \bar{\mathbf{s}}_l(n) + \mathbf{n}(n). \quad (6.19)$$

Note that i) no constraint has to be set on  $\mathbf{W}$  for the symbol recovery, ii) the PRP interference cancellation procedure proposed is generic and can be applied to any ST encoder  $\mathcal{M}$ .

Now the same detection algorithm as in [119] can be applied to the signal in (6.18). Noticing that

$$\mathbf{P}_P^N \mathbf{T}_{\text{ZP}} = \mathbf{T}_{\text{ZP}} \mathbf{P}_N^0,$$

we denote by

$$\begin{aligned}
\tilde{\mathbf{D}}_1 &:= \text{diag}\{\tilde{\mathbf{c}}_1\}, \\
\tilde{\mathbf{D}}_2 &:= \text{diag}\{\tilde{\mathbf{c}}_2\}, \\
\tilde{\mathbf{n}}(2i) &:= \mathbf{F}_P \mathbf{n}(2i) \text{ and} \\
\tilde{\mathbf{n}}(2i+1) &:= \mathbf{F}_P \mathbf{P}_P^N \mathbf{n}^*(2i+1);
\end{aligned}$$

if we switch to the frequency domain by computing

$$\begin{aligned}
\tilde{\mathbf{r}}(2i) &= \mathbf{F}_P \mathbf{r}^{\text{ZP}}(2i), \\
\tilde{\mathbf{r}}(2i+1) &= \mathbf{F}_P (\mathbf{P}_P^N \mathbf{r}^{\text{ZP}}(2i+1))^*,
\end{aligned} \tag{6.20}$$

exploiting the fact that  $\mathbf{C}_l = \mathbf{F}_P^H \tilde{\mathbf{D}}_l \mathbf{F}_P$ ,  $1 \leq l \leq 2$ , we can write as in [119]:

$$\begin{bmatrix} \tilde{\mathbf{r}}(2i) \\ \tilde{\mathbf{r}}(2i+1) \end{bmatrix} = \underbrace{\begin{bmatrix} \tilde{\mathbf{D}}_1 & \tilde{\mathbf{D}}_2 \\ \tilde{\mathbf{D}}_2^* & -\tilde{\mathbf{D}}_1^* \end{bmatrix}}_{=\tilde{\mathbf{D}}} \begin{bmatrix} \mathbf{F}_P \mathbf{T}_{\text{ZPS}}(2i) \\ \mathbf{F}_P \mathbf{T}_{\text{ZPS}}(2i+1) \end{bmatrix} + \begin{bmatrix} \tilde{\mathbf{n}}(2i) \\ \tilde{\mathbf{n}}(2i+1) \end{bmatrix}$$

where  $\tilde{\mathbf{D}}$  is an orthogonal channel matrix. Thus multiplying  $[\tilde{\mathbf{r}}(2i)^T, \tilde{\mathbf{r}}(2i+1)^T]^T$  by  $\tilde{\mathbf{D}}^H$  achieves the separation of the transmitted signals  $\mathbf{s}(2i)$  and  $\mathbf{s}(2i+1)$ , and it can be shown [119] that full transmit diversity is achieved. Note that the separation of signals allows to use the same equalization schemes as in the single-antenna case discussed in chapter 3.

## 6.4.2 Decoding based on diagonalization of pseudo-circulant channel matrices

The ST data encoder  $\mathcal{M}$  considered here is based on a modification version of the Alamouti scheme [93] and outputs blocks of  $N_t \times M$  vectors with  $N_t = M = 2$ . The modification proposed are required for enabling the equalization structure that is detailed below: it exploits the diagonalization properties of pseudo-circulant matrices similar to the equalization matrix proposed by theorem (3.5.1) in the SISO case.  $\mathcal{M}$  and  $\mathcal{W}$  are specified such that they generate the following matrix  $\mathbf{Q}(i) := \{\mathbf{q}_l(2i+k), 1 \leq l \leq 2, 0 \leq k < 2\}$  at the antennas outputs:

$$\mathbf{Q}(i) := \begin{bmatrix} \begin{bmatrix} \mathbf{s}(2i) \\ \alpha(2i)\mathbf{p} \end{bmatrix} & -\mathbf{P}_P^0 \mathbf{Q}_{\beta(i)} \begin{bmatrix} \mathbf{s}^*(2i+1) \\ \beta^*(i)\alpha^*(2i+1)\mathbf{p}^* \end{bmatrix} \\ \begin{bmatrix} \mathbf{s}(2i+1) \\ \alpha(2i)\mathbf{p} \end{bmatrix} & \mathbf{P}_P^0 \mathbf{Q}_{\beta(i)} \begin{bmatrix} \mathbf{s}^*(2i) \\ \beta^*(i)\alpha^*(2i+1)\mathbf{p}^* \end{bmatrix} \end{bmatrix}$$

$\mathbf{P}_P^0$  being a permutation matrix defined as previously (inverting the order of the vector elements),  $\alpha(i) \in \mathbb{C}$  with  $|\alpha(i)| = 1$  being pseudo-random complex weighting factors as defined in chapter 3 with  $\alpha(2i+1) = \beta(i)\alpha(2i)$  and  $\beta(i) = \alpha^*(2i-1)/\alpha(2i)$ .  $\mathbf{Q}_{\beta(i)}$  is defined as:

$$\mathbf{Q}_{\beta(i)} = \begin{bmatrix} \mathbf{0}_{D \times N} & \beta(i) \cdot \mathbf{I}_D \\ \mathbf{I}_N & \mathbf{0}_{N \times D} \end{bmatrix}.$$

The  $D \times 1$  postfix vector  $\mathbf{p}$  is chosen such that it has hermitian symmetry, i.e. with defining  $(\cdot)^F$  as an operator that reads the vector argument in inverse order, we obtain:  $(\mathbf{p}^*)^F = \mathbf{p}$ . Similar to [4], the channels are represented by  $P \times P$  pseudo-circulant channel matrices  $\mathbf{C}_l^{\beta(i)}$ ,  $1 \leq l \leq 2$ . These are identical to standard circulant convolution matrices with the upper triangular part multiplied by the scalar factor  $\beta(i)$ , i.e.  $\mathbf{C}_l^{\beta(i)} := \mathbf{C}_l^{\text{ISI}} + \beta(i)\mathbf{C}_l^{\text{IBI}}$ .

With  $\mathbf{R}(i) := [\mathbf{r}^T(2i) \ \mathbf{r}^T(2i+1)]^T$  and the noise matrix  $\mathbf{N}(i) = [\mathbf{n}^T(2i) \ \mathbf{n}^T(2i+1)]^T$ , the received signals over  $M = 2$  symbol times are given as follows:

$$\mathbf{R}(i) = \begin{bmatrix} \sum_{l=1}^2 [\mathbf{C}_l^{\text{IBI}} \mathbf{q}_l(2i-1) + \mathbf{C}_l^{\text{ISI}} \mathbf{q}_l(2i)] \\ \sum_{l=1}^2 [\mathbf{C}_l^{\text{IBI}} \mathbf{q}_l(2i) + \mathbf{C}_l^{\text{ISI}} \mathbf{q}_l(2i+1)] \end{bmatrix} + \mathbf{N}(i)$$

Exploiting the fact that  $(\mathbf{P}_P^0 \mathbf{C}_l^{\beta(i)} \mathbf{P}_P^0)^* = (\mathbf{C}_l^{\beta(i)})^H$  and  $\mathbf{Q}_{\beta(i)} \mathbf{C}_l^{\beta(i)} = \mathbf{C}_l^{\beta(i)} \mathbf{Q}_{\beta(i)}$ , since both are diagonal in the same basis, we compute:

$$\begin{aligned} \hat{\mathbf{R}}(i) &:= \begin{bmatrix} \mathbf{r}(2i) + 2\mathbf{p}_1^{\beta(i)}(i) \\ \mathbf{Q}_{\beta(i)}^H \left( \mathbf{P}_P^0 \left( \mathbf{r}(2i+1) + \mathbf{p}_2^{\beta(i)}(i) \right) \right)^* \end{bmatrix} \\ &= \underbrace{\begin{bmatrix} \mathbf{C}_1^{\beta(i)} & \mathbf{C}_2^{\beta(i)} \\ (\mathbf{C}_2^{\beta(i)})^H & -(\mathbf{C}_1^{\beta(i)})^H \end{bmatrix}}_{=\mathbf{W}_H(i)} \begin{bmatrix} \begin{bmatrix} \mathbf{s}(2i) \\ \alpha(2i)\mathbf{p} \end{bmatrix} \\ \begin{bmatrix} \mathbf{s}(2i+1) \\ \alpha(2i)\mathbf{p} \end{bmatrix} \end{bmatrix}, \\ \mathbf{p}_1^{\beta(i)}(i) &:= \alpha(2i)\beta(i)\mathbf{C}_1^{\text{IBI}}\mathbf{T}_P\mathbf{p}, \tag{6.21} \\ \mathbf{p}_2^{\beta(i)}(i) &:= -2[\text{Re}\{\alpha(2i)\}\mathbf{C}_1^{\text{IBI}} + j\text{Im}\{\alpha(2i)\}\mathbf{C}_2^{\text{IBI}}]\mathbf{T}_P\mathbf{p}. \tag{6.22} \end{aligned}$$

Corresponding to Alamouti's derivations [93], the data symbols can be straightforwardly separated by pre-multiplication of  $\hat{\mathbf{R}}(i)$  by the hermitian of the upper channel matrix  $\mathbf{W}_H(i)$ , since  $\mathbf{W}_H^H(i)\mathbf{W}_H(i)$  is a block diagonal matrix. The equalization based on pseudo circulant channel matrices is then performed on  $\mathbf{W}_H^H(i)\hat{\mathbf{R}}(i)$ , as presented in chapter 3. The MIMO channel estimation presented in section 6.3 is performed on  $\mathbf{R}(i)$ .

In practice, however, the equalization procedure contains an interference suppression step based on the calculation of (6.21) and (6.22). This calculation requires the use of channel estimates in the matrix  $\mathbf{C}_1^{\text{IBI}}$ . Since such a suppression step is not required in the approach presented in section 6.4.1, the latter approach is typically preferred.

## 6.5 Simulation results

Figures 6.2 to 6.9 presents Bit Error Rate (BER) and Packet Error Rate (PER) simulation results that have been obtained based on an MTMR system with two transmit and one receive antennas in the context of

the 5.2GHz IEEE802.11a WLAN standard. All simulations have been performed for BPSK, QPSK, QAM-16 and QAM-64 symbols, a convolutional code with code rate of  $R = 1/2$  (133o/171o) and uncorrelated BRAN-A channels [37] with mean unit power. The frame length is set such that 72 OFDM data symbols are used for any constellation type, each transmitted over at least 2000 channel realizations. Dummy symbols are added prior and following the frame in order to allow a seamless postfix based CIR estimation. The pseudo-random weighting factors are chosen to be a zero-mean pseudo-random  $\pm 1$  sequence. Different mobility conditions have been considered: no mobility (0m/s) and 32m/s of mobility. At the receiver side, the Doppler frequency and the noise variance are assumed to be known; the channel power delay profile, however, is typically hard to obtain in practice and it is thus assumed to be unknown. In the MMSE estimation matrix derivations, a rectangular profile over the postfix duration is assumed. The following systems are compared:

- modified IEEE802.11a standard using Alamouti STBC (CP-OFDM), with ZF equalization and MMSE MIMO channel estimation based on preambles;
- MTMR PRP-OFDM modulator with ZP-OFDM decoding as presented in section 6.4.1, with MMSE equalization, channel estimation based on 41 received Alamouti blocks of 2 PRP-OFDM symbols (from 20 before to 20 after the latest block) for BPSK, QPSK and QAM-16. For QAM-64, 121 received Alamouti blocks are used due to the increased constraints on the CIR MSE. No preambles sequences are introduced at the header of the frames.

Considering the BPSK and QPSK simulation results presented in Figures 6.2 to 6.5

Without mobility and using an Overlap-Add (OLA) based low-complexity decoding approach (similar to chapter 3.7 for the STSR case), the PRP-OFDM MTMR receiver outperforms a standard CP-OFDM architecture by approx. 1dB for BPSK and QPSK constellations. For QAM-16 and QAM-64, both schemes show comparable performances with a slight advantage for PRP-OFDM. The more complex MMSE decoding approach, however, lets the PRP-OFDM scheme outperform the classical scheme by approx. 1.5dB in all cases and shows performance results that are close to the known-channel limit.

In the presence of mobility and without tracking, CP-OFDM operating at 5GHz carrier frequency combined with a preamble based channel estimation is unsuitable for mobility levels that are higher than pedestrian mobility (see analysis for the STSR case in chapter 3.8). The PRP-OFDM scheme in combination with Wiener filtering for channel estimation as detailed in chapter 3.3.2, section *Block based CIR update based on Wiener filtering (increased latency)* shows the following results for a mobility of 32m/s at 5GHz carrier frequency:

1. BPSK simulation results show a small performance degradation for the time-variant scenario compared to the MMSE decoding approach applied in a static context; the loss is approx. 0.2dB for the BER results and 0.3dB for the PER results.
2. QPSK simulation results also show a small performance degradation for the time-variant scenario; approx. 0.3dB and 0.4dB are lost for the BER and PER results respectively.
3. QAM-16 simulation results illustrate the impact of an insufficient MSE of the CIR estimates. While the time-variant performance results are close to the time-invariant observations, there is a degradation for C/I higher than approx. 14dB. Still, the system performance allows an application of the proposed scheme in a practical scenario at the given mobility.

4. QAM-64 applies PRP-OFDM based channel estimation over an observation size of 121 STC blocks. Still, it is not sufficient since the performance degradation is visible above approx. 17dB. It is obvious that the proposed scheme needs to be combined with other CIR estimation approaches in order to deliver satisfying results.

## 6.6 Conclusion

A new OFDM modulation scheme based on pseudo random postfix insertion has been presented for multiple antenna systems. It has been shown that the postfix can be, similar to the data stream, encoded based on a suitable STC. This allows a semi-blind identification of the MIMO channel in the receiver requiring a very low arithmetical complexity. The simulation results given for an Alamouti based MTMR system with two transmit and one receive antennas show that the proposed CIR estimation techniques work very robustly, even in a high mobility scenario (mobility up to 30m/s is considered here) applying constellation settings BPSK, QPSK or QAM-16. QAM-64 constellations should not rely on PRP-OFDM based channel estimation alone, but should be combined with different approaches (e.g. in combination with rotating carrier based CIR estimation, iterative interference suppression, etc.).

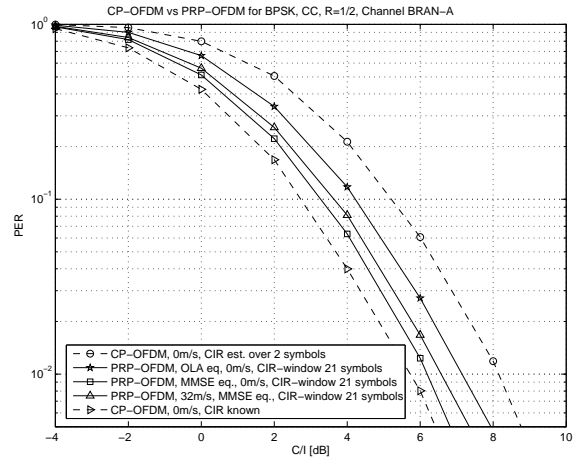
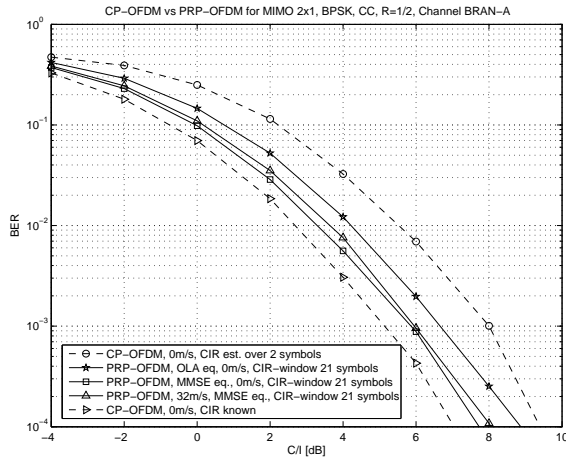


Figure 6.2: BER for IEEE802.11a, MIMO 2x1, Figure 6.3: PER for IEEE802.11a, MIMO 2x1, BRAN channel model A, BPSK, different decoding approaches.

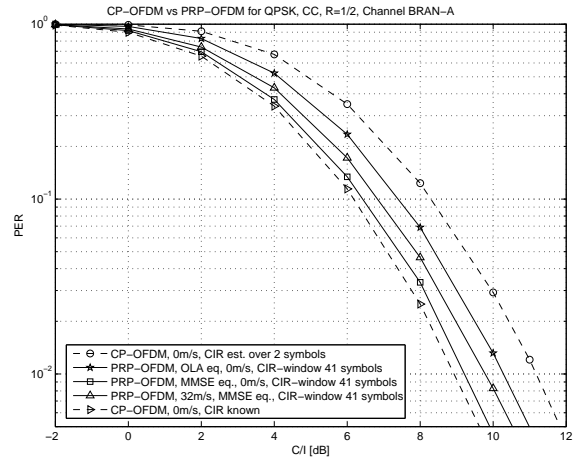
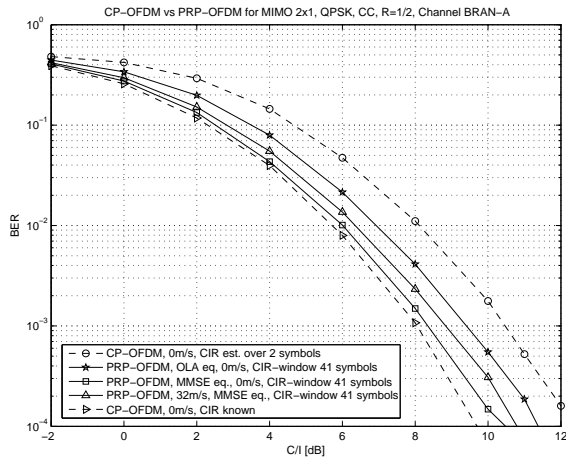


Figure 6.4: BER for IEEE802.11a, MIMO 2x1, Figure 6.5: PER for IEEE802.11a, MIMO 2x1, BRAN channel model A, QPSK, different decoding approaches.

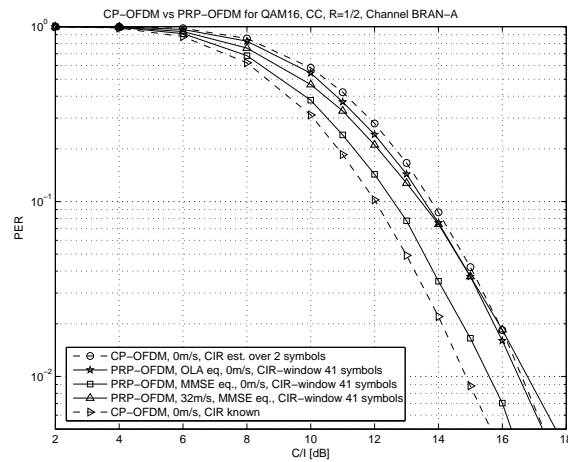
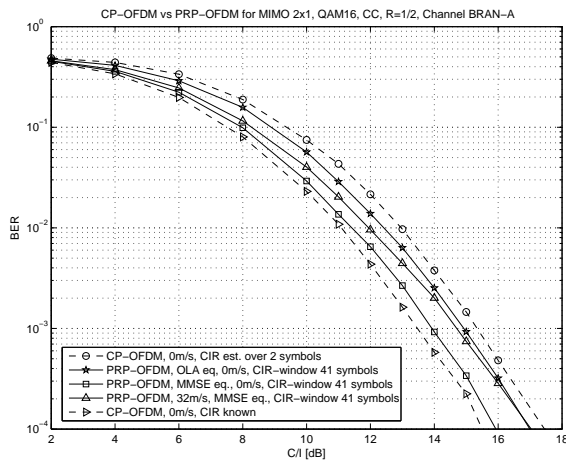


Figure 6.6: BER for IEEE802.11a, MIMO 2x1, BRAN channel model A, QAM16, different decoding approaches, Doppler environment. Figure 6.7: PER for IEEE802.11a, MIMO 2x1, BRAN channel model A, QAM16, different decoding approaches, Doppler environment.

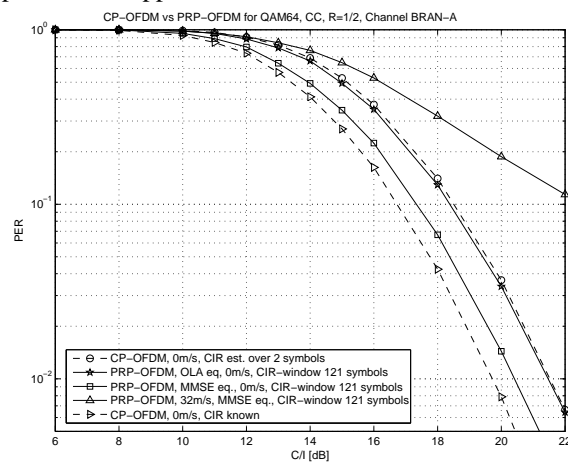
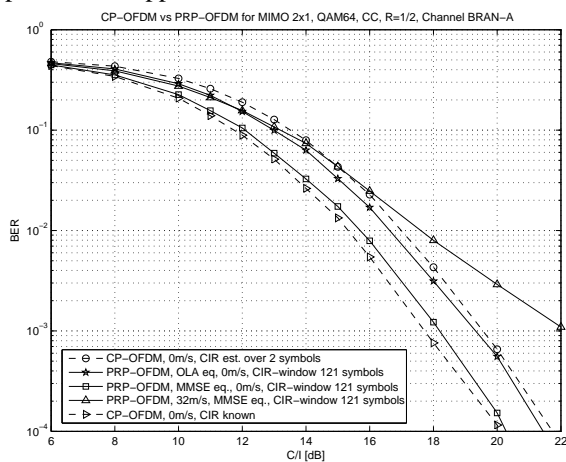


Figure 6.8: BER for IEEE802.11a, MIMO 2x1, BRAN channel model A, QAM64, different decoding approaches, Doppler environment. Figure 6.9: PER for IEEE802.11a, MIMO 2x1, BRAN channel model A, QAM64, different decoding approaches, Doppler environment.



## Chapter 7

# Iterative Interference Suppression

This chapter presents an approach which helps to *iteratively* improve the Pseudo Random Postfix OFDM (PRP-OFDM) based channel estimation by exploiting soft-output decoder messages.

### 7.1 Introduction

The general principles of the Pseudo Random Postfix OFDM (PRP-OFDM) modulation scheme have been introduced in chapters 3, 4, 5 and 6 of this thesis: the cyclic prefix extension of classical Cyclic Prefix OFDM (CP-OFDM) is replaced by a known postfix weighted by a pseudo random scalar sequence changing at the OFDM block rate. This way, unlike for classical OFDM modulators, the receiver can exploit an additional information: the prior knowledge of a part of the transmitted block and track channel variations. Chapter 3 details several equalization and decoding schemes compatible with PRP-OFDM.

With PRP-OFDM, an estimate of the CIR can be derived by a simple averaging of the time domain OFDM received block. The averaging is required in order to cancel the interference of the samples carrying useful information on the pseudo-random postfix (assumed to be zero-mean). A practical trade-off needs to be established between the length of the averaging window and the resulting amount of residual interference impacting the channel estimation accuracy. For a large averaging window and in a typical scenario, [7] shows that PRP-OFDM CIR estimation outperforms schemes relying on rotating pilot patterns interpolation in terms of mean-square-error (MSE) up to an SNR of approx. 15dB.

Considering the results of chapters 3 and 6, however, one understands that there are the following two main limiting factors for PRP-OFDM based channel estimation:

1. higher order constellations (QAM-64, etc.) require a high SNR working point (e.g., targeting a PER of  $10^{-2}$  in the context of the simulation conditions defined in chapter 3.8 for channel BRAN-A, approx. 21dB of C/I are required) and thus correspondingly precise channel estimates; the corresponding window sizes of PRP-OFDM based channel estimation then become impractically large: e.g., targeting a CIR estimation of 24dB, a window size of approx. 252 postfix observations is required (based on a minimum dimension circulant diagonalization for the CIR estimation as

detailed in chapter 3.3). Standard PRP-OFDM channel estimation approaches are thus unsuitable for higher order constellation symbols in a practical context. Note that standard CP-OFDM systems typically target an estimation MSE (mean square error) of approx.  $\text{MSE}^{-1} \approx \text{SNR} + 3\text{dB}$  (e.g. IEEE802.11a [56]).

2. in the context of very high mobility, the channel is highly time-variant. As a consequence, even the Wiener based channel estimators presented in chapter 3.3.2 are insufficient, since postfixes cannot be considered if they are convolved by a CIR that is de-correlated from the CIR to be estimated (the Wiener filter then introduces a weighting factor close to zero). Again, the MSE of the CIR estimates is insufficient and will impact the system performance.

In order to solve these issue, this chapter proposes an iterative CIR estimation scheme. While the first CIR estimation step is typically performed based on a mean-value and de-convolution calculation as presented in chapter 3, it is refined exploiting the outputs of a soft output decoder which makes PRP-OFDM suitable for high throughput systems. As a result, an accurate CIR estimation is possible applying a small observation window size.

The added complexity introduced by this iterative data interference cancellation on the channel estimation can be mitigated when the system considered already implements an advanced coding scheme such as turbo code which requires already the presence of a forward backward decoder in the receiver.

The chapter is organized as follows. Section 7.2 settles the notations and defines the PRP-OFDM modulator. The new iterative channel estimation technique is compared to classical one and discussed in section 7.3, followed by practical considerations in section 7.3.3. Finally section 7.4 provides simulation results.

## 7.2 Notations and PRP-OFDM modulator

This section briefly recalls the baseband discrete-time block equivalent model of a  $N$  carrier PRP-OFDM system. The  $i$ th  $N \times 1$  input digital vector<sup>1</sup>  $\tilde{\mathbf{s}}_N(i)$  is first modulated by the IFFT matrix  $\mathbf{F}_N^H := \frac{1}{\sqrt{N}} \left( W_N^{ij} \right)^H$ ,  $0 \leq i < N, 0 \leq j < N$  and  $W_N := e^{-j\frac{2\pi}{N}}$ . Then, a deterministic postfix vector  $\mathbf{p}_D := (p_0, \dots, p_{D-1})^T$  weighted by a pseudo random value  $\alpha(i) \in \mathbb{C}, |\alpha(i)| = 1$  is appended to the IFFT outputs  $\mathbf{s}_N(i) := \mathbf{F}_N^H \tilde{\mathbf{s}}_N(i)$ . A pseudo random  $\alpha(i)$  prevents the postfix time domain signal from being deterministic and avoids thus spectral peaks, see chapter 4. With  $P := N + D$ , the corresponding  $P \times 1$  transmitted vector is  $\mathbf{s}_P(i) := \mathbf{F}_{ZP}^H \tilde{\mathbf{s}}_N(i) + \alpha(i) \mathbf{p}_P$ , where

$$\mathbf{F}_{ZP}^H := \begin{bmatrix} \mathbf{I}_N \\ \mathbf{0}_{D,N} \end{bmatrix}_{P \times N} \mathbf{F}_N^H \quad \text{and} \quad \mathbf{p}_P := (\mathbf{0}_{1,N} \mathbf{p}_D^T)^T$$

The samples of  $\mathbf{s}_P(i)$  are then sent sequentially through the channel modeled here as a  $L$ th-order FIR  $C(z) := \sum_{n=0}^L c_n z^{-n}$  of impulse response  $\mathbf{c}_L = (c_0, \dots, c_L)$ . The OFDM system is designed such that the postfix duration exceeds the channel memory  $L < D$ .

<sup>1</sup>Lower (upper) boldface symbols will be used for column vectors (matrices) sometimes with subscripts  $N, D$  or  $P$  emphasizing their sizes (for square matrices only); tilde will denote frequency domain quantities; argument  $i$  will be used to index blocks of symbols;  $^H$  ( $^T$ ) will denote Hermitian (Transpose).

Let  $\mathbf{C}_{\text{ISI}}(P)$  and  $\mathbf{C}_{\text{IBI}}(P)$  be respectively the Toeplitz inferior and superior triangular matrices of first column:  $[c_0, c_1, \dots, c_L, 0, \dots, 0]^T$  and first row  $[0, \dots, 0, c_L, \dots, c_1]$ . As already explained in [80], the channel convolution can be modeled by  $\mathbf{r}_P(i) := \mathbf{C}_{\text{ISI}}\mathbf{s}_P(i) + \mathbf{C}_{\text{IBI}}\mathbf{s}_P(i-1) + \mathbf{n}_P(i)$ .  $\mathbf{C}_{\text{ISI}}(P)$  and  $\mathbf{C}_{\text{IBI}}(P)$  represent respectively the intra and inter block interference. Since  $\mathbf{s}_P(i) = \mathbf{F}_{ZP}^H \tilde{\mathbf{s}}_N(i) + \alpha(i)\mathbf{p}_P$ , we have:

$$\mathbf{r}_P(i) = (\mathbf{C}_{\text{ISI}} + \beta_i \mathbf{C}_{\text{IBI}})\mathbf{s}_P(i) + \mathbf{n}_P(i)$$

where  $\beta_i := \frac{\alpha(i-1)}{\alpha(i)}$  and  $\mathbf{n}_P(i)$  is the  $i$ th AWGN vector of element variance  $\sigma_n^2$ . Note that  $\mathbf{C}_{\beta_i} := (\mathbf{C}_{\text{ISI}} + \beta_i \mathbf{C}_{\text{IBI}})$  is pseudo circulant: i.e. a circulant matrix whose  $(D-1) \times (D-1)$  upper triangular part is weighted by  $\beta_i$ .

The expression of the received block is thus:

$$\begin{aligned} \mathbf{r}_P(i) &= \mathbf{C}_{\beta_i} (\mathbf{F}_{ZP}^H \tilde{\mathbf{s}}_N(i) + \alpha(i)\mathbf{p}_P) + \mathbf{n}_P(i) \\ &= \mathbf{C}_{\beta_i} \begin{pmatrix} \mathbf{F}_N^H \tilde{\mathbf{s}}_N(i) \\ \alpha(i)\mathbf{p}_D \end{pmatrix} + \mathbf{n}_P(i) \end{aligned} \quad (7.1)$$

With these notations, CIR estimation is discussed in the following.

## 7.3 Channel estimation

Below the standard low-complexity PRP-OFDM CIR estimation technique detailed in chapter 3 based on interference suppression by mean value calculation is briefly recalled. Then a description of the proposed iterative scheme improving the CIR estimate MSE follows. All derivations are detailed in the static context, extension to mobility environment is possible applying the techniques presented in [5, 7].

### 7.3.1 Standard channel estimation

Define  $\mathbf{C}_{\text{CIR}}(D) := \mathbf{C}_{\text{ISI}}(D) + \mathbf{C}_{\text{IBI}}(D)$  as the  $D \times D$  circulant channel matrix of first row  $\text{row}_0(\mathbf{C}_{\text{CIR}}(D)) = [c_0, 0, \dots, 0, c_L, \dots, c_1]$ . Note that  $\mathbf{C}_{\text{ISI}}(D)$  and  $\mathbf{C}_{\text{IBI}}(D)$  contain respectively the lower and upper triangular parts of  $\mathbf{C}_{\text{CIR}}(D)$ .

Denoting by  $\mathbf{s}_N(i) := [s_0(i), \dots, s_{N-1}(i)]^T$ , splitting this vector in 2 parts:

$$\begin{aligned} \mathbf{s}_{N,0}(i) &:= [s_0(i), \dots, s_{D-1}(i)]^T, \\ \mathbf{s}_{N,1}(i) &:= [s_{N-D}(i), \dots, s_{N-1}(i)]^T, \end{aligned} \quad (7.2)$$

and performing the same operations for the noise vector:

$$\begin{aligned} \mathbf{n}_P(i) &:= [n_0(i), \dots, n_{P-1}(i)]^T, \\ \mathbf{n}_{D,0}(i) &:= [n_0(i), \dots, n_{D-1}(i)]^T, \\ \mathbf{n}_{D,1}(i) &:= [n_{P-D}(i), \dots, n_{P-1}(i)]^T, \end{aligned}$$

the received vector  $\mathbf{r}_P(i)$  can be expressed as:

$$\mathbf{r}_P(i) = \begin{pmatrix} \mathbf{C}_{\text{ISI}}(D)\mathbf{s}_{N,0}(i) + \alpha(i-1)\mathbf{C}_{\text{IBI}}(D)\mathbf{p}_D + \mathbf{n}_{D,0} \\ \vdots \\ \mathbf{C}_{\text{IBI}}(D)\mathbf{s}_{N,1}(i) + \alpha(i)\mathbf{C}_{\text{ISI}}(D)\mathbf{p}_D + \mathbf{n}_{D,1} \end{pmatrix}. \quad (7.3)$$

As usual the transmitted time domain signal  $\mathbf{s}_N(i)$  is assumed zero-mean. Thus the first  $D$  samples  $\mathbf{r}_{P,0}(i)$  of  $\mathbf{r}_P(i)$  and its last  $D$  samples  $\mathbf{r}_{P,1}(i)$  can be exploited very easily to retrieve the channel matrices relying on the deterministic nature of the postfix as follows:

$$\begin{aligned} \hat{\mathbf{r}}_{c,0} &:= \mathbb{E} \left[ \frac{\mathbf{r}_{P,0}(i)}{\alpha(i-1)} \right] = \mathbf{C}_{\text{IBI}}(D)\mathbf{p}_D, \\ \hat{\mathbf{r}}_{c,1} &:= \mathbb{E} \left[ \frac{\mathbf{r}_{P,1}(i)}{\alpha(i)} \right] = \mathbf{C}_{\text{ISI}}(D)\mathbf{p}_D. \end{aligned} \quad (7.4)$$

Since  $\mathbf{C}_{\text{ISI}}(D) + \mathbf{C}_{\text{IBI}}(D) = \mathbf{C}_{\text{CIRC}}(D)$  is circulant and diagonalizable in the frequency domain  $\mathbf{F}_D$  combining equations (7.4) and using the commutativity of the convolution yields:

$$\begin{aligned} \hat{\mathbf{r}}_c &:= \hat{\mathbf{r}}_{c,0} + \hat{\mathbf{r}}_{c,1} \\ &= \mathbf{C}_{\text{CIRC}}(D)\mathbf{p}_D \end{aligned} \quad (7.5)$$

$$\begin{aligned} &= \mathbf{P}_D \mathbf{c}_D \\ &= \mathbf{F}_D^H \tilde{\mathbf{P}}_D \mathbf{F}_D \mathbf{c}_D, \end{aligned} \quad (7.6)$$

where  $\mathbf{P}_D$  is a  $D \times D$  circulant matrix with first row  $\text{row}_0(\mathbf{P}_D) := [p_0, p_{D-1}, p_{D-2}, \dots, p_1]$  and  $\tilde{\mathbf{P}}_D := \text{diag}\{\mathbf{F}_D \mathbf{p}_D\}$ .

Since in practice the expectation  $\mathbb{E}[\cdot]$  in (7.4) is approximated by a mean value calculation over a limited number  $Z$  of symbols, we can model the estimation error as noise  $\tilde{\mathbf{n}}_D$ .

Assuming both the received OFDM time domain data samples and  $\mathbf{n}_P$  to be Gaussian of respective covariances  $\sigma_s^2 \mathbf{I}_N$  and  $\sigma_n^2 \mathbf{I}_P$ , the covariance of  $\tilde{\mathbf{n}}_D$  is:

$$\begin{aligned} \mathbf{R}_{\tilde{\mathbf{n}}_D} &:= \mathbb{E} [\tilde{\mathbf{n}}_D \tilde{\mathbf{n}}_D^H] \\ &= \frac{\sigma_s^2 + 2\sigma_n^2}{Z} \mathbf{I}_D. \end{aligned}$$

Thus, an estimate of the CIR  $\hat{\mathbf{c}}_D$  can be retrieved by either a ZF or MMSE approach as discussed in chapter 3.

### 7.3.2 The new iterative channel estimation

The iterative estimation scheme presented here requires an initial CIR estimate which is for example obtained by the techniques presented above. In order to prepare the presentation of the detailed algorithm, the following theorem is defined:

**Theorem 7.3.1** Define the latest CIR estimated  $\hat{\mathbf{c}}^{k-1}(i)$  represented by matrix  $\mathbf{C}_{\beta_i}^{k-1}(i)$  multiplication. Denote by  $\tilde{\mathbf{r}}_{N,eq}^{k-1}(i) = \tilde{\mathbf{s}}_N(i) + \tilde{\mathbf{w}}_N^{k-1}$  the frequency domain equalized vector  $\mathbf{r}_P(i)$  ( $\tilde{\mathbf{w}}_N^{k-1}$  representing the residual error) performed with the CIR estimate  $\hat{\mathbf{c}}^{k-1}(i)$  of the previous step. With  $p(\tilde{\mathbf{s}}_N(i) = \mathbf{a}_N | \tilde{\mathbf{r}}_{N,eq}^{k-1}(i))$  being the likelihood that  $\mathbf{a}_N$  was sent knowing the received vector  $\tilde{\mathbf{r}}_{N,eq}^{k-1}(i)$ , the optimum time domain interference estimate in the minimum MSE sense is thus given by

$$\mathbf{u}_P^k(i) = \sum_{\mathbf{a}_N \in [a_0, \dots, a_{Q_M-1}]^N} p(\tilde{\mathbf{s}}_N(i) = \mathbf{a}_N | \tilde{\mathbf{r}}_{N,eq}^{k-1}(i)) \mathbf{C}_{\beta_i}^{k-1} \mathbf{F}_{ZP}^H \mathbf{a}_N(i) \quad (7.7)$$

$\{a_n \in \mathbb{C}, n \in [0, \dots, Q_M - 1]\}$  is the set of constellation symbols (alphabet) and  $Q_M$  the constellation order.  $\square$

### Proof of theorem 7.3.1:

Define  $\check{\mathbf{r}}_P^k(i) = \mathbf{r}_P(i) - \mathbf{C}_{\beta_i}^{k-1}(i) \alpha(i) \mathbf{p}_P$  as the received vector after subtraction of the zero-forcing PRP interference estimate based on the previous CIR estimate  $\mathbf{C}_{\beta_i}^{k-1}(i)$ . Assuming that  $\mathbf{u}_P^k(i)$  is a vector used in order to reduce the interference onto the postfix convolved by the channel in  $\mathbf{r}_P(i)$ , the remaining total square error is given by

$$\varepsilon^2(i) = \sum_{\mathbf{a}_N \in [a_0, \dots, a_{Q_M-1}]^N} p(\tilde{\mathbf{s}}_N(i) = \mathbf{a}_N | \tilde{\mathbf{r}}_{N,eq}^{k-1}(i)) \mathbb{E} \tau \left\{ \left( \check{\mathbf{r}}_P(\tilde{\mathbf{s}}_N(i) = \mathbf{a}_N) - \mathbf{u}_P^k(i) \right) \left( \check{\mathbf{r}}_P(\tilde{\mathbf{s}}_N(i) = \mathbf{a}_N) - \mathbf{u}_P^k(i) \right)^H \right\}$$

where  $\tau\{\cdot\}$  is the trace matrix operator. The optimum  $\mathbf{u}_P^k(i)$  is found by setting

$$\frac{\partial \varepsilon^2(i)}{\partial (\mathbf{u}_P^k(i))^*} = \sum_{\mathbf{a}_N \in [a_0, \dots, a_{Q_M-1}]^N} p(\tilde{\mathbf{s}}_N(i) = \mathbf{a}_N | \tilde{\mathbf{r}}_{N,eq}^{k-1}(i)) (\mathbf{u}_P^k(i) - \mathbf{C}_{\beta_i}^{k-1} \mathbf{F}_{ZP}^H \mathbf{a}_N(i)) = \mathbf{0}$$

which leads to the expression given by theorem 7.3.1. Q.E.D.

Finally, the iterative CIR estimation is performed in several steps:

1. Initial CIR estimation: at iteration  $k = 0$ , perform an initial CIR estimation  $\hat{\mathbf{c}}^0(i)$ , for example as proposed in section 7.3.1.
2. Increment iteration index:  $k \leftarrow k + 1$
3. Perform FEC decoding based on latest CIR estimates  $\hat{\mathbf{c}}^{k-1}(i)$ : buffer the outputs of the soft-output decoder which indicate the bit-probabilities of the  $l$ th encoded bit of the constellation on carrier  $n$  of OFDM symbol  $i$ :  $p_l^k(x_n(i))$  with  $n \in [0, \dots, N - 1]$  and  $l \in [0, \dots, \log_2(Q_M) - 1]$ ;  $Q_M$  is the constellation order.
4. Interference estimation: as detailed in section 7.3.3 the interference estimation  $\mathbf{u}_P^k(i)$  from OFDM data symbol  $i$  is generated based on the bit-probabilities  $p_l^k(x_n(i))$  and the latest CIR estimates  $\hat{\mathbf{c}}^{k-1}(i)$  as given by theorem 7.3.1.

5. Interference suppression: subtract estimated interference from received vector  $\mathbf{r}_P(i)$  and form a new observation vector:  $\tilde{\mathbf{r}}_P^k(i) = \mathbf{r}_P(i) - \mathbf{u}_P^k(i)$ .
6. CIR estimation: derive a new CIR estimate  $\hat{\mathbf{c}}^k(i)$  from  $\tilde{\mathbf{r}}_P^k(i)$  e.g. as proposed in section 7.3.1. The resulting  $\hat{\mathbf{c}}^k(i)$  yields to a more accurate estimate since interference of the OFDM data symbols on the postfix convolved by the channel has been reduced.
7. Iterate: until a given performance criterion is met go to step 2.

The iterative CIR estimation is compatible to any FEC decoder which delivers at its output bit-probabilities of encoded information bits among which are the SOVA (Soft-Output-Viterbi-Algorithm) decoders and forward backward algorithm. If such a decoder is applied for the sake of CIR estimation only, the complexity increase is considerable. However, if the proposed technique is used in a system where iterative decoding is used anyhow (e.g. in the context of Turbo Codes, etc.), the additional complexity can be considered for implementation.

### 7.3.3 Practical considerations related to Iterative Interference Suppression

This section details the practical derivation of some of the quantities required by the above presented Iterative Interference Suppression based CIR estimation algorithm.

The expression  $p(\tilde{\mathbf{s}}_N(i) = \mathbf{a}_N | \tilde{\mathbf{r}}_{N,eq}^{k-1}(i))$  is calculated using Bayes' rule:

$$p(\tilde{\mathbf{s}}_N(i) = \mathbf{a}_N | \tilde{\mathbf{r}}_{N,eq}^{k-1}(i)) = \frac{p(\tilde{\mathbf{r}}_{N,eq}^{k-1}(i) | \tilde{\mathbf{s}}_N(i) = \mathbf{a}_N) p(\tilde{\mathbf{s}}_N(i) = \mathbf{a}_N)}{p(\tilde{\mathbf{r}}_{N,eq}^{k-1}(i))} \quad (7.8)$$

The a-priori probabilities  $p(\tilde{\mathbf{s}}_N(i) = \mathbf{a}_N) = \prod_{n=0}^{N-1} p(\tilde{s}_n(i) = a_n)$  are obtained by exploiting the bit-probabilities  $b_l(a_n)$  of the soft-decoder outputs:

$$p(\tilde{s}_n(i) = a_n) = \prod_{l=0}^{\log_2(Q_M)-1} p(b_l(a_n))$$

assuming that the bits are independent. This property is usually assured by a large interleaver. The distribution of the received samples  $p(\tilde{\mathbf{r}}_{N,eq}^{k-1}(i) | \tilde{\mathbf{s}}_N(i) = \mathbf{a}_N)$  is given by a multivariate Gaussian probability density function (PDF) with  $\mathbf{R}_{\tilde{\mathbf{w}}_N^{k-1}, \tilde{\mathbf{w}}_N^{k-1}} = \mathbf{E}[\tilde{\mathbf{w}}_N^{k-1}(\tilde{\mathbf{w}}_N^{k-1})^H]$  ( $\tilde{\mathbf{w}}_N^{k-1}$  represents the residual error in the frequency domain equalized vector  $\tilde{\mathbf{r}}_{N,eq}^{k-1}(i) = \tilde{\mathbf{s}}_N(i) + \tilde{\mathbf{w}}_N^{k-1}$ ):

$$p(\tilde{\mathbf{r}}_{N,eq}^{k-1}(i) | \tilde{\mathbf{s}}_N(i) = \mathbf{a}_N) = \pi^{-N} \det^{-1} \left\{ \mathbf{R}_{\tilde{\mathbf{w}}_N^{k-1}, \tilde{\mathbf{w}}_N^{k-1}} \right\} \exp \left\{ -(\tilde{\mathbf{r}}_{N,eq}^{k-1}(i) - \mathbf{a}_N)^H \mathbf{R}_{\tilde{\mathbf{w}}_N^{k-1}, \tilde{\mathbf{w}}_N^{k-1}}^{-1} (\tilde{\mathbf{r}}_{N,eq}^{k-1}(i) - \mathbf{a}_N) \right\}$$

The expression  $p(\tilde{\mathbf{r}}_{N,eq}^{k-1}(i))$  is calculated according to (7.8) by exploiting

$$\sum_{\mathbf{a} \in [a_0, \dots, a_{Q_M-1}]^N} p(\tilde{\mathbf{s}}_N(i) = \mathbf{a}_N | \tilde{\mathbf{r}}_{N,eq}^{k-1}(i)) = 1.$$

If  $\mathbf{R}_{\tilde{\mathbf{w}}_N^{k-1}, \tilde{\mathbf{w}}_N^{k-1}}$  is diagonal (or approximated by a matrix containing its diagonal elements only), (7.7)

can be considerably simplified, since  $p(\tilde{\mathbf{s}}_N(i) = \mathbf{a}_N | \tilde{\mathbf{r}}_{N,eq}^{k-1}(i)) = \prod_{n=0}^{N-1} p(\tilde{s}_n = a_n | \tilde{r}_n^{k-1}(i))$ :

$$\mathbf{u}_P(i) = \sum_{n=0}^{N-1} \sum_{a_n \in [a_0, \dots, a_{Q_M-1}]} p(\tilde{s}_n = a_n | \tilde{r}_n^{k-1}(i)) \mathbf{C}_{\beta_i}^{k-1} \mathbf{F}_{ZP}^H \mathbf{a}_N^{(n)}(i)$$

with  $\mathbf{a}_N^{(n)} = (0, \dots, 0, a_n(i), 0, \dots, 0)^T$  is derived from vector  $\mathbf{a}_N$  in which only the  $n$ th element is non-zero.

## 7.4 Simulation Results

In order to illustrate the performances of our approach, simulations have been performed in the IEEE802.11a [56] WLAN context: a  $N = 64$  carrier 20MHz bandwidth broadband wireless system operating in the 5.2GHz band using the 16 sample postfix defined in chapter 4, Tab. 4.2. The frame length is chosen to be 72 OFDM symbols for all constellation types. Dummy OFDM/postfix symbols are introduced prior and following the frame in order to allow a seamless CIR estimation. The CP-OFDM modulator is replaced by a PRP-OFDM modulator. A rate  $R = 1/2$ , constraint length  $K = 7$  Convolutional Code (CC) (o171/o133) is used before bit interleaving followed by 64QAM constellation mapping. The pseudo-random weighting factors are chosen to be a zero-mean pseudo-random  $\pm 1$  sequence.

Monte Carlo simulations are run and averaged over at least 2500 realizations of a normalized BRAN-A [37] frequency selective channel without Doppler in order to obtain BER curves.

Based on a SOVA decoder, figure 7.1 illustrates several important properties of PRP-OFDM combined with Iterative Interference Suppression:

1. for a fixed carrier-over-interference (C/I) ratio of  $C/I = 24dB$  that the MSE of the CIR is decreased by approx. 12dB after three iterations using the new algorithm proposed in section 7.3.2 compared to the initial estimates obtained by the algorithm proposed in section 7.3.1.
2. this gain varies only slightly with the size of the observation window for the mean-value calculation *postfix convolved by CIR plus noise*. I.e. Iterative Interference Suppression is applicable to high SNR scenarios where correspondingly low MSE values for the CIR estimates are required. Moreover, Iterative Interference Suppression is also suitable for a very high mobility scenario combined with lower order constellations and a very small window size for CIR estimation: the iterative process considerably improves the CIR estimation MSE (e.g., approx. 12dB are gained with a single iteration assuming a mean window size of 20 OFDM symbols).
3. the gain in MSE is considerable for the first iteration (approx. 12dB in all cases); however, the differences are small for further iterations. In practice, a single iteration may be sufficient.

Concerning the performance evaluation of the Iterative Interference Suppression, the time-invariant (improvement for higher order constellations) and time-variant (very high mobility for lower order constellations) are considered independently:

1. **time invariant case:** The BER/PER results (of decoded bits) for a mean-value calculation window size of 31 are given by Figure 7.2 and 7.3 for QAM-64 constellations and by Figures 7.4 and 7.5 for QAM-16 constellations. Using QAM-16 constellations in combination with the (relatively small) window size of 31 symbols for PRP-OFDM based channel estimation does not lead to a visible error floor in the considered SNR range, but the PER results show that over 1dB is lost compared to standard CP-OFDM schemes. This loss is regained after a single iteration applying the Iterative Interference Suppression. In the case of QAM-64, the performance degradation of basic PRP-OFDM based channel estimation compared to standard CP-OFDM is important: there is approx. 4dB loss at a BER of  $10^{-4}$  and the loss in PER is even higher. Again, a single iteration is sufficient in order to obtain satisfying results, even improving the performance compared to standard CP-OFDM by approx. 0.5dB.
2. **time variant case:** The mobility context is evaluated based on QPSK symbols and a window size of only 5 OFDM symbols for PRP-OFDM based channel estimation. As expected, the system performance changes only slightly when the mobility is increased from 0m/s (cf. Figure 7.6 for BER, Figure 7.7 for PER) to 36m/s (cf. Figure 7.8 for BER, Figure 7.9 for PER) and finally to 72m/s (cf. Figure 7.10 for BER, Figure 7.11 for PER). Obviously, the resulting system performance is approx. 0.75dB below the standard CP-OFDM case in BER and approx. 2dB in PER. Still, these results show that acceptable performance results are achievable in presence of extremely high Doppler and low system latency due to a small observation window for PRP-OFDM based channel estimation.

## 7.5 Conclusion

A new iterative interference cancellation scheme for PRP-OFDM based systems has been proposed. In a typical example the MSE of the resulting CIR estimated is improved by approx. 12dB over three iterations. This makes PRP-OFDM modulators applicable to higher order constellations, e.g. 64QAM, etc. For the reasons given in section 7.4, the proposed scheme can be applied in high mobility scenarios without losing throughput nor spectral efficiency compared to CP-OFDM systems designed for a static environment, since no additional redundancy in terms of pilot tones, learning symbols, etc. is necessary.

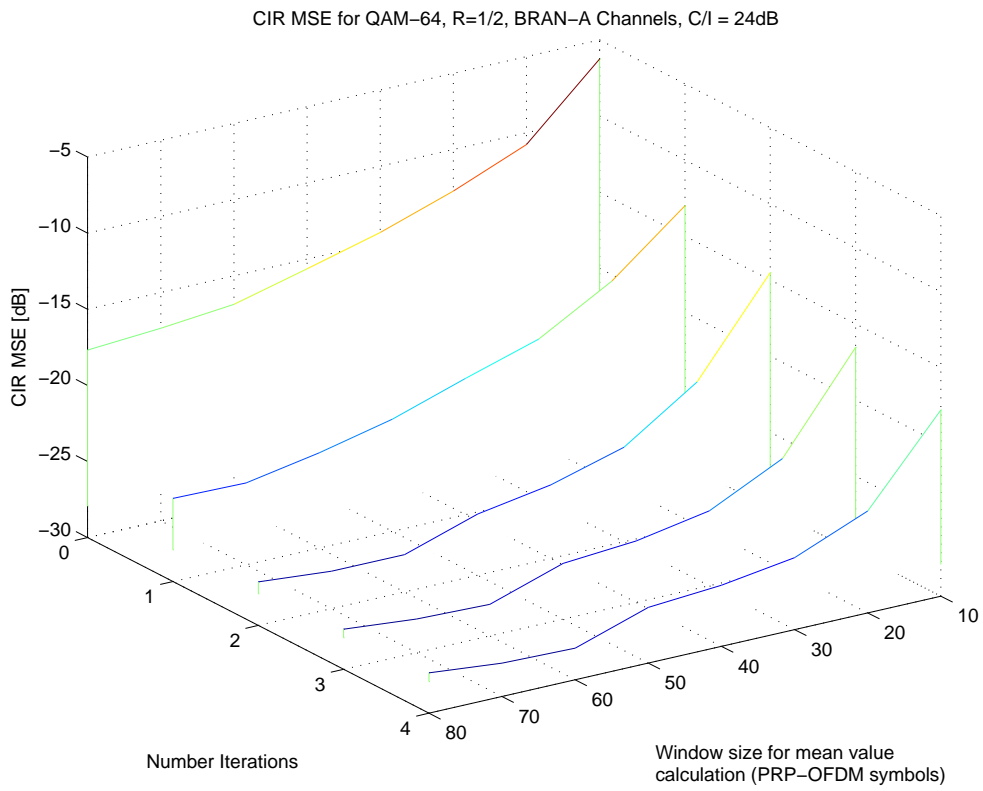


Figure 7.1: CIR MSE for 64QAM, BRAN-A, C/I=24dB.

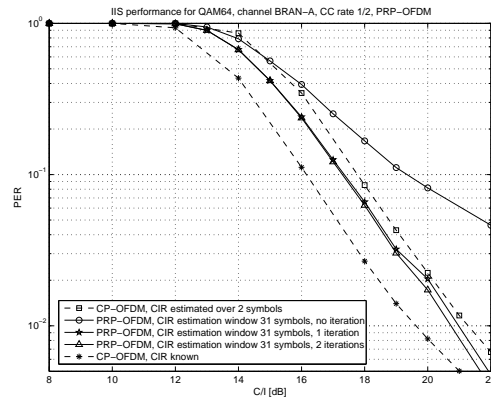
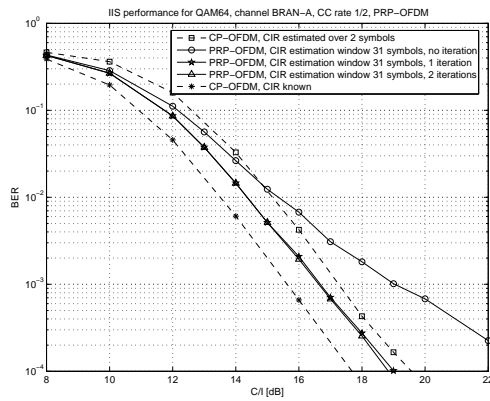


Figure 7.2: BER for IEEE802.11a, BRAN channel model A, QAM64, iterative interference cancellation. Figure 7.3: PER for IEEE802.11a, BRAN channel model A, QAM64, iterative interference cancellation.

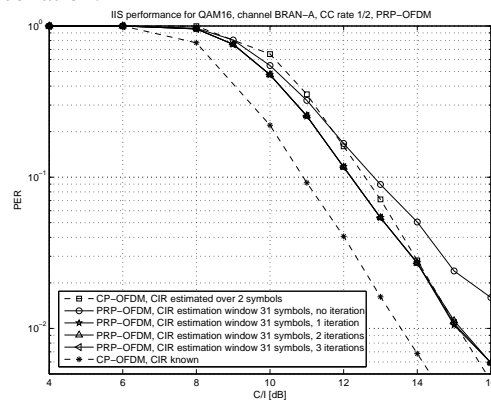
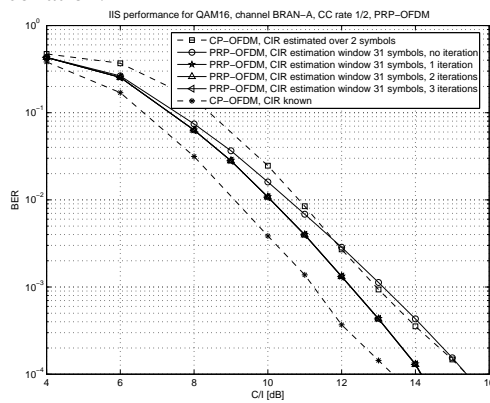


Figure 7.4: BER for IEEE802.11a, BRAN channel model A, QAM16, iterative interference cancellation. Figure 7.5: PER for IEEE802.11a, BRAN channel model A, QAM16, iterative interference cancellation.

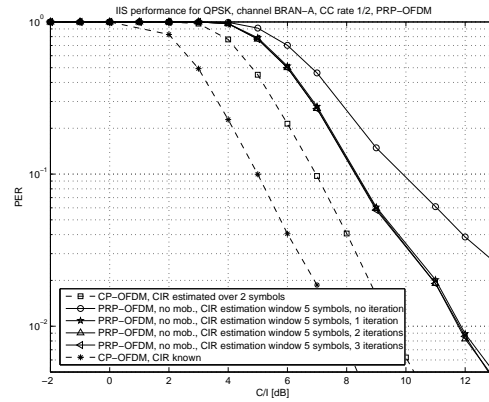
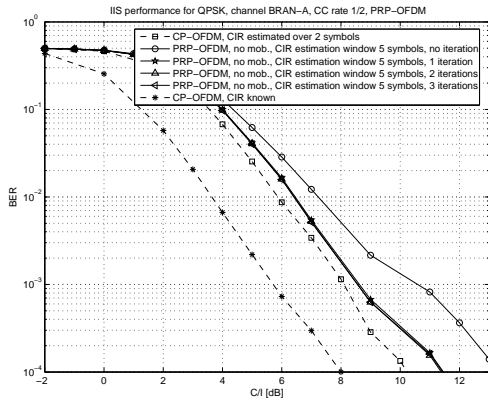


Figure 7.6: BER for IEEE802.11a, BRAN channel model A, QPSK, iterative interference cancellation. Figure 7.7: PER for IEEE802.11a, BRAN channel model A, QPSK, iterative interference cancellation.

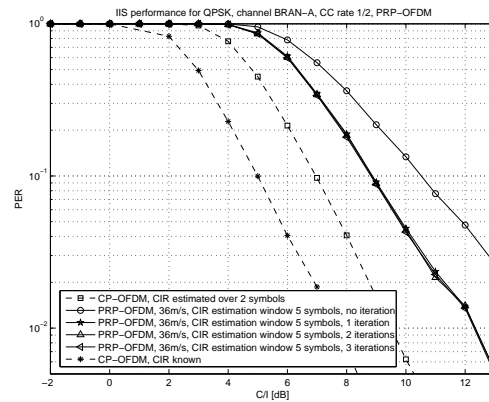
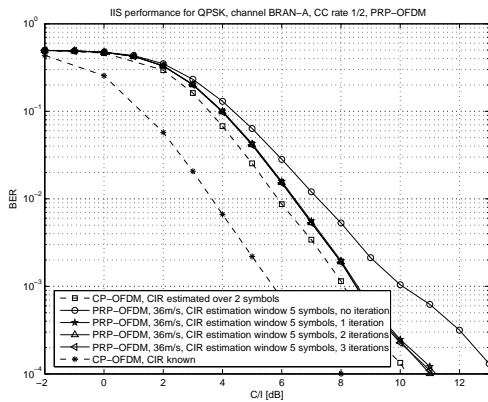


Figure 7.8: BER for IEEE802.11a, 36m/s, BRAN channel model A, QPSK, iterative interference cancellation. Figure 7.9: PER for IEEE802.11a, 36m/s, BRAN channel model A, QPSK, iterative interference cancellation.

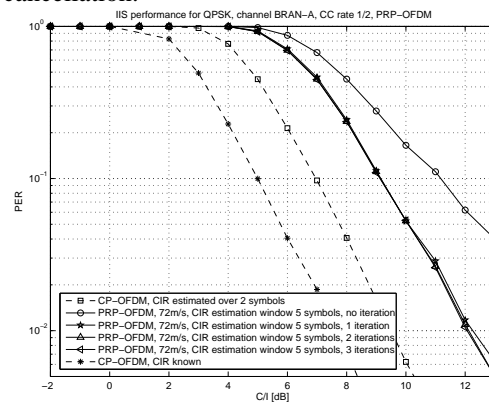
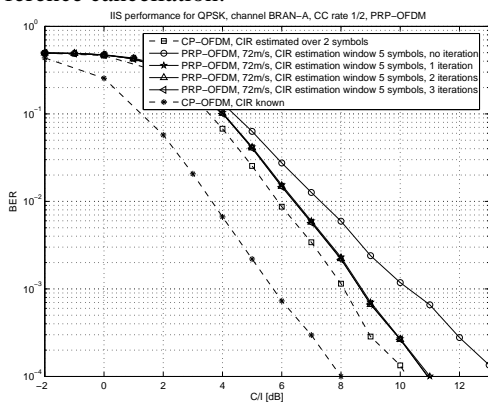


Figure 7.10: BER for IEEE802.11a, 72m/s, BRAN channel model A, QPSK, iterative interference cancellation. Figure 7.11: PER for IEEE802.11a, 72m/s, BRAN channel model A, QPSK, iterative interference cancellation.



## Chapter 8

# Low Density Parity Check (LDPC) Coding for OFDM

This chapter illustrates how to adapt the LDPC code word mapping onto OFDM carriers assuming perfect Channel State Information (CSI) knowledge [27, 28].

### 8.1 Introduction

Low Density Parity Check (LDPC) codes have been extensively studied, originally by [91, 120] and more recently by [121–123] and others. Initially, regular codes were studied and shown to exhibit a threshold phenomenon: with the block length tending towards infinity, an arbitrarily small bit-error-rate (BER) can be achieved for any Signal-to-Noise Ratio (SNR) level above a given threshold. [91] first observed this behavior for binary symmetrical channels (BCS). It was then generalized by [124] to randomly constructed irregular codes and further extended by [123] to various binary-input channels (BCS, Laplace, AWGN) and several decoding algorithms including the belief propagation (sum-product) algorithm. Also in [123], a general concentration theorem was proven: the decoder performance on random graphs converges to its expected value as the length of the code increases.

Based on these results, LDPC codes have been designed outperforming turbo codes [90] on Additive White Gaussian Noise (AWGN) channels [125]. While rather precise derivation techniques exist for asymptotic LDPC codes [92] under the pseudonym *density evolution*, the derivation complexity is important and has been subject to further studies: e.g., [125] proposes an elegant way to deal numerically with the calculation of the distribution of combined random variables (RVs) as they occur in [92]’s algorithm. The same authors introduce a simplified technique based on a Gaussian approximation (message densities are approximated to be Gaussian or Gaussian mixtures for irregular LDPC codes) [126]: they prove that the calculation complexity is reduced by several orders of magnitude while the results often are as accurate as the ones obtained from full density evolution.

Please note that there is no simple way to express updating message densities in the framework of turbo decoding and thus Monte Carlo simulation based techniques are typically used in order to analyze

the approximate evolution of Gaussian messages (*Exit Charts*) [127, 128].

While the practical problem of how to efficiently encode an LDPC code has been addressed in [129], many other issues have only been considered from a theoretical point of view (e.g. limited to AWGN channels). In the framework of this thesis, we focus on such a practical context by considering the efficient use of LDPC codes for Orthogonal Frequency Division Multiplexing (OFDM) based systems in combination with frequency selective fading channels. In the framework of this chapter, the case of a time invariant propagation channel is considered as it typically occurs in Wireless Local Area Network (WLAN) systems, e.g. IEEE802.11a/n [56, 58]. For this purpose, we build on results and ideas of [130, 131]: LDPC analysis techniques are derived for OFDM systems by approximating the frequency domain channel as a step-profile where each sub-band is characterized by a constant complex channel coefficient. For each sub-band, a sub-LDPC code is defined and considered for the global optimization. Moreover, a new optimization technique is proposed taking the number of iterations in the LDPC decoding process as well as the resulting error probability of data bits into account. This allows to optimize the allocation of data and redundancy bits which is not possible for *density evolution* based approaches, since the error probability asymptotically tends to zero above a given SNR threshold for both, data and redundancy bits.

In this chapter, we extend the LDPC optimization algorithm of [130, 131] to a sub-carrier based expression (omitting the notion of sub-bands covering several carriers): exploiting that in the context of OFDM the frequency selective fading channel is transformed into a set of parallel attenuations in the discrete frequency domain. Both, the derivation of optimum LDPC codes and the carrier-allocation (which can be interpreted as an adaptive interleaving) for data and redundancy bits are studied in a time-invariant context [27, 28]. While both optimization steps are ideally performed jointly, the carrier-allocation algorithm is straightforwardly applicable to existing LDPC codes which are not necessarily optimized for a given frequency selective propagation channel. The corresponding results will prove to be straightforwardly applicable to a context where LDPC codes and/or the corresponding carrier mapping are derived based on approximate estimates of the propagation channel. Thanks to the Gaussian approximation, a reliable result is expected (relying on the conclusions of [126]) at low arithmetical calculation complexity requirements. The proposed architectures are thus applicable to practical hardware implementation. A typical example is a closed-loop WLAN system where the propagation channel is known to the transmitter (TX) and receiver (RX) and thus suitable LDPC codes can be negotiated prior to transmission.

This chapter is organized as follows. Section 8.2 defines the notations and assumptions we use. The presentation of a new optimization procedure adapted to the OFDM context follows in section 8.3: two different low-complexity algorithms are derived based on different assumptions on the structure of the LDPC code. Simulation results and a final conclusion are respectively given in sections 8.4 and 8.5.

## 8.2 Notations and definitions

This section briefly presents the basic definitions introduced in chapters 2 and 3 for an  $N$  carrier PRP-OFDM system. The  $i$ th  $N \times 1$  input digital vector<sup>1</sup>  $\tilde{\mathbf{s}}_N(i)$  is first modulated by the IFFT matrix  $\mathbf{F}_N^H := \frac{1}{\sqrt{N}} \left( W_N^{ij} \right)^H, 0 \leq i < N, 0 \leq j < N$  where  $W_N := e^{-j\frac{2\pi}{N}}$ . Then, a deterministic postfix vector  $\mathbf{p}_D :=$

<sup>1</sup>Lower (upper) boldface symbols will be used for column vectors (matrices) sometimes with subscripts  $N$  or  $P$  emphasizing their sizes (for square matrices only); tilde denotes frequency domain quantities; argument  $i$  will be used to index blocks of symbols;  $^H$  ( $^T$ ) denotes Hermitian (Transpose).

$(p_0, \dots, p_{D-1})^T$  weighted by a pseudo random value  $\alpha(i) \in \mathbb{C}$  is appended to the IFFT outputs  $\mathbf{s}_N(i)$ . With  $P := N + D$ , the corresponding  $P \times 1$  transmitted vector is  $\mathbf{s}_P(i) := \mathbf{F}_{\text{ZP}}^H \tilde{\mathbf{s}}_N(i) + \alpha(i) \mathbf{p}_P$ , where

$$\mathbf{F}_{\text{ZP}}^H := \begin{bmatrix} \mathbf{I}_N \\ \mathbf{0}_{D,N} \end{bmatrix}_{P \times N} \quad \mathbf{F}_N^H \quad \text{and} \quad \mathbf{p}_P := (\mathbf{0}_{1,N} \mathbf{p}_D^T)^T$$

Without loss of generality, the elements of  $\mathbf{s}_N(i) = \mathbf{F}_N^H \tilde{\mathbf{s}}_N(i)$  are assumed to be i.i.d. and zero mean random variables of variance  $\sigma_s^2 = 1$  which are independent of  $\alpha(i) \mathbf{p}_D$ . The samples of  $\mathbf{s}_P(i)$  are then sent sequentially through the channel, modeled here as an  $L$ th-order FIR filter  $C(z) := \sum_{n=0}^L c_n z^{-n}$ . The OFDM system is designed such that the postfix duration exceeds the channel memory  $L < D$ .

Let  $\mathbf{C}_{\text{ISI}}(P)$  and  $\mathbf{C}_{\text{IBI}}(P)$  be respectively the Toeplitz lower and upper triangular matrices of first column  $[c_0, c_1, \dots, c_L, 0, \dots, 0]^T$  and first row  $[0, \dots, 0, c_L, \dots, c_1]$ . As already explained in [80], the channel convolution can be expressed as  $\mathbf{r}_P(i) := \mathbf{C}_{\text{ISI}}(P) \mathbf{s}_P(i) + \mathbf{C}_{\text{IBI}}(P) \mathbf{s}_P(i-1) + \mathbf{n}_P(i)$ .  $\mathbf{C}_{\text{ISI}}(P)$  and  $\mathbf{C}_{\text{IBI}}(P)$  represent respectively the intra-symbol and inter-block interference.  $\mathbf{n}_P(i)$  is the  $i$ th AWGN vector of i.i.d. elements with variance  $\sigma_n^2$ . Since  $\mathbf{s}_P(i) = \mathbf{F}_{\text{ZP}}^H \tilde{\mathbf{s}}_N(i) + \alpha(i) \mathbf{p}_P$ , we have:

$$\mathbf{r}_P(i) = (\mathbf{C}_{\text{ISI}} + \beta_i \mathbf{C}_{\text{IBI}}) \mathbf{s}_P(i) + \mathbf{n}_P(i) \quad (8.1)$$

where  $\beta_i := \frac{\alpha(i-1)}{\alpha(i)}$ . Note that  $\mathbf{C}_{\beta_i} := (\mathbf{C}_{\text{ISI}} + \beta_i \mathbf{C}_{\text{IBI}})$  is pseudo circulant: i.e. a circulant matrix whose  $(D-1) \times (D-1)$  upper right triangular part is weighted by  $\beta_i$ . Such a matrix is no longer diagonal on a standard Fourier basis, but on a new one still allowing an efficient implementation based on FFTs (see appendix A).

The expression of the received block thus becomes:

$$\begin{aligned} \mathbf{r}_P(i) &= \mathbf{C}_{\beta_i} (\mathbf{F}_{\text{ZP}}^H \tilde{\mathbf{s}}_N(i) + \alpha(i) \mathbf{p}_P) + \mathbf{n}_P(i) \\ &= \mathbf{C}_{\beta_i} \begin{pmatrix} \mathbf{F}_N^H \tilde{\mathbf{s}}_N(i) \\ \alpha(i) \mathbf{p}_D \end{pmatrix} + \mathbf{n}_P(i) \end{aligned}$$

Several equalization approaches are presented in chapter 3. Assuming the application of a low-complexity Overlap-Add (OLA) based decoding architecture, the following expression is obtained with  $\mathbf{C}_{\text{CIRC}}(N) := \mathbf{C}_{\text{IBI}}(N) + \mathbf{C}_{\text{ISI}}(N)$ :

$$\begin{aligned} \mathbf{r}_N &= \mathbf{C}_{\text{CIRC}}(N) \mathbf{s}_N(i) + \mathbf{n}_N(i) \\ &= \mathbf{F}_N^H \tilde{\mathbf{D}}_C \tilde{\mathbf{s}}_N(i) + \mathbf{n}_N(i) \end{aligned} \quad (8.2)$$

$$\tilde{\mathbf{r}}_N = \tilde{\mathbf{D}}_C \tilde{\mathbf{s}}_N(i) + \tilde{\mathbf{n}}_N(i) \quad (8.3)$$

with  $\tilde{\mathbf{r}}_N = \mathbf{F}_N \mathbf{r}_N(i)$  and  $\tilde{\mathbf{n}}_N(i) = \mathbf{F}_N \mathbf{n}_N(i)$ . The circulant channel matrix  $\mathbf{C}_{\text{CIRC}}(N) = \mathbf{F}_N^H \tilde{\mathbf{D}}_C \mathbf{F}_N$  is diagonal on a Fourier basis with  $\tilde{\mathbf{D}}_C = \text{diag}\{\mathbf{F}_N [c_0, c_1, \dots, c_L, 0, \dots, 0]^T\}$ .  $\text{diag}\{\cdot\}$  transforms a vector into a diagonal matrix. Thus, each carrier is weighted by its corresponding complex channel coefficient given in  $\tilde{\mathbf{D}}_C = \text{diag}\{\tilde{c}_0, \dots, \tilde{c}_{N-1}\}$ . Note that equation (8.3) also corresponds to the received expression in a standard Cyclic-Prefix OFDM (CP-OFDM) transceiver context. The LDPC mapping approach presented below is thus directly applicable to CP-OFDM system, too.

[130] points out that the choice of the constellation mapping (i.e. the set of  $\tilde{\mathbf{s}}_N(i)$  amplitudes) plays an important role for the system performance analysis if data bits are encoded based on LDPC

Codes. Log-likelihood ratio (LLR) based messages generated from BPSK and QPSK constellations are Gaussian, symmetric and consistent as required for density evolution [123] (the consistency condition guarantees that the error probability is a large sense decreasing function over the iteration number  $l$ ; moreover, this condition guarantees that the block error probability tends towards zero if and only if the message densities tend towards a Dirac mass at infinity). The symmetry condition, however, is not valid for M-QAM constellations with  $M > 4$  [130, 131]. In order to resolve the issue, [132] proposes an i.i.d. channel adaptation technique where the data bit sequence is combined with a pseudo-random i.i.d. bit sequence. As a result, the symmetry condition is verified on the messages.

Defining  $t_c$  as the variable node degree and  $t_r$  as the parity check node degree, a regular LDPC code characterized by the parameter set  $(Z_{LDPC}, t_c, t_r)$  is a linear block code defined by a sparse parity check matrix  $\mathbf{H}$  of dimension  $Z_{LDPC} \times M_{LDPC}$  with  $Z_{LDPC} = \frac{t_c}{t_r} M_{LDPC}$  [120]. The code words  $\mathbf{m}_{M_{LDPC}}$  consists of  $M_{LDPC}$  bits which all satisfy  $Z_{LDPC}$  parity check equations:

$$\mathbf{H}\mathbf{m}_{M_{LDPC}} = \mathbf{0}_{Z_{LDPC},1} \quad (8.4)$$

There are  $K_{LDPC} = M_{LDPC} - Z_{LDPC}$  information bits and the code rate is  $R \geq 1 - \frac{t_c}{t_r}$  (there only is equality if the matrix  $\mathbf{H}$  is full rank). Such a code can be graphically represented by a so-called *factor graph* [133]. Fig.8.1 illustrates such a graph for  $(M = 9, t_c = 2, t_r = 3)$ :

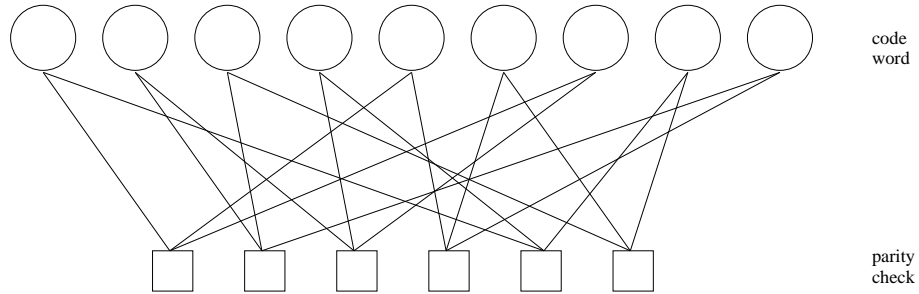


Figure 8.1: Example of a factor graph.

The corresponding  $\mathbf{H}$  matrix is presented by [130]:

$$\mathbf{H} = \begin{pmatrix} 1 & 0 & 0 & 0 & 1 & 0 & 1 & 0 & 0 \\ 0 & 1 & 1 & 0 & 0 & 0 & 0 & 0 & 1 \\ 0 & 1 & 0 & 1 & 0 & 0 & 1 & 0 & 0 \\ 0 & 0 & 0 & 0 & 1 & 1 & 0 & 0 & 1 \\ 1 & 0 & 0 & 1 & 0 & 0 & 0 & 1 & 0 \\ 0 & 0 & 1 & 0 & 0 & 1 & 0 & 1 & 0 \end{pmatrix} \quad (8.5)$$

Fig.8.1 helps to identify *cycles* of length  $v$  which is a path comprising  $v$  edges closing back on itself. An important code design parameter is the *girth* of a graph: it defines the minimum cycle length of a graph and should be as large as possible (note that the optimization of LDPC codes is typically performed under the *local tree assumption*, i.e. the girth is assumed to be large enough such that the sub-graph forms a tree and the incoming messages to every node are therefore independent).

A further generalization of LDPC codes has been introduced by [124] with *irregular* LDPC codes characterized by a non-uniform distribution of '1's over the rows and columns of the  $\mathbf{H}$  matrix. [124] shows that good irregular codes outperform regular ones. Typically, the code is represented by two polynomials;  $\lambda_i$  ( $\rho_j$ ) respectively represent the percentage of branches connected to variable nodes (check nodes) of degree  $i$  ( $j$ ).  $t_{c,max}$  ( $t_{r,max}$ ) is the maximum connection degree of variable nodes (check nodes):

$$\lambda(x) = \sum_{i=2}^{t_{c,max}} \lambda_i x^{i-1} \quad (8.6)$$

$$\rho(x) = \sum_{j=2}^{t_{r,max}} \rho_j x^{j-1} \quad (8.7)$$

Both polynomials are link to each other via the code rate  $R$ :

$$(1-R) \sum_{i=2}^{t_{c,max}} \frac{\lambda_i}{i} = \sum_{j=2}^{t_{r,max}} \frac{\rho_j}{j}.$$

In a another common representation,  $\lambda_i$  in (8.6) is replaced by

$$\tilde{\lambda}_i = \frac{\lambda_i/i}{\sum_{k=2}^{t_{c,max}} \lambda_k/k}$$

and  $\rho_j$  in (8.7) is replaced by

$$\tilde{\rho}_i = \frac{\rho_i/i}{\sum_{k=2}^{t_{r,max}} \rho_k/k}.$$

In the framework of this thesis, only *systematic* LDPC codes are considered; this is proper because practically only systematic codes are used in reality. The corresponding generating matrix  $\mathbf{G}$  of the LDPC code is applied to the initial vector of information bits  $\mathbf{b}$  as follows:  $\mathbf{m} = \mathbf{G}\mathbf{b}$  with  $\mathbf{H}\mathbf{G} = \mathbf{0}$ . Moreover, the analysis is limited to binary LDPC codes (i.e. all elements are  $\in GF(2)$ ). Non-binary codes with elements  $\in GF(Q)$  have been proven to provide improved performances, but require a decoding complexity which rises exponentially with  $q = \log_2(Q)$  [134].

As commonly used, we choose to work with LLR messages in combination with received carrier amplitudes  $r$ :

$$v = \log \frac{p(r|x=1)}{p(r|x=-1)}$$

are the output messages of variable node where  $x$  is the bit value of the corresponding node. Likewise, the output messages of a check node are defined as

$$u = \log \frac{p(r'|x'=1)}{p(r'|x'=-1)}$$

where  $x'$  is the bit value of the variable node arriving from the check node and  $r'$  contains all information available to a check node up to the present iteration. Under sum-product decoding [126],  $v$  is equal to the sum of all the incoming LLRs:

$$v = u_0 + \sum_{i=1}^{d_v-1} u_i \quad (8.8)$$

where  $u_0$  is the observed LLR of the decoded bit and  $u_i, i = 1, \dots, d_v - 1$  represent all incoming LLRs from neighbors of the variable node except from the check node that will get the message  $v$  (i.e. its input must be independent of its previous output). The  $u$  messages are then recalculated based on the so-called ‘‘tanh’’ rule [135, 136]:

$$\tanh\left(\frac{u}{2}\right) = \prod_{j=1}^{d_c-1} \tanh\left(\frac{v_j}{2}\right) \quad (8.9)$$

where  $v_j, j = 1, \dots, d_c - 1$  are the incoming LLRs from the  $d_c - 1$  neighbors of a check node. Note that the message of the node itself ( $j = 0$ ) is omitted in the product calculation.

In the case of QPSK mapping, [130] shows that the messages corresponding to the real (imaginary) part of the  $k^{\text{th}}$  OFDM carrier is  $u_{0,2k}$  ( $u_{0,2k+1}$ ) and depends on the frequency domain channel coefficient  $\tilde{c}_k$  and the noise variance  $\sigma_{n,k}^2$  of the corresponding carrier (assuming that the amplitude  $\tilde{s} = 1$  has been sent on the corresponding carrier):

$$\begin{aligned} u_{0,2k} &:= \frac{4|\tilde{c}_k|^2}{\sigma_{n,k}^2} + \frac{4}{\sigma_{n,k}^2} \Re\{\tilde{c}_k^* \tilde{n}_k\} \\ u_{0,2k+1} &:= \frac{4|\tilde{c}_k|^2}{\sigma_{n,k}^2} + \frac{4}{\sigma_{n,k}^2} \Im\{\tilde{c}_k^* \tilde{n}_k\} \end{aligned}$$

$\Re(\cdot)$  ( $\Im(\cdot)$ ) represents the real (imaginary) part of the argument. The corresponding distribution is Gaussian, symmetric and consistent (i.e.  $f(x) = e^x f(-x) \forall x \in \mathbb{R}$ ):

$$f_{u_{0,2k}} = f_{u_{0,2k+1}} = \mathcal{N}\left(\frac{4|\tilde{c}_k|^2}{\sigma_{n,k}^2}, \frac{8|\tilde{c}_k|^2}{\sigma_{n,k}^2}\right)$$

With the notations and definitions presented above, the following sections will show how to derive a suitable LDPC code assuming the channel is known and time-invariant.

### 8.3 LDPC Code optimization with known and time-invariant channel

We choose to perform the optimization of LDPC codes based on the *Gaussian Approximation* assumption which has been studied and validated in [126] due to its inherent low-complexity implementation properties. However, instead of performing an asymptotic threshold optimization (i.e. a joint search for a  $\mathbf{H}$  matrix and a minimum SNR level which lead to error free decoding properties if the matrix size and the number of decoding iterations tends towards infinity) we apply the idea of [130] to optimize the error probability of useful data bits with a fixed number of iterations. As [130] mentions correctly, such an approach may be slightly inconsistent, since asymptotic and non-asymptotic properties are mixed up. However, this analysis is better adapted to a practical case requiring a limited number of decoding iterations and [130] shows that the results of the corresponding code optimization has shown satisfying performances for small code word sizes.

In the following sections, important properties of the *Gaussian Approximation* are first recalled. It is shown that a generic optimization of the LDPC code-word mapping onto OFDM carriers is difficult to achieve; instead, we propose to apply in typical practical scenarios the following two analysis approaches which are sub-optimum approximations:

1. it will be shown that the LDPC code-word should be mapped onto OFDM carriers such that the message values from all variable nodes in the factor graph should be identical in the belief propagation decoding. In an asymptotic context (number OFDM carriers  $N \rightarrow \infty$ , LDPC codeword size  $\rightarrow \infty$ , number of different node degrees  $\rightarrow \infty$ ) this is theoretically feasible; note that [130, 131] observed an identical behavior if new LDPC codes are derived for a given propagation channel and in combination with OFDM symbols. In practice, however, a small number of different node degrees is often defined and this result leads to a sub-optimum optimization result.
2. a second order approximation of the message updating equation of the *Gaussian Approximation* approach will be used in order to optimize the LDPC code-word mapping onto OFDM carriers.

### 8.3.1 Properties of the Gaussian Approximation applied to the analysis of message passing decoding

Denoting the mean values of  $u$  ( $v$ ) by  $m_u$  ( $m_v$ ), the update equation (8.8) at iteration  $l$  becomes for every node with  $d_v$  branches [126]:

$$m_v^{(l)} = m_{u_0} + (d_v - 1)m_u^{(l-1)} \quad (8.10)$$

with  $m_u^{(0)} = 0$ . This means that the arriving messages to each node are assumed to be identical for the whole graph. The difference lies in the fact that more messages are arriving at the higher order nodes and thus the corresponding bit reliabilities are improved. For  $m_u^{(l)}$ , equation (8.9) leads to the following expression [126]:

$$\mathbb{E} \left[ \tanh \left( \frac{u^{(l)}}{2} \right) \right] = \mathbb{E} \left[ \tanh \left( \frac{v^{(l)}}{2} \right) \right]^{d_v - 1} \quad (8.11)$$

In the case of OFDM systems, the initial LLR message depends on the channel coefficient  $\tilde{c}_k$  of the corresponding carrier  $k$  providing the bit information [130]:  $m_{u_0} = m_{u_0}(\tilde{c}_k)$ . [130] further derives the updating equation of  $m_u^{(l)}$  based on an approximation of  $\tilde{\mathbf{c}}$  by a step-function characterized by a constant channel coefficient per step and representing each step by a corresponding LDPC sub-code. In the following, we avoid this step function approximation by expressing the updating equation based on the channel coefficient of each OFDM carrier and the node connection degree (i.e. number of branches)  $\zeta(k)$  of each bit modulated on the corresponding sub-carrier. The incoming means  $m_u^{(l-1)}$  in (8.10) are, however, still assumed to be constant for each nodes. The corresponding updating equation is expressed with the help of  $\phi(x)$  (convex for  $x > 0$ ) defined in [126] (see same reference for low complexity approximations of  $\phi(x)$ )

$$\phi(x) := \begin{cases} 1 - \frac{1}{\sqrt{4\pi x}} \int_{\mathbb{R}} \tanh\left(\frac{u}{2}\right) e^{-\frac{(u-x)^2}{4x}} du & \text{if } x > 0 \\ 1 & \text{if } x = 0 \end{cases}$$

as presented in (8.12):

$$m_u^{(l)} = \sum_{j=2}^{l_r, \max} \rho_j \left\{ \phi^{-1} \left\{ 1 - \left[ \underbrace{\frac{1}{N} \sum_{k=0}^{N-1} \left( 1 - \phi \left( m_{u_0}(\tilde{c}_k) + (\zeta(k) - 1)m_u^{(l-1)} \right) \right)}_{=\mathbb{E} \left[ \tanh \left( \frac{v^{(l)}(k)}{2} \right) \right] \text{ with } d_c=j} \right]} \right\}^{j-1} \right\} \quad (8.12)$$

argument of  $\phi^{-1}(1-x)$  is  $\left( 1 - \mathbb{E} \left[ \tanh \left( \frac{u^{(l)}(k)}{2} \right) \right] \right)$ , the result is the distribution of  $u$  (via mean value)

The mean distribution is given by the sum of mean values weighted by occurrence probability

After a maximum number of  $l = L$  iterations, the output means corresponding to carrier  $k$  are calculated taking *all* incoming  $m_u^{(L)}$  into account:

$$m_{u,k} = m_{u_0}(\tilde{c}_k) + \zeta(k)m_u^{(L)} \quad (8.13)$$

Prior to the calculation of the BER, we define

$$\psi(k) := \begin{cases} 2 & \text{if carrier } k \text{ carries 2 data bits} \\ 1 & \text{if carrier } k \text{ carries 1 data bit} \\ 0 & \text{if carrier } k \text{ carries 2 redundancy bits} \end{cases}$$

The BER is then calculated based on the results of [130] with  $Q(x) = \frac{1}{2\pi} \int_x^\infty e^{-\frac{t^2}{2}} dt$ :

$$\begin{aligned} P_e &= \frac{1}{\sum_{k=0}^{N-1} \psi(k)} \sum_{k=0}^{N-1} \psi(k) \int_{-\infty}^0 \frac{1}{\sqrt{4\pi m_{u,k}}} e^{-\frac{(x-m_{u,k})^2}{4m_{u,k}}} dx \\ &= \frac{1}{\sum_{k=0}^{N-1} \psi(k)} \sum_{k=0}^{N-1} \psi(k) Q \left( \sqrt{\frac{m_{u_0}(\tilde{c}_k) + \zeta(k)m_u^{(L)}}{2}} \right) \end{aligned} \quad (8.14)$$

The optimization of the data bit attribution to OFDM carriers  $\psi(x)$  is obtained as follows:

$$\psi(k)_{\forall k} = \underset{\psi(k)_{\forall k}}{\operatorname{argmin}} P_e(\tilde{\mathbf{c}}, (\sigma_{n,k})_{\forall k}, \psi(k)). \quad (8.15)$$

The following section will study the optimization of the LDPC code word mapping onto OFDM carriers with the goal to minimize the decoding error probability.

### 8.3.2 Direct interpretation of the message passing update equation

The goal is to choose the LDPC code-word mapping onto OFDM carriers such that the message passing LDPC code decoding algorithm provides optimum performance result as defined in equation (8.15). For this purpose, the channel coefficients of the different OFDM carriers are taken into account as well as the variable/check node degrees of the applied LDPC code.

The optimization is prepared by the definition of the following theorems:

**Theorem 8.3.1** *Jensen's inequality:* With  $f(\cdot)$  being a convex function, it is  $\frac{\sum_{i=0}^{N-1} f(x_i)}{N} \geq f\left(\frac{\sum_{i=0}^{N-1} x_i}{N}\right)$ .

**Proof of theorem 8.3.1:** See [137, 138].

**Theorem 8.3.2** *It is  $\phi^{-1}\left\{1 - \left[1 - \frac{1}{2}[\phi(m_{u_0}(c_k) + \varepsilon) + \phi(m_{u_0} - \varepsilon)]\right]^{j-1}\right\} < \phi^{-1}\left\{1 - [1 - \phi(m_{u_0}(c_k))]\right\}^{j-1}$  for  $\varepsilon > 0$ ,  $m_{u_0}(c_k) > 0$  and  $j \in (2, \dots, t_{r,max})$ .*  $\square$

**Proof of theorem 8.3.2:** The application of theorem 8.3.1 immediately leads to the expression given by theorem 8.3.2. Q.E.D.

In order to maximize  $m_u^{(l)}$  in (8.12), it is required to minimize  $\sum_{k=0}^{N-1} \phi\left(m_{u_0}(\tilde{c}_k) + (\zeta(k) - 1)m_u^{(l-1)}\right)$ . Using theorem 8.3.1 with equation (8.12), it is obvious that this goal is achieved if the arguments of  $\phi(\cdot)$  are equal for all  $k$ :

$$\frac{1}{N} \sum_{k=0}^{N-1} \phi\left(m_{u_0}(\tilde{c}_k) + (\zeta(k) - 1)m_u^{(l-1)}\right) \geq \phi\left(\frac{1}{N} \sum_{k=0}^{N-1} \left(m_{u_0}(\tilde{c}_k) + (\zeta(k) - 1)m_u^{(l-1)}\right)\right) \quad (8.16)$$

with equality for

$$\left(m_{u_0}(\tilde{c}_k) + (\zeta(k) - 1)m_u^{(l-1)}\right) = \left(m_{u_0}(\tilde{c}_{k'}) + (\zeta(k') - 1)m_u^{(l-1)}\right), \forall k, k'. \quad (8.17)$$

Equation (8.17) guarantees that all messages leaving the variable nodes and arriving at the check nodes in the factor graph are of identical value. If this property is given, the LDPC code-word mapping is optimum (with the limitations inherent to the *Gaussian Approximation* approach). Note that we assume for the optimization process that the observed messages  $m_{u_0}(\tilde{c}_k)$  have the correct sign with respect to the corresponding information bit that it carries.

If equality cannot be achieved (due to the given channel coefficients  $\tilde{c}_k$ , a limited number of different variable node degrees  $\zeta(k) - 1$ , etc.), theorem 8.3.2 gives some arguments that equality should be

achieved as closely as possible in terms of absolute difference to the optimum. For this case, further results are derived in the following section by a second order approximation of the message passing update equation.

### 8.3.3 Second order approximation of the message passing update equation

The goal of this section is to continue on the problem that has been addressed in the previous section: an optimum carrier mapping (i.e. attribution of  $m_{u_0}(\tilde{c}_k)$  to node degrees  $\zeta(k)$ ) needs to be found such that the expression  $m_u^{(l)}$  in equation (8.12) is maximized. This goal requires to minimize  $\sum_{k=0}^{N-1} \phi(m_{u_0}(\tilde{c}_k) + (\zeta(k) - 1)m_u^{(l-1)})$  in (8.12).

The asymptotic analysis presented in section 8.3.2 is applicable if the set of available channel coefficients and variable node degrees allows to create messages of identical value leaving the variable nodes in the message passing decoder as defined in equation (8.17). In a practical scenario typically few different node degrees are defined and the results of the asymptotic analysis are sub-optimum (e.g., it is the case for the TGnSync LDPC code [41]). This context is addressed in this section by evaluation of a second order approximation of (8.12) and its use in (8.12) by a second order approximation of  $\phi(x)$  and a first order approximation of  $\phi^{-1}(x)$ . We start the optimization by observing that the mean value of the argument of  $\phi(\cdot)$  in equation (8.12) is

$$\begin{aligned} x_0 &:= \frac{1}{N} \sum_{k=0}^{N-1} \left( m_{u_0}(\tilde{c}_k) + (\zeta(k) - 1)m_u^{(l-1)} \right) \\ &= \left( \frac{1}{N} \sum_{k=0}^{N-1} m_{u_0}(\tilde{c}_k) \right) + \left( \frac{1}{N} \sum_{k=0}^{N-1} (\zeta(k) - 1)m_u^{(l-1)} \right) \end{aligned}$$

Note that  $x_0$  is independent of the mapping of the LDPC code-words onto OFDM carriers. Section 8.3.2 has shown that the mapping is ideally chosen such that  $m_{u_0}(\tilde{c}_k) + (\zeta(k) - 1)m_u^{(l-1)}$  is approx. constant for all carriers  $k$  and thus  $x_0 \approx m_{u_0}(\tilde{c}_k) + (\zeta(k) - 1)m_u^{(l-1)} \approx \text{const} \forall k$ . We therefore choose to develop  $\phi(\cdot)$  around the point  $x_0$  with constants  $\alpha_\phi, \beta_\phi, \gamma_\phi$ .

$$\phi(x) = \phi(x_0) + \frac{\partial \phi}{\partial x}(x_0)(x - x_0) + \frac{\partial^2 \phi}{2! \partial x^2}(x_0)(x - x_0)^2 + O(x^3) \quad (8.18)$$

$$\approx \alpha_\phi + \beta_\phi(x - x_0) + \gamma_\phi(x - x_0)^2 \quad (8.19)$$

Note in particular that  $\left. \frac{\partial \phi}{\partial x}(x) \right|_{x>0} < 0$  (i.e.  $\beta_\phi < 0$ ) and  $\left. \frac{\partial^2 \phi}{\partial x^2}(x) \right|_{x>0} > 0$  (i.e.  $\gamma_\phi > 0$ ). Concerning  $\phi^{-1}(x)$ , it is  $\left. \frac{\partial \phi^{-1}}{\partial x}(x) \right|_{x>0} < 0$ .

$\sum_{k=0}^{N-1} \phi(m_{u_0}(\tilde{c}_k) + (\zeta(k) - 1)m_u^{(l-1)})$  is thus approximated as follows:

$$\sum_{k=0}^{N-1} \phi(m_{u_0}(\tilde{c}_k) + (\zeta(k) - 1)m_u^{(l-1)}) \approx \underbrace{\left( \sum_{k=0}^{N-1} \alpha_\phi \right)}_{=f_1(\cdot)} + \underbrace{\left( \beta_\phi \sum_{k=0}^{N-1} (m_{u_0}(\tilde{c}_k) + (\zeta(k) - 1)m_u^{(l-1)} - x_0) \right)}_{=f_2(\cdot)} + \underbrace{\left( \gamma_\phi \sum_{k=0}^{N-1} (m_{u_0}(\tilde{c}_k) + (\zeta(k) - 1)m_u^{(l-1)} - x_0)^2 \right)}_{=f_3(\cdot)} \quad (8.20)$$

$$\approx \underbrace{\tilde{f}_1(\cdot)}_{=\text{const}} + \gamma_\phi \sum_{k=0}^{N-1} m_{u_0}(\tilde{c}_k) \zeta(k) m_u^{(l-1)} \quad (8.21)$$

Note that  $\tilde{f}_1(\cdot)$  is defined to cover all contributions that are independent of the LDPC code word mapping onto OFDM carriers. As discussed in section 8.3.2, equation (8.21) needs to be minimized in order to maximize the resulting messages  $m_u^{(l)}$  in the update equation (8.12). The solution is given by the following theorem:

**Theorem 8.3.3** *In order to minimize equation (8.21), it is sufficient to minimize  $\sum_{k=0}^{N-1} m_{u_0}(\tilde{c}_k) \zeta(k)$ . This goal is achieved by attributing the smallest channel coefficients  $|\tilde{c}_k|$  to the highest degree variable nodes and vice versa.  $\square$*

**Proof of theorem 8.3.3:** It is  $m_{u_0}(\tilde{c}_k) \zeta(k) + m_{u_0}(\tilde{c}_{k'}) \zeta(k') < m_{u_0}(\tilde{c}_k) \zeta(k') + m_{u_0}(\tilde{c}_{k'}) \zeta(k)$ ,  $\forall k, k'$  if  $m_{u_0}(\tilde{c}_k) < m_{u_0}(\tilde{c}_{k'})$  and  $\zeta(k') < \zeta(k)$ , since this inequality can be rewritten as

$$\underbrace{(m_{u_0}(\tilde{c}_k) - m_{u_0}(\tilde{c}_{k'}))}_{<0} \underbrace{(\zeta(k) - \zeta(k'))}_{>0} < 0. \text{ Applying this property to all elements of } \sum_{k=0}^{N-1} m_{u_0}(\tilde{c}_k) \zeta(k) \text{ leads}$$

to theorem 8.3.3. Q.E.D.

Theorem 8.3.3 complements the results of section 8.3.2 for optimizing the update equation (8.12) in the case that the elements  $m_{u_0}(\tilde{c}_k) + (\zeta(k) - 1)m_u^{(l-1)}$  cannot be guaranteed to be constant  $\forall k$ : the smallest channel coefficients  $|\tilde{c}_k|$  should be attributed to the highest degree variable nodes and vice versa. Based on this results derived above, a LDPC code word mapping algorithm is derived in the following section.

### 8.3.4 An algorithm for LDPC code word mapping onto OFDM carriers

The optimization of the LDPC code word mapping onto OFDM carriers is based on the following comments with respect to the results derived in the previous sections:

1.  $P_e$  given by equation (8.14) is calculated over the data bits only; redundancy bits are not considered for the final BER.
2. Typically, an LDPC code is larger than one OFDM symbol; still, the equation (8.14) is applicable if the length of the codeword is an integer multiple of the number of bits modulated in one OFDM symbol.
3. Both, the resulting degree distributions  $\lambda(x)$ ,  $\rho(x)$  and the data bit attribution to OFDM carriers depends on the channel coefficients  $\mathbf{c}$ .
4. Ideally, a joint optimization of  $\lambda(x)$ ,  $\rho(x)$  and the data bit attribution to OFDM carriers is performed. However, the optimization of the BER expression (8.14) may also be performed based on a given LDPC code. In the simulation results section, it will be shown that the resulting data bit attribution to OFDM carriers can improve the code performance considerable compared to a poor choice.

If only an optimization concerning the data bit attribution to OFDM carriers is required for a given LDPC code, the upper result can be interpreted in a first approximation as follows: In order to minimize the BER, the expression  $m_{u_0(\tilde{c}_k)} + \zeta(k)m_u^{(L)}$  in (8.14) must be as large as possible. Thus,

1. since  $P_e$  is calculated only over useful data bits, use lowest order nodes (i.e.  $\zeta(k)$  is minimum) for redundancy nodes and maximize thus  $\zeta(k)m_u^{(L)}$ .
2. moreover, put data bits on the strongest carriers (i.e.  $|c_k|$  is maximum) in order to maximize  $m_{u_0(\tilde{c}_k)}$ .
3. assure a maximum final  $m_u^{(L)}$ . It turns out from theorems 8.3.1, 8.3.2 and 8.3.3 that this is achieved if the argument of  $\phi(\cdot)$  in (8.11) is as homogeneous as possible; in particular, very small arguments should be avoided. Consequently, high order nodes (i.e.  $\zeta(k)$  is large) should be attributed to small  $|c_k|$  and low order nodes (i.e.  $\zeta(k)$  is small) to large  $|c_k|$ .
4. if homogeneous arguments of  $\phi(\cdot)$  in (8.11) cannot be achieved in all cases, try to maximize the arguments for these exceptions since  $\phi(x \rightarrow \infty) \rightarrow 0$ .

This observation is illustrated in Fig.8.2 for an exemplary OFDM channel and an imaginary LDPC code of rate  $R = 1/2$  with variable node degrees 2, 3 and 4:

It is interesting to note that [130, 131] observe an identical behavior in a different context: the corresponding authors search a new LDPC code for a given OFDM propagation channel profile (while we present in this chapter how to perform an optimum mapping for any **given** LDPC code). At the output of the optimization process, they obtain results identical to properties of Fig.8.2 - however without further analyzing the underlying mechanisms.

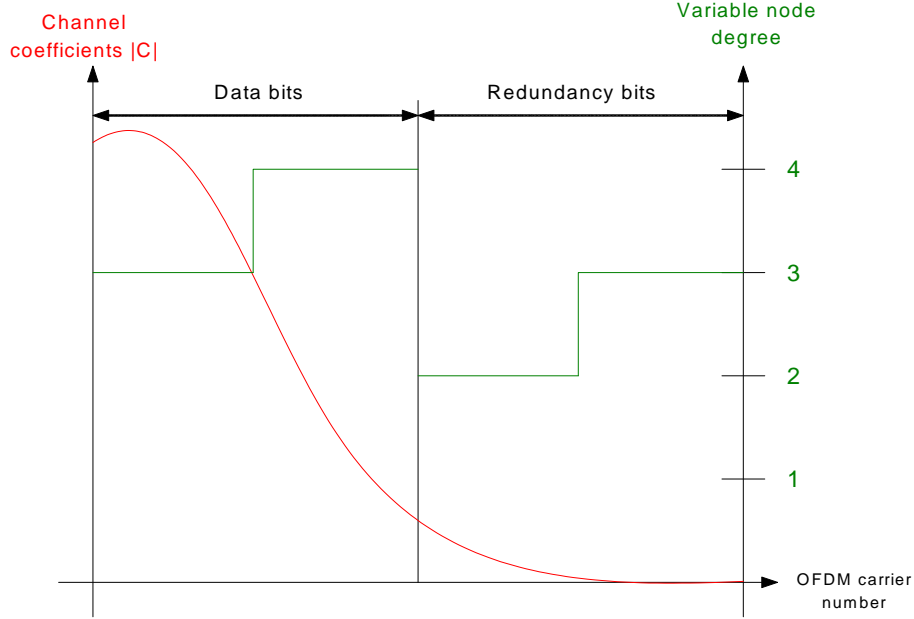


Figure 8.2: Example of LDPC code-word assignment.

In order to apply this LDPC code-word mapping in a practical context with a limited number  $N$  of OFDM carriers and a given LDPC code by a matrix  $\mathbf{H}$  of limited dimension, the following mapping algorithm is proposed based on the upper observations:

1. Assume that BPSK constellations are used for explanation sake. We further assume that all  $M_{LDPC}$  bits of an LDPC code-word  $\mathbf{m}_{M_{LDPC}}$  fit into  $P$  OFDM symbols, where the first  $K_{LDPC} = M_{LDPC} - Z_{LDPC}$  entries of  $\mathbf{m}_{M_{LDPC}}$  are information bits  $\mathbf{m}_k^{\text{Data}}$  and the remaining ones are redundancy bits  $\mathbf{m}_{Z_{LDPC}}^{\text{Red}}$ . Each OFDM symbol is defined to consist of  $N$  carriers, of which  $\bar{N} < N$  are attributed to data/redundancy symbols, i.e.  $M_{LDPC} = P\bar{N}$ . The channel coefficients of the  $\bar{N}$  used OFDM carriers are regrouped in the vector  $\tilde{\mathbf{c}}_{\bar{N}} := [\tilde{c}_0, \dots, \tilde{c}_{\bar{N}-1}]^T$ . The variable node degrees (i.e. the number of ones in the column of the LDPC code  $\mathbf{H}$  matrix corresponding to a specific code-word bit) of all  $M_{LDPC}$  code-word bits shall be contained in a vector  $\mathbf{w}_{M_{LDPC}}$ ; its first  $K_{LDPC} = M_{LDPC} - Z_{LDPC}$  entries  $\mathbf{w}_{K_{LDPC}}^{\text{Data}}$  are linked to data bits while the remaining ones  $\mathbf{w}_{Z_{LDPC}}^{\text{Red}}$  are linked to redundancy bits.
2. Duplicate the complex valued channel coefficients vector  $\tilde{\mathbf{c}}_{\bar{N}} := [\tilde{c}_0, \dots, \tilde{c}_{\bar{N}-1}]^T$   $P$  times and keep the result in the vector  $\tilde{\mathbf{c}}_{P\bar{N}} := \underbrace{\begin{bmatrix} \tilde{\mathbf{c}}_{\bar{N}}^T \\ \dots \\ \tilde{\mathbf{c}}_{\bar{N}}^T \end{bmatrix}}_{P \text{ times}}^T$ .
3. With  $|\tilde{\mathbf{c}}_{\bar{N}}| = [|\tilde{c}_0|, \dots, |\tilde{c}_{\bar{N}-1}|]^T$ , sort  $|\tilde{\mathbf{c}}_{P\bar{N}}|$  starting with the smallest element (up to the largest one); the vector  $\mathbf{p}_{|\tilde{\mathbf{c}}_{P\bar{N}}|} := [p_0, \dots, p_{P\bar{N}-1}]^T$  shall contain the sorting result as integer elements:  $p_0$  points to the position in  $|\tilde{\mathbf{c}}_{P\bar{N}}|$  with the smallest element, etc.
4. Split the pointer vector  $\mathbf{p}_{|\tilde{\mathbf{c}}_{P\bar{N}}|} := [p_0, \dots, p_{P\bar{N}-1}]^T$  into two parts:  $\mathbf{p}_{|\tilde{\mathbf{c}}_{P\bar{N}}|}^{\text{Red}} := [p_0, \dots, p_{Z_{LDPC}-1}]^T$  contains pointers to the channel coefficients that will be assigned to redundancy bits and  $\mathbf{p}_{|\tilde{\mathbf{c}}_{P\bar{N}}|}^{\text{Data}} := [p_{Z_{LDPC}}, \dots, p_{P\bar{N}-1}]^T$  contains pointers to the channel coefficients that will be assigned to data bits.



The column weights of the resulting  $\mathbf{H}$  matrix are illustrated in Fig.8.3 for a code-word size of 576 bits.

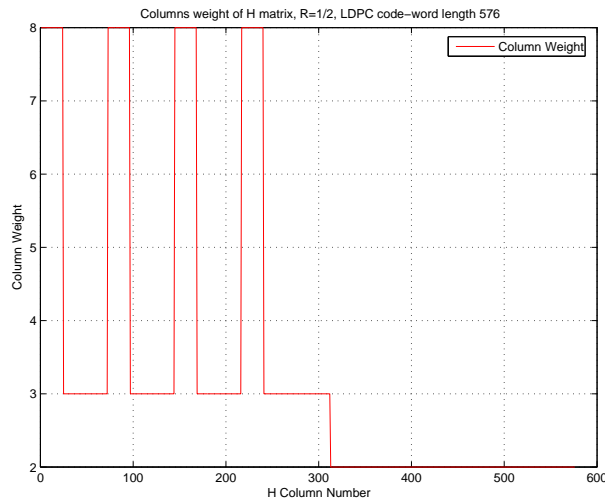


Figure 8.3: LDPC column weights, 576 bits code-word.

Simulations are performed over here for the 576 bits LDPC-codewords (15.000 code words are simulated per SNR value combined with the normalized BRAN-A channel definitions [37]) applying the mapping optimization approach are presented in Fig.8.4 and Fig.8.5 for the BER and PER respectively (only the data bits are used for BER/PER calculation, the redundancy bits are not considered); one LDPC code-word of 576 bits each is considered to be a packet. It should be pointed out that the PER results are improved by approximately 0.95dB at a PER of  $10^{-2}$ . As noted in section 8.3.4, if homogeneous arguments of  $\phi(\cdot)$  in (8.11) cannot be achieved in all cases, it is proposed to maximize the arguments for these exceptions (since  $\phi(x \rightarrow \infty) \rightarrow 0$ ). Finally, the impact of a (slightly) sub-optimum LDPC interleaving is illustrated in Fig.8.6 and Fig.8.7 by rotating the optimized carrier mapping vector. This test illustrates the sensibility of the LDPC interleaving. As a result, a very small difference is observed ( $< 0.1$ dB) for a small rotation of 2.5% of all carriers (14 carriers); however, this gap increases for larger rotations: the difference is approximately 0.25dB for a rotation of 20% of all carriers (115 carriers).

## 8.5 Conclusion

We have proposed in this chapter a simple way to derive optimum degree distributions and an optimum carrier attribution to data/redundancy nodes of different degree in the context of an OFDM system: it is sufficient to sort the available variable node degree values of the LDPC code and the absolute values of the frequency domain channel coefficients in order to derive a suitable mapping. This result can be interpreted as an optimum interleaver adapted to a given propagation channel. Simulation results show that a gain of approximately 0.95dB in PER performance can be achieved in a typical scenario. Due to the simplicity of the proposed approach, it is expected to be straightforwardly applicable in the context of systems such as IEEE802.11n WLANs: the study results have been presented at the IEEE 802.11n standardization group; they are currently under consideration for implementation in the standard [31,32].

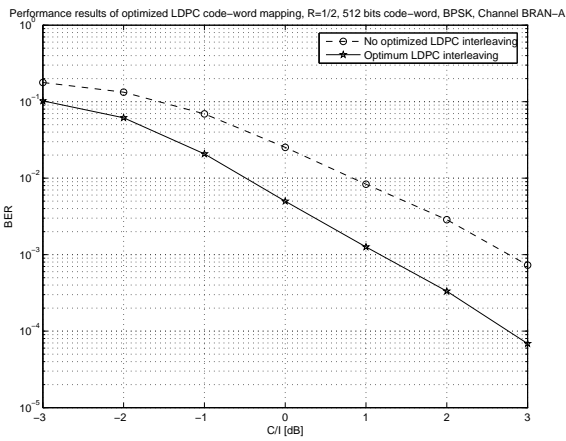


Figure 8.4: BER for LDPC code performance after optimization, channel BRAN-A, 576 bits code-word.

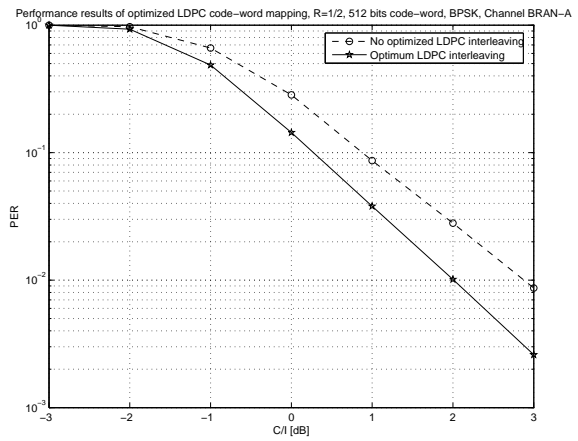


Figure 8.5: PER for LDPC code performance after optimization, channel BRAN-A, 576 bits code-word.

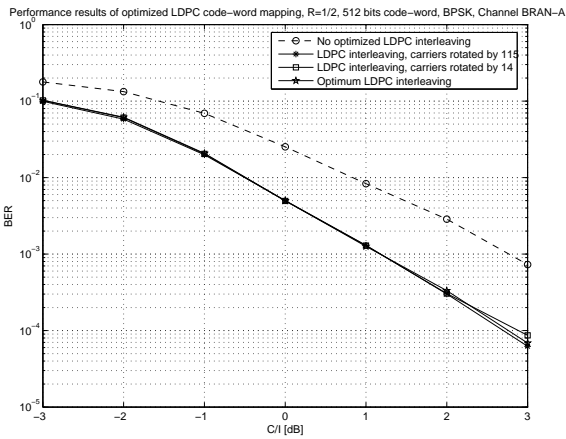


Figure 8.6: BER for LDPC code performance after different optimization approaches (including circular rotation), channel BRAN-A, 576 bits code-word.

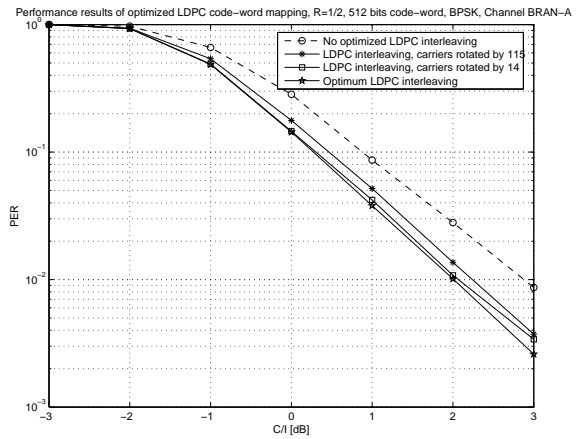


Figure 8.7: PER for LDPC code performance after different optimization approaches (including circular rotation), channel BRAN-A, 576 bits code-word.

## Chapter 9

# Conclusion

This thesis deals with detailed studies of the following two main topics

- Proposal of an improved OFDM modulation scheme applying a deterministic pseudo-randomly weighted postfix sequence instead of a cyclic prefix as it is used for standard CP-OFDM: **Pseudo Random Postfix OFDM (PRP-OFDM)**.
- Derivation of an optimum mapping of LDPC code-word bits onto OFDM carriers based on known channel state information (CSI).

In the context of the first item, the proposal of the novel Pseudo-Random-Postfix OFDM scheme, it is furthermore shown how to derive suitable finite postfix sequences and how to estimate/track the channel impulse response in a time-invariant and time-variant scenario. In the given typical examples, a mobility up to 72m/s is demonstrated to be applicable based on BPSK, QPSK and QAM-16 constellations at a carrier frequency of 5.2GHz. Finally, time and frequency synchronization refinement techniques are detailed; they allow to constantly refine an initial (preamble-based) synchronization.

Concerning the optimized LDPC code-word mapping onto OFDM carriers taking into account that the knowledge of channel attenuations is available, two different approaches are presented in order to derive an optimum mapping. The first approach is optimum if a homogeneous messages can be achieved in the belief propagation decoder, while the second approach is a refinement taking the practical case into account where only few different node degrees exist an homogeneous messages are not feasible.

This thesis thus addresses two related, but still distinct problems in the framework of OFDM systems. As a result, the PRP-OFDM study presents a ready-to-use toolkit that allows to implement a high-velocity OFDM system with minimum redundancy overhead. The LDPC chapter also provides a simple algorithm that is ready to be implemented in a practical system.

## Further study topics

Further study topics and follow-up work of this thesis may include the following items

- Study of sub-optimum, but reduced-complexity channel estimation/tracking architectures. In particular, the multiplication with large estimation matrices as proposed in chapter 3 is a limiting factor if the observation window size grows. It may, for example, be possible to obtain separate CIR estimates for each OFDM symbol within the observation window. By means of suitable combination approaches, it is expected to achieve CIR estimates suitable for the equalization steps.
- The impact of the availability of the channel power delay profile (PDP) needs further consideration. Since it is unlikely that a perfect estimate of the PDP is available in a practical system implementation, all simulations in this thesis are based on a rectangular PDP with its length corresponding to the PRP-OFDM postfix size. It may though be possible to inject the knowledge of typical TX/RX filter designs in the approximation of the PDP, since the observed channel corresponds to the convolution of TX/RX filters by the over-the-air propagation channel. Moreover, it is expected that real propagation channels can be better approximated by a ramp function, depending on the considered frequency band.
- The proposed Iterative-Interference-Suppression approaches are leading to satisfying results after few iterations (typically one iteration is sufficient). However, they are numerically complex as illustrated in Appendix C. A future topic is to find look-up table based architectures leading to a trade-off in terms of memory requirements and calculation complexity. In particular the calculation requirements of the interference suppression vector in function of the a-posteri probability outputs of the soft-output decoder in the receiver are expected to be optimized.
- Considering the LDPC code-word mapping optimization, a future study topic is to consider the availability of several LDPC codes for each code-rate and block size. It is thus possible not only to optimize the mapping for one single code with a given channel impulse response, but also to choose the most suitable LDPC coding matrix for the considered scenario.

## Appendix A

# Proof of Diagonalization Properties of Pseudo circulant matrices

This appendix details the proof of the diagonalization of pseudo circulant matrices [81]. These matrices correspond to standard circulant convolution matrices with the difference that the upper triangular part is weighted by a complex factor  $\alpha$ . In the framework of this paper, it is assumed that  $|\alpha| = 1$ .

**Proposition:** The matrix  $\mathbf{C}_\alpha$  defined as

$$\begin{aligned} \mathbf{C}_\alpha &:= \begin{bmatrix} c_0 & \alpha \cdot c_{N-1} & \alpha \cdot c_{N-2} & \rightarrow & \alpha \cdot c_1 \\ c_1 & c_0 & \alpha \cdot c_{N-1} & \rightarrow & \alpha \cdot c_2 \\ \downarrow & \searrow & \searrow & \searrow & \downarrow \\ c_{N-1} & \rightarrow & \rightarrow & \rightarrow & c_0 \end{bmatrix} \\ &= \mathbf{C}_{\text{ISI}} + \alpha \cdot \mathbf{C}_{\text{IBI}}, \end{aligned}$$

is diagonalized as follows:

$$\mathbf{C}_\alpha = \mathbf{V}_N^{-1} \text{diag} \left\{ C \left( \alpha^{-\frac{1}{N}} \right), \dots, C \left( \alpha^{-\frac{1}{N}} e^{j \frac{2\pi(N-1)}{N}} \right) \right\} \mathbf{V}_N$$

with

$$\begin{aligned} \mathbf{V}_N &:= \left( \frac{1}{N} \sum_{n=0}^{N-1} |\alpha|^{-\frac{2n}{N}} \right)^{\frac{1}{2}} \mathbf{F}_N \text{diag} \left\{ 1, \dots, \alpha^{\frac{N-1}{N}} \right\}, \\ \mathbf{F}_N &:= \frac{1}{\sqrt{N}} \left( W_N^{ij} \right)_{0 \leq i < N, 0 \leq j < N}, W_N := e^{-j \frac{2\pi}{N}}, \\ C(z) &:= \sum_{n=0}^{N-1} c_n z^{-n} \text{ and } z, \alpha, c_0, \dots, c_{N-1} \in \mathbb{C}. \end{aligned}$$

**Proof:**  $\mathbf{C}_\alpha$  can be rewritten as

$$\begin{aligned}\mathbf{C}_\alpha &= c_0 \mathbf{I}_N + c_1 \mathbf{J}_N^1 + \dots + c_{N-1} \mathbf{J}_N^{N-1}, \\ \mathbf{J}_N^n &:= \begin{bmatrix} \mathbf{0}_{n,(N-n)} & \alpha \mathbf{I}_n \\ \mathbf{I}_{(N-n)} & \mathbf{0}_{(N-n),n} \end{bmatrix}, n = 1, \dots, N.\end{aligned}$$

Denoting by  $(\lambda_k, \mathbf{x}_k)$  the eigenvalues and associated eigenvectors of  $\mathbf{J}_N$ ,  $(\lambda_k^n, \mathbf{x}_k)$  are the corresponding ones for  $\mathbf{J}_N^n$ .  $\lambda_k$  is obtained by setting  $\det(\mathbf{J}^N - \lambda_k^N \mathbf{I}_N) = (\alpha - \lambda_k^N)^N = 0$ . Thus  $\lambda_k = \alpha^{\frac{1}{N}} = |\alpha|^{\frac{1}{N}} e^{j \frac{\phi(\alpha)}{N}} e^{-j 2\pi \frac{k}{N}}$ ,  $k = 0, \dots, N-1$  where  $\phi(\alpha)$  is the phase of  $\alpha$ . By setting  $\mathbf{J}_N \mathbf{x}_k = \lambda_k \mathbf{x}_k$ , the unitary eigenvectors of  $\mathbf{J}_N$  can be verified to be

$$\mathbf{x}_k = \left( \sum_{n=0}^{N-1} |\alpha|^{-\frac{2n}{N}} \right)^{-\frac{1}{2}} \begin{bmatrix} 1 \\ |\alpha|^{-\frac{1}{N}} e^{-j\phi(\alpha)\frac{1}{N}} e^{jk\frac{2\pi}{N}} \\ \dots \\ |\alpha|^{-\frac{N-1}{N}} e^{-j\phi(\alpha)\frac{N-1}{N}} e^{jk\frac{2\pi(N-1)}{N}} \end{bmatrix}$$

with  $k = 0, \dots, N-1$ . Stacking all the  $\mathbf{x}_k$  in matrix  $\mathbf{X}_N$ , we have:

$$\begin{aligned}\mathbf{X}_N &:= [\mathbf{x}_0 \ \mathbf{x}_1 \ \dots \ \mathbf{x}_{N-1}] = \\ &\left[ \frac{1}{N} \sum_{n=0}^{N-1} |\alpha|^{-\frac{2n}{N}} \right]^{-\frac{1}{2}} \text{diag} \left\{ 1, \dots, \alpha^{-\frac{N-1}{N}} \right\} \mathbf{F}_N^H.\end{aligned}$$

Since  $\mathbf{x}_k$  is an eigenvector of  $\mathbf{J}_N$  associated to  $\lambda_k$ , one can easily verify that  $\mathbf{C}_\alpha \mathbf{x}_k = c_1 \mathbf{x}_k + c_1 (\mathbf{J}_N \mathbf{x}_k) + \dots + c_{N-1} (\mathbf{J}_N^{N-1} \mathbf{x}_k) = C(\lambda_k^{-1}) \mathbf{x}_k$ . This shows that  $(C(\lambda_k^{-1}), \mathbf{x}_k)$  are the eigenvalues of  $\mathbf{C}_\alpha$ . Thus,  $\mathbf{X}_N^{-1} \mathbf{C}_\alpha \mathbf{X}_N = \text{diag}\{C(\lambda_0^{-1}), \dots, C(\lambda_{N-1}^{-1})\}$  which proves that:

$$\mathbf{C}_\alpha = \mathbf{X}_N \text{diag} \left\{ C \left( \alpha^{-\frac{1}{N}} \right), \dots, C \left( \alpha^{-\frac{1}{N}} e^{j \frac{2\pi(N-1)}{N}} \right) \right\} \mathbf{X}_N^{-1}$$

Since  $\mathbf{V}_N = \mathbf{X}_N^{-1}$  we reach the desired result: QED.

## Appendix B

# Biased and unbiased MMSE equalizers

Based on a received PRP-OFDM signal as derived in chapter 3

$$\begin{aligned}\mathbf{r}_P(i) &= \mathbf{C}_{\beta_i} (\mathbf{F}_{ZP}^H \tilde{\mathbf{s}}_N(i) + \alpha(i) \mathbf{p}_P) + \mathbf{n}_P(i) \\ &= \mathbf{C}_{\beta_i} \begin{pmatrix} \mathbf{F}_N^H \tilde{\mathbf{s}}_N(i) \\ \alpha(i) \mathbf{p}_D \end{pmatrix} + \mathbf{n}_P(i),\end{aligned}\tag{B.1}$$

this section derives a standard *biased* MMSE equalizer and an *unbiased* MMSE equalizer as introduced by [42–44].

### B.1 Biased MMSE equalizer

**Theorem B.1.1** *The biased equalization matrix in the MMSE sense for retrieving an estimate of  $\tilde{\mathbf{s}}_N(i)$  in (B.1) is given by*

$$\begin{aligned}\mathbf{G}_{MMSE}^{\text{PRP}} &:= \mathbf{F}_N [\mathbf{I}_N \mathbf{0}_{N,D}] \mathbf{R}_{s_p} \mathbf{C}_{\beta_i}^H \mathbf{Q}^{-1} \\ &= \mathbf{F}_N [\mathbf{I}_N \mathbf{0}_{N,D}] \mathbf{R}_{s_p} \mathbf{V}_P^H(i) \mathbf{D}_i^H \hat{\mathbf{Q}}^{-1} \mathbf{V}_P(i),\end{aligned}$$

with  $\mathbf{Q} := \mathbf{R}_{n_p} + \mathbf{C}_{\beta_i} \mathbf{R}_{s_p} \mathbf{C}_{\beta_i}^H$ ,  $\hat{\mathbf{Q}} := \mathbf{R}_{n_p} + \mathbf{D}_i \hat{\mathbf{R}}_{s_p} \mathbf{D}_i^H$ ,  $\mathbf{R}_{n_p} := \mathbb{E}[\mathbf{n}_P(i) \mathbf{n}_P^H(i)] = \sigma_n^2 \mathbf{I}_P$ ,  $\mathbf{R}_{s_p} := \mathbb{E}[\mathbf{s}_P(i) \mathbf{s}_P^H(i)]$ ,  $\hat{\mathbf{R}}_{s_p} := \mathbf{V}_P(i) \mathbf{R}_{s_p} \mathbf{V}_P^H(i)$ .  
□

**Proof of Theorem B.1.1:** With (B.1) the received signal after equalization by the  $N \times P$  equalization matrix  $\mathbf{G}_{MMSE}^{\text{PRP}}$  is

$$\tilde{\mathbf{r}}_N^{eq}(i) := \mathbf{G}_{MMSE}^{\text{PRP}} \mathbf{C}_{\beta_i} \begin{pmatrix} \mathbf{F}_N^H \tilde{\mathbf{s}}_N(i) \\ \alpha(i) \mathbf{p}_D \end{pmatrix} + \mathbf{G}_{MMSE}^{\text{PRP}} \mathbf{n}_P(i)$$

The resulting MSE  $\varepsilon$  to be minimized in function of  $\mathbf{G}_{\text{MMSE}}^{\text{PRP}}$  is thus

$$\varepsilon := \text{tr} \left\{ \mathbf{E} \left[ \left( \tilde{\mathbf{r}}_N^{eq}(i) - \tilde{\mathbf{s}}_N(i) \right) \left( \tilde{\mathbf{r}}_N^{eq}(i) - \tilde{\mathbf{s}}_N(i) \right)^H \right] \right\}$$

The MMSE is found by setting  $\frac{\partial \varepsilon}{\partial (\mathbf{G}_{\text{MMSE}}^{\text{PRP}})^*} = \mathbf{0}$  [108, 139]:

$$\frac{\partial \varepsilon}{\partial (\mathbf{G}_{\text{MMSE}}^{\text{PRP}})^*} = \mathbf{G}_{\text{MMSE}}^{\text{PRP}} \mathbf{C}_{\beta_i} \mathbf{R}_{s_p} \mathbf{C}_{\beta_i}^H + \mathbf{G}_{\text{MMSE}}^{\text{PRP}} \mathbf{R}_{\mathbf{n}_p} - \mathbf{E} \left[ \tilde{\mathbf{s}}_N(i) \begin{pmatrix} \mathbf{F}_N^H \tilde{\mathbf{s}}_N(i) \\ \alpha(i) \mathbf{p}_D \end{pmatrix}^H \right] \mathbf{C}_{\beta_i} \quad (\text{B.2})$$

Since  $\alpha(i) \mathbf{p}_D$  and  $\tilde{\mathbf{s}}_N(i)$  are assumed to be independent and  $\mathbf{R}_{s_N} = \sigma_s^2 \mathbf{I}$ :

$$\begin{aligned} \mathbf{E} \left[ \tilde{\mathbf{s}}_N(i) \begin{pmatrix} \mathbf{F}_N^H \tilde{\mathbf{s}}_N(i) \\ \alpha(i) \mathbf{p}_D \end{pmatrix}^H \right] &= [\mathbf{R}_{s_N} \mathbf{0}_{N,D}] \mathbf{F}_N, \\ &= \mathbf{F}_N \mathbf{R}_{s_N} [\mathbf{I}_N \mathbf{0}_{N,D}], \\ &= \mathbf{F}_N [\mathbf{I}_N \mathbf{0}_{N,D}] \mathbf{R}_{s_p}, \end{aligned}$$

exploiting

$$\mathbf{R}_{s_N} = [\mathbf{I}_N \mathbf{0}_{N,D}] \mathbf{R}_{s_p} [\mathbf{I}_N \mathbf{0}_{N,D}]^H$$

$\mathbf{R}_{s_N} [\mathbf{I}_N \mathbf{0}_{N,D}] = [\mathbf{I}_N \mathbf{0}_{N,D}] \mathbf{R}_{s_p}$  is not generally true for full matrices  $\mathbf{R}_{s_N}$  and  $\mathbf{R}_{s_p}$  and only holds since  $\alpha(i) \mathbf{p}_D$  and  $\tilde{\mathbf{s}}_N(i)$  are independent. Forcing (B.2) to zero leads to the MMSE equalizer  $\mathbf{G}_{\text{MMSE}}^{\text{PRP}}$  given in the proposition. Q.E.D.

## B.2 Unbiased MMSE equalizer

**Theorem B.2.1** *The unbiased equalization matrix in the MMSE sense for retrieving an estimate of  $\tilde{\mathbf{s}}_N(i)$  in (B.1) is given by*

$$\begin{aligned} \mathbf{G}_{\text{MMSE,unb}}^{\text{PRP}} &:= (\mathbf{R}_{s_N} - \text{diag} \{ \lambda_0, \dots, \lambda_{N-1} \}) \mathbf{F}_N \mathbf{C}_o^H \left[ \mathbf{C}_{\beta_i} \mathbf{R}_{s_p} \mathbf{C}_{\beta_i}^H + \mathbf{R}_{\mathbf{n}} \right]^{-1} \\ &= \hat{\mathbf{G}} \mathbf{G}_{\text{MMSE}}^{\text{PRP}} \\ \hat{\mathbf{G}} &:= \mathbf{I} - \text{diag} \{ \lambda_0, \dots, \lambda_{N-1} \} \mathbf{R}_{s_N}^{-1} \\ \lambda_n &:= [\mathbf{R}_{s_N} \mathbf{B}_i - \mathbf{I}_N]_{n,n} / [\mathbf{B}_i]_{n,n} \\ \mathbf{B}_i &:= \mathbf{F}_N \mathbf{C}_o^H \left[ \mathbf{C}_{\beta_i} \mathbf{R}_{s_p} \mathbf{C}_{\beta_i}^H + \mathbf{R}_{\mathbf{n}} \right]^{-1} \mathbf{C}_o \mathbf{F}_N^H \end{aligned}$$

where  $\mathbf{R}_{s_N} = [\mathbf{I}_N \mathbf{0}_{N,D}] \mathbf{R}_{s_p} [\mathbf{I}_N \mathbf{0}_{N,D}]^H$  is assumed to be diagonal,  $\mathbf{R}_{s_p} = \mathbf{E} [\mathbf{s}_p(i) \mathbf{s}_p^H(i)]$  and  $\mathbf{C}_o$  is the  $P \times N$  matrix containing  $\mathbf{C}_{\text{ISI}}(P)$   $N$  first columns.

□

**Proof of Theorem B.2.1:** Denote by  $\mathbf{G}_{\text{MMSE,unb}}^{\text{PRP}}$  the  $N \times P$  MMSE matrix equalizer for a system where the original data vector has been multiplied by a pseudo circulant channel matrix  $\mathbf{C}$  as explained in appendix A. Thus, the  $i$ th equalized received OFDM vector is  $\tilde{\mathbf{r}}_N^{eq}(i) := \mathbf{G}_{\text{MMSE,unb}}^{\text{PRP}} (\mathbf{C}_{\beta_i} \mathbf{s}_P(i) + \mathbf{n}(i))$ . In consequence, the estimation error on carrier  $n$  is given by

$$\begin{aligned} \varepsilon_n(i) &:= \tilde{r}_n(i) - \tilde{s}_n(i) \\ &= [(\mathbf{G}_{\text{MMSE,unb}}^{\text{PRP}} \mathbf{C}_{\beta_i} \mathbf{s}_P(i) - \tilde{\mathbf{s}}_N(i)) + \mathbf{G}_{\text{MMSE,unb}}^{\text{PRP}} \mathbf{n}(i)]_n \end{aligned}$$

where  $[\cdot]_k$  indicates the  $k$ th vector element. The offset on carrier  $n$  is then given by

$$\begin{aligned} \varepsilon_{\text{offset},n}(i) &:= \mathbb{E}[\varepsilon_n(i) | \tilde{s}_n(i)] \\ &= \mathbb{E} \left[ \left( \mathbf{G}_{\text{MMSE,unb}}^{\text{PRP}} \mathbf{C}_{\beta_i} \mathbf{s}_P - \tilde{\mathbf{s}}_N(i) \right)_n | \tilde{s}_n(i) \right] \\ &= \left[ \mathbf{G}_{\text{MMSE,unb}}^{\text{PRP}} \mathbf{C}_o \mathbf{F}_N^H \begin{pmatrix} \mathbf{0}_{n-1,1} \\ \tilde{s}_n(i) \\ \mathbf{0}_{N-n-1,1} \end{pmatrix} \right]_n + \underbrace{\mathbb{E} \left[ \mathbf{G}_{\text{MMSE,unb}}^{\text{PRP}} \mathbf{C}_{\beta_i} \begin{pmatrix} \mathbf{0}_{N,1} \\ \alpha(i) \mathbf{p}_D \end{pmatrix} \right]_n}_{=0, \text{ since } \mathbb{E}[\alpha(i)]=0} \\ &= \tilde{s}_n(i) [\mathbf{G}_{\text{MMSE,unb}}^{\text{PRP}} \mathbf{C}_o \mathbf{F}_N^H - \mathbf{I}_N]_{n,n}, \end{aligned} \quad (\text{B.3})$$

where  $[\cdot]_{j,k}$  is the operator isolating row  $j$  and column  $k$  element of a matrix.  $\mathbf{C}_o$  is the  $P \times N$  matrix containing  $\mathbf{C}_{\text{ISI}}(P)$   $N$  first columns. In accordance to the definition of Lagrange multipliers [104], the following term  $C(\mathbf{G}_{\text{MMSE,unb}}^{\text{PRP}})$  is added to the cost function  $J := \mathbb{E} [|\mathbf{G}_{\text{MMSE,unb}}^{\text{PRP}} \mathbf{r}_P(i) - \tilde{\mathbf{s}}_N(i)|^2]$  that is minimized in order to derive  $\mathbf{G}_{\text{MMSE,unb}}^{\text{PRP}}$ :

$$\begin{aligned} C(\mathbf{G}_{\text{MMSE,unb}}^{\text{PRP}}) &:= 2 \sum_{k=0}^{N-1} \text{Re} \left\{ \lambda_k^* [\mathbf{G}_{\text{MMSE,unb}}^{\text{PRP}} \mathbf{C}_o \mathbf{F}_N^H - \mathbf{I}_N]_{k,k} \right\} \\ \frac{\partial C(\mathbf{G}_{\text{MMSE,unb}}^{\text{PRP}})}{\partial [\mathbf{G}_{\text{MMSE,unb}}^{\text{PRP}}]_{j,k}^*} &= \lambda_j [\mathbf{F}_N \mathbf{C}_o^H]_{j,k} \\ \frac{\partial C(\mathbf{G}_{\text{MMSE,unb}}^{\text{PRP}})}{\partial (\mathbf{G}_{\text{MMSE,unb}}^{\text{PRP}})^*} &= \text{diag} \{ \lambda_0, \dots, \lambda_{N-1} \} (\mathbf{F}_N \mathbf{C}_o^H) \end{aligned}$$

Thus,

$$\frac{\partial C(\mathbf{G}_{\text{MMSE,unb}}^{\text{PRP}})}{\partial (\mathbf{G}_{\text{MMSE,unb}}^{\text{PRP}})^*} = \text{diag} \{ \lambda_0, \dots, \lambda_{N-1} \} (\mathbf{F}_N \mathbf{C}_o^H)$$

and the minimization of the total cost function  $\frac{\partial (J+C(\mathbf{G}_{\text{MMSE,unb}}^{\text{PRP}}))}{\partial (\mathbf{G}_{\text{MMSE,unb}}^{\text{PRP}})^*} = \mathbf{0}$  results in

$$\mathbf{G}_{\text{MMSE,unb}}^{\text{PRP}} = (\mathbf{F}_N \mathbf{R}_{s_N} \mathbf{F}_N^H - \text{diag} \{ \lambda_0, \dots, \lambda_{N-1} \}) \mathbf{F}_N \mathbf{C}_o^H [\mathbf{C}_{\beta_i} \mathbf{R}_{s_P} \mathbf{C}_{\beta_i}^H + \mathbf{R}_n]^{-1}$$

The  $\mathbf{D}_\lambda = (\lambda_0, \dots, \lambda_{N-1})^T$  introduce additional degrees of freedom and are used in order to force  $\varepsilon_{\text{offset},n}(i) = 0$ . Using (B.3), this condition is expressed by

$$[\mathbf{G}_{\text{MMSE,unb}}^{\text{PRP}} \mathbf{C}_o \mathbf{F}_N^H - \mathbf{I}]_{n,n} = 0 \quad \forall n \quad (\text{B.4})$$

It is straightforward to show that the resulting expressions for  $\lambda_0, \dots, \lambda_{N-1}$  are the ones given by the theorem; With  $\mathbf{B}_i = \mathbf{F}_N \mathbf{C}_o^H \left[ \mathbf{C}_{\beta_i} \mathbf{R}_{s_p} \mathbf{C}_{\beta_i}^H + \mathbf{R}_n \right]^{-1} \mathbf{C}_o \mathbf{F}_N^H$ :

$$\sum_k \left[ \mathbf{F}_N \mathbf{R}_{s_N} \mathbf{F}_N^H - \mathbf{D}\lambda \right]_{n,k} [\mathbf{B}_i]_{k,n} = 1 \quad \forall n$$

and thus

$$\begin{aligned} [\mathbf{F}_n \mathbf{R}_{s_N, s_N} \mathbf{B}_i - \mathbf{I}_N]_{n,n} &= [\mathbf{D}\lambda \mathbf{F}_N \mathbf{B}_i]_{n,n} \\ &= \lambda_n [\mathbf{F}_N \mathbf{B}_i]_{n,n} \\ &= 0 \end{aligned}$$

leading to the resulting expressions are for diagonal  $\mathbf{R}_{\tilde{s}_N}$

$$\lambda_n = [\mathbf{R}_{\tilde{s}_N} \mathbf{B}_i - \mathbf{I}_N]_{n,n} / [\mathbf{B}_i]_{n,n}, n = 0, \dots, N-1$$

Q.E.D.

## Appendix C

# Complexity Considerations

This Appendix gives calculation complexity estimates for the PRP-OFDM related channel estimation and equalization approaches presented in chapters 3 to 7.

### C.1 The complexity of basic operations

The complexity of the operations used is expressed by the number of *real multiplications* ( $\mu_{\mathbb{R}}$ ) and *real additions* ( $\alpha_{\mathbb{R}}$ ) necessary in order to perform the calculation. Tab. C.1 presents the complexity of basic complex operations in  $\mu_{\mathbb{R}}$  and  $\alpha_{\mathbb{R}}$  [140, 141].

Operations	Abbreviation	$\mathbb{R}$ multiplications	$\mathbb{R}$ additions
real multiplication	$\mu_{\mathbb{R}}$	1	–
real addition	$\alpha_{\mathbb{R}}$	–	1
complex multiplication	$\mu_{\mathbb{C}}$	3	3
complex addition	$\alpha_{\mathbb{C}}$	–	2
real $\times$ complex multiplication	$\mu_{\mathbb{RC}}$	2	–
complex $N$ -points FFT	$\text{DFT}_{\mathbb{C}}(N)$	$\rightarrow$ section C.2	$\rightarrow$ section C.2

Table C.1: *The complexity of basic operations.*

### C.2 The complexity of Fast Fourier Transformation (FFT) algorithms

Tab. C.2 presents the complexity of different FFT algorithms. Wherever possible, we use the *radix-4 FFT* ( $N$  must be a number that can be expressed as  $N = 4^x, x \in \mathbb{N}^+$ ). The *split-radix* offers the lightest load whereas the *radix-4* is more power consuming; the *radix-2* comes last. On the other hand, however efficient the *split-radix* algorithm is, its memory access requirements are greater than for *radix-4* [142].

FFT type	$\mathbb{R}$ multiplications	$\mathbb{R}$ additions	RAM access
radix-2	$\frac{3 \cdot N}{2} \cdot \log_2(N) - 5 \cdot N + 8$	$\frac{7 \cdot N}{2} \cdot \log_2(N) - 5 \cdot N + 8$	$4 \cdot N \cdot \log_2(N)$
radix-4	$\frac{9 \cdot N}{8} \cdot \log_2(N) - \frac{43}{12} \cdot N + \frac{16}{3}$	$\frac{25 \cdot N}{8} \cdot \log_2(N) - \frac{43}{12} \cdot N + \frac{16}{3}$	$2 \cdot N \cdot \log_2(N)$
split-radix	$N \cdot \log_2(N) - 3 \cdot N + 4$	$3 \cdot N \cdot \log_2(N) - 3 \cdot N + 4$	$3 \cdot N \cdot \log_2(N)$

Table C.2: *The complexity of FFT operations.*

### C.3 PRP-OFDM Complexity Evaluation

The parameters that are used in the complexity evaluation correspond to the notations in chapters 2 to 7. They are recalled in Tab. C.3

Parameter	Comments
$D$	Size of the postfix sequence
$K$	Number of iterations for Iterative Interference Suppression (IIS)
$N$	Number of OFDM carriers
$P$	Number of samples per OFDM symbol plus postfix sequence
$Q_M$	Modulation order
$Z$	Observation window size of channel estimation in number of OFDM symbols

Table C.3: *Notations.*

The following considerations have been taken into account for the complexity evaluation:

- The derivation of estimation and/or equalization matrices is not considered in the complexity evaluation, since they are assumed to be precalculated. In a practical application, they are preferably stored in look-up tables.
- Any multiplication/division of samples by the pseudo-random weighting postfix factors  $\alpha(i)$  is not considered in the complexity evaluation;  $\alpha(i)$  is assumed to be chosen such that these operations are negligible, e.g.  $\alpha(i) \in (\pm 1)$  or  $\alpha(i) \in (\pm 1, \pm j)$ .
- The Fast Fourier Transform of a vector of size  $D \times 1$  followed by  $N - D$  ( $P - D$ ) padding zeros is assumed to require the calculation complexity  $\text{DFT}_{\mathbb{C}}(N)$  ( $\text{DFT}_{\mathbb{C}}(P)$ ). It should be noted, however, that the corresponding generic FFT architecture can be further optimized taking the fixed zero positions into account.
- The frequency domain channel coefficients are obtained by performing an FFT on the estimated postfix sequence convolved by the channel divided by the frequency domain postfix coefficients (ZF equalization) or by division by the corresponding MMSE coefficients (MMSE equalization). These complex divisions are evaluated as a complex multiplication since the corresponding multiplicative coefficients can be pre-calculated. Note that in practice, a full complex multiplier may not even be necessary, since an optimized hard-wired architecture may be used for each frequency domain channel equalization coefficient.
- The channel estimation step is assumed to include the estimation of the postfix sequence convolved by the channel; this result is re-used by transforming PRP-OFDM symbols to ZP-OFDM.

### C.3.1 Generic Complexity Evaluation

The following table Tab. C.4 resumes the complexity of the basic PRP-OFDM related channel estimation and equalization approaches presented in chapters 3 to 7.

Index	Operation	Complexity
1	$N$ -point frequency domain CIR estimation based on $ZD \times 1$ observation vector	$D \times (DZ - 1)\alpha_{\mathbb{C}}, (D^2Z + N)\mu_{\mathbb{C}}, \text{DFT}_{\mathbb{C}}(N)$
2	$P$ -point frequency domain CIR estimation based on $ZD \times 1$ observation vector	$D \times (DZ - 1)\alpha_{\mathbb{C}}, (D^2Z + P)\mu_{\mathbb{C}}, \text{DFT}_{\mathbb{C}}(P)$
3	$N$ -point frequency domain CIR estimation based on $2ZD \times 1$ observation vector	$D \times (2DZ - 1)\alpha_{\mathbb{C}}, (2D^2Z + N)\mu_{\mathbb{C}}, \text{DFT}_{\mathbb{C}}(N)$
4	$P$ -point frequency domain CIR estimation based on $2ZD \times 1$ observation vector	$D \times (2DZ - 1)\alpha_{\mathbb{C}}, (2D^2Z + P)\mu_{\mathbb{C}}, \text{DFT}_{\mathbb{C}}(P)$
5	Interference Suppression step for one CIR estimation	$2DZ\alpha_{\mathbb{C}}, ZNQ_M\mu_{\mathbb{R}\mathbb{C}}, N2D \times (2D - 1)\mu_{\mathbb{C}}, Z \text{DFT}_{\mathbb{C}}(N)$
6	CP-OFDM ZF equalization	$N\mu_{\mathbb{C}}, 1 \text{DFT}_{\mathbb{C}}(N)$
7	MMSE equalization of one OFDM symbol (pseudo-circulant $P \times P$ CIR matrix equalization)	$N \times (P - 1)\alpha_{\mathbb{C}}, NP\mu_{\mathbb{C}}$ (FFT included)
8	MMSE equalization of one OFDM symbol (transformation to ZP-OFDM and matrix equalization)	$D + N \times (P - 1)\alpha_{\mathbb{C}}, NP\mu_{\mathbb{C}}$ (FFT included)
9	OLA equalization of one OFDM symbol	$6D\alpha_{\mathbb{C}}, N\mu_{\mathbb{C}}, \text{DFT}_{\mathbb{C}}(N)$

Table C.4: *Generic Complexity Evaluation.*

### C.3.2 Numerical Examples

Tab. C.5 gives some numerical examples on calculation complexity for an IEEE802.11a [56] related parameter set:  $N = 64, D = 16, Q_M = 16, K = 1, Z = 41$ .

## C.4 Conclusion

The complexity evaluation presented in this Appendix reveals that the optimum MMSE based channel estimation and symbol equalization approaches are of a considerable complexity: symbol equalization is approx. 38.4 times more complex compared to standard CP-OFDM. As it is stated in the general conclusions chapter 9, future work should consider complexity reduction of the proposed approaches. For this purpose, some directions are given by [39] for the ZP-OFDM related equalization structures. The low-complexity OLA equalization approach, however, is only of limited complexity increase and thus PRP-OFDM in combination with such a decoder is an alternative to existing CP-OFDM systems.

Index	Operation	$\mu_{\mathbb{R}}$	$\alpha_{\mathbb{R}}$
1	$N$ -point frequency domain CIR estimation based on $ZD \times 1$ observation vector	31888	53616
2	$N$ -point frequency domain CIR estimation based on $2ZD \times 1$ observation vector	63376	106096
3	Interference Suppression step for one CIR estimation	282960	233104
4	CP-OFDM ZF equalization	400	1168
5	MMSE equalization of one OFDM symbol (pseudo-circulant $P \times P$ CIR matrix equalization) <b>Normalized by CP-OFDM complexity</b>	38.4	21.8
6	MMSE equalization of one OFDM symbol (transformation to ZP-OFDM and matrix equalization) <b>Normalized by CP-OFDM complexity</b>	38.4	21.8
7	OLA equalization of one OFDM symbol <b>Normalized by CP-OFDM complexity</b>	1	1.16

Table C.5: Numerical Examples on Complexity Evaluation.

## Appendix D

# Modeling of the channel evolution in a Doppler context

This section resumes the modeling of the channel impulse response and its covariance in a time-variant Doppler environment as studied by [105]; in the context of this thesis, the validity of the so-called *Jakes* Doppler spectrum is assumed as derived in the latter reference. Then, several modeling approaches with different accuracy vs complexity trade-offs are presented. These models will help to derive suitable channel estimators following standard *Wiener* and *Kalman* filtering approaches [104].

### D.1 Modeling time-variant channels

The relation between a time-variant channel impulse response  $\mathbf{c}(n_0)$  and  $\mathbf{c}(n_1)$  at instants  $t_0 = n_0\Delta T$  and  $t_1 = n_1\Delta T$  respectively can be formalized as follows:

$$\mathbf{c}(n_1) = \alpha_{\mathbf{c}}(n_0, n_1)\mathbf{c}(n_0) + \check{\mathbf{c}}(n_0).$$

$\check{\mathbf{c}}(n_0)$  is the so-called *process-noise* which is Gaussian. Following the derivations in [105], the factor  $\alpha_{\mathbf{c}}(n_0, n_1)$  is

$$\begin{aligned} \alpha_{\mathbf{c}}(n_0, n_1) &= \frac{\mathbf{E} [c_l(n_0)c_l^*(n_1)]}{\mathbf{E} [|c_l(n_0)|^2]} \\ &= J_0(2\pi f_D |n_1 - n_0| \Delta T) \end{aligned}$$

where  $c_l(n)$  is the  $l^{\text{th}}$  component of the CIR  $\mathbf{c}(n)$  at instant  $T_n = n\Delta T$ ,  $J_0(\cdot)$  is the  $0^{\text{th}}$  order Bessel function of the first kind and  $f_D$  the Doppler frequency.

In the framework of this thesis, this model is assumed to be exact. In the following, two simplified and sub-optimum models are derived suitable for use with *Wiener* and *Kalman* filtering theory.

## D.2 Auto-Regressive model of first order

Recent publications discuss the possibility to approximate Jakes' model by an order-one Auto-Regressive (AR) filter given by [106] and illustrated by Fig.D.1.

$$\mathbf{c}(n+1) = J_0(2\pi f_D T_1) \mathbf{c}(n) + \check{\mathbf{c}}(n+1) \quad (\text{D.1})$$

$\check{\mathbf{c}}(n+1)$  is the so-called process-noise.

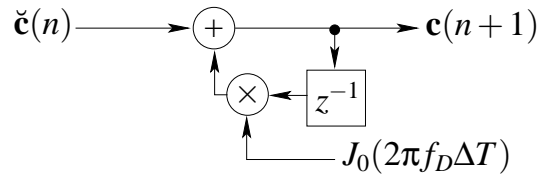


Figure D.1: Order one AR Doppler model.

This model has several advantages; in particular, an MMSE estimator of the CIR  $\mathbf{c}(0)$  based on noisy observations  $\mathbf{c}(n) + \mathbf{n}(n)$  is straightforwardly derived by Kalman filtering [104, 107]. Rewriting equation (D.1) as

$$\begin{cases} \mathbf{c}(0) = \check{\mathbf{c}}(0) \\ \mathbf{c}(1) = J_0(2\pi f_D T_1) \check{\mathbf{c}}(0) + \check{\mathbf{c}}(1) \\ \vdots \\ \mathbf{c}(n) = \sum_{k=0}^n J_0^k(2\pi f_D T_1) \check{\mathbf{c}}(n-k) \end{cases}$$

clearly shows that the AR model inherently approximates  $J_0(2\pi f_D k \Delta T)$  by  $J_0^k(2\pi f_D \Delta T)$ . The latter expression is justified by the Bessel function addition theorem stating

$$J_0(x+y) = \sum_{k=-\infty}^{\infty} (-1)^k J_k(x) J_k(y) \approx J_0(x) J_0(y) \quad (\text{D.2})$$

for small  $x$  and  $y$ . However, these approximations are not quite valid in the context of high Doppler frequencies which occur, for example, in the context of high mobility WLANs or at high carrier frequencies if their application is required over the duration of a long packet.

This motivates the Moving-Average (MA) based approach presented in the following.

### D.3 Moving Average model

The MA filter approach is based on expressing the time domain channel vector  $\mathbf{c}(n)$  by the following set of equations:

$$\begin{cases} \mathbf{c}(0) = \check{\mathbf{c}}(0) \\ \mathbf{c}(1) = J_0(2\pi f_D T_1) \check{\mathbf{c}}(0) + \check{\mathbf{c}}(1) \\ \vdots \\ \mathbf{c}(n) = \sum_{k=0}^n J_0(2\pi f_D T_k) \check{\mathbf{c}}(n-k) \end{cases} \quad (\text{D.3})$$

The norm of the process noise  $\check{\mathbf{c}}(n)$  is such that the norm of  $\mathbf{c}(n)$  is dependent of  $n$ : in the framework of this thesis, it is assumed without loss of generality  $E[\mathbf{c}^H(n)\mathbf{c}(n)] = 1$ . The corresponding filter is illustrated in Fig.D.2.

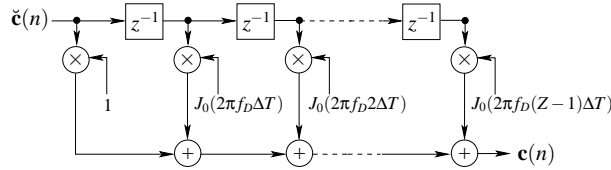


Figure D.2: MA Doppler model.

Since the Pseudo Random Postfix OFDM modulation provides means for channel tracking even at high Doppler frequencies, the Doppler model applied throughout this paper is based on the MA model presented before, conveniently rewritten as follows:

$$\mathbf{c}(n) = \sum_{k=0}^n J_0(2\pi f_D T_k) \check{\mathbf{c}}(n-k). \quad (\text{D.4})$$

with  $\check{\mathbf{c}}(k) = \mathbf{0}$  for  $k < 0$ . Similar to Kalman filter theory [104], so-called process-noise vectors  $\check{\mathbf{c}}(n)$  are introduced with  $E[\check{\mathbf{c}}(n)\check{\mathbf{c}}^H(k)] = \mathbf{0}$  for  $n \neq k$  and  $\check{\mathbf{c}}(0) = \mathbf{c}(0)$ . They represent the evolution of the CIR in time. This representation directly follows from Jake's model (see above) and is very suitable for high mobility WLAN environments. Please note that (contrary to the AR model), (D.4) is *not* compatible with the standard Kalman filter process equation, usually expressed as [104] (note that a Kalman filter can be derived for a general AR-MA model):

$$\mathbf{c}(n) = \mathbf{F}(n, n-1)\mathbf{c}(n-1) + \check{\mathbf{c}}(n).$$

$\mathbf{F}(n, n-1)$  is the transition matrix and  $\check{\mathbf{c}}(n)$  is the so-called process noise which is i.i.d. and Gaussian. Thus, a MMSE estimator of  $\mathbf{c}(0)$  based on noisy observations

$$\bar{\mathbf{c}}(n) = \mathbf{c}(n) + \mathbf{n}(n), n = 0, \dots, N-1 \quad (\text{D.5})$$

is complex to handle by Kalman filters contrary to the example shown by [107] for the AR model. A feasible (but complex) solution is to express the MA filter by the corresponding equivalent AR model (of infinite order), to truncate it and to derive the Kalman filter based on this approximation [143]. More suitable alternative solutions are discussed in chapter 3 of this thesis. There, the simulation section illustrates the limited validity of the different modeling approach.

## Appendix E

# Permutation product theorem for correlation and channel matrices

This section proves in the context of time synchronization refinement the product of the circulant channel matrix by the correlation matrix is merely commutative up to a transpose operator:

**Proposition:** Given a  $P \times P$   $J$ -circulant correlation matrix  $\mathbf{M}_J$  as defined by (5.6)

$$\mathbf{M}_J = \begin{bmatrix} p_0 & p_1 & \cdots & p_{D-1} & 0 & \rightarrow & \rightarrow & 0 \\ p_1 & & \nearrow & & & & & p_0 \\ \vdots & \nearrow & & & & & & \vdots \\ p_{D-1} & & & & & & & p_{D-2} \\ 0 & & & & & & & p_{D-1} \\ 0 & & & & & & \nearrow & 0 \\ 0 & & & & & \nearrow & \nearrow & 0 \\ \downarrow & & & & \nearrow & \nearrow & \nearrow & \downarrow \\ 0 & p_0 & \cdots & p_{D-2} & p_{D-1} & 0 & \rightarrow & 0 \end{bmatrix}$$

and a  $P \times P$  circulant convolution matrix  $\mathbf{C}_{\text{CIRC}}(P)$ , the following expression holds:

$$\mathbf{M}_J \mathbf{C}_{\text{CIRC}}(P) = \mathbf{H}_{\text{CIRC}}^T(P) \mathbf{M}_J.$$

**Proof:**  $\mathbf{M}_J$  and  $\mathbf{C}_{\text{CIRC}}(P)$  are diagonalized as

$$\mathbf{M}_J = \mathbf{F}_P \mathbf{D}_J \mathbf{F}_P, \mathbf{C}_{\text{CIRC}}(P) = \mathbf{F}_P^H \mathbf{D}_H \mathbf{F}_P$$

where  $\mathbf{D}_J$  and  $\mathbf{D}_H$  are diagonal matrices. Thus,

$$\begin{aligned} \mathbf{M}_J \mathbf{C}_{\text{CIRC}}(P) &= \mathbf{F}_P \mathbf{D}_H \mathbf{D}_J \mathbf{F}_P = \mathbf{F}_P \mathbf{D}_H \mathbf{F}_P^H \mathbf{M}_J \\ &= \mathbf{F}_P \mathbf{F}_P \mathbf{C}_{\text{CIRC}}(P) \mathbf{F}_P^H \mathbf{F}_P^H \mathbf{M}_J \\ &= \mathbf{P} \mathbf{C}_{\text{CIRC}}(P) \mathbf{P} \mathbf{M}_J = \mathbf{H}_{\text{CIRC}}^T(P) \mathbf{M}_J, \end{aligned}$$

where  $\mathbf{P}$  is the permutation matrix with  $[\mathbf{P}]_{n, \text{modulo}(N-n, N)} = 1, n = 0, \dots, N-1$  and zero otherwise. Q.E.D.



## Appendix F

# Complex derivation

This chapter recalls some useful rules on derivatives with respect to a complex matrix. In particular, the derivation of the *trace* of a matrix expression is discussed, since the corresponding result is often used throughout the document.

As proposed in [104, 139, 144], we define the partial derivatives of a scalar function  $J(\mathbf{X})$  with respect to a complex matrix  $\mathbf{X}$  as follows:

$$\begin{aligned} \left[ \frac{\partial J(\mathbf{X})}{\partial \mathbf{X}} \right]_{kl} &:= \frac{1}{2} \left[ \frac{\partial J(\mathbf{X})}{\partial x_{kl}^{\text{Re}}} - j \frac{\partial J(\mathbf{X})}{\partial x_{kl}^{\text{Im}}} \right] \\ \left[ \frac{\partial J(\mathbf{X})}{\partial \mathbf{X}^*} \right]_{kl} &:= \frac{1}{2} \left[ \frac{\partial J(\mathbf{X})}{\partial x_{kl}^{\text{Re}}} + j \frac{\partial J(\mathbf{X})}{\partial x_{kl}^{\text{Im}}} \right] \end{aligned}$$

with  $\mathbf{x} = [x_{kl}]_{\forall k, \forall l}$  with  $x_{kl} := x_{kl}^{\text{Re}} + jx_{kl}^{\text{Im}}$ .

The complex gradient can be defined as proposed in [104, 145]:

$$\nabla J(\mathbf{X}) := 2 \frac{\partial}{\partial \mathbf{X}^*} J(\mathbf{X}) \tag{F.1}$$

As detailed in [104], cost functions as they occur in an engineering context are often not *holomorph* (or *analytic*). A differential algebra adapted to *non-holomorph* functions has been proposed by [146]. The upper definitions are in accordance with these results.

Useful partial derivatives with respect to  $\mathbf{X}^*$  are presented in the following with  $\tau(\mathbf{X})$  denoting the trace of matrix  $\mathbf{X}$  [139]:

$$\frac{\partial}{\partial \mathbf{X}^*} \tau(\mathbf{X}) = \mathbf{0} \quad (\text{F.2})$$

$$\frac{\partial}{\partial \mathbf{X}^*} \tau(\mathbf{X}^H) = \mathbf{I} \quad (\text{F.3})$$

$$\frac{\partial}{\partial \mathbf{X}^*} \tau(\mathbf{A}\mathbf{X}^H\mathbf{B}) = \mathbf{B}\mathbf{A} \quad (\text{F.4})$$

$$\frac{\partial}{\partial \mathbf{X}^*} \tau(\mathbf{A}\mathbf{X}^*\mathbf{B}) = \mathbf{A}^T\mathbf{B}^T \quad (\text{F.5})$$

$$\frac{\partial}{\partial \mathbf{X}^*} \tau(\mathbf{A}\mathbf{X}\mathbf{B}) = \mathbf{0} \quad (\text{F.6})$$

$$\frac{\partial}{\partial \mathbf{X}^*} \tau(\mathbf{X}^k) = \mathbf{0} \quad (\text{F.7})$$

$$\frac{\partial}{\partial \mathbf{X}^*} \tau((\mathbf{X}^H)^k) = k(\mathbf{X}^H)^{k-1} \quad (\text{F.8})$$

$$\frac{\partial}{\partial \mathbf{X}^*} \tau(\mathbf{X}^H\mathbf{A}\mathbf{X}\mathbf{B}) = \mathbf{A}\mathbf{X}\mathbf{B} \quad (\text{F.9})$$

$$\frac{\partial}{\partial \mathbf{X}^*} \tau(\mathbf{X}^H\mathbf{A}\mathbf{X}^H\mathbf{B}) = \mathbf{A}\mathbf{X}^H\mathbf{B} + \mathbf{B}\mathbf{X}^H\mathbf{A} \quad (\text{F.10})$$

$$\frac{\partial}{\partial \mathbf{X}^*} \tau(\mathbf{X}^{-1}) = \mathbf{0} \quad (\text{F.11})$$

$$\frac{\partial}{\partial \mathbf{X}^*} \tau(e^{\mathbf{X}}) = \mathbf{0} \quad (\text{F.12})$$

# List of Tables

1	Analyse des postfixes (16 échantillons postfix). . . . .	ix
2	Analyse des postfixes (32 échantillons postfix). . . . .	x
3	Analyse des postfixes (48 échantillons postfix). . . . .	x
2.1	Parameters of the 2Tx modes in 20MHz bandwidth (48 data subcarriers) . . . . .	21
2.2	Parameters of the 3Tx and 4Tx modes in 20MHz bandwidth (48 data subcarriers) . . . . .	21
3.1	Time domain samples of a suitable postfix. . . . .	43
4.1	Time domain samples of a suitable postfix (Kaiser Window, 16 samples). . . . .	66
4.2	Time domain samples of a suitable postfix (optimized 16 samples postfix). . . . .	70
4.3	Comparison on postfix trade-offs (16 samples postfix). . . . .	70
4.4	Time domain samples of a suitable postfix (Kaiser Window, 32 Samples). . . . .	71
4.5	Time domain samples of a suitable postfix (optimized 32 samples postfix). . . . .	71
4.6	Comparison on postfix trade-offs (32 samples postfix). . . . .	72
4.7	Time domain samples of a suitable postfix (Kaiser Window, 48 Samples). . . . .	72
4.8	Time domain samples of a suitable postfix (optimized 48 samples postfix). . . . .	73
4.9	Comparison on postfix trade-offs (48 samples postfix). . . . .	73
5.1	Time domain samples of a suitable postfix (low PAPR). . . . .	87
C.1	<i>The complexity of basic operations.</i> . . . . .	141

C.2	<i>The complexity of FFT operations.</i>	142
C.3	<i>Notations.</i>	142
C.4	<i>Generic Complexity Evaluation.</i>	143
C.5	<i>Numerical Examples on Complexity Evaluation.</i>	144

# List of Figures

1	Modèle discret du modulateur CP-OFDM. . . . .	iv
2	Modèle discret du modulateur ZP-OFDM. . . . .	iv
3	Modèle discret du modulateur PRP-OFDM. . . . .	v
4	Estimation du canal à latence minimale. . . . .	vi
5	Estimation du canal à erreur moyenne quadratique minimale. . . . .	vii
6	BER pour IEEE802.11a, BRAN canal A, QPSK. . . . .	vii
7	PER pour IEEE802.11a, BRAN canal A, QPSK. . . . .	vii
8	BER pour IEEE802.11a, BRAN canal A, QPSK. . . . .	viii
9	BER pour IEEE802.11a, BRAN canal A, MAQ-16. . . . .	viii
10	PER pour IEEE802.11a, BRAN canal A, MAQ-16. . . . .	viii
11	Différents postfixes en domaine temporel (16 échantillons). . . . .	xi
12	Différents postfixes en domaine fréquentiel (16 échantillons). . . . .	xi
13	Différents postfixes en domaine temporel (32 échantillons). . . . .	xii
14	Différents postfixes en domaine fréquentiel (32 échantillons). . . . .	xii
15	Différents postfixes en domaine temporel (48 échantillons). . . . .	xiii
16	Différents postfixes en domaine fréquentiel (48 échantillons). . . . .	xiii
17	Modèle discret du modulateur MTMR PRP-OFDM. . . . .	xv
18	BER pour IEEE802.11a, MIMO 2x1, BRAN canal A, QPSK. . . . .	xvi
19	PER pour IEEE802.11a, MIMO 2x1, BRAN canal A, QPSK. . . . .	xvi

20	BER pour IEEE802.11a, MIMO 2x1, BRAN canal A, MAQ-16, Doppler. . . . .	xvi
21	PER pour IEEE802.11a, MIMO 2x1, BRAN canal A, MAQ-16, Doppler. . . . .	xvi
22	Erreur moyenne quadratique du CIR pour MAQ-64, BRAN-A, C/I=24dB. . . . .	xviii
23	Exemple de l'optimisation du mapping des mots de code LDPC. . . . .	xix
24	BER pour code LDPC après optimisation, canal BRAN-A, 576 bits mot de code. . . . .	xix
25	PER pour code LDPC après optimisation, canal BRAN-A, 576 bits mot de code. . . . .	xix
2.1	Continuous CP-OFDM modulator. . . . .	7
2.2	Continuous PRP-OFDM modulator. . . . .	8
2.3	Illustration of the synthesis of $u(z)$ based on its polyphase components . . . . .	10
2.4	Equivalence between a linear scalar filter and the representation as polyphase sub-band filtering. . . . .	12
2.5	Illustration of Inter-Block-Interference. . . . .	13
2.6	Discrete model of the CP-OFDM transceiver. . . . .	14
2.7	Parallel frequency domain representation of CP-OFDM. . . . .	15
2.8	Discrete model of the PRP-OFDM transceiver. . . . .	16
2.9	Discrete model of the ZP-OFDM transceiver. . . . .	16
2.10	IEEE802.11n MITMOT transmitter architecture. . . . .	20
3.1	Discrete model of the PRP-OFDM transceiver. . . . .	24
3.2	Circularization for PRP-OFDM. . . . .	25
3.3	Postfixes with different trade-offs in frequency domain. . . . .	28
3.4	Illustration of channel extraction (representation in frequency domain). . . . .	28
3.5	Illustration of noise amplification by de-convolution (representation in frequency domain). . . . .	29
3.6	Received symbols exploited for channel estimation (minimum latency). . . . .	33
3.7	Received symbols exploited for channel estimation (increased latency). . . . .	34
3.8	Discrete model of the PRP-OFDM OLA demodulator. . . . .	42

---

3.9	MSE of CIR estimates in Doppler scenario, no mobility (channel power profile is assumed to be rectangular). . . . .	44
3.10	MSE of CIR estimates in Doppler scenario, no mobility (exact channel power profile is known). . . . .	44
3.11	MSE of CIR estimates in Doppler scenario, mobility 36m/s (channel power profile is assumed to be rectangular). . . . .	45
3.12	MSE of CIR estimates in Doppler scenario, mobility 36m/s (exact channel power profile is known). . . . .	45
3.13	MSE of CIR estimates in Doppler scenario, mobility 72m/s (channel power profile is assumed to be rectangular). . . . .	45
3.14	MSE of CIR estimates in Doppler scenario, mobility 72m/s (exact channel power profile is known). . . . .	45
3.15	BER for IEEE802.11a, BRAN channel model A, BPSK, different decoding approaches. . . . .	46
3.16	PER for IEEE802.11a, BRAN channel model A, BPSK, different decoding approaches. . . . .	46
3.17	BER for IEEE802.11a, BRAN channel model A, QPSK, different decoding approaches. . . . .	47
3.18	PER for IEEE802.11a, BRAN channel model A, QPSK, different decoding approaches. . . . .	47
3.19	BER for IEEE802.11a, BRAN channel model A, QPSK, different decoding approaches, Doppler environment. . . . .	47
3.20	PER for IEEE802.11a, BRAN channel model A, QPSK, different decoding approaches, Doppler environment. . . . .	47
3.21	BER for IEEE802.11a, BRAN channel model A, QAM16, different decoding approaches. . . . .	47
3.22	PER for IEEE802.11a, BRAN channel model A, QAM16, different decoding approaches. . . . .	47
3.23	BER for IEEE802.11a, BRAN channel model A, QAM16, different decoding approaches, Doppler environment. . . . .	48
3.24	PER for IEEE802.11a, BRAN channel model A, QAM16, different decoding approaches, Doppler environment. . . . .	48
3.25	BER for IEEE802.11a, BRAN channel model A, QAM64, different decoding approaches. . . . .	48
3.26	PER for IEEE802.11a, BRAN channel model A, QAM64, different decoding approaches. . . . .	48
3.27	BER for IEEE802.11a, BRAN channel model C, BPSK, different decoding approaches. . . . .	49
3.28	PER for IEEE802.11a, BRAN channel model C, BPSK, different decoding approaches. . . . .	49
3.29	BER for IEEE802.11a, BRAN channel model C, QPSK, different decoding approaches. . . . .	49

3.30	PER for IEEE802.11a, BRAN channel model C, QPSK, different decoding approaches. . . . .	49
3.31	BER for IEEE802.11a, BRAN channel model C, QPSK, different decoding approaches, Doppler environment. . . . .	50
3.32	PER for IEEE802.11a, BRAN channel model C, QPSK, different decoding approaches, Doppler environment. . . . .	50
3.33	BER for IEEE802.11a, BRAN channel model C, QPSK, different decoding approaches, Doppler environment. . . . .	50
3.34	PER for IEEE802.11a, BRAN channel model C, QPSK, different decoding approaches, Doppler environment. . . . .	50
3.35	BER for IEEE802.11a, BRAN channel model C, QAM16, different decoding approaches. . . . .	50
3.36	PER for IEEE802.11a, BRAN channel model C, QAM16, different decoding approaches. . . . .	50
3.37	BER for IEEE802.11a, BRAN channel model C, QAM16, different decoding approaches, Doppler environment. . . . .	51
3.38	PER for IEEE802.11a, BRAN channel model C, QAM16, different decoding approaches, Doppler environment. . . . .	51
3.39	BER for IEEE802.11a, BRAN channel model C, QAM64, different decoding approaches. . . . .	51
3.40	PER for IEEE802.11a, BRAN channel model C, QAM64, different decoding approaches. . . . .	51
3.41	BER for IEEE802.11a, BRAN channel model E, BPSK, different decoding approaches. . . . .	52
3.42	PER for IEEE802.11a, BRAN channel model E, BPSK, different decoding approaches. . . . .	52
3.43	BER for IEEE802.11a, BRAN channel model E, QPSK, different decoding approaches. . . . .	52
3.44	PER for IEEE802.11a, BRAN channel model E, QPSK, different decoding approaches. . . . .	52
3.45	BER for IEEE802.11a, BRAN channel model E, QPSK, different decoding approaches, Doppler environment. . . . .	53
3.46	PER for IEEE802.11a, BRAN channel model E, QPSK, different decoding approaches, Doppler environment. . . . .	53
3.47	BER for IEEE802.11a, BRAN channel model E, QAM16, different decoding approaches. . . . .	53
3.48	PER for IEEE802.11a, BRAN channel model E, QAM16, different decoding approaches. . . . .	53
3.49	BER for IEEE802.11a, BRAN channel model E, QAM16, different decoding approaches, Doppler environment. . . . .	53

---

3.50	PER for IEEE802.11a, BRAN channel model E, QAM16, different decoding approaches, Doppler environment. . . . .	53
3.51	BER for IEEE802.11a, BRAN channel model E, QAM64, different decoding approaches. . . . .	54
3.52	PER for IEEE802.11a, BRAN channel model E, QAM64, different decoding approaches. . . . .	54
3.53	BER for IEEE802.11a, BRAN channel model A uncoded, BPSK, different decoding approaches. . . . .	55
3.54	PER for IEEE802.11a, BRAN channel model A uncoded, BPSK, different decoding approaches. . . . .	55
3.55	BER for IEEE802.11a, BRAN channel model A uncoded, QPSK, different decoding approaches. . . . .	55
3.56	PER for IEEE802.11a, BRAN channel model A uncoded, QPSK, different decoding approaches. . . . .	55
3.57	BER for IEEE802.11a, BRAN channel model A uncoded, QAM16, different decoding approaches. . . . .	55
3.58	PER for IEEE802.11a, BRAN channel model A uncoded, QAM16, different decoding approaches. . . . .	55
4.1	Discrete model of the PRP-OFDM modulator. . . . .	58
4.2	Transmission Spectrum Mask of IEEE802.11a. . . . .	60
4.3	Time Domain Signal generation by means of an IFFT for IEEE802.11a. . . . .	60
4.4	A typical transmitter implementation of IEEE802.11a. . . . .	62
4.5	Postfixes with different trade-offs in time domain (16 samples). . . . .	67
4.6	Postfixes with different trade-offs in frequency domain (16 samples). . . . .	67
4.7	Postfixes with different trade-offs in time domain (32 samples). . . . .	68
4.8	Postfixes with different trade-offs in frequency domain (32 samples). . . . .	68
4.9	Postfixes with different trade-offs in time domain (48 samples). . . . .	69
4.10	Postfixes with different trade-offs in frequency domain (48 samples). . . . .	69
5.1	Illustration of FS refinement (1). . . . .	83
5.2	Illustration of FS refinement (2). . . . .	84
5.3	Synchronization offset probabilities. . . . .	87
5.4	Example: mean estimated frequency offset. . . . .	88

5.5	Example: standard deviation of the mean estimated frequency offset. . . . .	88
6.1	Discrete model of the MTMR PRP-OFDM modulator. . . . .	90
6.2	BER for IEEE802.11a, MIMO 2x1, BRAN channel model A, BPSK, different decoding approaches. 102	
6.3	PER for IEEE802.11a, MIMO 2x1, BRAN channel model A, BPSK, different decoding approaches. 102	
6.4	BER for IEEE802.11a, MIMO 2x1, BRAN channel model A, QPSK, different decoding approaches. 102	
6.5	PER for IEEE802.11a, MIMO 2x1, BRAN channel model A, QPSK, different decoding approaches. 102	
6.6	BER for IEEE802.11a, MIMO 2x1, BRAN channel model A, QAM16, different decoding approaches, Doppler environment. . . . .	103
6.7	PER for IEEE802.11a, MIMO 2x1, BRAN channel model A, QAM16, different decoding approaches, Doppler environment. . . . .	103
6.8	BER for IEEE802.11a, MIMO 2x1, BRAN channel model A, QAM64, different decoding approaches, Doppler environment. . . . .	103
6.9	PER for IEEE802.11a, MIMO 2x1, BRAN channel model A, QAM64, different decoding approaches, Doppler environment. . . . .	103
7.1	CIR MSE for 64QAM, BRAN-A, C/I=24dB. . . . .	113
7.2	BER for IEEE802.11a, BRAN channel model A, QAM64, iterative interference cancellation. . .	114
7.3	PER for IEEE802.11a, BRAN channel model A, QAM64, iterative interference cancellation. . .	114
7.4	BER for IEEE802.11a, BRAN channel model A, QAM16, iterative interference cancellation. . .	114
7.5	PER for IEEE802.11a, BRAN channel model A, QAM16, iterative interference cancellation. . .	114
7.6	BER for IEEE802.11a, BRAN channel model A, QPSK, iterative interference cancellation. . . .	115
7.7	PER for IEEE802.11a, BRAN channel model A, QPSK, iterative interference cancellation. . . .	115
7.8	BER for IEEE802.11a, 36m/s, BRAN channel model A, QPSK, iterative interference cancellation. 115	
7.9	PER for IEEE802.11a, 36m/s, BRAN channel model A, QPSK, iterative interference cancellation. 115	
7.10	BER for IEEE802.11a, 72m/s, BRAN channel model A, QPSK, iterative interference cancellation. 115	
7.11	PER for IEEE802.11a, 72m/s, BRAN channel model A, QPSK, iterative interference cancellation. 115	

---

8.1	Example of a factor graph. . . . .	120
8.2	Example of LDPC code-word assignment. . . . .	129
8.3	LDPC column weights, 576 bits code-word. . . . .	131
8.4	BER for LDPC code performance after optimization, channel BRAN-A, 576 bits code-word. . .	132
8.5	PER for LDPC code performance after optimization, channel BRAN-A, 576 bits code-word. . .	132
8.6	BER for LDPC code performance after different optimization approaches (including circular rotation), channel BRAN-A, 576 bits code-word. . . . .	132
8.7	PER for LDPC code performance after different optimization approaches (including circular rotation), channel BRAN-A, 576 bits code-word. . . . .	132
D.1	Order one AR Doppler model. . . . .	146
D.2	MA Doppler model. . . . .	147







---

# Bibliography

- [1] Markus Muck, Marc de Courville, and Pierre Duhamel. A Pseudorandom Postfix OFDM modulator - Semi-blind channel estimation and equalization. *IEEE Transactions on Signal Processing*, 54(3):1005–1017, March 2006.
- [2] Markus Muck, Marc de Courville, and Pierre Duhamel. Synchronization Refinement in the context of the Pseudo Random Postfix OFDM modulation scheme. *Submitted to IEEE Transactions on Wireless Communications, 2006*.
- [3] M. Muck, M. de Courville, and M. Debbah. Pseudo Random Postfix OFDM based modulator for next generation 60GHz WLANs. In *Proceedings of the Mobile IST Summit*, Aveiro, Portugal, June 2003.
- [4] Markus Muck, Marc de Courville, Merouane Debbah, and Pierre Duhamel. A Pseudo Random Postfix OFDM modulator and inherent channel estimation techniques. In *GLOBECOM conference records*, San Francisco, USA, December 2003.
- [5] Markus Muck, Alexandre Ribeiro Dias, Marc de Courville, and Pierre Duhamel. A Pseudo Random Postfix OFDM based modulator for multiple antennae systems. In *Proceedings of the Int. Conf. on Communications*, 2004.
- [6] Markus Muck, Marc De Courville, and Pierre Duhamel. Postfix Design for Pseudo Random Postfix OFDM Modulators. In *9th International OFDM Workshop*, Dresden, Gemany, September 2004.
- [7] Kai-Uwe Schmidt, Markus Muck, Jens Schoenthier, and Marc de Courville. Time or Frequency Domain Pilots for Channel Tracking in Wireless OFDM Systems? In *International OFDM Workshop*, Dresden, Germany, September 2004.
- [8] Markus Muck, Marc de Courville, Xavier Miet, and Pierre Duhamel. Iterative Interference Suppression for Pseudo Random Postfix OFDM based Channel Estimation. In *IEEE International Conference on Acoustics, Speech, and Signal Processing*, Philadelphia, USA, March 2005.
- [9] M. Muck and J. P. Javaudin. Advanced OFDM Modulators considered in the IST-WINNER framework for future wireless systems. In *Proceedings of the Mobile IST Summit*, Dresden, Germany, June 2005.
- [10] Markus Muck, Laurent Mazet, and Marc de Courville. Pseudo Random Postfix OFDM based channel estimation in a Doppler scenario. In *Proceedings of the Mobile IST Summit*, Dresden, Germany, June 2005.

- [11] Markus Muck, Philippe Bernardin, Patrick Labé, Xavier Miet, Dirk Pannicke, and Jens Schönthier. Prototyping of a hybrid 5GHz/60GHz OFDM WLAN system in the framework of IST-BroadWay. In *Proceedings of the Mobile IST Summit*, Dresden, Germany, June 2005.
- [12] Markus Muck, Xavier Miet, Marc de Courville, and Pierre Duhamel. A Successive Minimum-Mean-Square-Error OFDM-Data-Symbol Cancellation Scheme for Channel Estimation in the Pseudo-Random-Postfix OFDM Context. In *Defensive Publication*. Patent Database, 2004.
- [13] David Falconer, Stefan Kaiser, Marc De Courville, Rui Dinis, Jean-Philippe Javaudin, Tad Matsumoto, Markus Muck, and Arne Svensson. WWRF Working Group 4 White Paper: Broadband Frequency Domain-Based Air-Interfaces for Future-Generation Wireless Systems. In *Wireless World Research Forum, 13th meeting*, Jeju Island, Korea, March 2005.
- [14] Patrick Labbé, Markus Muck, Jens Schoentier, Dirk Pannicke, Konstantinos Ntagkounakis, and Emil Entchev. Final project report, IST-2001-32686 BroadWay project. Technical report, IST-BROADWAY project, IST-2001-32686, available at <http://www.ist-broadway.org>, 2005.
- [15] Markus Muck, Jens Schoentier, and Dirk Pannicke. Final BroadWay Base-Band Description and Evaluation, IST-2001-32686 BroadWay project. Technical report, IST-BROADWAY project, IST-2001-32686, available at <http://www.ist-broadway.org>, 2005.
- [16] Patrick Labbé, Jérémy Gosteau, Markus Muck, and Joerg Pamp. Evaluation and verification of the micro and macro diversity concepts for 60GHz type of applications, Release II, IST-2001-32686 BroadWay project. Technical report, IST-BROADWAY project, IST-2001-32686, available at <http://www.ist-broadway.org>, 2005.
- [17] Jens Schoentier, Markus Muck, Konstantinos Ntagkounakis, and Emil Entchev. Demonstration of key system elements, Release II, IST-2001-32686 BroadWay project. Technical report, IST-BROADWAY project, IST-2001-32686, available at <http://www.ist-broadway.org>, 2005.
- [18] Markus Muck, Dirk Pannicke, Jens Schoentier, and Jochen Ertel. Extended Baseband Algorithms Implementation and Test Results Document, IST-2001-32686 BroadWay project. Technical report, IST-BROADWAY project, IST-2001-32686, available at <http://www.ist-broadway.org>, 2004.
- [19] Markus Muck, Jens Schoentier, Kai-Uwe Schmidt, and Michael Benedix. Algorithm Enhancement Definition, Release III, IST-2001-32686 BroadWay project. Technical report, IST-BROADWAY project, IST-2001-32686, available at <http://www.ist-broadway.org>, 2004.
- [20] Markus Muck, Jens Schoentier, Sven Zeisberg, Veronique Buzenac-Settineri, Sebastien Simoens, Laurent Mazet, and Marc de Courville. BroadWay Baseband Requirements, IST-2001-32686 BroadWay project. Technical report, IST-BROADWAY project, IST-2001-32686, available at <http://www.ist-broadway.org>, 2005.
- [21] Auer G., Bogucka H., Bonnet J., Costa E., Falahati S., Falconer D., Galda D., Hamon M.-H., Javaudin J.-P., Kansanen K., Klang G., Langowski A., Lestable T., Li Z., Muck M., Nyström J., Piatyszek A., Richter G., Sternad M., Tujkovic D., Tyczka P., Wesolowski K., Teng Y., and Zimmermann E. Deliberable D2.1: Identification of Radio-Link Technologies. Technical report, IST-WINNER project, IST-2003-507581, available at <http://www.ist-winner.org>, 2004.
- [22] Gunther Auer, David Bateman, Jérôme Bonnet, David Falconer, Jean-Philippe Javaudin, Markus Muck, Gerd Richter, Andreas Saul, Sandro Sital, Krzysztof Wesolowski, and Janusz Pochmara.

- Deliverable D2.2: Feasibility of Multi-Bandwidth Transmissions. Technical report, IST-WINNER project, IST-2003-507581, available at <http://www.ist-winner.org>, 2004.
- [23] Gunther Auer, Jérôme Bonnet, Elena Costa, Zbigniew Dlugaszewski, David Falconer, Rainer Grünheid, Marie-Hélène Hamon, Jean-Philippe Javaudin, Kimmo Kansanen, Göran Klang, Chan Tong Lam, Jouko Leinonen, Thierry Lestable, Zexian Li, Benjamin Ng, Markus Muck, Stephan Stiglmayr, Maryam Sabbaghian, Yong Teng, Nenad Veselinovic, Krzysztof Wesolowski, and Ernesto Zimmermann. Deliverable D2.3: Assessment of Radio-link technologies. Technical report, IST-WINNER project, IST-2003-507581, available at <http://www.ist-winner.org>, 2005.
- [24] Angeliki Alexiou, Gunther Auer, Johan Axnäs, David Bateman, Mats Bengtsson, Ting Chen, Pedro Coronel, Elena Costa, Martin Döttling, Sorour Falahati, David Falconer, Gharavi Leila, Reiner Grünheid, Martin Haardt, Jean-Philippe Javaudin, Niklas Johansson, Volker Jungnickel, Ateet Kapur, Juha Karjalainen, Thanh Tung Kim, Ole Klein, Patrick Labbé, Jouko Leinonen, Thierry Lestable, Zexian Li, Geneviève Mange, Abdelkader Medles, Markus Muck, Sebastian Obermanns, Pirjo Pasanen, Adam Piatyszek, Stéphanie Rouquette-Léveil, Thomas Sälzer, Wolfgang Schott, Sandro Sital, Per Skillermark, Anti Sorri, Veljko Stankovic, Mikael Sternad, Kai-Erik Sunell, Tommy Svensson, Yong Teng, Samuli Visuri, Krzysztof Wesolowski, Thorsten Wild, and Ernesto Zimmermann. Deliverable D2.9: Implementation Impact of Candidate Key Technologies. Technical report, IST-WINNER project, IST-2003-507581, available at <http://www.ist-winner.org>, 2005.
- [25] Marten Sundberg. Pseudo random postfix (prp) ofdm. Technical report, Ericsson Research and Department of Signals and Systems at Uppsala University, 2005.
- [26] Yi Ma, Na Yi, and Rahim Tafazolli. Channel Estimation for PRP-OFDM in Slowly Time-Varying Channel: First-Order or Second-Order Statistics ? *IEEE Signal Processing Letters*, to appear, 2006.
- [27] Markus Muck, Stéphanie Rouquette-Léveil, and Marc de Courville. Reconfigurable Low Density Parity Check (LDPC) Code Interleaving for OFDM. In *Submitted to the IST Mobile Wireless and Communication Summit Conference*, Greece, June 2006.
- [28] Markus Muck, Stéphanie Rouquette-Léveil, and Marc de Courville. Reconfigurable Low Density Parity Check (LDPC) Code Interleaving for SISO and MIMO OFDM Systems. In *Submitted to the IEEE International Workshop on Signal Processing Advances for Wireless Communications (SPAWC)*, Cannes, France, June 2006.
- [29] M. de Courville, S. Zeisberg, Markus Muck, and J. Schönthier. BroadWay: the Way to Broadband Access at 60GHz. In *International Conference on Telecommunications*, Beijing, China, June 2002.
- [30] W. Mohr, L. Hiebinger, J. von Häfen, E. M. Diaz, P. Gelpi, T. Jämsä, G. Malmgren, P. Ojanen, and D. C. Schultz. The WINNER project: Research for new radio interfaces for better mobile services. In *Proceedings of the Mobile IST Summit*, Lyon, France, June 2004.
- [31] Sean Coffey and Adrian Stephens and Markus Muck and Marc de Courville and Stéphanie Rouquette-Léveil and Jean-Noël Patillon et al. Joint Proposal: High throughput extension to the 802.11 Standard: PHY, IEEE 802.11-05/1102r2. Standard Proposal, IEEE Standards Department, Vancouver, Canada, November 2005.

- [32] Sean Coffey and Adrian Stephens and Markus Muck and Marc de Courville and Stéphanie Rouquette-Léveil and Jean-Noël Patillon et al. Joint Proposal: High throughput extension to the 802.11 Standard: MAC, IEEE 802.11-05/1095r2. Standard Proposal, IEEE Standards Department, Vancouver, Canada, November 2005.
- [33] Markus Muck, Marc de Courville, Stéphanie Rouquette-Léveil, Jean-Noël Patillon, Sebastien Simoens, Alexandre Ribeiro Dias, Karine Gosse, Brian Classon, Keith Blankenship. Full proposal for IEEE802.11n: Mac and mImo Techniques for MOre Throughput, detailed specification, IEEE802.11-04/1372r4. Standard Proposal, IEEE Standards Department, Monterey, California, USA, January 2005.
- [34] Markus Muck, Marc de Courville, Stéphanie Rouquette-Léveil, Jean-Noël Patillon, Sebastien Simoens, Alexandre Ribeiro Dias, Karine Gosse, Brian Classon, Keith Blankenship. Full proposal for IEEE802.11n: Mac and mImo Techniques for MOre Throughput, functional requirements, IEEE802.11-04/01370r2. Standard Proposal, IEEE Standards Department, Monterey, California, USA, January 2005.
- [35] Markus Muck, Marc de Courville, Stéphanie Rouquette-Léveil, Jean-Noël Patillon, Sebastien Simoens, Alexandre Ribeiro Dias, Karine Gosse, Brian Classon, Keith Blankenship. Full proposal for IEEE802.11n: Mac and mImo Techniques for MOre Throughput, simulation results, IEEE802.11-04/1371r1. Standard Proposal, IEEE Standards Department, Monterey, California, USA, January 2005.
- [36] Markus Muck, Marc de Courville, Stéphanie Rouquette-Léveil, Jean-Noël Patillon, Sebastien Simoens, Alexandre Ribeiro Dias, Karine Gosse, Brian Classon, Keith Blankenship. Full proposal for IEEE802.11n: Mac and mImo Techniques for MOre Throughput, presentation, IEEE802.11-04/1369r7. Standard Proposal, IEEE Standards Department, Monterey, California, USA, January 2005.
- [37] ETSI Normalization Committee. Channel Models for HIPERLAN/2 in different indoor scenarios. Norme ETSI, document 3ERI085B, European Telecommunications Standards Institute, Sophia-Antipolis, Valbonne, France, 1998.
- [38] T. M. Schmidl and Donald C. Cox. Robust Frequency and Timing Synchronization for OFDM. *IEEE Trans. on Communications*, 45, December 1997.
- [39] Bertrand Muquet. *Novel receiver and decoding schemes for wireless OFDM systems with cyclic prefix or zero padding*. PhD thesis, Motorola Labs Paris and École Nationale Supérieure des Télécommunications, September 2001.
- [40] B. Muquet, Z. Wang, G. B. Giannakis, M. de Courville, and P. Duhamel. Cyclic Prefixing or Zero Padding for Wireless Multicarrier Transmissions ? *IEEE Trans. on Communications*, December 2002.
- [41] Syed Aon Mujtaba et al. TGnSync IEEE 802.11n Proposal, IEEE 802.11-04/0889r6. IEEE, USA, 2005. available at <http://www.tgnsync.org>.
- [42] J.M. Cioffi, G.P. Dudevoir, M.V. Eyuboglu, and G.D. Forney. MMSE decision feedback equalizers and coding- Part I: equalization results. *IEEE Trans. on Communications*, pages 2582–2594, October 1995.

- [43] J.M. Cioffi, G.P. Dudevoir, M.V. Eyuboglu, and G.D. Forney. MMSE decision feedback equalizers and coding- Part II: coding results. *IEEE Trans. on Communications*, pages 2595–2604, October 1995.
- [44] S. Verdú. *Multiuser Detection*. Cambridge University Press, 1998.
- [45] R. W. Chang. Synthesis of band-limited orthogonal signals for multichannel data transmission. *Bell Sys. Tech. Journal*, 45, December 1966.
- [46] Yao Xiao. Master's thesis. *Louisiana State University*, 2001.
- [47] S. B. Weinstein and P. M. Ebert. Data Transmission by Frequency-Division Multiplexing using the Discrete Fourier Transform. *IEEE Trans. on Communications*, 19(5):628–634, October 1971.
- [48] A. Peled and A. Ruiz. Frequency Domain Data Transmission using Reduced Computational Complexity Algorithms. In *IEEE International Conference on Acoustics, Speech, and Signal Processing*, pages 964–967, Denver, USA, April 1980.
- [49] B. Hirosaki. An Analysis of Automatic Equalizers for Orthogonally Multiplexed QAM Systems. *IEEE Trans. on Communications*, 28(1):73–83, January 1980.
- [50] L. J. Cimini. Analysis and simulation of a digital mobile channel using orthogonal frequency division multiple access multiplexing. *IEEE Transactions on Communications*, pages 665–675, 1985.
- [51] M. Alard and R. Lassale. Principles of Modulation and Channel Coding for Digital Broadcasting for Mobile Receivers. *European Broadcasting Union Review Technical*, 224:168–190, August 1987.
- [52] I. Kalet. The Multitone Channel. *IEEE Trans. on Communications*, 37:119–124, February 1989.
- [53] ANSI T1E1.4 Committee Contribution. The DWMT: a multicarrier transceiver for ADSL using M-band wavelets. Technical report, ANSI, March 1993.
- [54] ETSI Normalization Committee. Radio Broadcasting Systems, Digital Audio Broadcasting (DAB) to mobile, portable and fixed receivers. Norme ETSI, document ETS 300 401, European Telecommunications Standards Institute, Sophia-Antipolis, Valbonne, France, 1995–1997.
- [55] ETSI Normalization Committee. Digital Broadcasting Systems for Television, Sound and Data Services; Framing Structure, Channel Coding and Modulation for Digital Terrestrial Television. Norme ETSI, document pr ETS 300 744, European Telecommunications Standards Institute, Sophia-Antipolis, Valbonne, France, 1996.
- [56] IEEE 802.11a. Part 11: Wireless LAN Medium Access Control (MAC) and Physical Layer specifications (PHY) - High Speed Physical Layer in the 5GHz band. IEEE Std 802.11a-1999, IEEE Standards Department, New York, January 1999.
- [57] Broadband Radio Access Networks (BRAN). " High Performance Radio Local Area Network - Type 2; System Overview ". Technical Report 101683, ETSI, October 1999.
- [58] Sean Coffey et al. WWiSE IEEE 802.11n Proposal, IEEE 802.11-05/0150r1. Atlanta IEEE plenary meeting, USA, March 2005. available at <http://www.wwise.org/>.

- [59] Marc de Courville. *Utilisation de bases orthogonales pour l'algorithmique adaptative et l'égalisation des systèmes multiporteuses*. PhD thesis, École Nationale Supérieure des Télécommunications, October 1996.
- [60] S. Kaiser. Trade-Off between Channel Coding and Spreading in Multi-Carrier CDMA. In *IEEE Spread Spectrum Techniques And Applications Proceedings*, volume 3, pages 1366–1370, 4th International Symposium, 1996.
- [61] Mérouane Debbah. *Linear Precoders for Wireless Communications*. PhD thesis, Motorola Labs Paris and Université de Marne la Vallée, September 2002.
- [62] H. Rohling, K. Brüninghaus, and R. Grünheid. Comparison of Multiple Access Schemes for an OFDM Downlink System. In K. Fazel and G. P. Fettweis, editors, *Multi-Carrier Spread Spectrum*, pages 23–30. Kluwer Academix Publishers, Norwell, MA 02061, USA, 1997.
- [63] M. Schnell and S. Kaiser. Diversity considerations for mc-cdma systems in mobile communications. In *International Symposium on Spread Spectrum Techniques & Applications*, pages 131–135, Mainz, Germany, September 1996.
- [64] W.G. Teich, A. Bury, J. Egle, M. Nold, and J. Lindner. Iterative detection algorithms for extended MC-CDMA. In *IEEE Spread Spectrum Techniques And Applications Proceedings*, volume 1, pages 184–188, 5th International Symposium, 1998.
- [65] Jürgen Lindner. MC-CDMA and its Relation to General Multiuser/Multisubchannel Transmission Systems. In *International Symposium on Spread Spectrum Techniques & Applications*, pages 115–121, Mainz, Germany, September 1996.
- [66] H. Sari, Y. Levy, and G. Karam. Orthogonal Frequency-Division Multiple Access For The Return Channel On CATV Networks. *International Conference on Telecommunications*, 1:52–57, April 1996.
- [67] K. S. Jacobsen, J. A. C. Bingham, and J. M. Cioffi. Synchronized DMT for multipoint-to-point communications on HFC networks. In *GLOBECOM conference records*, volume 2, pages 963–966, November 1995.
- [68] B. Le Floch, M. Alard, and C. Berrou. Coded orthogonal frequency division multiplex (TV broadcasting). *Proceedings of the IEEE*, 83(6):982–996, June 1995.
- [69] J. P. Javaudin, C. Dubuc, D. Lacroix, and M. Earnshaw. An OFDM Evolution to the UMTS High High Speed Download Packet Access. In *Proceedings of the IEEE Vehicular Technology Conference, Fall*, Los Angeles, USA, September 2004.
- [70] G.B. Giannakis. Filterbanks for blind channel identification and equalization. *IEEE Signal Processing Letters*, 4(6):184–187, June 1997.
- [71] A. Scaglione, G.B. Giannakis, and S. Barbarossa. Redundant filterbank precoders and equalizers - Part I: unification and optimal designs. *IEEE Trans. on Signal Processing*, 47:1988–2006, July 1999.
- [72] A. Scaglione, G.B. Giannakis, and S. Barbarossa. Redundant filterbank precoders and equalizers - Part II: blind channel estimation, synchronization and direct equalization. *IEEE Trans. on Signal Processing*, 47:2007–2022, July 1999.

- [73] Z. Wang and G.B. Giannakis. Wireless multicarrier communications: where Fourier meets Shannon. *IEEE Signal Processing Magazine*, 17:29–48, May 2000.
- [74] G. B. Giannakis. Filterbanks for blind channel identification and equalization . *IEEE Signal Processing Letters* , pages 184–187, June 1997.
- [75] B. Muquet, M. de Courville, P. Duhamel, and G.B. Giannakis. OFDM with Trailing Zeros versus OFDM with Cyclic Prefix: Links, Comparisons and Application to the HiperLAN/2 System. In *Proceedings of the Int. Conf. on Communications*, volume 2, pages 1049–1053, New-Orleans, USA, June 2000.
- [76] B. Muquet, M. de Courville, G.B. Giannakis, Z. Wang, and P. Duhamel. Reduced Complexity Equalizers for Zero-Padded OFDM transmissions. In *IEEE International Conference on Acoustics, Speech, and Signal Processing*, Istanbul, Turkey, June 2000.
- [77] L. Deneire, B. Gyselinckx, and M. Engels. Training Sequence versus Cyclic Prefix - A New Look on Single Carrier Communication . *IEEE Communication Letters* , July 2001.
- [78] R. Cendrillon and M. Moonen. Efficient Equalizers For Single And Multi-Carrier Environments With Known Symbol Padding. *International Symposium on Spread Spectrum Techniques & Applications*, August 2001.
- [79] M. de Courville and P. Duhamel. Une approche signal des systèmes multiporteuses OFDM. In Hermes, editor, *Traitement du signal pour les communications numériques*. Philippe Loubaton, Norwell, MA 02061, USA, 2004.
- [80] A. Akansu, P. Duhamel, X. Lin, and M. de Courville. Orthogonal Transmultiplexers in Communication : A Review. *IEEE Trans. on Signal Processing*, 46(4):979–995, April 1998.
- [81] P. P. Vaidyanathan. *Multirate Systems and Filter Banks*. Prentice Hall, Englewood Cliffs, New Jersey, USA, 1993.
- [82] ETSI Normalization Committee. Digital broadcasting systems for television, sound and data services; Framing structure, channel coding and modulation for 11/12 GHz satellite services,. Norme ETSI, document pr ETS 300 421, European Telecommunications Standards Institute, Sophia-Antipolis, Valbonne, France, 1994.
- [83] P. Hoehner, S. Kaiser, and P. Robertson. Pilot-symbol-aided channel estimation in time and frequency. *GLOBECOM Conference Records (Phoenix, USA)*, pages 90–96, November 1997.
- [84] J. K. Cavers. An Analysis of Pilot Symbol Assisted Modulation for Rayleigh Fading Channels. *IEEE Trans. on Veh. Technol.*, 40(4):686–693, November 1991.
- [85] S. Oho and G. B. Giannakis. Average Rate Optimal PSAM Transmissions Over Time-Selective Fading Channels. *IEEE Trans. on Wireless Communications*, 1(4):712–720, October 2002.
- [86] Ming-Xian Chang and Yu T. Su. Blind and Semiblind Detections of OFDM Signals in Fading Channels. *IEEE Trans. on Communications*, 52(5):744–754, May 2004.
- [87] Bertrand Muquet, Shengli Zhou, and Georgios B. Giannakis. Subspace-based Estimation of Frequency-Selective Channels for Space-Time Block Precoded Transmissions. In *11th IEEE Statistical Signal Processing Workshop*, Singapore, August 2001.

- [88] A.P. Petropulu, R. Zhang, and R. Lin. "Blind OFDM Channel Estimation through Simple Linear Precoding". *IEEE Transactions on Wireless Communications*, March 2004.
- [89] J. G. Proakis. *Digital Communications*. Mc Graw Hill, New York, USA, 3rd ed., 1995.
- [90] C. Berrou, C. Glavieux, and P. Thitimajshima. Near Shannon limit error-correcting coding and decoding: Turbo-codes. In *Proceedings of the Int. Conf. on Communications*, pages 1064–1070, Geneva, Switzerland, May 1993.
- [91] R.G. Gallager. *Low-Density Parity-Check Codes*. Cambridge, MA: MIT Press, 1963.
- [92] T. J. Richardson, M. A. Shokrollahi, and R. Urbanke. Design of Capacity-Approaching Irregular Low-Density Parity-Check Codes. *IEEE Transactions on Information Theory*, 47:619–637, 2001.
- [93] S.M. Alamouti. A Simple Transmit Diversity Technique for Wireless Communications. *IEEE Journal on Selected Areas in Communications*, 16(8):1451–1458, October 1998.
- [94] M. Moeneclaey. The Effect of Synchronisation Errors on the Performance of Orthogonal Frequency-Division Multiplexed (OFDM) Systems. In *Proceedings of COST254 Workshop on Emerging Techniques for Communication Terminals*, Toulouse, France, 1997.
- [95] T. M. Schmidl and D. C. Cox. Robust frequency and timing synchronization for OFDM. *IEEE Trans. on Communications*, 45(12):1613–1621, December 1997.
- [96] Paul H. Moose. A Technique for Orthogonal Frequency Division Multiplexing Frequency Offset Correction. *IEEE Trans. on Communications*, 42(10):2908–2914, October 1994.
- [97] M. Peeters T. Pollet. Synchronization with DMT Modulation. *IEEE Communications Magazine*, 37(4), April 1999.
- [98] Jan-Jaap van de Beek, Magnus Sandell, and Per Ola Borgesson. ML Estimation of Time and Frequency Offset in OFDM Systems. *IEEE Trans. on Signal Processing*, 45(7):1800–1805, July 1997.
- [99] J. Tellado-Mourello. *Peak to average power reduction for multicarrier modulation*. PhD thesis, Stanford University, September 1999.
- [100] V. Aue, G.P. Fettweis, and R. Valenzuela. A comparison of the performance of linearly equalized single carrier and coded OFDM over frequency selective fading channels using the random coding technique. In *Proceedings of the Int. Conf. on Communications*, May 1998.
- [101] W. Zou and W. Yiyang. COFDM: an overview. *IEEE Trans. on Broadcasting*, 41:1–8, March 1995.
- [102] R. van Nee and R. Prasad. *OFDM for wireless multimedia communications*. Artech House Publishers, Boston, USA, 2000.
- [103] Alben Mihovska, Thorsten Wild, Tommy Svensson, Mikael Sternad, Monica Navarro, Stephan Pfletschinger, David Falconer, Chan Tong Lam, Florence Danilo-Lemoine, Armin Dammann, Simon Plass, Gunther Auer, Jérôme Bonnet, David Astély, Johan Axnäs, Niklas Johansson, Göran Klang, Magnus Olsson, Per Skillermark, Kai-Erik Sunell, Marie-Hélène Hamon, Rodolphe Legouable, Mylène Pischella, Thomas Sälzer, Pedro Coronel, Wolfgang Schott, Mats Bengtsson, Angeliki Alexiou, Abdelkader Medles, Markus Muck, Elias Tragos, Carl Eklund, Kari Kalliojärvi, Antti Sorri, Samuli Visuri, Yong Teng, Ole Klein, Ralf Pabst, Keith Roberts, Zbigniew

- Dlugaszewski, Adam Piatyszek, Michal Wodczak, Thierry Lestable, Vaia Sdralia, Elena Costa, Martin Döttling, Jörn von Häfen, Eiman Mohyeldin, Karsten Brüninghaus, Bill 'Xinqun' Liu, David Thomas, Eduard A. Jorswieck, Volker Jungnickel, Malte Schellmann, Aydin Sezgin, Tobias Frank, Ting Chen, Rainer Grünheid, Stephan Stiglmayr, Emilio Mino, Ernesto Zimmermann, Martin Fuchs, Veljko Stankovic, Martin Haardt, Mohammad Abaii, Yajian Liu, Kari Hooli, Juha Karjalainen, and Zexian Li. Deliverable D2.10: Final report on identified RI key technologies, system concept, and their assessment. Technical report, IST-WINNER project, IST-2003-507581, available at <http://www.ist-winner.org>, 2005.
- [104] S. Haykin. *Adaptive Filter Theory*. Prentice-Hall, Englewood Cliffs, New Jersey, USA, 1986.
- [105] J. William C. Jakes, editor. *Microwave Mobile Communications*. John Wiley and sons, New York, 1974.
- [106] P. Chang H. Wang. On verifying the first-order Markovian assumption for a Rayleigh fading channel model. *IEEE Trans. Veh. Technol.*, 45, May 1996.
- [107] Z. Liu, X. Ma, and G. B. Giannakis. Space-Time Coding and Kalman Filtering for Time-Selective Fading Channels. *IEEE Trans. on Communications*, 50, February 2002.
- [108] Steven M. Kay. *Fundamentals of Statistical Signal Processing : Estimation Theory*. Prentice-Hall, Englewood Cliffs, New Jersey, USA, 1993.
- [109] E. O. Brigham. *The Fast Fourier Transform*. Prentice-Hall, Englewood Cliffs, New Jersey, USA, 1974.
- [110] ETSI Normalization Committee. Broadband Radio Access Networks (BRAN); HIPERLAN Type 2; Physical (PHY) Layer. Norme ETSI, document RTS0023003-R2, European Telecommunications Standards Institute, Sophia-Antipolis, Valbonne, France, February 2001.
- [111] W. A. Gardner. *Cyclostationarity in Communications and Signal Processing*. IEEE Press, New York, USA, 1994.
- [112] A. V. Oppenheim and R. W. Schaffer. *Discrete-Time Signal Processing*. Prentice-Hall, Englewood Cliffs, New Jersey, USA, 1989.
- [113] W. Rieger, M. Haas, C. Huber, G. Lehner, and W. M. Rucker. A novel approach to the 2D-TM inverse electromagnetic medium scattering problem. *IEEE Trans. on Magnetics*, 35:1566–1569, May 1999.
- [114] Y. Chen, N. Smavatkul, and S. Emeott. Power management for VoIP over IEEE 802.11 WLAN. *IEEE Wireless Communications and Networking Conference*, 3:1648 – 1653, 2004.
- [115] N. Chen, M. Tanaka, and R. Heaton. OFDM Timing Synchronization under Multi-Path Channels. *Proceedings of the IEEE Vehicular Technology Conference, Spring*, 1:378 – 382, 2003.
- [116] Markus Muck, Jens Schönthier, and Kai-Uwe Schmidt. Algorithm Enhancement Definition. Technical report, Deliverable D7R3 of IST-BROADWAY project IST-2001-32686, available at <http://www.ist-broadway.org>, 2004.
- [117] Shengli Zhou, Xiaoli Ma, and Georgios B. Giannakis. Space-Time Coding and Kalman Filtering for Time-Selective Fading Channels. *IEEE Transactions on Communications*, Volume 50:183 – 186, February 2002.

- [118] V. Tarokh, H. Jafarkhani, and A.R. Calderbank. Space-Time Block Codes from Orthogonal Designs. *IEEE Trans. on Information Theory*, 45(5):1456–1467, July 1999.
- [119] Shengli Zhou and Georgios B. Giannakis. Space-Time Coding With Maximum Diversity Gains Over Frequency-Selective Fading Channels. *IEEE Signal Processing Letters*, 8:269–272, October 2001.
- [120] R.G. Gallager. Low-Density Parity-Check Codes. *IRE Transactions on Information Theory*, IT-8:21–28, 1962.
- [121] M. Sipser and D. A. Spielmann. Expander Codes. *IEEE Transactions on Information Theory*, 42:1710–1722, 1996.
- [122] D. J. C. MacKay and R. M. Neal. Near Shannon limit performance of low-density parity check codes. *Electron. Lett.*, 32:1645–1646, 1996.
- [123] T. J. Richardson and R. Urbanke. The capacity of low-density parity check codes under message passing decoding. *IEEE Transactions on Information Theory*, 47:599–618, 2001.
- [124] M. Luby, M. Mitzenmacher, A. Shokrollahi, and D. Spielmann. Analysis of low-density codes and improved designs using irregular graph. *Proc. 30th Annual ACM Symposium on Theory of Computing*, pages 249–258, 1998.
- [125] Sae-Young Chung, Jr. G. David Forney, Thomas J. Richardson, and Rüdiger Urbanke. On the Design of Low-Density Parity-Check Codes within 0.0045 dB of the Shannon Limit. *IEEE Communications Letters*, pages 58–60, 2001.
- [126] Sae-Young Chung, T. J. Richardson, and R. Urbanke. Analysis of Sum-Product Decoding Low-Density Parity-Check Codes Using a Gaussian Approximation. *IEEE Transactions on Information Theory*, 47:657–670, 2001.
- [127] S. ten Brink. Iterative decoding trajectories of parallel concatenated codes. *3rd IEEE ITG Conf. Source and Channel Coding*, 2000.
- [128] S. ten Brink. Rate one-half code for approaching the Shannon limit by 0.1 dB. *Electron. Letters*, 36:1293–1294, 2000.
- [129] T. J. Richardson and R. Urbanke. Efficient Encoding of Low-Density Parity-Check Codes. *IEEE Transactions on Information Theory*, 47:638–656, 2001.
- [130] Valérian Mannoni. *Optimisation des codes LDPC pour les communications multi-porteuses*. PhD thesis, Univeristy of Reims, Champagne-Ardenne, France, June 2004.
- [131] V. Mannoni, D. Declercq, and G. Gelle. Optimized Irregular Low-Density Parity-Check Codes for Multicarrier Modulations over Frequency-Selective Channels. *EURASIP Journal on Applied Signal Processing*, 36:1536–1546, 2004.
- [132] J. Hou, P. H. Siegel, L. B. Milstein, and H. D. Pfister. Capacity-Approaching Bandwidth-Efficient Coded Modulation Schemes Based on Low-Density Parity-Check Codes. *IEEE Transactions on Information Theory*, 49:2141–2155, 2003.
- [133] F. R. Kschischang, B. J. Frey, and H.-A. Loeliger. Factor Graphs and the Sum-product Algorithm. *IEEE Transactions on Information Theory*, 47:498–519, 2001.

- [134] David Declercq. Optimisation et performances des codes LDPC pour des canaux non-standards. *Habilitation Thesis, University of Cergy-Pontoise, France, 2003.*
- [135] C. R. Hartmann and L. D. Rudolph. An optimum symbol-by-symbol decoding rule for linear codes. *IEEE Transactions on Information Theory*, IT-22:514–517, 1976.
- [136] J. Hagenauer, E. Offer, and L. Papke. Iterative decoding of binary block and convolutional codes. *IEEE Transactions on Information Theory*, 42:429–445, 1996.
- [137] J. L. W. V. Jensen. Sur les fonctions convexes et les inégalités entre les valeurs moyennes. *Acta Math.*, 30:175 – 193, 1906.
- [138] S. G. Krantz. *Handbook of Complex Variables*. Boston, MA: Birkhäuser, 1999.
- [139] Marcel Joho. *A Systematic Approach to Adaptive Algorithms for Multichannel System Identification, Inverse Modeling, and Blind Identification*. PhD thesis, Swiss Federal Institute of Technology, October 2000.
- [140] Emmanuel C. Ifeachor and Barrie W. Jervis. *Digital Signal Processing: A Practical Approach*. Addison Wesley publishing company, electronic systems engineering series edition, 1993.
- [141] Marc de Courville and Pierre Duhamel. Adaptive Filtering in Subbands Using a Weighted Criterion. *IEEE Trans. on Signal Processing*, 46(9):2359–2371, September 1998.
- [142] Pierre Duhamel and Martin Vetterli. Fast Fourier Transforms: A Tutorial Review and a State of the Art. *Signal Processing*, (19):259–299, 1990.
- [143] Rupul Safaya. A Multipath Channel Estimation Algorithm using a Kalman filter. Master Thesis, Illinois Institute Of Technology, Chicago, IL., 1997.
- [144] D. H. Brandwood. A complex gradient operator and its application in adaptive array theory. *Proceedings of the IEE*, pages 11–16, 1983.
- [145] C. W. Therrien. *Discrete Random Signals and Statistical Signal Processing*. Prentice Hall, New Jersey, 1992.
- [146] L. Schwartz. *Cours d'Analyse*. Ecole Polytechnique, Paris, 1948.

## Patents

- Markus Muck, Marc de Courville, Stephanie Rouquette-Leveil. Irregular systematic LDPC code-word mapping onto OFDM Carriers in the framework of IEEE802.11n Submitted to the European Patent Office, 2005
- Markus Muck, Alexandre Ribeiro Dias, Marc de Courville. OFDM channel estimation and tracking for multiple transmit antennas European Patent EP03292120.7, 2003
- Markus Muck, Marc de Courville, Mérouane Debbah. Channel Estimation Using The Guard Interval Of A Multicarrier Signal World Patent WO 2004/064344, European Patent EP 1 416 689, 2002

